JOINT TRANSPORTATION
RESEARCH PROGRAM
INDIANA DEPARTMENT OF TRANSPORTATION
AND PURDUE UNIVERSITY

Development of Protocols for Reuse Assessment of Existing Foundations in Bridge Rehabilitation and Replacement Projects

Jeehee Lim, Rodrigo Salgado, Monica Prezzi, Yao Wang, Fei Han

SPR-4516 • Report Number: FHWA/IN/JTRP-2023/23 • DOI: 10.5703/1288284317654

RECOMMENDED CITATION

Lim, J., Salgado, R., Prezzi, M., Wang, Y., & Han, F. (2023). *Development of protocols for reuse assessment of existing foundations in bridge rehabilitation and replacement projects* (Joint Transportation Research Program Publication No. FHWA/IN/JTRP-2023/23). West Lafayette, IN: Purdue University. https://doi.org/10.5703/1288284317654

AUTHORS

Jeehee Lim
Graduate Researcher
Lyles School of Civil Engineering
Purdue University

Rodrigo Salgado, PhD
Charles Pankow Professor in Civil Engineering
Lyles School of Civil Engineering
(765) 494-5030
rodrigo@ecn.purdue.edu
Purdue University

Monica Prezzi, PhD
Professor of Civil Engineering
Lyles School of Civil Engineering
Purdue University

Yao Wang
Graduate Researcher
Lyles School of Civil Engineering
Purdue University

Fei Han, PhD
Civil and Environmental Engineering Assistant Professor
University of New Hampshire

JOINT TRANSPORTATION RESEARCH PROGRAM

The Joint Transportation Research Program serves as a vehicle for INDOT collaboration with higher education institutions and industry in Indiana to facilitate innovation that results in continuous improvement in the planning, design, construction, operation, management and economic efficiency of the Indiana transportation infrastructure. https://engineering.purdue.edu/JTRP/index_html

Published reports of the Joint Transportation Research Program are available at http://docs.lib.purdue.edu/jtrp/.

NOTICE

TECHNICAL REPORT DOCUMENTATION PAGE

1. Report No. FHWA/IN/JTRP-2023/23	**2. Government Accession No.**	**3. Recipient's Catalog No.**
4. Title and Subtitle Development of Protocols for Reuse Assessment of Existing Foundations in Bridge Rehabilitation and Replacement Projects		**5. Report Date** August 2023 **6. Performing Organization Code**
7. Author(s) Jeehee Lim, Rodrigo Salgado, Monica Prezzi, Yao Wang, and Fei Han		**8. Performing Organization Report No.** FHWA/IN/JTRP-2023/23
9. Performing Organization Name and Address Joint Transportation Research Program Hall for Discovery and Learning Research (DLR), Suite 204 207 S. Martin Jischke Drive West Lafayette, IN 47907		**10. Work Unit No.** **11. Contract or Grant No.** SPR-4516
12. Sponsoring Agency Name and Address Indiana Department of Transportation (SPR) State Office Building 100 North Senate Avenue Indianapolis, IN 46204		**13. Type of Report and Period Covered** Final Report **14. Sponsoring Agency Code**

15. Supplementary Notes

Conducted in cooperation with the U.S. Department of Transportation, Federal Highway Administration.

16. Abstract

The existing foundations of a bridge can sometimes be reused. This may occur when a completely new bridge is built but also in bridge or superstructure widening projects. Reuse of existing foundations not only eliminates the costs associated with demolishing and disposing of old foundations, but also reduces the costs of the design and construction of new foundation elements. However, several challenges exist, including assessing the structural integrity, estimating the current capacity, estimating the remaining service life, and considering current design codes and specifications of the existing foundations, and clear guidelines for foundation reuse. The absence of foundation reuse guidelines by INDOT hinders the reuse of bridge foundations and prevents design consultants from designing new structures using existing foundations. In this project, comprehensive foundation reuse guidelines were developed in the form of flow charts based on a literature review on bridge foundation reuse design—including technical publications and existing standards and codes—and a set of analyses. The proposed guidelines include detailed guidance on inspection of the structural integrity of existing foundations, determination of as-built geometry of existing foundations, capacity estimation of existing foundations, minimum requirements for foundation reuse, and selection of foundation reuse solutions. The proposed guidelines for foundation reuse design were tested in an ongoing INDOT project. From the implementation project, we found that a complete site investigation that produces reliable estimation of soil profile and properties, is essential to determine whether there is reserve capacity in existing foundations. Additional site investigation is generally worth doing, not only to account for any strengthening of the soil that may have occurred over time, but also because of the greater accuracy in interpretation and analysis that results. We also found that use of the most current, cutting-edge methods can be useful in estimating the reserve capacity of existing foundations, and that design checks using different design codes can produce contrasting results.

17. Key Words foundation reuse, foundation reuse design guidelines, inspection of existing foundations, capacity estimation of existing foundations, selection of foundation reuse solutions, pile cap contribution, group efficiencies.	**18. Distribution Statement** No restrictions. This document is available through the National Technical Information Service, Springfield, VA 22161.

19. Security Classif. (of this report) Unclassified	**20. Security Classif. (of this page)** Unclassified	**21. No. of Pages** 105 including appendices	**22. Price**

EXECUTIVE SUMMARY

Introduction

The existing foundations of a bridge can be reused for bridge or superstructure widening, bridge or superstructure replacement, bridge repurposing, seismic retrofitting of bridge foundations, bridge rehabilitation, clearance increase, or other retrofitting purposes. Reuse of existing foundations not only eliminates the costs associated with demolition of old foundations and their disposal, but also reduces the costs of the design and construction of new foundation elements. However, there are challenges, including the assessment of the structural integrity of existing foundations, estimation of the current capacity of existing foundations, estimation of the remaining service life of the existing foundations, the application of current design codes and specifications to existing foundations that were constructed based on old design codes and specifications, and lack of clear guidelines for foundation reuse. The absence of foundation reuse guidelines in INDOT's toolbox hinders the reuse of bridge foundations and also prevents design consultants from designing new structures using existing foundations. In this project, foundation reuse protocols are proposed to serve as guidance for INDOT engineers to systematically assess the possibility of reusing existing foundations and to consistently come up with reliable solutions for bridge rehabilitation and replacement projects. The proposed guidelines for foundation reuse design were evaluated and implemented in one ongoing INDOT bridge rehabilitation and widening project.

To reuse existing foundations in bridge replacement and bridge rehabilitation projects, it is very important to accurately estimate the bearing capacity of the existing foundations by using current design methods and current standards. Current design standards do not include the load carrying capacity that develops due to the interaction of the pile cap and the soil bearing the cap in the total capacity calculation of the pile groups supporting bridge piers. The effect of the interactions between individual piles in a group and the soil surrounding them is accounted for by using a single group efficiency value, which is capped at 1 to be conservative. However, recent studies showed that the contribution of a soil-supported pile cap to the total bearing capacity of the group is not negligible. Group efficiency values can also be greater than 1, depending on group layout, location of the individual piles, settlement level and type of resistance. Accordingly, a series of realistic numerical simulations of axially loaded pile groups was performed using realistic soil models and fine meshes in Finite Element (FE) analyses, which included a parametric study of the impact of the pile cap on the total pile group resistance and pile efficiency values. Different advanced two-surface constitutive models were used to realistically simulate the behavior of sand and clay, separately. The commercial software Abaqus/CAE (SIMULIA, 2021) was used to perform the FE analyses. In the analyses, different soil profiles that are typical in Indiana, pile group layouts (1×5, 2×5, to 3×5), pile diameters B (14 inches and 23.6 inches), pile-to-pile spacings ($3B$ and $5B$), and pile-to-cap edge distances ($2B$ and $6B$) were carefully considered.

Findings

Protocols for foundation reuse were proposed, in the form of flow charts, in this study. Determination of the as-built geometry of existing foundations is the first step when considering foundation reuse. After determining the as-built geometry of the existing foundations, their structural integrity should be assessed through inspection. If the structural integrity of existing foundations is sufficient for potential reuse with or without repairs, the available site investigation data should be collected and analyzed. If necessary, additional site investigation can be performed not only to determine an accurate design soil profile for the site, but also to investigate any time effects—like, for example, from consolidation or setup—on the current soil profile. Based on the as-built geometry of the existing foundations and the site investigation data, the capacities of existing foundations can be estimated. The current capacity of existing foundations can be estimated from consideration of historical records, inspection results, structural integrity evaluations, site investigation data, and load tests. Capacity estimation of existing foundations is one of the major challenges for foundation reuse, because of the uncertainties regarding historical records, inspection results, current site conditions, time effects on capacity, and remaining service life. It is recommended that foundation capacity predictions be made using the most current pile design methods and current site investigation data. These predictions can be complemented with data from load tests on existing foundations for an accurate capacity estimation. Next, both geotechnical and structural design checks must be performed based on updated design loads, current soil profile conditions, and the estimated current capacities of existing foundations. If the existing foundations do not pass the design checks, they can be repaired or strengthened by adding newly installed piles to increase their capacity, or the superstructure design loads can be reduced by, for example, using lighter materials. Another option to consider is strengthening ground conditions by using ground engineering methods. If none of these methods work, then the existing foundations will need to be completely replaced by new foundations.

The proposed guidelines for foundation reuse design were evaluated and implemented for an ongoing INDOT bridge rehabilitation and widening project on I-465 over 71st street. From the implementation project, we found that a "loam" layer in the soil profile, which is typical in Indiana soil profiles, may be difficult to classify as either a sandy soil or clayey soil, but a correct classification is very important, because most of the design methods—including traditional ones contained in AASHTO (AASHTO, 2020) and current methods—are developed for either sand or clay. Depending on the classification, the estimated capacities can be substantially different, even for the same SPT or CPT cone resistance values. In addition, an accurate site investigation is essential to estimate whether the existing foundations have reserve in capacity. Obtaining additional site investigation data is advantageous, not only to account for any strengthening of the soil that may have occurred in time, but also because of the greater accuracy in interpretation and analysis that results. We also found that capacity estimation using the state-of-the-art methods is useful in estimating the reserve capacity of existing foundations, and design checks using different design codes can produce contrasting results.

Additionally, we performed studies on the bearing capacity of the pile cap and the individual efficiencies of the piles in a pile group. Based on the results of the realistic, advanced FE analyses performed in this study, the pile cap contribution towards the total capacity of the pile-supported foundation in sand can be significant. It ranges from 12% to 80% depending on the target settlement level of the pile group. The percentage of the pile cap contribution to the total pile group capacity varies with the settlement of the pile cap, cap size, and soil profile. Features of the soil profile that were considered are soil types, relative density of

sand layers, thickness of the loose layer in a loose-over-dense soil profile, and the existence of a dense sand layer at the top of the soil profile.

The efficiencies of individual piles in a pile group increase as the pile cap settlement increases. It is lower than 1 when the pile cap settlement is very small but can be greater than 1 as settlement increases. The efficiencies for the shaft resistance typically increase at higher rates than the efficiencies for the base resistance as the settlement increases from 0 to 100 mm (4 inches). The amount and rate of change of shaft and base efficiencies at the different settlement levels considered in this study depend on group layout, soil profile, and location of the pile in a group.

Implementation

Comprehensive foundation reuse guidelines were developed in the form of flow charts based on a comprehensive literature review on bridge foundation reuse design, which includes technical publications and existing standards and codes. The proposed guidelines include detailed guidance on the inspection of existing foundations to assess their structural integrity, determination of as-built geometry of the existing foundations, capacity estimation of the existing foundations, minimum requirements for foundation reuse, and selection of foundation reuse solutions.

The proposed guidelines for foundation reuse were implemented in an ongoing INDOT bridge rehabilitation and widening project on I-465 over 71st street. Following the proposed guidelines, the research team, with collaboration from INDOT engineers, fulfilled the following: (1) reviewed available historical records; (2) analyzed inspection results; (3) interpreted available site investigation data and proposed performing additional CPT tests to better estimate soil properties; (4) reanalyzed soil profile conditions, including the data from the additionally performed CPT; (5) determined the as-built geometry of the existing foundations; (6) estimated the bearing capacities of the existing foundations using different design methods; (7) performed design checks following different design codes (ASD, LFD, and LFRD design frameworks); (8) analyzed the selected solution of strengthening the existing foundations with new piles; (9) estimated the capacities of new foundations; and (10) reperformed design checks following different design codes (ASD, LFD, and LFRD design frameworks). These analyses were performed for research and illustration purposes only.

From the implementation project, we found that the "loam" layer—"loam" being a common soil classification used by drillers in Indiana—may be difficult to classify as either a sandy soil or clayey soil, but a correct classification is very important, because most of the design methods— including traditional ones contained in AASHTO (AASHTO, 2020) and current methods—are specified for either sand or clay. In addition, an accurate site investigation is essential to estimate whether the existing foundations have reserve capacity, and additional site investigation is generally worth it, not only to account for any strengthening of the soil that may have occurred in time, but also because of the greater accuracy in interpretation and analysis that results. We also found that the capacity estimation using state-of-the-art CPT-based methods can be useful in estimating the reserve capacity of the existing foundations, and design checks using different design codes can produce contrasting results. These findings can be useful in future INDOT bridge rehabilitation and widening projects, which are common applications of foundation reuse in Indiana.

Additionally, we extracted the pile cap contribution towards the total pile group capacity and the pile efficiencies from simulation results. Based on a series of realistic, advanced finite-element analyses of soil-supported pile groups, we found that (1) the pile cap contribution towards the total capacity of the pile-supported foundation in sand is significant (12% to 80%, depending on the settlement level, for the pile groups considered in this study), and (2) the efficiencies of individual piles in a pile group increase as the pile cap settlement increases. The efficiencies are lower than 1 when the pile cap settlement is very small but can be greater than 1 as settlement increases. These findings can be implemented in pile group designs with further studies.

An equation for the unit pile cap capacity was developed based on a series of realistic, advanced finite-element analyses of soil-supported pile groups. The proposed equation predicts the pile cap capacities of pile groups with various group layouts (1×5, 2×5, to 3×5), pile diameters B (14 inches and 23.6 inches), pile-to-pile spacings ($3B$ and $5B$), and pile-to-cap edge distances ($2B$ and $6B$) in uniform loose and dense sands.

CONTENTS

LIST OF TABLES

LIST OF FIGURES

1. INTRODUCTION

1.1 Background

When a bridge is replaced or retrofitted, it may be advantageous to reuse its existing foundation elements (e.g., footings or piles and pile cap) if they are able to provide sufficient bearing capacity to support the new or retrofitted bridge. Reuse of existing foundations not only eliminates the costs associated with demolition of old foundations and their disposal, but also reduces the costs of the design and construction of new foundation elements. For example, the reuse of foundations for the reconstruction of the Milton-Madison Bridge between Kentucky and Indiana resulted in savings of $50 million (Tiberio, 2015). In addition to significant cost savings, benefits of reusing existing foundations include reduced project delivery timelines, improved safety, no ROW procurement, no utility relocations, and minimum environmental impact (Davis et al., 2019). In this type of work, engineers are held to a negligence standard (Salgado, 2022b); however, the standard of care in the foundation reuse area is still fluid. Because the geometry and condition of the foundations are often unknown, this creates a risk that is specific to this type of application. Additional uncertainties include any changes that have happened to the soil and the soil-foundation interface over the life of the existing structure and whether design methods then used were to conservative or unconservative. What should a prudent engineer do when designing a reuse solution remains object of study.

Foundation reuse can be defined by "the use of an existing foundation or substructure of a bridge, in whole or in part, when the existing foundation has been evaluated for new loads" (Agrawal et al., 2018). Foundation reuse does not include the cases where the loads do not change, such as in bridge deck replacements. The existing foundations of a bridge can be reused for bridge or superstructure widening, bridge or superstructure replacement, bridge repurposing, retrofitting of bridge foundations for seismic conditions or other purposes, or clearance increase. NCHRP Synthesis 505 (Boeckmann, 2019; Boeckmann & Loehr, 2017) performed a web-based survey to agencies in the USA and Canada and obtained responses from 45 US state DOTs and 8 Canadian provinces. In a question about applications for foundation reuse, 82% of the respondents chose the bridge or superstructure widening application, and 80% of the respondents chose the bridge or superstructure replacement application. Seismic retrofit of bridge foundations, increase of clearance, and bridge repurposing were chosen by 30%, 30% and 24% of the respondents, respectively, while only 2% of the respondents chose scour retrofit and cantilever retaining wall as applications for foundation reuse.

According to the survey performed by NCHRP Synthesis 505 (Boeckmann, 2019; Boeckmann & Loehr, 2017) and discussions in the workshop hosted by FHWA's Foundation Characterization Program in 2013 (Boeckmann & Loehr, 2017) and in the DFI's 46th annual Conference on Deep Foundations in Las Vegas in 2021 (Boeckmann & Shields, 2022), the major challenges for reuse of existing foundations of a bridge are the following.

- Assessment of structural integrity of the existing foundations.
- Estimation of current capacity of the existing foundations.
- Estimation of remaining service life of the existing foundations.
- Consideration of current design codes and specifications to existing foundations constructed based on old design codes and specifications.
- Lack of clear guidelines for foundation reuse.

The absence of foundation reuse guidelines in INDOT's toolbox hinders the reuse of bridge foundations and also prevents design consultants from designing new structures using existing foundations. There is not at present a systematic manner, based on current science and engineering, to address this problem. In this research, foundation reuse protocols are proposed to serve as guidance for INDOT engineers to systematically assess the possibility of reusing existing foundations and to consistently come up with reliable solutions for bridge rehabilitation and replacement projects.

1.2 Pile Group Capacity and Contribution of Pile Cap

To reuse existing foundations in bridge replacement projects, it is very important to accurately estimate the load capacity of the existing foundations by using current, reliable design methods and current standards. Typically, the foundation design methods that were used to design the existing foundations of old bridges are mostly empirical and thus tend to be conservative. Empirical pile design methods were developed based on results of pile load tests for the specific site conditions in which these tests were performed; thus, generalization of these methods to capture several important factors, such as friction degradation due to driving, cross-sectional shape (e.g., solid cross section versus hollow ones; square versus circular sections) and other factors is not advisable.

According to the design standards (AASHTO, 2020; INDOT, 2018), the load-carrying capacity that develops due to the interaction of the pile cap and the soil bearing the cap is not considered for pile group-supported bridge foundations. However, recent studies have demonstrated that the contribution of a soil-supported pile cap to the total bearing capacity of the group is not negligible and could be considered in cases in which scouring is not expected to occur. In addition, according to the AASHTO design manual (AASHTO, 2020), the effect of the interactions between individual piles in a group and the soil surrounding them is accounted for by using a single group efficiency value, which is capped at 1 to be conservative. This efficiency

factor does not depend on the configuration of the individual piles in the pile group, settlement level, type of resistances (pile shaft versus pile base) or soil layering.

Results of model- and small-scale load tests on pile groups with caps supported by soil have shown that the pile cap capacity accounts for about 10%–40% of the total pile group capacity (Park et al., 2012; Senna et al., 1993), depending on pile spacing and soil conditions. In the Sagamore bridge monitoring projects (SPR-4165 and SPR-4546), the pile cap capacity has been measured to be approximately 20% of the total foundation capacity (Han, Marashi, et al., 2020; Han, Prezzi, et al., 2020). Numerical studies on pile group response have demonstrated that group efficiency values can be greater than 1 depending on group layout, location of individual piles in the group, settlement level and type of resistances (Han et al., 2015; Han, Salgado, et al., 2019). Being able to account for the pile cap capacity and to consider group efficiency values greater than 1 when evaluating the total load capacity of existing foundations can lead to more widespread foundation reuse and significant cost savings for INDOT. Therefore, a comprehensive understanding of (1) the contribution of cap capacity to the total foundation capacity, and (2) the effect of the pile cap on the mobilization of base and shaft resistances of individual piles in a group is essential to accurately reevaluate the load capacity of existing pile groups to be reused.

In order to account for the effect of the pile cap on pile group capacity, researchers have used both analytical (Butterfield & Banerjee, 1971; Chow & Teh, 1991; Shen et al., 2000) and numerical (Huang et al., 2011; McCabe & Lehane, 2006; Ottaviani, 1976) approaches to model the response of pile groups subjected to axial loads. These studies improved the understanding of pile group response to loading. However, the use of simple constitutive models (e.g., linear elastic models or linear elastic, perfectly-plastic models with the Mohr-Coulomb yield criterion) and the use of coarse meshes in finite-element (FE) simulations limit the application of the results in design.

In this research, a parametric study involving a series of realistic numerical simulations of axially loaded pile groups was performed by using realistic soil models and fine meshes in FE analyses. Pile group configurations that are commonly used to support bridges in Indiana were analyzed to study the effect of soil layering, pile cap size, pile group layout, and pile-to-pile spacing on the bearing capacity mobilization of pile groups.

1.3 Reuse Protocols by Other DOTs

While INDOT and other DOTs have been reusing existing foundations, none of the DOTs have complete policies or guidelines on foundation reuse in place. Several DOTs have started to include a discussion of foundation reuse in their bridge design manuals (IDOT, 2011; MaineDOT, 2018; MassDOT, 2013; ODOT, 2020). MaineDOT (2018) provides suggestions for the reuse of two types of foundations which are timber piles and granite or stone substructure, and IDOT (2011), MassDOT (2013), ODOT (2020) provide requirements for foundation reuse and guidelines on specifications, inspection and estimation of the capacity of existing foundations. Table 1.1 summarizes the existence of foundation reuse guidelines in other DOTs.

In addition, FHWA and a few DOTs (e.g., MDOT and MoDOT) have explored design methods and decision criteria for foundation reuse (Agrawal et al., 2018; Aktan & Attanayake, 2015; Boeckmann & Loehr, 2017; Boeckmann et al., 2018; Collin & Jalinoos, 2014). Yet, these attempts are still preliminary and incomplete. Foundation reuse protocols developed especially for Indiana can be implemented by INDOT, accounting for the site conditions and foundation types commonly seen in Indiana.

TABLE 1.1
Foundation reuse protocols in other DOTs

	Detailed Guidelines for the Assessment of Existing Foundations				
DOT	**Specifications**	**Integrity Check**	**Capacity Check**	**Service Life Check**	**Note**
MaineDOT (2018)	×	–	–	×	Detailed guidelines only for timber piles and granite or stone substructures
Illinois DOT (IDOT, 2011)	✓	–	✓	×	Simple guidelines (minimum requirements) for foundation reuse are given
Massachusetts DOT (MASSDOT, 2013)	✓	✓	✓	–	Simple guidelines (minimum requirements) for bridge rehabilitation are given
Ohio DOT (ODOT, 2020)	✓	✓	✓	×	Simple guidelines (minimum requirements) for foundation reuse are given

Note:
✓ = Yes.
× = No.
– = Recommended without detailed guidelines.

TABLE 1.2
Foundation reuse case histories

Reference	Case Name	Location	General Description	Foundation Type	Superstructure Type	Primary Drivers for Reuse
Agrawal et al. (2018)	I-44 Bridge over Gasconade River	MO	Existing substructure repaired and reused. Temporary substructure built to support the bridge before slide.	Massive pneumatic caissons keyed into bedrock	Truss	–
Agrawal et al. (2018)	Fast-14 Replacement Project	MA	14 bridges replaced on original substructures with minimal repairs.	–	Steel girders with composite concrete decks	–
Agrawal et al. (2018)	Lake Mary Bridge	Flagstaff, AZ	Replacement of superstructure with reuse of the existing foundations considered.	Masonry footings	Steel girders-Continuous; 3-span	Economic
Agrawal et al. (2018)	Milton Madison Bridge	Between Madison, IN and Milton, KY	Bridge replaced using slide-in-place construction on many of the original piers that required minimal bridge closures.	Caissons	Truss; 5-span	Economic/ABC
Agrawal et al. (2018)	North Torrey Pines Bridge	Del Mar, CA	A significant retrofit program was undertaken to correct existing issues with respect to seismic problems.	Footing and piles	Concrete girders; 15-span	Historical
Agrawal et al. (2018)	Georgia Street Bridge	San Diego, CA	Two replacement alternatives and two retrofit alternatives were considered.	Spread footing	Three-rib Concrete arch;	Historical
Agrawal et al. (2018)	Huey P. Long Bridge	Jefferson Parish, LA	New trusses were installed outside of the original trusses and connected to widened portions of the piers using a steel transfer frame.	Caissons	Truss	Economic
Agrawal et al. (2018)	Manahawkin Bay Bridges	Ocean County, NJ	The final construction plan involved the construction of a new bridge next to the existing main bridge to allow diversion of the eastbound traffic onto the new structure.	Timber pile	Concrete girders	Economic
Agrawal et al. (2018)	US Route 2A Bridge	Haynesville, ME	Replacement of the superstructure while reusing the substructure and pile foundations without modification.	Timber pile; 3-span	Steel girders; 3-span	Economic
Agrawal et al. (2018)	US Route 1 Viaduct	Bath, ME	The reconstructed bridge maintained the original geometry (no spans removed), while all above ground components (piers, abutments, superstructure, etc.) were replaced.	Footings and steel piles	Steel girders 20-span	Economic/ABC
Agrawal et al. (2018)	Mississagi River Bridge	Ontario, Canada	Replacement of the superstructure with reuse of the existing piers.	Spread footing/steel sheet piling	Steel girders; 5-span	Economic
Agrawal et al. (2018)	Henley Street Bridge	Knoxville, TN	The replacement bridge utilized the existing piers and arch ribs but replaced the deck and spandrel columns.	Spread footing	Concrete arch; 6 spans	Historical

Continued

TABLE 1.2
(Continued)

Reference	Case Name	Location	General Description	Foundation Type	Superstructure Type	Primary Drivers for Reuse
Agrawal et al. (2018)	Jackson Road over MA Route 2	Lancaster, MA	Bridge replaced. The existing substructure components, including abutments, piers, and timber piles were reused.	Pile (timber piles)	Steel girders; simply-supported spans	Economic/ABC
Agrawal et al. (2018)	Cedar Street over MA Route 9	Wellesley, MA	The superstructure was in poor condition and in need of replacement. Substructure considered reuse.	Footings and steel piles	Steel girders; 2-span	Economic/ABC
Agrawal et al. (2018)	Bay of Quinte Skyway	Ontario, Canada	The preliminary evaluation showed that reusing the caissons was economically, environmentally, and socially beneficial.	Caissons (socketed into bedrock)	Steel girders;17-span	Economic
Agrawal et al. (2018)	Crowchild Trail Bridge	Alberta, Canada	The bridge was widened to provide one additional travel lane in each direction and to realign ramps at the ends of the bridge.	Footing/Pile	Steel girders; 10-span	Economic/ Environmental
Agrawal et al., (2018); Collin & Jalinoos, (2014)	Hurricane Deck Bridge	MO	A new alignment was used that reduced the span lengths and increased the number of piers from 4 to 7.	Caissons	Truss	Economic
Agrawal et al., (2018); Collin & Jalinoos, (2014); Jalinoos, (2015); Jalinoos et al., (2016); LeGrand (2015)	I-95 corridor Bridges	VA	11 bridges replaced with full substructure reuse. 9 bridges installed with cathodic protection, 1 with ECE, 1 with ECE and cathodic protection.		New Lightweight Concrete decks (lowering loading by about 7%)	
Boeckmann & Loehr, (2017)	Bowker Overpass	Boston, MA	–	Steel pipe piles	Four-span concrete slab deck atop steel stringers	
Boeckmann & Loehr, (2017)	Hunt Road over I-495	Lowell, MA	Replacement of the abutment backfill with lightweight geofoam to reduce the dead load on the piles and satisfy the HS-25 scenario. Analysis of the pier footings indicated that the allowable bearing resistance listed on the plans was sufficient for all loading scenarios considered. The footings were recommended for reuse without modification.	Abutments on 12-inch diameter unreinforced cast-in-place concrete piles; Piers are on spread footings	The bridge consists of a concrete deck atop steel beams resting on two concrete abutments and four multi-column concrete piers.	

Note: ABC = Accelerated Bridge Construction.

1.4 Case Histories of Foundation Reuse

There are several historic cases of foundation reuse discussed in the literature. Table 1.2 is summarized from (Agrawal et al., 2018) and (Boeckmann & Loehr, 2017). From the twenty cases selected, sixteen involved structural integrity checks of the foundation elements, five involved as-built geometry determination, nine involved additional site investigation, three used finite element analysis to assess the capacity of the foundation elements, five included life cycle investigations, and only one mentioned further monitoring of the structure. Table 1.2 provides general information for the selected cases.

2. PILE CAP CONTRIBUTION TO PILE GROUP CAPACITY

2.1 Finite-Element Analyses of Pile Groups

2.1.1 Constitutive Models

A comprehensive understanding of soil-pile group response to axial loading can be achieved by performing Finite Element Analyses (FEA). The use of realistic constitutive models is necessary to obtain accurate analysis results. Simple constitutive models, such as a linear elastic model or a linearly elastic-perfectly plastic model with the Mohr-Coulomb yield criterion are not capable of capturing the complex response of the soil surrounding a pile or a pile group (Han et al., 2015; Han, Salgado, et al., 2019).

In this study, two advanced two-surface constitutive models are used to simulate the behavior of sand and clay: the sand model developed by Loukidis and Salgado (2009) is used to simulate sand layers and the clay model developed by Chakraborty, Salgado, and Loukidis (2013) is used to simulate clay layers. Both models are based on critical-state soil mechanics and use a bounding surface to capture the peak strength of soil and a dilatancy surface to capture the dilatancy (plastic volume change during shearing) of soil before it reaches critical state under continuous monotonic shearing. These soil models are able to capture the highly nonlinear response of soil to loading under various loading paths with consideration of initial fabric, initial stress state and initial density (i.e., relative density D_R of sand and over consolidation ratio OCR of clay). In addition, the clay model can capture the increase in shear strength with increasing loading rate and the decrease in shear strength all the way to the residual strength with consideration of the change in fabric under extensive shearing. The values of the model parameters for sand and clay are presented in Table 2.1 and Table 2.2, respectively. In the case of sand, we selected for the simulations Ottawa sand, which is a medium-sized silica sand with rounded-to-subrounded particles, and for clay, we considered Boston Blue Clay (BBC), which is an inorganic clay of low-to-medium plasticity that does not have a residual state. In our analyses, the rate of loading applied at the top of the pile cap is high enough to produce an undrained response for clay, but sufficiently low to produce a negligible strain-rate effect on the shear strength of clay, and a drained response for sand. In the analyses, the applied

TABLE 2.1
Model parameters used for sand (Ottawa sand)

Parameter Groups	Parameter Symbol	Parameter Value
Small-Strain Parameters	ν	0.15
	C_g	611
	n_g	0.437
	γ_1	0.00065
	α_1	0.47
Critical State	Γ_c	0.78
	λ	0.081
	ξ	0.196
	M_{cc}	1.21
Bounding Surface	k_b	1.9
Dilatancy	D_0	1.31
	k_d	2.2
Plastic Modulus	h_1	2.2
	h_2	0.24
	e_{lim}	0.81
	μ	1.2
Stress-Induced Anisotropy	c_1	0.71
	c_2	0.78
	n_s	0.35
Inherent Anisotropy	α	0.31
	k_h	0.39
Yield Surface Radius	m	0.05

TABLE 2.2
Model parameters used for clay (Boston Blue Clay)

Parameter Groups	Parameter Symbol	Parameter Value
Small-Strain Parameters	ν	0.25
	C_g	250
	ζ	5
	κ	0.036
Normal Consolidation Line	N	1.138
	λ	0.187
Stress Anisotropy	$K_{0,NC}$	0.53
Shear Strength	M_{cc}	1.305
	n_s	0.2
	k_b	0.0
	ρ	2.7
Dilatancy Surface	D_0	1
Flow Rule	c_2	0.95
	ξ	0.31
Plastic Modulus	h_0	1.1
Yield Surface Radius	m	0.05

velocity gradually increased from 0 to 20 mm/s (0.787 inches/s) within the first second and kept constant until the end of the simulation.

Advanced soil models for sand and clay are implemented through user-defined material subroutines (VUMAT) in the commercial software Abaqus/CAE (SIMULIA, 2017). The Jaumann rates are considered for both models in the VUMAT to capture the effect of rigid-body rotation in the analyses. Since the soil models are developed based on effective stresses (with effective stress = total stress minus pore-water pressure), the pore-water pressure in a soil element is separately calculated within the VUMAT. The initial pore-water pressure is the hydrostatic pore-water pressure for both sand and clay layers. During the application of loading, the excess pore-water pressure is zero for sand layers under drained conditions, while the excess pore-water pressure rate $\dot{u}$ for a given computation step for a clay layer under undrained conditions is calculated using

$$\dot{u} = \frac{K_w}{n}\dot{\varepsilon}_v \qquad \text{(Eq. 2.1)}$$

where K_w is the bulk modulus of water, n is the porosity and $\dot{\varepsilon}_v$ is the volumetric strain rate.

The piles and the pile cap are modeled by using a linear-elastic model with Young's modulus E of 50 GPa (7,252,000 psi), Poisson's ratio v of 0.2 and unit weight of 25 kN/m^3 (159 pcf).

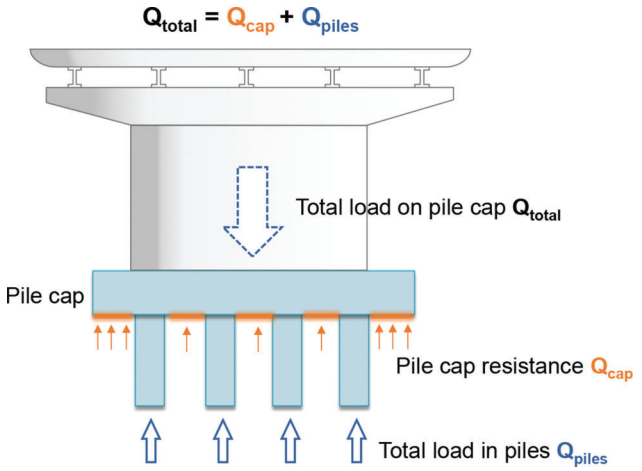

Figure 2.1 Force equilibrium for a pile group supporting a bridge pier.

2.1.2 Analysis Configuration

Pile groups with a rigid pile cap are often used to support bridge piers and bents and to transfer structural loads to the ground. As shown in Figure 2.1, when the superstructure loads (from the bridge deck, beams, and bridge pier) are applied on the pile cap, part of the load is carried by the piles in the group below the pile cap, and the remaining load is carried by the soil that is immediately below the pile cap. The total applied load Q_{total} is equal to the summation of the pile resistance Q_{pile} and the cap resistance Q_{cap}:

$$Q_{total} = Q_{cap} + Q_{piles} \qquad \text{(Eq. 2.2)}$$

In the analyses, three different pile group configurations (1×5, 2×5, and 3×5) are considered with different pile diameters B (0.36 m (14 inches) and 0.6 m (23.6 inches)), pile-to-pile spacings s_p ($3B$ and $5B$) and pile-to-cap edge distances s_{edg} ($2B$ and $6B$). Only pile groups having soil-supported pile caps—which have the pile caps resting on the ground surface—are considered to evaluate the effect of the pile cap on the load capacity of the pile group. Table 2.3 provides a summary of the pile group configurations considered in the analyses.

The four different soil profiles shown in Figure 2.2—loose-over-dense sand (profile 1), normally consolidated (NC) clay over dense sand (profile 2), loose sand sandwiched between two layers of dense sand (profile 3), and over consolidated (OC) clay underlain by NC clay and dense sand at the bottom (profile 4)—are considered in the analyses. Relative densities D_R of 40% and 80% are used for the loose and dense sand layers, respectively, and over consolidation ratios (OCR) of 5 and 10 are considered for the OC clay. To evaluate the effect of soil layering on the contribution of the pile cap to the total capacity of the pile group, the thicknesses of the top and middle layers were varied. Table 2.4 provides the values of the thicknesses of the top and middle layers used in the analyses.

Considering the symmetries in the pile group configurations, one-quarter of the problem domains are modeled in the simulations. Figure 2.3 shows the simulation domain of a 3×5 pile group. As shown in the figure, only one-quarter of the entire domain is considered as the simulation domain. Figure 2.3 also shows the applied boundary conditions to the simulation domain.

TABLE 2.3
Pile group configurations considered in the analyses

Group Configuration	Pile Diameter B (M)	Pile Length L (M)	Pile-to-Pile Spacing S_p	Pile-to-Cap Edge Distance S_{edg}
1×5	0.36, 0.6 (14 inches, 23.6 inches)	10 (32.8 ft)	$3B$, $5B$	$2B$, $6B$
2×5	0.36 (14 inches)	10 (32.8 ft)	$3B$	$2B$
3×5	0.36 (14 inches)	10 (32.8 ft)	$3B$	$2B$

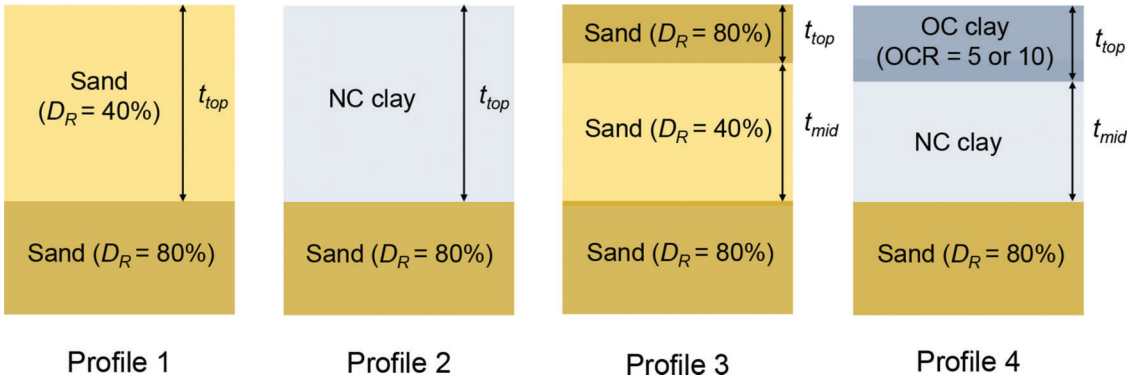

Figure 2.2 Soil profiles considered in the analyses.

TABLE 2.4
Thicknesses of top and middle layers considered in the analyses

Soil Profile	Thickness of Top Layer t_{top}	Thickness of the Middle Layer t_{mid}
Profile 1	0, 0.5B_{cap}, B_{cap}, 1.5B_{cap}, 2B_{cap}, 2.5B_{cap}, 3B_{cap}, 10 m (32.8 ft), 10 m (32.8 ft) + 2B, 20 m (65.6 ft)	–
Profile 2	0, B_{cap}, 2B_{cap}, 10 m (32.8 ft), 10 m (32.8 ft) + 2B, 20 m (65.6 ft)	–
Profile 3	0, 0.5B_{cap}, B_{cap}, 1.5B_{cap}, 2B_{cap}, 10 m (32.8 ft)	10 m (32.8 ft) – t_{top}
Profile 4	0, 0.5B_{cap}, B_{cap}, 1.5B_{cap}, 10 m (32.8 ft)	10 m (32.8 ft) – t_{top}

Note: B_{cap} = shorter length of the pile cap.

For materials like soils that show a softening response with loading, finite-element analyses results are dependent on the mesh configuration. Therefore, use of a fine mesh configuration that can capture the development of strain localization (shear bands) next to the pile shaft and base with loading is necessary to obtain realistic and accurate numerical analysis results for pile groups (Han, Salgado, et al., 2017; Loukidis & Salgado, 2008). For linear finite elements, which are the type of elements used in this study, the size of the elements located in the zones where shear bands develop should be the same as the thickness of shear bands measured experimentally, as done in load tests performed on piles in calibration chambers with visualization capabilities. According to Tehrani et al. (2015), Tovar-Valencia et al. (2018), the thickness of the shear band in sand next to the shaft of a pile loaded axially is of the order of 4 to 5 times the mean particle size D_{50} of the sand when the pile surface is rough. Han, Salgado, et al. (2017) suggested that for sand the element size should be 2 mm to 6 mm (0.0787–0.236 inches) below the pile base based on their parametric study. Janabi et al., (2022) observed from images collected during model footing load tests in sand a shear band thickness of about 7D_{50} to 8D_{50}. Given that the D_{50} of Ottawa sand is 0.4 mm (0.0157 inches) and these experimental observations, the estimated range of shear band thickness for Ottawa sand is 2 mm to 6 mm (0.0787–0.236 inches). Morgenstern and Tchalenko (1969, 1967) observed shear band thicknesses of 3 mm to 4 mm (0.118–0.157 inches) in kaolin clay from microscope photographs taken from specimens at different stages during direct shear tests. Thakur (2007, 2011) performed undrained plane-strain compression tests on Norwegian quick clay samples prepared between two glass plates and measured a shear band thickness of 3 mm to 5 mm (0.118–0.197 inches) by performing digital image correlation (DIC) analyses of the pictures of the samples taken during the tests. In this study, we used linear elements, 4 mm (0.157 inches) in size, next to the pile shaft, below the pile base and below the edges of the pile cap to capture the soil response in the shear bands in a realistic manner. Figure 2.4 shows the mesh configuration used for the analyses of a 3×5 pile group with B = 0.36 m (14 inches), $s_p = 3B$ and $s_{edg} = 2B$; the mesh consists of 8-noded, linear, hexahedral elements, with very fine meshing (elements 4 mm (0.157 inches) in size) in the vicinity of the shafts and bases of the piles and the edges of the pile cap.

The commercial software Abaqus/CAE (SIMULIA, 2021) was used to perform the analyses. Abaqus/Explicit was used to solve the analyses. In the analyses, the effects of installation of the pile group and of time on the stress state in the soil domain are not considered. The initial stress state in the soil is assumed to be close to its initial K_0-consolidated state. The soil and the piles and the soil and the pile cap are assumed to be in perfect contact. In the first step of the analyses, an initial K_0-consolidated stress field is assigned to all element Gauss points. Next, gravity is applied to the piles and the soil by applying the corresponding forces at element nodes. This is continued until the analyses reach a static equilibrium. Gravity is not applied to the pile cap to exclude the effect of the weight of the pile cap on the

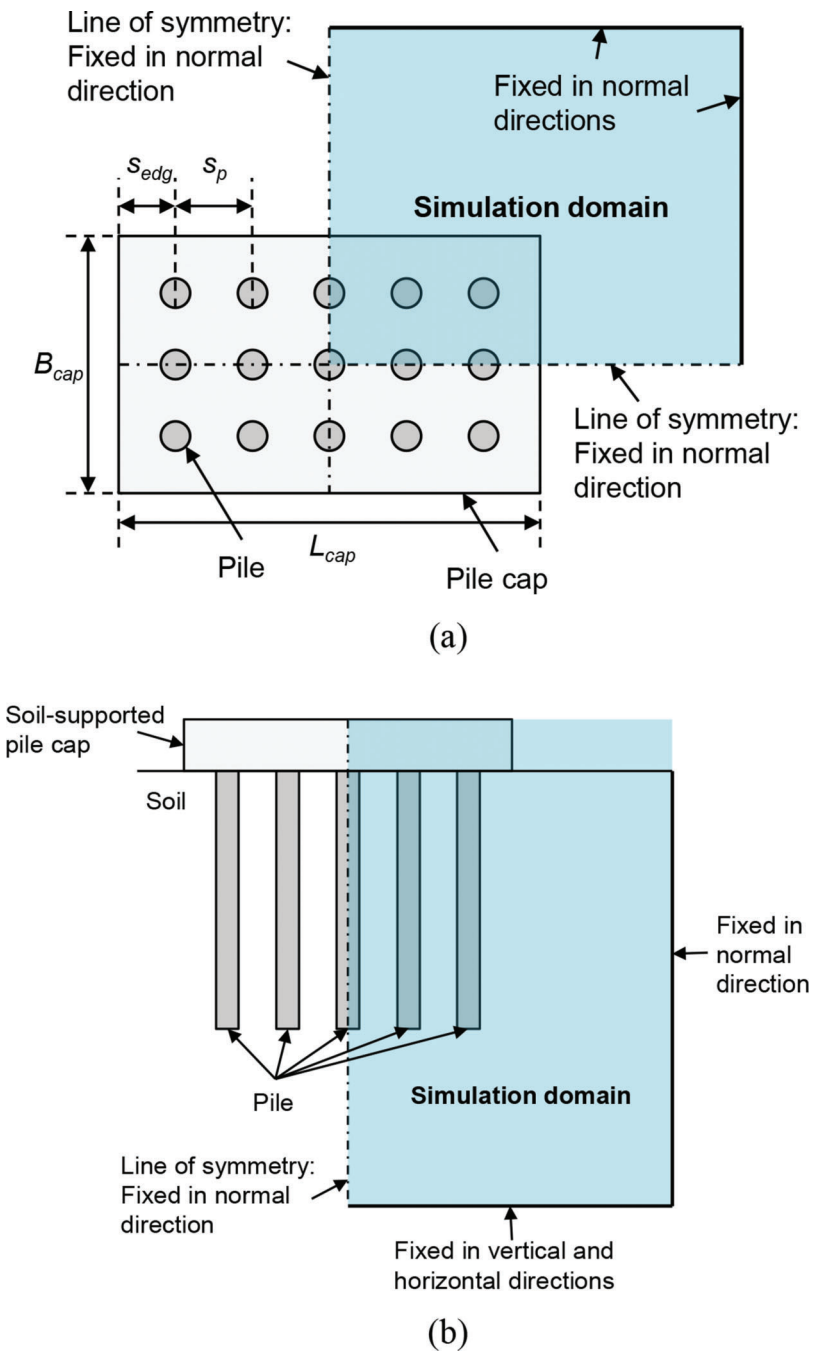

Figure 2.3 Simulation domain of the 3×5 pile group and its boundary conditions: (a) a plan view of the simulation domain, and (b) a side view of the simulation domain of the pile group.

load capacity of the pile group. In the second stage of the analyses, loading was simulated by applying a vertical velocity boundary condition at the top surface of the pile cap. The applied velocity gradually increased from 0 mm to 20 mm/s (0.787 inches/s) within the first second and kept constant until the total settlement of the pile cap reached 100 mm (4 inches).

The weight of the cap is not considered in the analyses because we do not know a priori the thickness of the pile cap that will be used in actual designs. Engineers can subtract the weight of the pile cap from the load capacity obtained from the analyses to calculate their net capacity at design time. Similarly, in footing analyses, we do not consider the weight of the footing. In group efficiency calculations, the weight of the cap also needs to be excluded from the load applied to the piles in the group to be consistent with the load applied to a single, isolated pile.

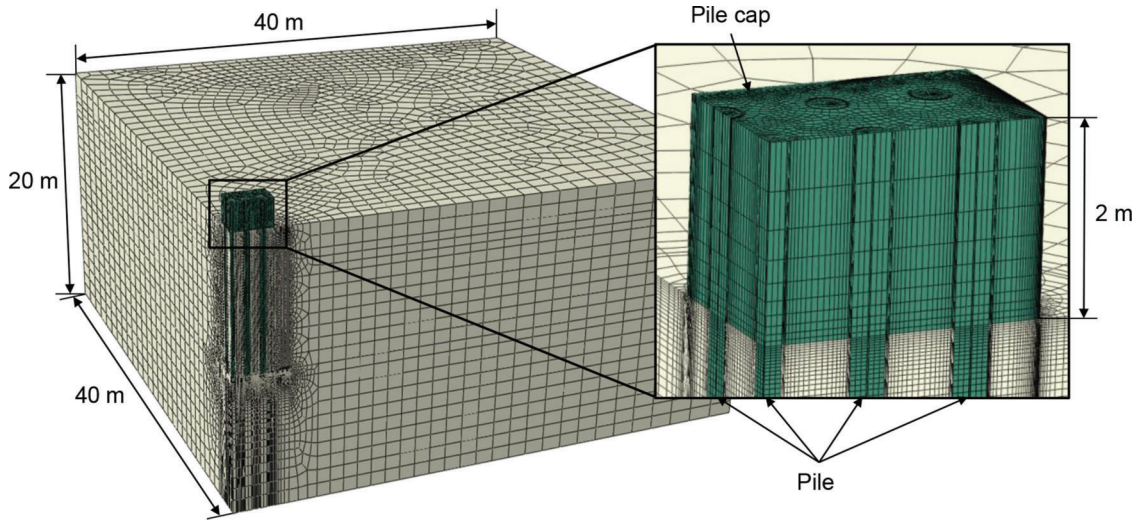

Figure 2.4 Mesh configuration used for the analyses of a 3×5 pile group with $B = 0.36$ m (14 inches), $s_p = 3B$, and $s_{edg} = 2B$.

2.2 Analyses Results

2.2.1 Pile Groups in Uniform Sand

2.2.1.1 Load-settlement curves. Axially-loaded pile groups with a soil-supported pile cap have three sources of resistance: the resistance developed by the pile cap bearing on soil and the base and shaft resistances of the individual piles in the pile group. Figure 2.5 shows a comparison of the mobilization of these axial resistances as a function of the pile cap settlement for the 1×5, 2×5, and 3×5 pile groups placed in uniform loose sand. The resistances of a single, isolated pile with the same geometry as the piles in the pile groups and placed in the same soil profile are also shown in the figure. Figure 2.5(a) shows the average total resistances per pile for the 1×5, 2×5, and 3×5 pile groups, and Figure 2.5(b), (c), and (d) show the average cap resistance per pile, the average base resistance per pile and the average shaft resistance per pile, respectively. As can be seen in Figure 2.5(a), all pile groups develop greater total axial resistances than the single, isolated pile. The greater total axial resistance per pile in pile groups than that of the single pile are mainly attributed to the resistances developed by the pile cap and the pile shafts, as shown in Figure 2.5(b) and (d).

For different pile groups, Figure 2.5(b) shows that the 1×5 pile group develops the largest cap resistance per pile and the 3×5 pile group develops the smallest cap resistance per pile. This indicates that the unit cap resistance of the 1×5 pile group is the largest, and the unit cap resistance of the 3×5 pile group is the smallest. This is because of the geometry of the pile cap. The geometry of the pile cap of the 3×5 pile group is closer to a square than the 1×5 pile group. As is the case with footings (a square footing has a smaller unit base resistance than a strip footing with the same width B if bearing on the same soil), the pile cap of the 3×5 pile group has a smaller unit resistance than the 1×5 pile group. However, we should note that the width B_{cap} of the pile cap of the 3×5 pile group is 1.5 times larger than the B_{cap} of the 1×5 pile group. The effects of the geometry of the cap and the width B_{cap} of the pile cap on the unit cap resistance need to be further investigated in future work to have a better understanding of the mobilization of the pile cap resistance with settlement.

Figure 2.5(c) shows that, as the settlement of the pile cap increases, the average base resistance of the piles in each of the pile groups is slightly greater than the resistance developed by a single, isolated pile. At a pile cap settlement of 100 mm (4 inches), the greatest average pile base resistance is observed for the 3×5 pile group and the smallest for the 1×5 pile group. The pile cap does not have much effect on the base resistances of the piles in a group at the beginning of the loading, but, as the settlement increases, the base resistances of the piles increase at a rate that depends on the size of the pile cap and group layout.

Figure 2.5(d) shows that the shaft resistances of the piles in the pile groups are smaller than that of the single, isolated pile in the beginning of the loading, but that this trend reverses as the pile cap settlement increases. The 3×5 pile group develops the smallest average shaft resistance and the 1×5 pile group develops the greatest average shaft resistance in the beginning of the loading. At a pile cap settlement of 100 mm (4 inches), the greatest average pile shaft resistance is observed for the 2×5 pile group and the smallest for the 1×5 pile group. The pile cap has a greater impact on the shaft resistance mobilization than base resistance mobilization for the piles in a group. In the beginning of the loading, the pile cap restricts the relative displacements between the pile shafts and the soil, so that smaller average shaft resistances are mobilized for the groups than for the single, isolated pile. However, as the settlement increases, the pile cap compresses the soil underneath it and generates additional confining stresses there. This pressure increase leads to shaft resistances for the piles in the group that are

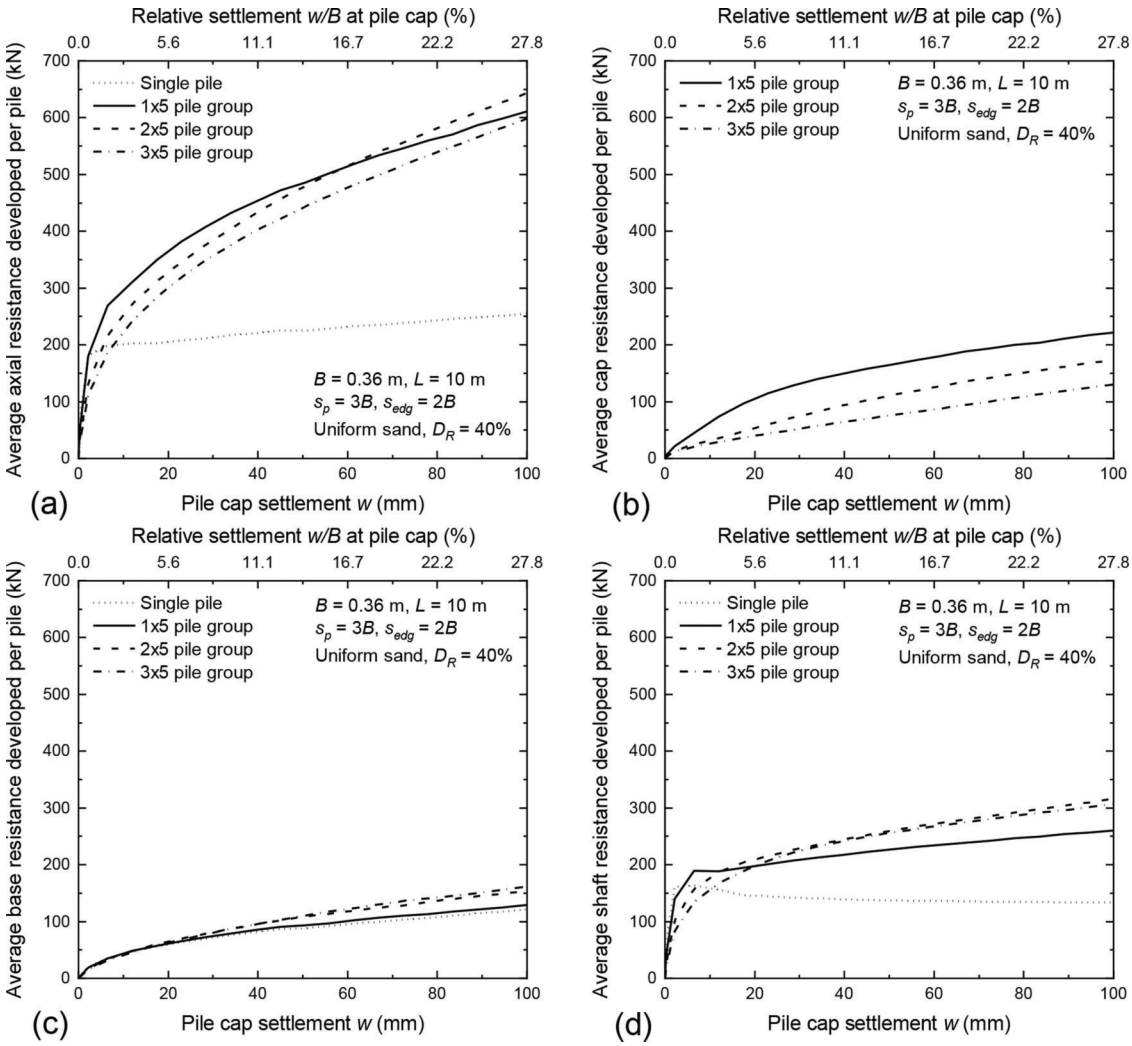

Figure 2.5 Comparison of the axial resistance mobilization as a function of pile cap settlement for the 1×5, 2×5, and 3×5 pile groups in uniform loose sand: (a) total resistance, (b) cap resistance, (c) base resistance, and (d) shaft resistance.

greater than those of a single pile. The increase in shaft resistance due to the presence of a soil-supported pile cap depends on the size of the pile cap and group layout.

Pile groups with soil-supported pile caps have two different effects on the mobilization of the base and shaft resistances of individual piles in the group: the effect due to the interaction between adjacent piles and the soil surrounding them and the effect of the pile cap-soil contact. For free-standing pile groups in sand, the interaction between adjacent piles has almost no effect on the base resistances of the piles in small groups (1×2, 1×3, and 2×2 groups); however, the effect of the pile cap on the shaft resistances of the piles in a group is not negligible (Han, Salgado, et al., 2019). At pile head settlements less than 2%–3% of the pile diameter, the interaction between piles delays the mobilization of the shaft resistances of the piles in a group when compared with single piles (the average shaft resistances of the piles in groups are smaller than that of single piles). At settlements greater than 2%–3% of the pile diameter, the shaft resistances of the piles in groups increase as the settlement increases and reach values of fully mobilized shaft resistances similar to that of a single, isolated pile (Han, Salgado, et al., 2019). Based on our simulation results, the pile groups with soil-supported pile caps develop greater average pile base and shaft resistances than the single, isolated pile, in general, as settlement increases up to 100 mm (4 inches). Again, this is mainly because of the contact between the pile cap and the soil underneath it; as load is transferred to the soil below the cap, the confining stress in the soil increases, which in turn leads to an increase in the base and shaft resistances.

Figure 2.6 shows a comparison of the axial resistance mobilization as a function of pile cap settlement for the 1×5, 2×5, and 3×5 pile groups placed in uniform dense sand. The resistances of a single, isolated pile with the same geometry as the piles in the groups and placed in the same soil profile are also shown in the figure for

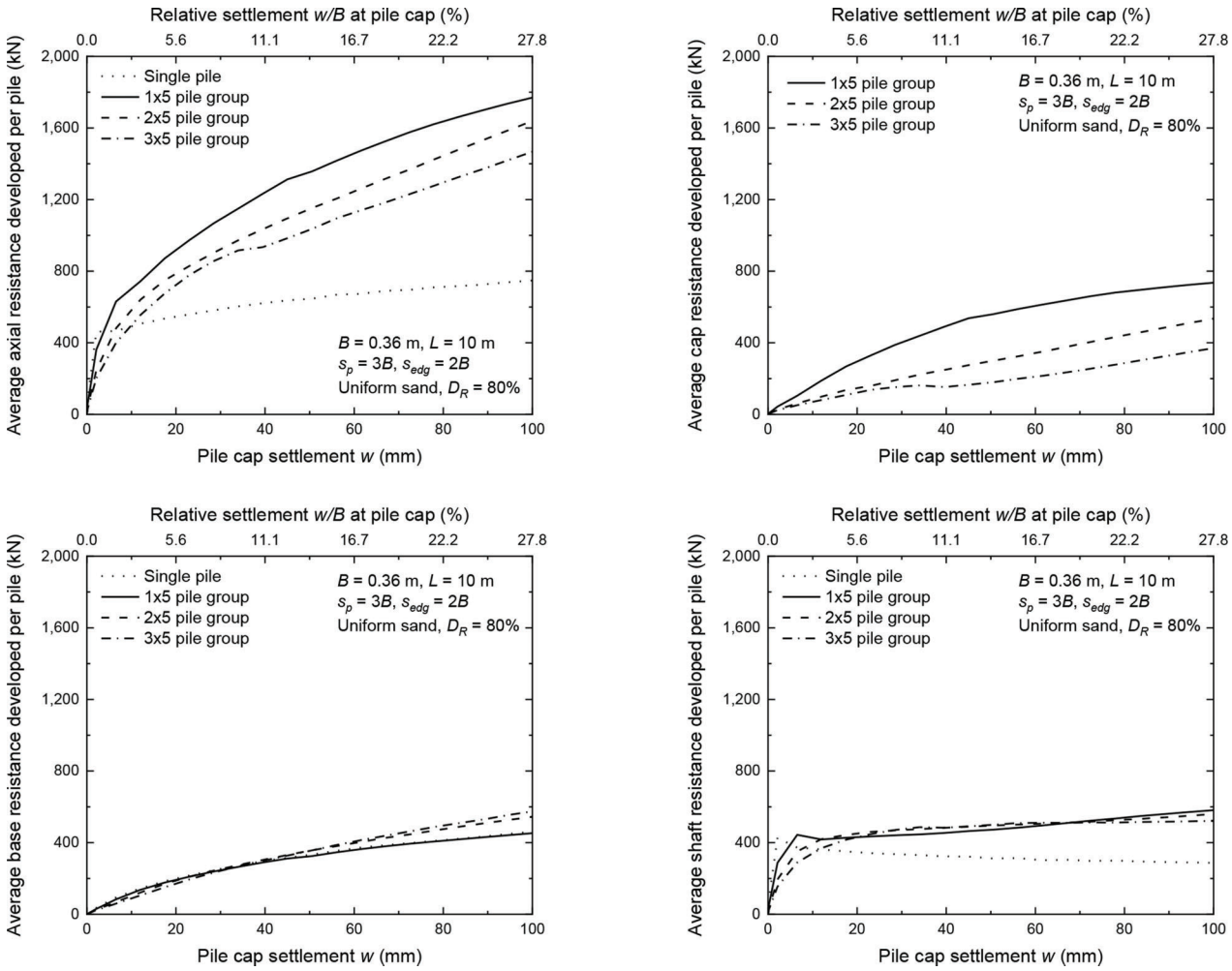

Figure 2.6 Comparison of the average axial pile resistances as a function of pile cap settlement for the 1×5, 2×5, and 3×5 pile groups in uniform dense sand: (a) total resistance, (b) cap resistance, (c) base resistance, and (d) shaft resistance.

reference. The general trends of the results are similar to those observed for the pile groups in uniform loose sand (see Figure 2.5).

Figures 2.7, 2.8, and 2.9 show base and shaft resistances of the individual piles in the 1×5, 2×5, and 3×5 pile groups in uniform sand. The resistances of a single, isolated pile with the same geometry as the piles in the group and placed in the same soil profile are also included in the figures for reference. Based on the FEA results, the individual piles in each pile group can be grouped into two or three pile categories that have almost the same base and shaft resistance mobilization response. Figure 2.10 shows the grouped individual piles in each pile group. The piles in the 1×5 and 2×5 pile groups can be grouped into a center pile category and a side pile category, whereas the piles in the 3×5 pile group can be grouped into a center pile category, a side pile category and a corner pile category depending on the location of the individual piles in the group.

2.2.1.2 Contribution of pile cap to the total resistance of the pile group. The contribution of the pile cap to the total resistance of the pile group is evaluated by the ratio between the pile cap resistance Q_{cap} and the total axial resistance Q_{total} of the pile group. Figure 2.11 shows the pile cap contribution to the total resistance at different pile cap settlements for three different pile group configurations in uniform sand. The pile cap contribution increases, in general, as the pile cap settlement increases. Figure 2.11(a) and Figure 2.11(b) show the results for pile groups in uniform loose sand and dense sand, respectively. As shown in the figures, the denser sand provides slightly higher cap contributions. The 1×5 pile group provides the largest cap contributions and the 3×5 pile group, the smallest cap contributions. For example, at a pile cap settlement of 100 mm, the cap contribution ratios for the 1×5 pile group in loose and dense sand are 36% and 42%, respectively, whereas those of the 3×5 pile group in loose and dense sand are 22% and 25%, respectively.

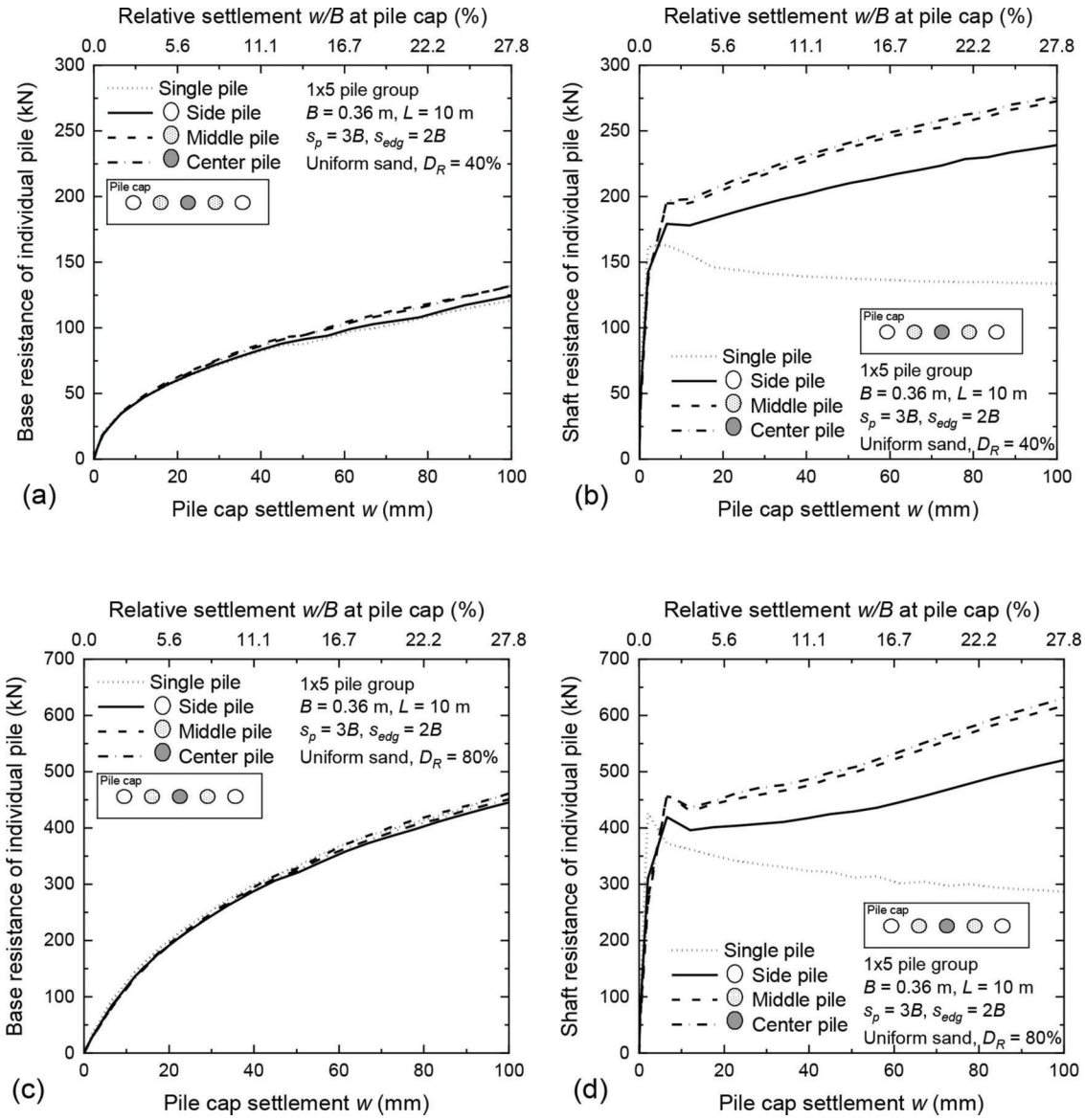

Figure 2.7 Base and shaft resistances of individual piles in 1×5 pile group in uniform sand: (a) base resistances of piles in loose sand, (b) shaft resistances of piles in loose sand, (c) base resistances of piles in dense sand, and (d) shaft resistances of piles in dense sand.

Figure 2.12 shows the unit pile cap resistances of different pile groups placed in uniform sand. As expected, the trends of these results are similar to those presented in Figure 2.11.

Figure 2.13 shows the pile cap contributions for the 1×5 pile groups with different pile diameters placed in uniform sand. The results show that, for the same pile length L, the cap contribution increases as the pile diameter B of the piles in the group increases from 0.36 m (14 inches) to 0.6 m (23.6 inches). For both cases, a pile-to-pile spacing s_p of $3B$ and a pile-to-cap edge distance s_{edg} of $2B$ are considered. Figure 2.14 shows the unit cap resistances of 1×5 pile groups for pile diameters of 0.36 m (14 inches) and 0.6 m (23.6 inches). The unit cap resistances of the 1×5 pile groups with different pile diameters are similar.

Figure 2.15 shows the pile cap contribution to the total resistance of 1×5 pile groups with different pile-to-pile spacings s_p and pile-to-cap edge distances s_{edg} placed in uniform sand. The results show that the cap contribution increases as the pile-to-pile spacing s_p and the pile-to-cap edge distance s_{edg} increase from $s_p = 3B$ and $s_{edg} = 2B$ to $s_p = 5B$ and $s_{edg} = 6B$. The greater cap contribution of the 1×5 pile group with $s_p = 5B$ and $s_{edg} = 6B$ is mainly because of the greater size of the pile cap, resulting in a relatively larger cap resistance than the resistances of the piles in the groups. When the unit cap resistances of the 1×5 pile groups with different s_p and s_{edg} are compared, the values of the unit cap resistances are similar, as shown in Figure 2.16.

Table 2.5 and Table 2.6 show summaries of unit cap capacities of the pile groups in uniform loose and dense sands.

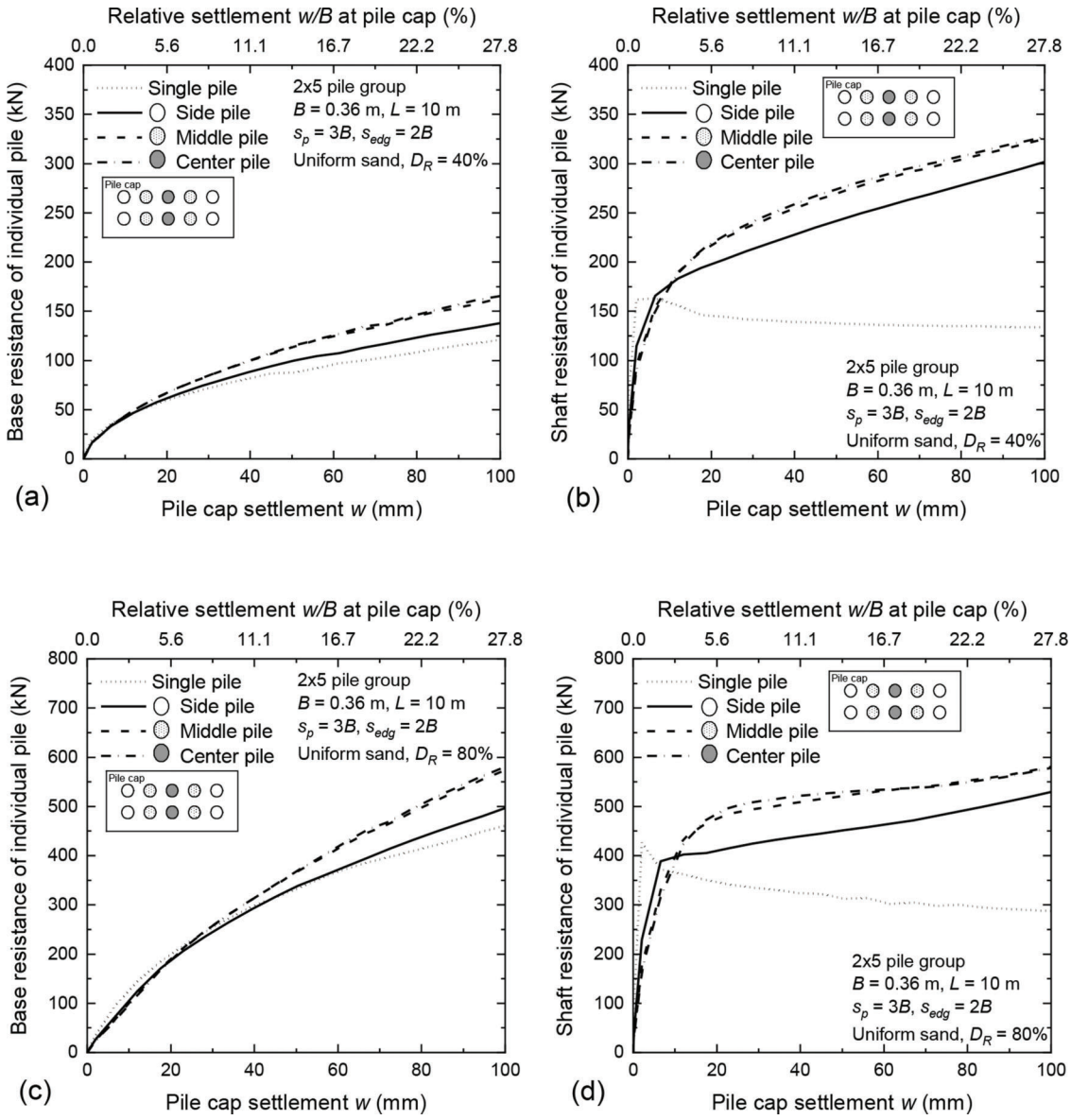

Figure 2.8 Base and shaft resistances of individual piles in 2×5 pile group in uniform sand: (a) base resistances of piles in loose sand, (b) shaft resistances of piles in loose sand, (c) base resistances of piles in dense sand, and (d) shaft resistances of piles in dense sand.

2.2.1.3 Group efficiencies. The effects of the pile-soil-pile interaction in a pile group and the pile cap-soil contact on the mobilization of the base and shaft resistances of the individual piles can be evaluated through the base and shaft efficiencies η_b and η_s, respectively, of the individual piles in the pile group as:

$$\eta_{b,i}(w) = \frac{Q_{b,i}(w)}{Q_{b,is}(w)} \qquad \text{(Eq. 2.3)}$$

$$\eta_{s,i}(w) = \frac{Q_{s,i}(w)}{Q_{s,is}(w)} \qquad \text{(Eq. 2.4)}$$

where $Q_{b,i}$ and $Q_{s,i}$ are the base and shaft resistances, respectively, of the i^{th} pile in the pile group; and $Q_{b,is}$ and $Q_{s,is}$ are the base and shaft resistances, respectively, of a single, isolated pile with the same geometry and placed in the same soil profile as the i^{th} pile of the pile group.

Figures 2.17, 2.18, and 2.19 show the base and shaft efficiencies (η_b and η_s, respectively) of the individual piles in the 1×5, 2×5, and 3×5 pile groups placed in uniform loose and dense sand. As shown in the figures, both the base and shaft efficiencies increase from values lower than 1 to values higher than 1 as the settlement increases from 0 mm to 100 mm (4 inches). In general, the base and shaft resistances of the piles in a group are mobilized at a slower rate than for the single pile because of the effects of the pile-soil-pile interaction in a pile group and the pile cap-soil contact. The figures also show that the change in base efficiencies is smaller than the change in shaft efficiencies. The effects of the pile-

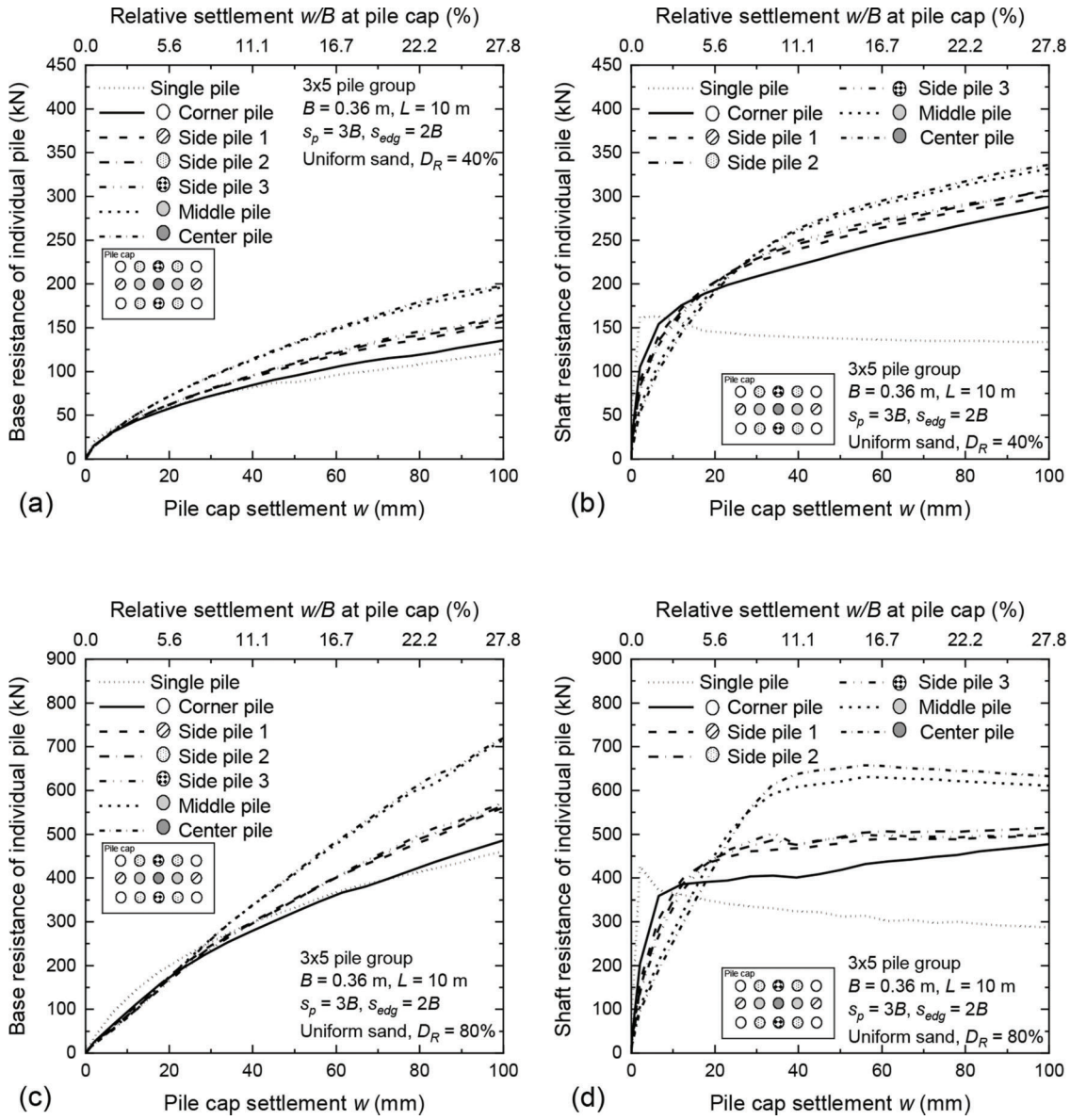

Figure 2.9 Base and shaft resistances of individual piles in 3×5 pile group in uniform sand: (a) base resistances of piles in loose sand, (b) shaft resistances of piles in loose sand, (c) base resistances of piles in dense sand, and (d) shaft resistances of piles in dense sand.

soil-pile interaction and the pile cap-soil contact are more significant for shaft resistance mobilization than for base resistance mobilization.

The shaft and base efficiencies and their rate of change with increasing settlement depend on the group layout. As shown in Figures 2.17, 2.18, and 2.19, the base and shaft efficiencies of the 1×5 pile group change the least while those of the 3×5 pile group change the most. For example, as the settlement increases from 0 mm to 100 mm (4 inches), the base efficiency of the center pile in the 1×5 pile group increases from 0.80 to 1.09 in loose sand and from 0.90 to 0.99 in dense sand, whereas the base efficiency of the center pile in the 3×5 pile group increases from 0.59 to 1.63 in loose sand and from 0.73 to 1.56 in dense sand. Similarly, as the settlement increases from 0 mm to 100 mm (4 inches), the shaft efficiency of the center pile in the 1×5 pile group increases from 0.55 to 2.05 in loose sand and from 0.52 to 2.18 in dense sand, whereas the shaft efficiency of the center pile in the 3×5 pile group increases from 0.2 to 2.5 in loose sand and from 0.2 to 2.17 in dense sand. These results reflect the fact that the size of the cap of the 3×5 pile group is greater than that of the 1×5 pile group; the larger the cap, the greater its impact on the mobilization of the base and shaft resistances of the piles in the group is.

The shaft and base efficiencies and their rate of change with increasing settlement also depend on the soil profile. From the results shown in Figures 2.17, 2.18, and 2.19, the change in both the base and shaft

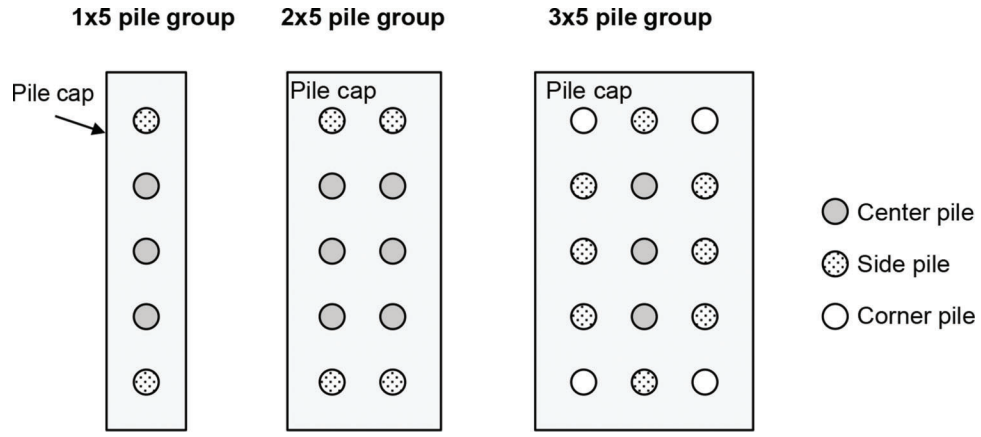

Figure 2.10 Grouping of individual piles in the 1×5, 2×5, and 3×5 pile groups depending on the location of each pile in the group.

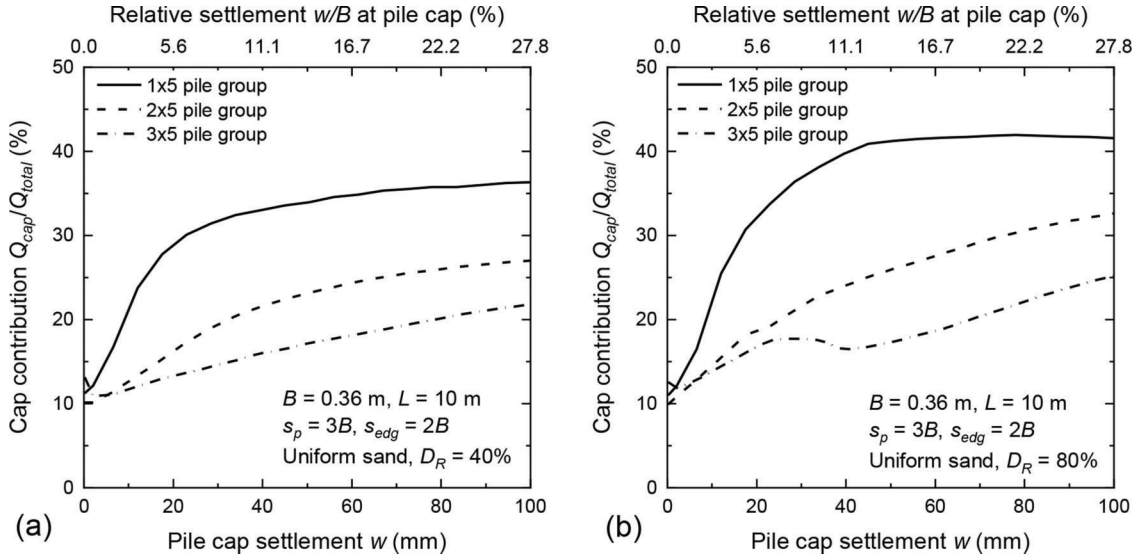

Figure 2.11 Pile cap contribution for 1×5, 2×5, and 3×5 pile groups in (a) uniform loose sand, and (b) uniform dense sand.

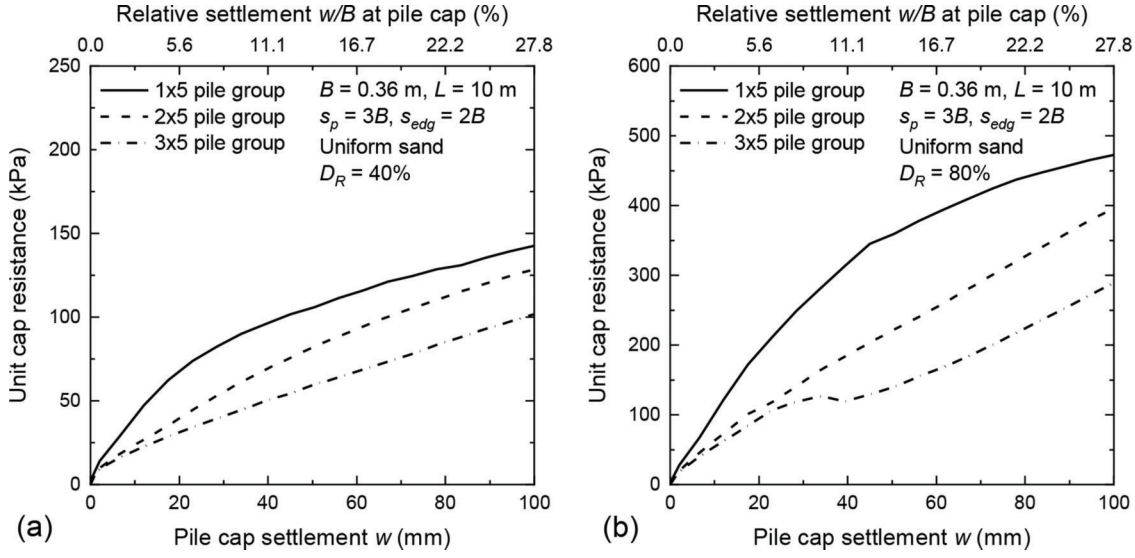

Figure 2.12 Unit cap resistances for 1×5, 2×5, and 3×5 pile groups in (a) uniform loose sand, and (b) uniform dense sand.

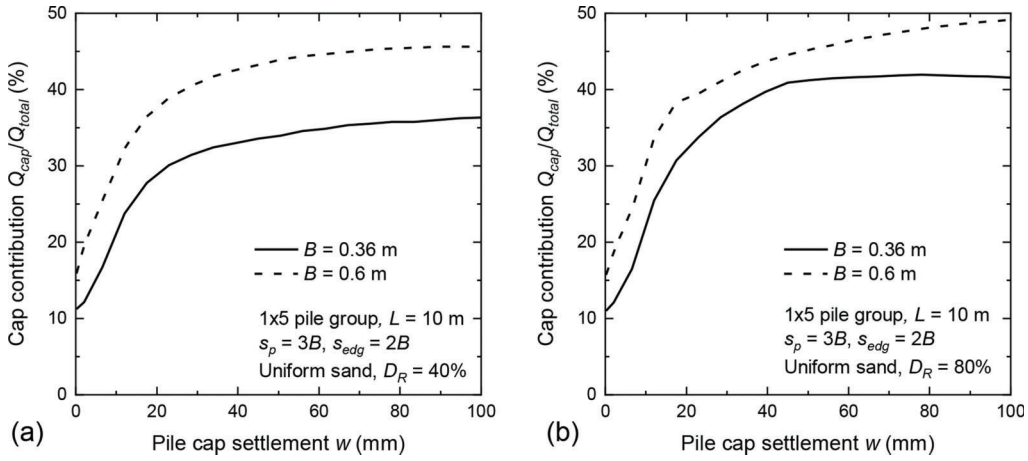

Figure 2.13 Pile cap constribution of 1×5 pile group for different pile diameter B in (a) uniform loose sand, and (b) uniform dense sand.

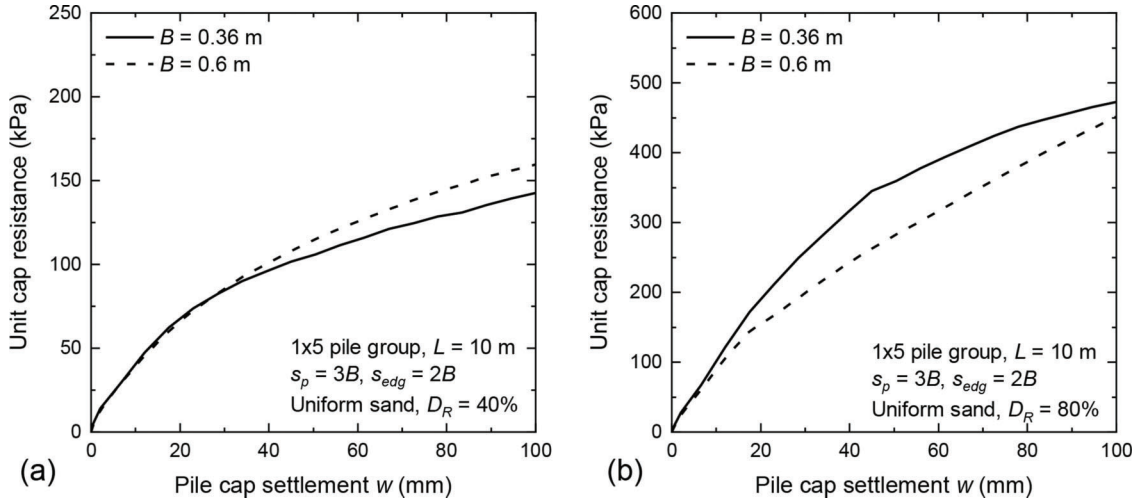

Figure 2.14 Unit cap resistance of 1×5 pile group for different pile diameter B in (a) uniform loose sand, and (b) uniform dense sand.

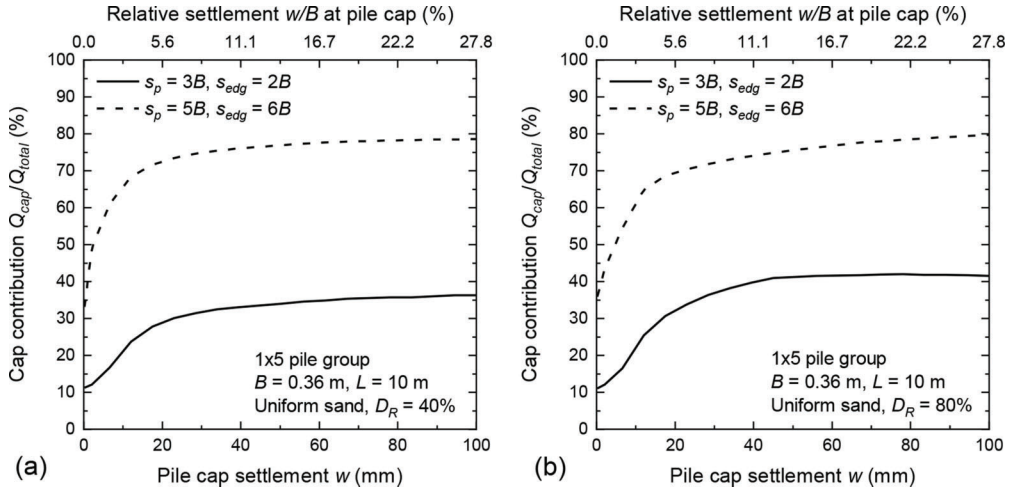

Figure 2.15 Pile cap contribution of 1×5 pile group for different pile-to-pile spacing s_p and pile-to-cap edge distance s_{edg} in (a) uniform loose sand, and (b) uniform dense sand.

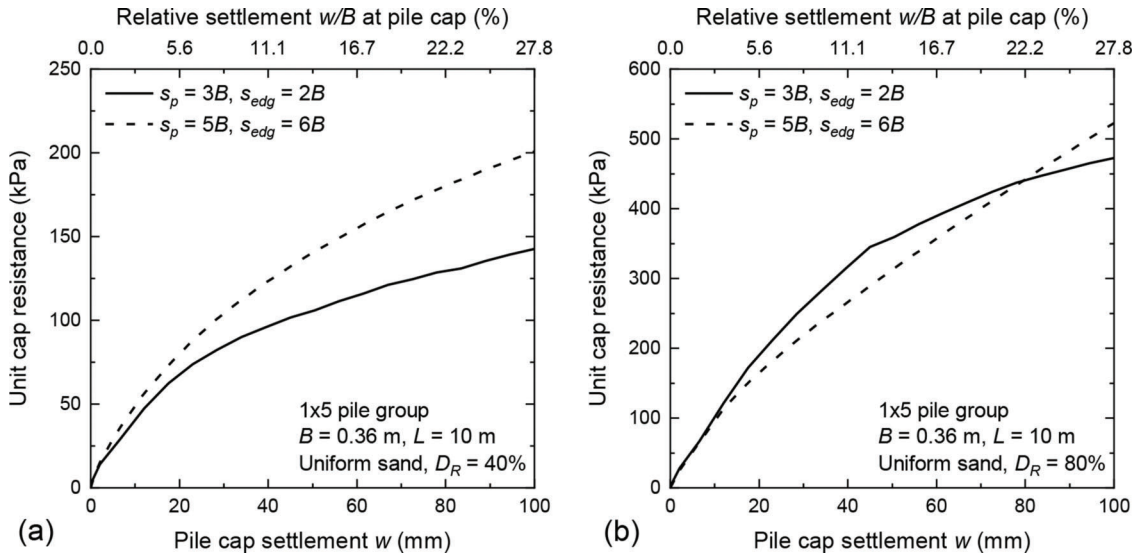

Figure 2.16 Unit cap resistance of 1×5 pile group for different pile-to-pile spacing s_p and pile-to-cap edge distance s_{edg} in (a) uniform loose sand, and (b) uniform dense sand.

TABLE 2.5
Summary of unit cap capacities in uniform loose sand

Group Configuration	Pile Diameter B (m)	Pile-to-Pile Spacing s_p	Pile-to-Cap Edge Distance s_{edg}	Shorter Length of the Pile Cap B_{cap} (m)	Longer Length of the Pile Cap L_{cap} (m)	Unit Cap Capacity at w = 50 mm (2 inches) (kPa)[1]	Unit Cap Capacity at w = 100 mm (4 inches) (kPa)[1]
1×5	0.36 (14 inches)	$3B$	$2B$	1.44 (4.72 ft)	5.76 (18.9 ft)	105.9 (2.21 ksf)	142.5 (2.98 ksf)
2×5	0.36 (14 inches)	$3B$	$2B$	2.52 (8.27 ft)	5.76 (18.9 ft)	82.4 (1.72 ksf)	128.7 (2.69 ksf)
3×5	0.36 (14 inches)	$3B$	$2B$	3.6 (11.8 ft)	5.76 (18.9 ft)	59.7 (1.25 ksf)	101.8 (2.13 ksf)
1×5	0.6 (23.6 inches)	$3B$	$2B$	2.4 (7.87 ft)	9.6 (31.5 ft)	115.3 (2.41 ksf)	159.5 (3.33 ksf)
1×5	0.36 (14 inches)	$5B$	$6B$	4.32 (14.2 ft)	11.52 (37.8 ft)	141.2 (2.95 ksf)	200.8 (4.19 ksf)

[1] w is the pile cap settlement.

TABLE 2.6
Summary of unit cap capacities in uniform dense sand

Group Configuration	Pile Diameter B (m)	Pile-to-Pile Spacing s_p	Pile-to-Cap Edge Distance s_{edg}	Shorter Length of the Pile Cap B_{cap} (m)	Longer Length of the Pile Cap L_{cap} (m)	Unit Cap Capacity at w = 50 mm (2 inches) (kPa)	Unit Cap Capacity at w = 100 mm (4 inches) (kPa)
1×5	0.36 (14 inches)	$3B$	$2B$	1.44 (4.72 ft)	5.76 (18.9 ft)	359.3 (7.50 ksf)	472.3 (9.86 ksf)
2×5	0.36 (14 inches)	$3B$	$2B$	2.52 (8.27 ft)	5.76 (18.9 ft)	222.1 (4.64 ksf)	396.3 (8.28 ksf)
3×5	0.36 (14 inches)	$3B$	$2B$	3.6 (11.8 ft)	5.76 (18.9 ft)	140.2 (2.93 ksf)	289.3 (6.04 ksf)
1×5	0.6 (23.6 inches)	$3B$	$2B$	2.4 (7.87 ft)	9.6 (31.5 ft)	282.9 (5.91 ksf)	451.4 (9.43 ksf)
1×5	0.36 (14 inches)	$5B$	$6B$	4.32 (14.2 ft)	11.52 (37.8 ft)	314.6 (6.57 ksf)	522.9 (10.92 ksf)

efficiencies of the piles in a group in dense sand is, in general, smaller than that in loose sand. For example, as the settlement increases from 0 mm to 100 mm (4 inches), the base and shaft efficiencies of the center piles in the 2×5 pile group increase from 0.67 to 1.36 and from 0.33 to 2.44, respectively, in loose sand; on the

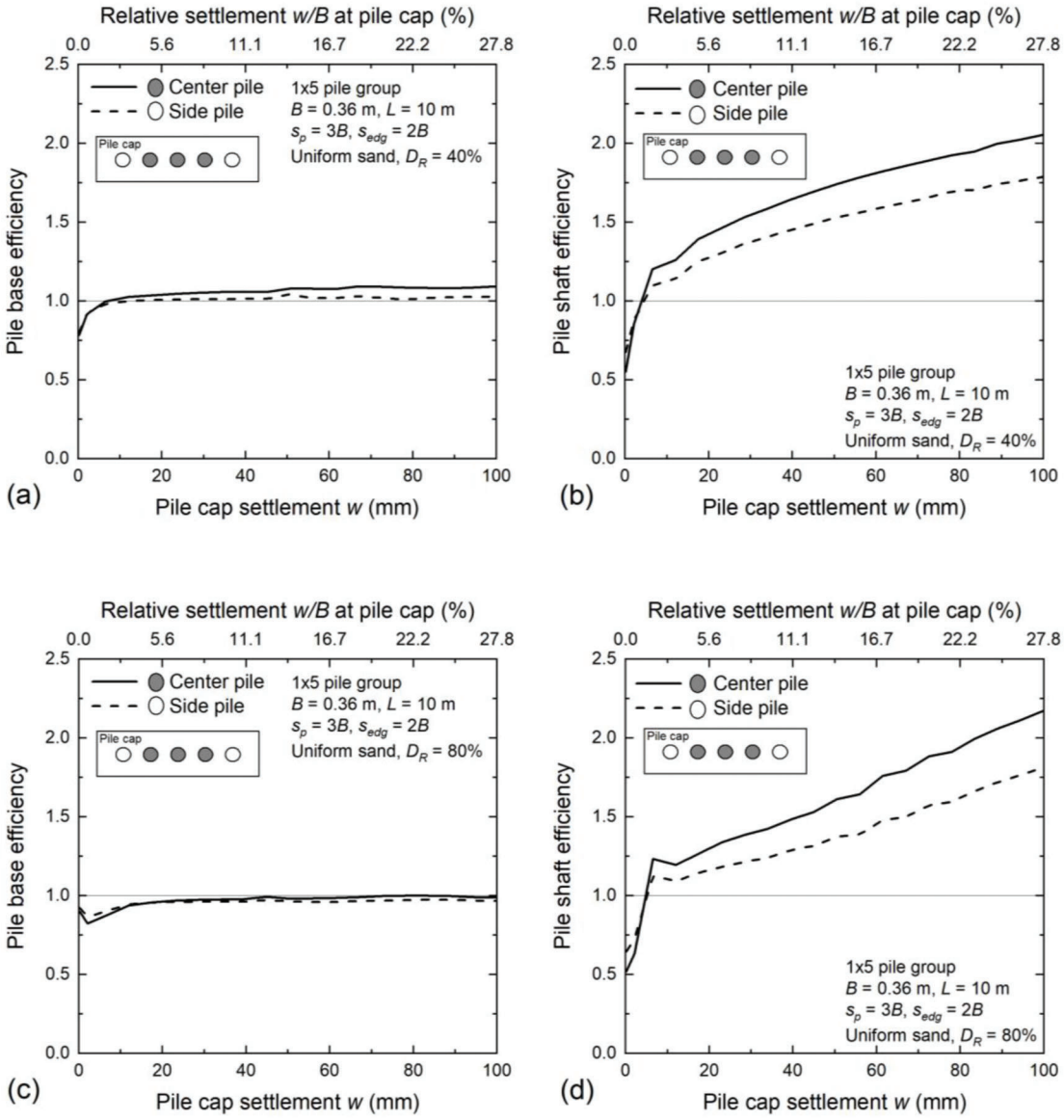

Figure 2.17 Efficiencies of individual piles in the 1×5 pile group in uniform sand: (a) base efficiencies η_b in loose sand, (b) shaft efficiencies η_s in loose sand, (c) base efficiencies η_b in dense sand, and (d) shaft efficiencies η_s in dense sand.

other hand, the efficiencies increase from 0.79 to 1.25 and from 0.32 to 2.02, respectively, in dense sand. These results can be explained by the fact that the denser the sand, the greater the strain localization in the zone immediately next to the pile is, affecting the pile-soil-pile and the pile cap-soil response.

Another factor that influences the shaft and base efficiencies and their rate of change with increasing settlement is the location of individual piles in a group. Figure 2.17 and Figure 2.18 show that in the 1×5 and 2×5 pile groups, both the base and shaft efficiencies of the center piles are smaller than those of the side piles in the beginning of the loading, but the efficiencies of the center piles increase at a faster rate and become greater than those of the side piles as the settlement increases from 0 mm to 100 mm (4 inches). For example, as the settlement increases from 0 mm to 100 mm (4 inches), the base and shaft efficiencies of the center piles in the 1×5 pile group in loose sand increase from 0.78 to 1.09 and from 0.55 to 2.05, respectively, while the base and shaft efficiencies of the side piles in the 1×5 pile group in loose sand increase from 0.8 to 1.03 and from 0.68 to 1.79, respectively. In the beginning of the loading of the 1×5 and 2×5 pile groups, the side piles carry more load than the center piles but as the settlement increases, then the center piles carry more load than the side piles. Figure 2.19 shows that, in the beginning of the loading of the 3×5 pile group, the center piles have the smallest base and shaft efficiencies, and the corner piles have the greatest base and shaft efficiencies,

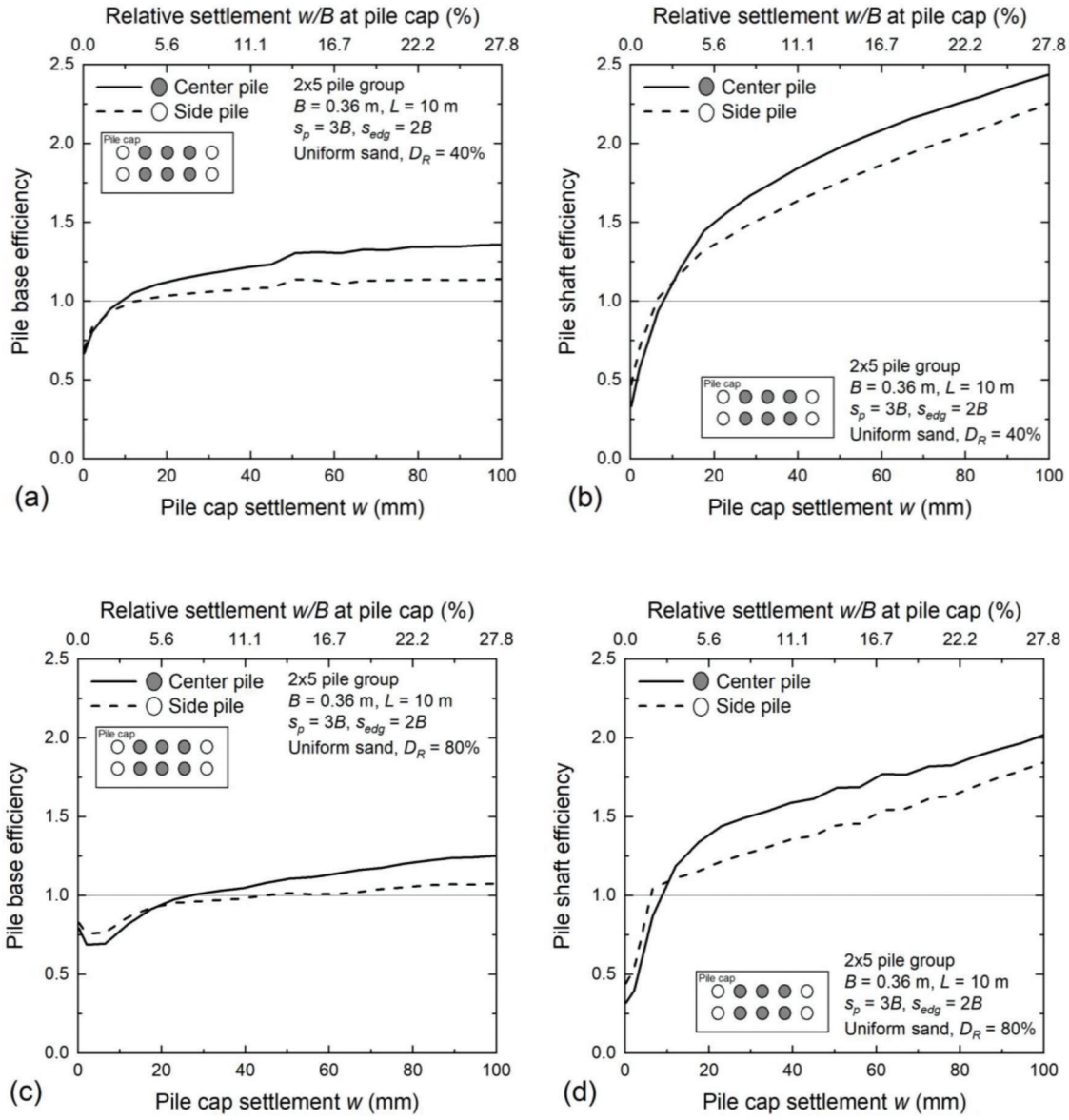

Figure 2.18 Efficiencies of individual piles in the 2×5 pile group in uniform sand: (a) base efficiencies η_b in loose sand, (b) shaft efficiencies η_s in loose sand, (c) base efficiencies η_b in dense sand, and (d) shaft efficiencies η_s in dense sand.

but, as the settlement increases, the base and shaft efficiencies of the center piles increase at the fastest rate and achieve higher values than those for the other piles in the group. In contrast, the efficiencies of the corner piles increase at the slowest rate and become the smallest. In the beginning of the loading, the corner piles carry more load than the center piles, but as the pile group settlement progresses, the opposite happens, with the center piles then carrying more load than the other piles.

Figure 2.20 shows the profiles of the unit shaft resistance mobilized along the pile shafts of the center, side and corner piles in the 3×5 pile group at different pile head settlements w_p (36 mm (1.4 inches), 50 mm (2 inches), and 100 mm (4 inches)). The profile of the limit unit shaft resistance mobilized at a pile head settlement of 36 mm (1.4 inches), which is 10% of the pile diameter B of a single, isolated pile placed in the same soil profile as the piles in the group is also plotted for reference. As discussed earlier, at settlements greater than 36 mm (1.4 inches), most of the load is carried by the center piles and the least is carried by the corner piles. In general, the unit shaft resistances of the piles in the 3×5 pile group are much higher than that of the single pile. In loose sand, the unit shaft resistances of all individual piles in the group continue to increase as the settlement increases. In dense sand, the changes in the unit shaft resistances of the center, side and corner piles depend on the depth of the pile being considered. As the settlement increases from 36 mm (1.4 inches) to 100 mm

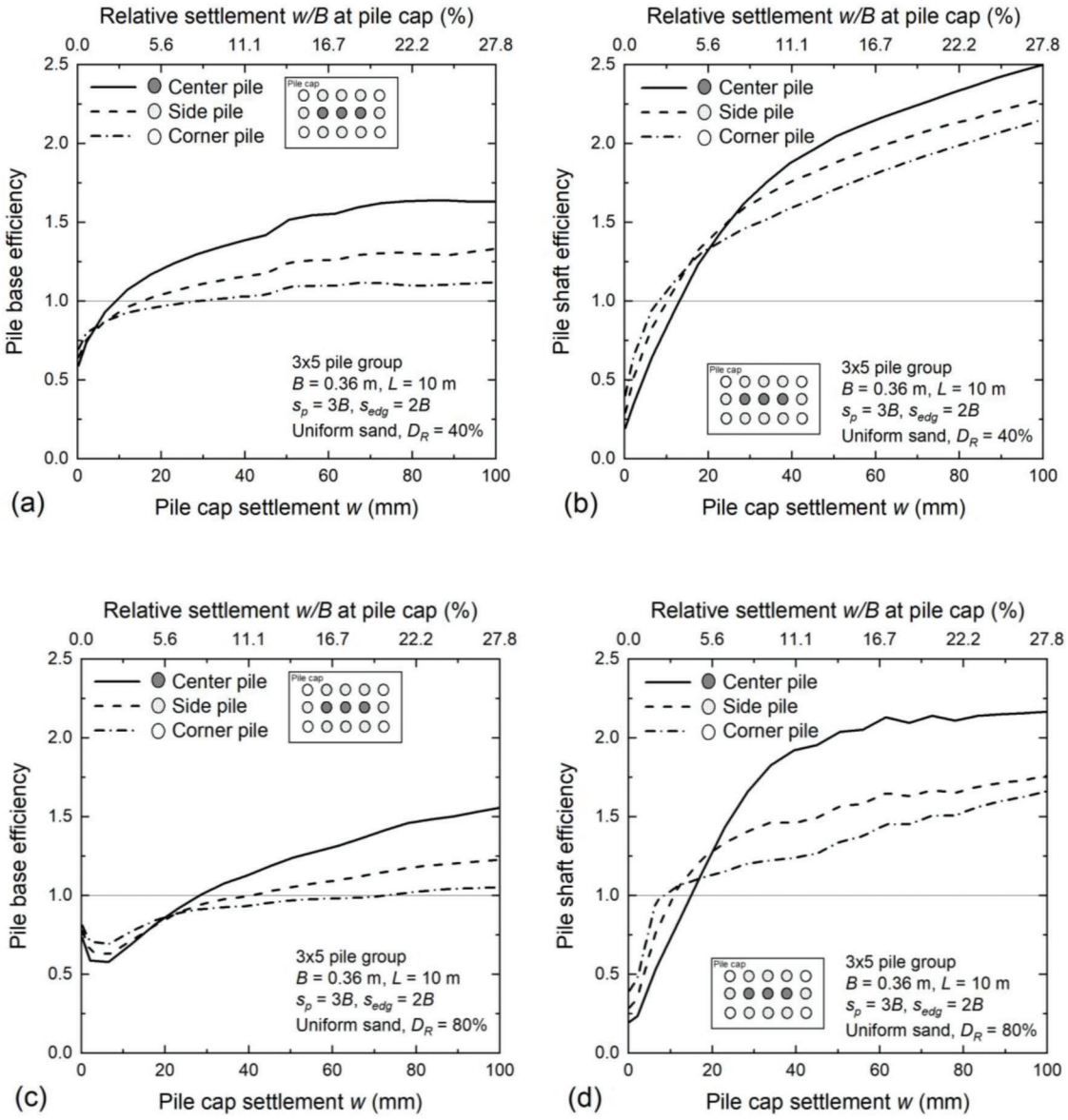

Figure 2.19 Efficiencies of individual piles in the 3×5 pile group in uniform sand: (a) base efficiencies η_b in loose sand, (b) shaft efficiencies η_s in loose sand, (c) base efficiencies η_b in dense sand, and (d) shaft efficiencies η_s in dense sand.

(4 inches), the unit shaft resistance of the center pile in the group in dense sand increases at depths smaller than 2 m (6.56 ft), but at depths greater than 3 m (9.84 ft), it decreases because of the effects of the cap on the lateral effective stress acting on the shafts of the piles. The unit shaft resistances of the side pile in the group in dense sand are almost the same at different settlement levels, and those of the corner pile increase slightly as the settlement increases from 36 mm (1.4 inches) to 100 mm (4 inches). These trends in the unit shat resistances with depth are similar to the trends of the lateral effective stress along the shafts of the piles in the group. For example, Figure 2.21 shows the average effective mean stress profiles calculated for soil elements next to the shaft of one of the center piles in the 3×5 pile group for pile head settlements w_p of 36 mm (1.4 inches), 50 mm (2 inches), and 100 mm (4 inches). The average mean effective stress at different depths is calculated by averaging pressures along the perimeter of the pile at each depth. The results for loose and dense sands are shown in Figure 2.21(a) and (b), respectively. The average mean effective stress profile calculated for the soil elements next to the shaft of a single, isolated pile placed in the same soil profile as the piles in the group for a pile head settlement w_p of 36 mm (1.4 inches) is also plotted for reference. The average mean effective stress profile for the single pile at settlements of 36 mm (1.4 inches), 50 mm (2 inches), and 100 mm (4 inches) are the same. The general trends of the mean effective stress profiles in the soil along the shaft of the center

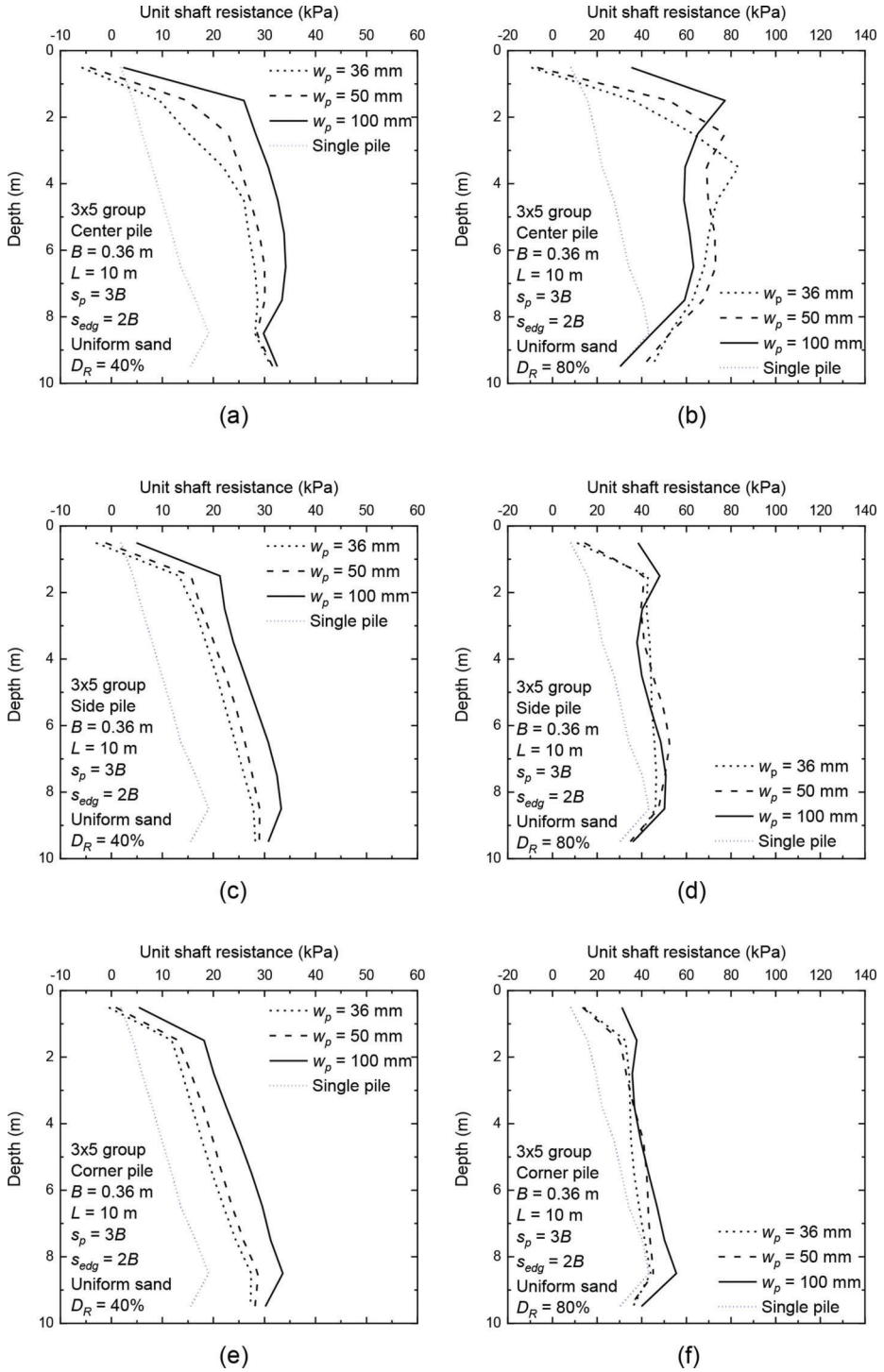

Figure 2.20 Development of unit shaft resistance along the pile shaft of an individual pile in the 3×5 pile group in loose and dense sands at different pile head settlements w_p: (a) center pile in loose sand, (b) center pile in dense sand, (c) side pile in loose sand, (d) side pile in dense sand, (e) corner pile in loose sand, and (f) corner pile in dense sand.

piles in the 3×5 pile group are very similar to those for the unit shaft resistances. The pressure profiles of the piles in the group are, in general, much greater than those calculated for the single pile (see Figure 2.21) because of the compressive loading effect on the soil below the pile cap. This increase in pressure makes the unit shaft resistances of the piles in the pile group greater than that of the single pile.

Figure 2.22 shows base and shaft efficiencies (η_b and η_s, respectively) of individual piles in the 1×5 pile groups with pile diameters of 0.36 m (14 inches) and 0.6 m (23.6 inches) and placed in uniform loose and dense sands.

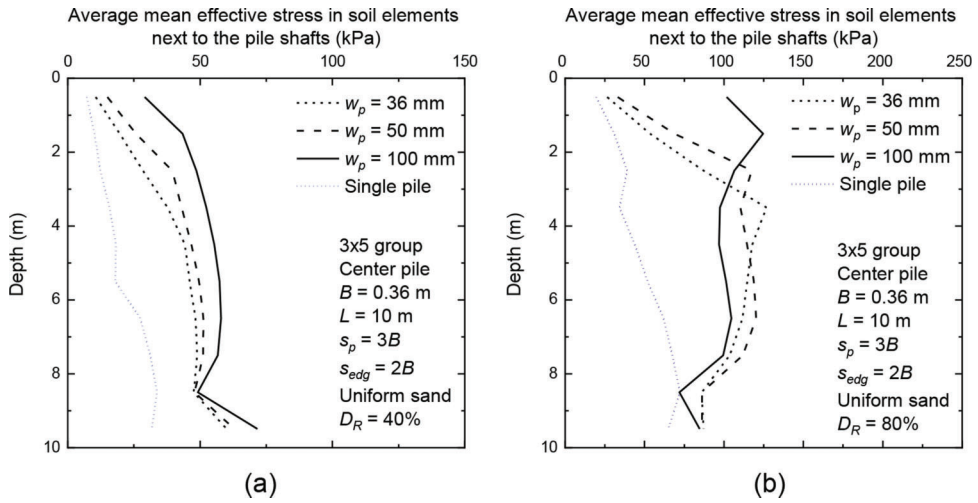

Figure 2.21 Average mean effective stress calculated for soil elements on the pile shaft of the center piles in the 3×5 pile group placed in (a) uniform loose sand, and (b) uniform dense sand at different depths.

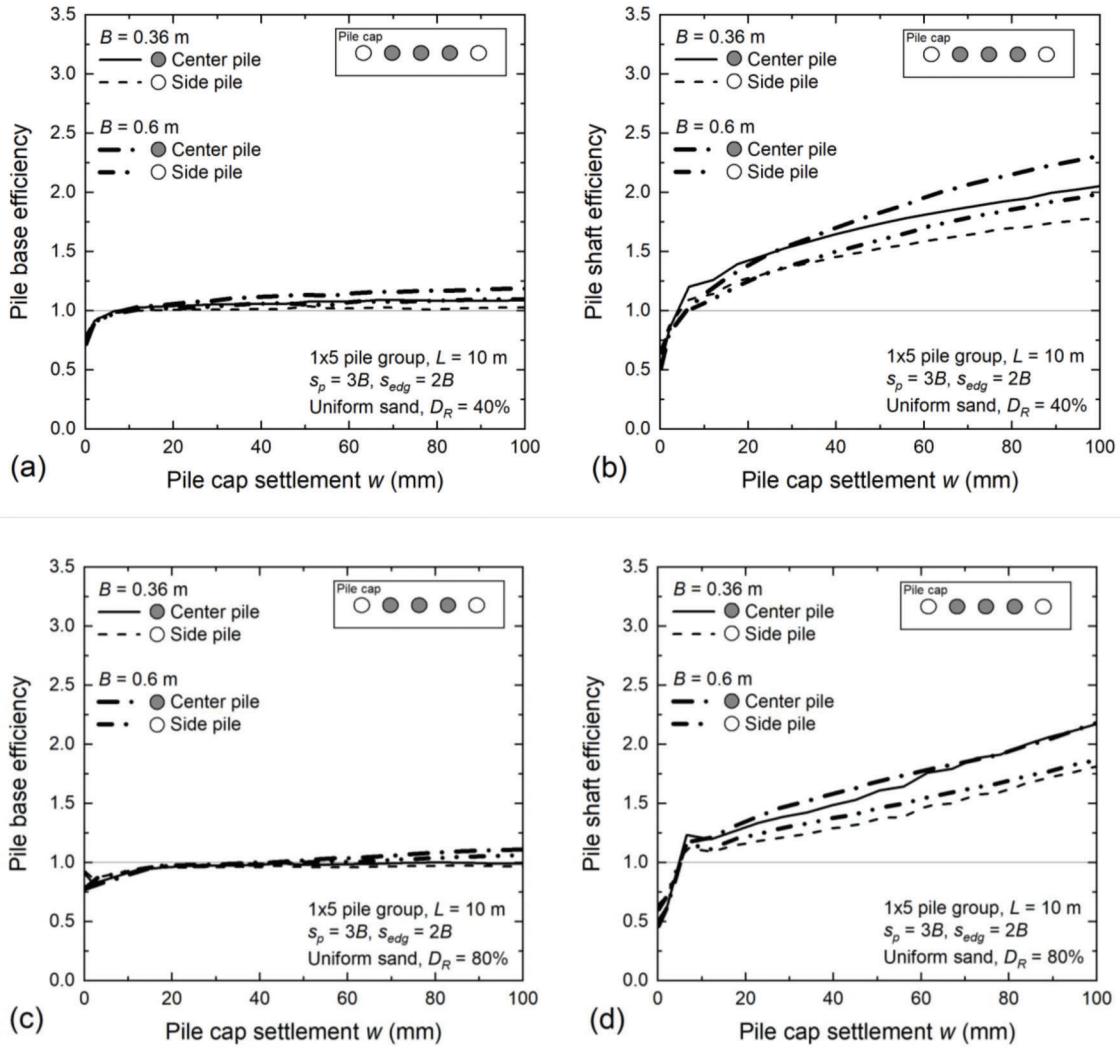

Figure 2.22 Efficiencies of individual piles in 1×5 pile group for different pile diameters B in uniform sand: (a) base efficiencies η_b in loose sand, (b) shaft efficiencies η_s in loose sand, (c) base efficiencies η_b in dense sand, and (d) shaft efficiencies η_s in dense sand.

A pile-to-pile spacing s_p of $3B$ and a pile-to-cap edge distance s_{edg} of $2B$ are considered for both cases. The 1×5 pile groups with different pile diameters have similar individual pile base and shaft efficiencies.

Figure 2.23 shows base and shaft efficiencies (η_b and η_s, respectively) of individual piles in the 1×5 pile group with pile-to-pile spacing s_p of $3B$ and pile-to-cap edge distance s_{edg} of $2B$, as well as with $s_p = 5B$ and $s_{edg} = 6B$. Both pile groups are placed in uniform loose or dense sand. The results show that the greater the s_p and s_{edg} are, the higher the base and shaft efficiencies are. This is because of the larger size of the pile cap of the pile group with $s_p = 5B$ and $s_{edg} = 6B$. For the pile groups with soil-supported pile caps, as s_p and s_{edg} increase, the size of the pile cap that is in contact with the soil also increases; the larger the pile cap is, the greater the base and shaft efficiencies of the piles in the pile group are. This results from the greater compressive loading of the larger pile cap on the soil below it. Figure 2.24 shows average mean effective stress profiles calculated for soil elements next to the shaft of the center piles in the 1×5 pile group with s_p of $3B$ and s_{edg} of $2B$ and the 1×5 pile group with $s_p = 5B$ and $s_{edg} = 6B$. Both pile groups are placed in uniform loose or dense sand. The average pressure profiles at pile head settlements w_p of 36 mm (1.4 inches), 50 mm (2 inches), and 100 mm (4 inches) are shown in the figure. The average pressure profile of the soil elements next to the

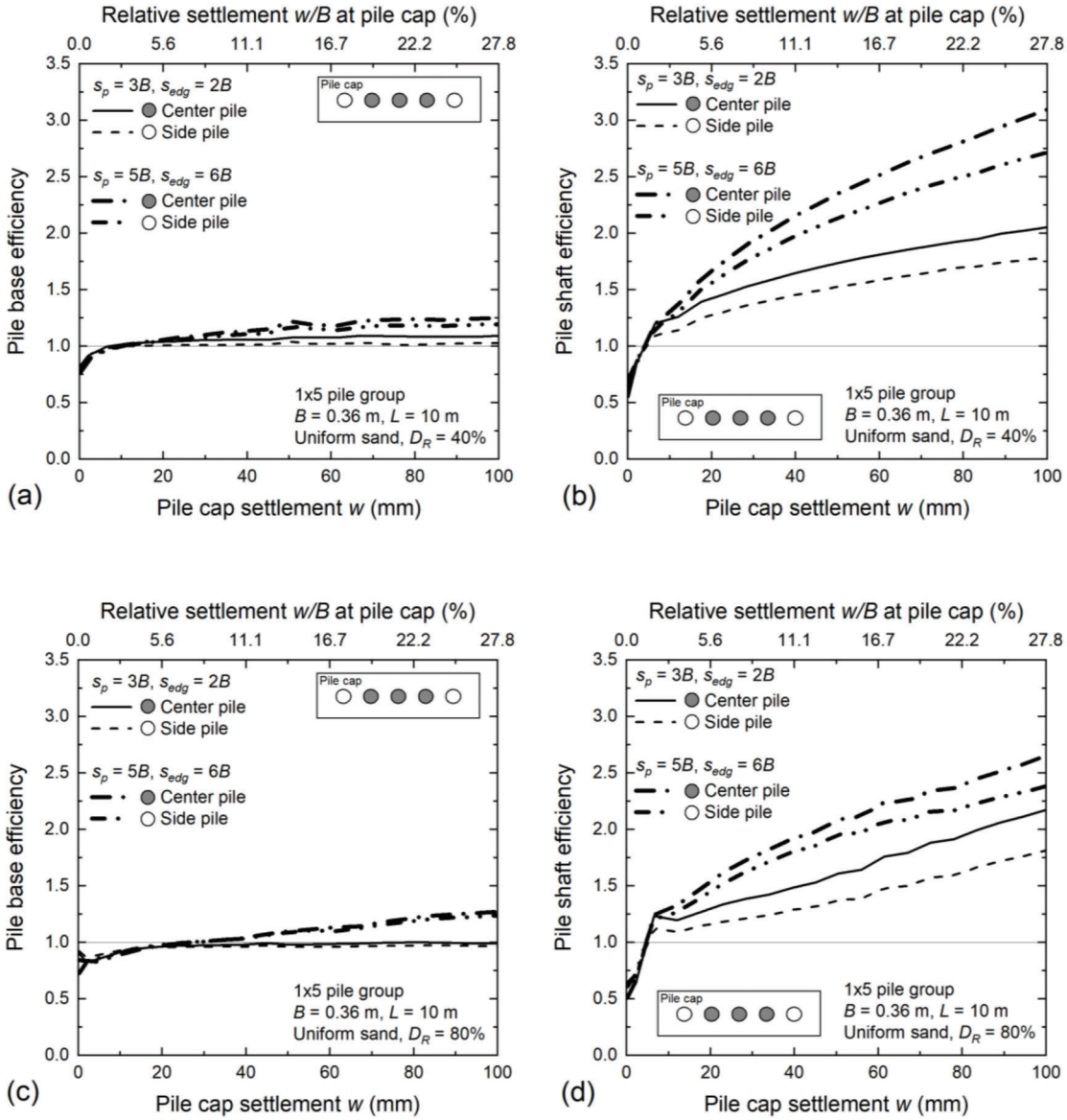

Figure 2.23 Efficiencies of individual piles in the 1×5 pile group for different pile-to-pile spacing s_p and pile-to-cap edge distance s_{edg} in uniform sand: (a) base efficiencies η_b in loose sand, (b) shaft efficiencies η_s in loose sand, (c) base efficiencies η_b in dense sand, and (d) shaft efficiencies η_s in dense sand.

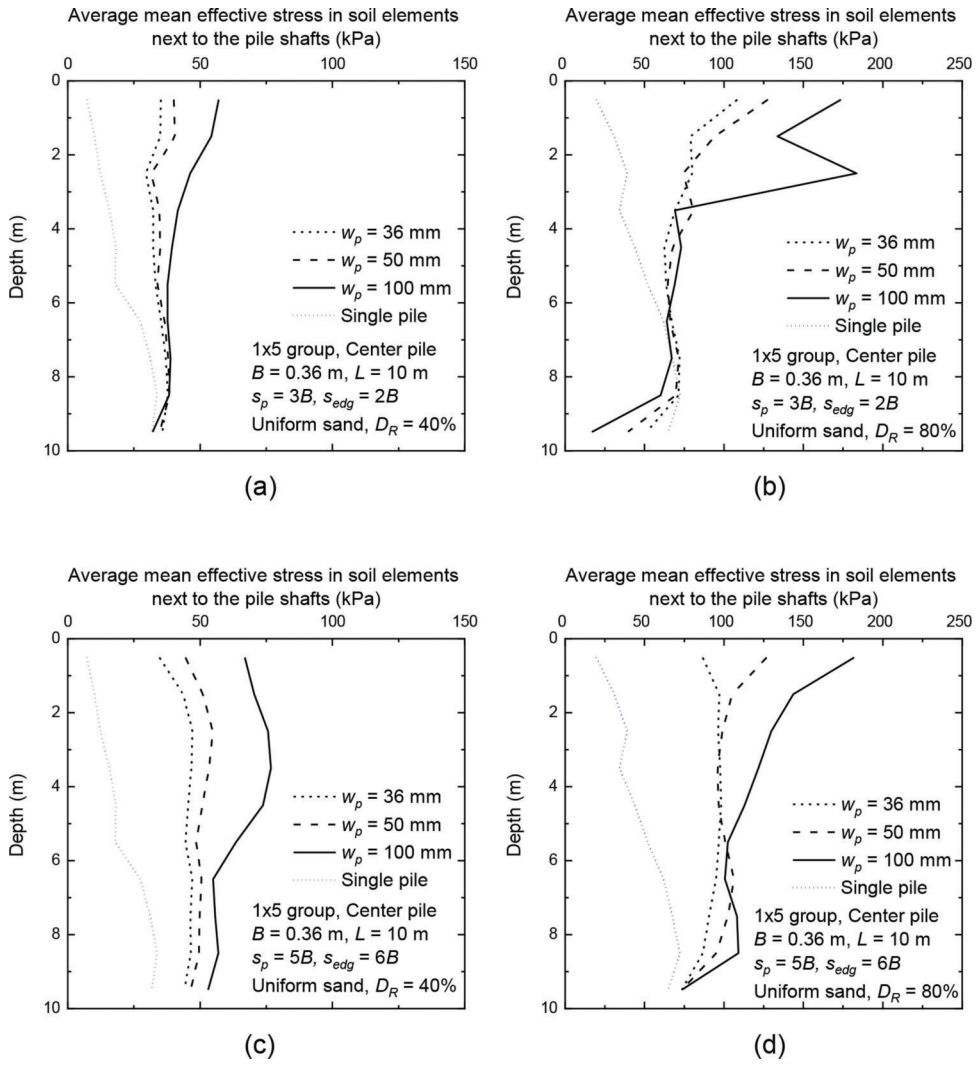

Figure 2.24 Average mean effective stress profiles calculated for soil elements on the pile shaft of the center pile in the 1×5 pile groups with (a) $s_p = 3B$ and $s_{edg} = 2B$ in loose sand, (b) $s_p = 3B$ and $s_{edg} = 2B$ in dense sand, (c) $s_p = 5B$ and $s_{edg} = 6B$ in loose sand, and (d) $s_p = 5B$ and $s_{edg} = 6B$ in dense sand.

shaft of the single pile placed in the same soil profile at the pile head settlements w_p of 36 mm (1.4 inches) is also plotted for reference. The average pressure profiles for the single, isolated pile at settlements of 36 mm (1.4 inches), 50 mm (2 inches), and 100 mm (4 inches) are the same. The mean effective stress generated in soil elements along the shaft of the center pile in the 1×5 pile group with $s_p = 5B$ and $s_{edg} = 6B$ is a slightly higher than that of the center pile in the 1×5 pile groups with s_p of $3B$ and s_{edg} of $2B$. In addition, the depth at which the pressure profile of the center pile in a group is greater than that of the single pile is deeper for the 1×5 pile group with $s_p = 5B$ and $s_{edg} = 6B$ than that for the 1×5 pile groups with s_p of $3B$ and s_{edg} of $2B$. This can be interpreted to be because of the larger influence zone of the larger pile cap. For this reason, the base and shaft efficiencies of the center pile in the 1×5 pile group with the larger pile cap are greater. The effects of s_p and s_{edg} on base and shaft efficiencies of individual piles for different pile group layouts can be further investigated in the future.

2.2.2 Pile Groups in Layered Soil

2.2.2.1 Tolerable settlements. For pile groups with soil-supported pile caps, the ultimate load settlement criterion of 10% of the diameter of a pile may be too small for certain designs. Reliance on the tolerable settlement criteria for bridges proposed by Bozozuk (1978) might be useful in those cases. According to Bozozuk (1978), a vertical settlement less than 50 mm is safe and tolerable for bridge structures, while a vertical settlement between 50 mm (2 inches) and 100 mm (4 inches) is harmful but still tolerable, and a vertical settlement greater than 100 mm (4 inches) is intolerable and is likely to cause heavy damage to the bridge

structures. Depending on the type and purpose of the structure being constructed, different values of tolerable settlements may be considered in design.

In this study, the resistance or contribution of the pile cap and the resistances or efficiencies of the individual piles in a pile group are evaluated at three different pile cap settlements: 10% of the pile diameter B, 50 mm (2 inches), and 100 mm (4 inches), so that engineers can choose a value for the tolerable settlement appropriate for the structure being designed.

2.2.2.2 Contribution of the pile cap. Figure 2.25 shows the pile cap contribution of the 1×5, 2×5, and 3×5 pile groups in loose-over-dense sand (profile 1) with various thicknesses t_{top} of the top loose sand layer. The cap contribution of the pile groups decreases as the thickness t_{top} of the loose sand layer increases up to the pile length L of 10 m (32.8 ft) and reaches the smallest value when t_{top} becomes equal to the pile length (the cap contribution of the 1×5 pile group decreases at the fastest rate while the cap contribution of the 3×5 pile group decreases at the slowest rate). As t_{top} increases from 0 to 10 m (32.8 ft), the cap contributions of the 1×5, 2×5, and 3×5 pile groups at a settlement of 50 mm (2 inches) decrease from 41% to 24% (with a minimum value of 21% at $t_{top} = 4.32$ m = 14.2 ft), from 26% to 16%, and from 17% to 12%, respectively. The cap contributions of the pile groups are almost constant and equal to the values obtained for the pile groups in uniform loose sand when t_{top} is greater than the pile length L. The cap contribution of pile groups in uniform loose sand are greater than those in loose-over-dense sand with $t_{top} = L$. The cap contributions of the 1×5, 2×5 and 3×5 pile groups in loose sand at a settlement of 50 mm (2 inches) are 34%, 23%, and 17%, respectively, whereas those in loose-over-dense sand with $t_{top} = L$ are 24%, 16% and 12%, respectively. This is because of the smaller base resistances of the piles in uniform loose sand than in loose-over-dense sand with $t_{top} = L$.

Figure 2.26 shows the unit cap resistances of the 1×5, 2×5, and 3×5 pile groups in loose-over-dense sand (profile 1) with various thicknesses t_{top} of the top loose sand layer. As t_{top} increases, the unit cap resistances of the pile groups decrease. The unit cap resistances of the 1×5, 2×5 and 3×5 pile groups for a settlement of 50 mm (2 inches) decrease from 359 kPa (7.5 ksf) to 106 kPa (2.2 ksf), from 222 kPa (4.6 ksf) to 82 kPa (1.7 ksf), and from 140 kPa (2.9 ksf) to 60 kPa (1.25 ksf), respectively, as the thickness of the top layer increases towards a thickness of 10 m (32.8 ft). The unit cap resistance of the 1×5 pile group decreases at the fastest rate and that of the 3×5 pile group decreases at the slowest rate.

Figure 2.27 and Figure 2.28 show the pile cap contribution towards total resistance and the unit cap resistance of the 1×5, 2×5, and 3×5 pile groups in normally-consolidated (NC) clay over dense sand (profile 2) with various thicknesses t_{top} of the top layer. The trends in these results are similar to those observed for the loose-over-dense sand (profile 1), but the decrease in the cap contribution is much faster as t_{top} increases. As t_{top} increases from 0 to 10 m (32.8 ft) (profile 2), the cap contributions of the 1×5, 2×5 and 3×5 pile groups at a settlement of 50 mm (2 inches) decrease from 41% to 3.5% (with a minimum value of 2.2% at $t_{top} = 1.44$ m = 4.72 ft), from 26% to 4.3% (with a minimum value of 3.4% at $t_{top} = 2.52$ m = 8.27 ft), and from 17% to 4.4% (with a minimum value of 3.6% at $t_{top} = 3.6$ m = 11.8 ft), respectively. The cap contributions of the 1×5, 2×5 and 3×5 pile groups in uniform NC clay at a settlement of 50 mm (2 inches) are 8.9%, 7.9% and 7.6%, respectively. The absolute values of the unit cap resistances are much smaller for the pile groups in normally-consolidated (NC) clay over dense sand (profile 2) than those in the loose-over-dense sand (profile 1). The unit cap resistances of the 1×5, 2×5 and 3×5 pile groups in profile 2 at a settlement of 50 mm (2 inches) decrease from 359 kPa (7.5 ksf) to 4.9 kPa (0.1 ksf), from 222 kPa (4.6 ksf) to 5.0 kPa (0.1 ksf), and from 140 kPa (2.9 ksf) to 5.1 kPa (0.1 ksf), respectively, as t_{top} increases from 0 m to 20 m (65.6 ft).

Figure 2.29 shows the pile cap contribution of the 1×5, 2×5 and 3×5 pile groups in loose sand sandwiched between two layers of dense sand (profile 3) with various thicknesses t_{top} of the top dense sand layer.

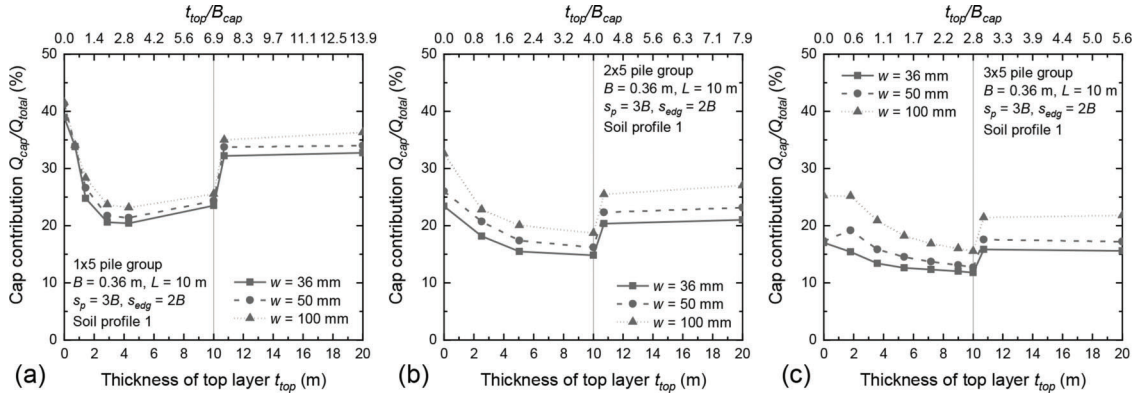

Figure 2.25 Pile cap contribution of pile groups in loose-over-dense sand (profile 1) with various thicknesses t_{top} of the top loose sand layer: (a) 1×5 pile group, (b) 2×5 pile group, and (c) 3×5 pile group.

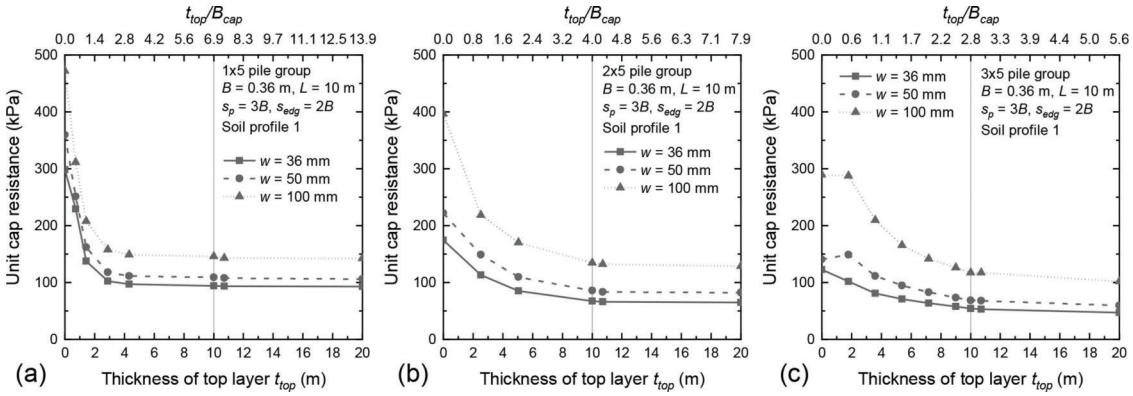

Figure 2.26 Unit cap resistance of pile groups in loose-over-dense sand (profile 1) with various thicknesses t_{top} of the top loose-sand layer: (a) 1×5 pile group, (b) 2×5 pile group, and (c) 3×5 pile group.

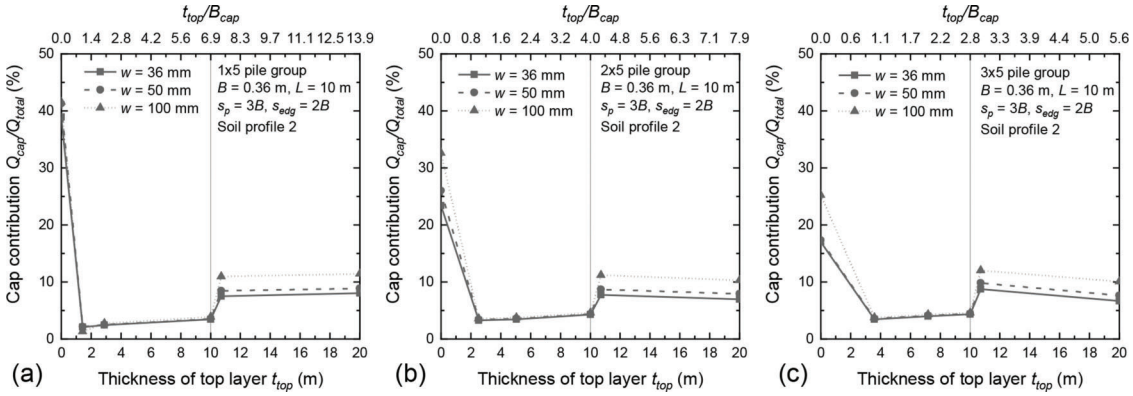

Figure 2.27 Pile cap contribution of pile groups in normally-consolidated (NC) clay over dense sand (profile 2) with various thicknesses t_{top} of the top NC clay layer: (a) 1×5 pile group, (b) 2×5 pile group, and (c) 3×5 pile group.

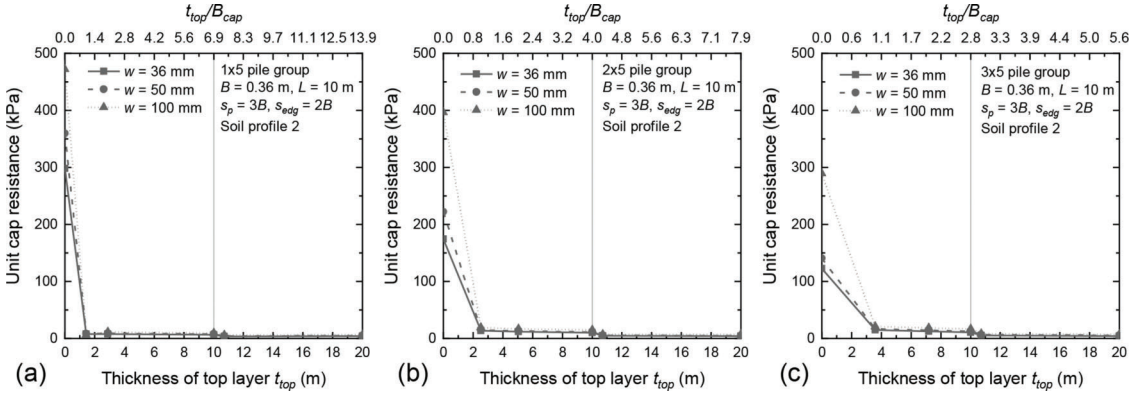

Figure 2.28 Unit cap resistances of pile groups in normally-consolidated (NC) clay over dense sand (profile 2) with various thicknesses t_{top} of the top NC clay layer: (a) 1×5 pile group, (b) 2×5 pile group, and (c) 3×5 pile group.

As the thickness of the top layer increases, the cap contribution of the pile groups increases, and most of the increases in cap contribution happens when t_{top} increases by just a few meters. The cap contributions of the 1×5, 2×5, and 3×5 pile groups at a settlement of 50 mm (2 inches) increase from 24% to 41%, from 16% to 26%, and from 13% to 17%, respectively, as t_{top} increases from 0 to 10 m (32.8 ft). The increase in cap contribution for the 1×5, 2×5, and 3×5 pile groups reach 68%, 67%, and 91% of their maximum cap contributions at t_{top} = 2.9 m (9.5 ft), 2.5 m (8.2 ft) and 1.8 m (5.9 ft), respectively. The effect of the stiff top layer on the pile cap contribution is the most significant for the 1×5 pile group and the least significant for the 3×5 pile group. Figure 2.30 shows the unit cap resistances of the 1×5, 2×5 and 3×5 pile groups in loose sand sandwiched between two layers of dense sand (profile 3) with various thicknesses t_{top} of the top dense layer. As the thickness of the stiff top layer increases, the unit cap resistances of the pile groups

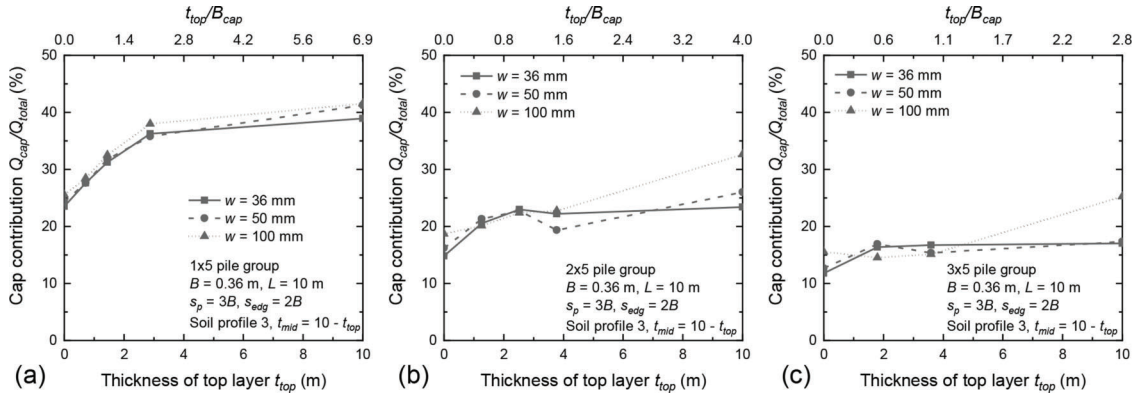

Figure 2.29 Pile cap contribution of pile groups in loose sand sandwiched between two layers of dense sand (profile 3) with various thicknesses t_{top} of the top dense sand layer: (a) 1×5 pile group, (b) 2×5 pile group, and (c) 3×5 pile group.

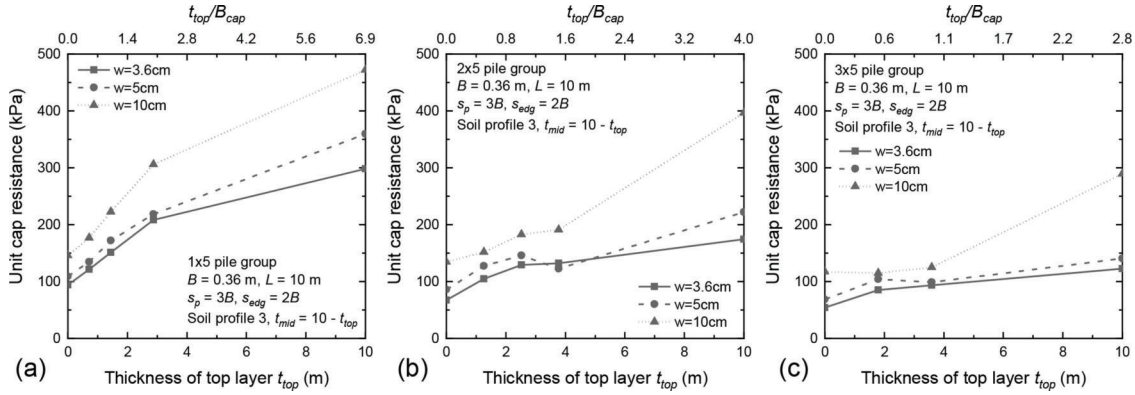

Figure 2.30 Unit cap resistances of the pile groups in loose sand sandwiched between two layers of dense sand (profile 3) with various thicknesses t_{top} of the top dense sand layer: (a) 1×5 pile group, (b) 2×5 pile group, and (c) 3×5 pile group.

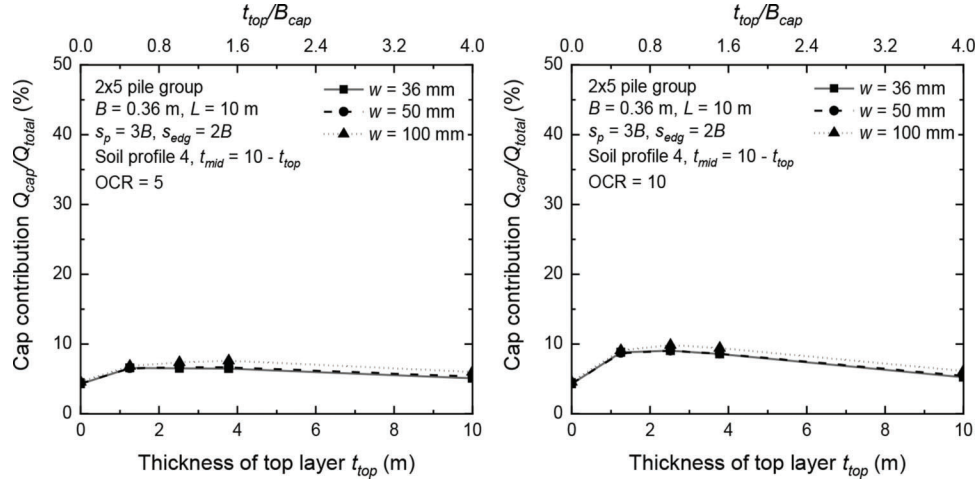

Figure 2.31 Pile cap contribution of 2×5 pile groups in over consolidated (OC) clay underlain by NC clay and dense sand at the bottom (profile 4) with various thicknesses t_{top} of the top OC clay layer: (a) OCR of 5 for the top OC clay, and (b) OCR of 10 for the top OC clay.

increase. The unit cap resistances of the 1×5, 2×5 and 3×5 pile groups at a settlement of 50 mm (2 inches) increase from 109 kPa (2.3 ksf) to 359 kPa (5.4 ksf), from 86 kPa (1.8 ksf) to 222 kPa (4.6 ksf), and from 68 kPa (1.4 ksf) to 140 kPa (2.9 ksf), respectively, as t_{top} increases from 0 to 10 m (32.8 ft).

Figure 2.31 and Figure 2.32 show the pile cap contribution and unit cap resistance of the 2×5 pile groups in overconsolidated (OC) clay underlain by NC clay and dense sand at the bottom (profile 4). Various thicknesses t_{top} of the top OC clay layer and OCR values of 5 and 10 are considered. The existence of the

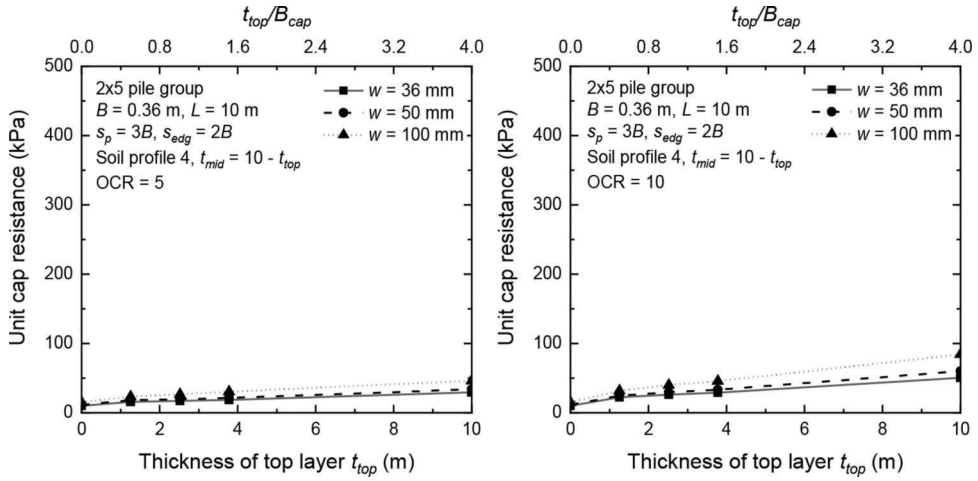

Figure 2.32 Unit cap resistance of the 2×5 pile groups in overconsolidated (OC) clay underlain by NC clay and dense sand at the bottom (profile 4) with various thicknesses t_{top} of the top OC clay layer: (a) OCR of 5 for the top OC clay, and (b) OCR of 10 for the top OC clay.

top OC clay layer increases the cap contribution and the unit cap resistance of the pile groups slightly, and the increases in cap contribution and unit cap resistance are greater for the OC clay with OCR equal to 10. The cap contributions at a settlement of 50 mm (2 inches) increase from 4.3% to 5.3% (with a maximum value of 6.7% at t_{top} = 2.52 m = 8.3 ft), and from 4.3% to 5.4% (with a maximum value of 9.1% at t_{top} = 2.52 m = 8.3 ft) for the OC clay with OCR of 5 and 10, respectively, as t_{top} increases from 0 to 10 m (32.8 ft). The unit cap resistances at a settlement of 50 mm (2 inches) increase from 12 kPa (0.25 ksf) to 34 kPa (0.71 ksf) and 60 kPa (1.25 ksf) for the OC clay with OCR of 5 and 10, respectively, as t_{top} increases from 0 to 10 m (32.8 ft). As the OCR of the top layer increases from 5 to 10, the cap contributions and the unit cap capacities at a settlement of 50 mm (2 inches) at t_{top} = 10 m (32.8 ft) increases from 5.3% to 5.4% and 34 kPa (0.71 ksf) to 60 kPa (1.25 ksf), respectively.

2.2.2.3 Group efficiencies. Figure 2.33 shows the base and shaft efficiencies of individual piles in the 3×5 pile groups in loose-over-dense sand (profile 1) with various thicknesses t_{top} of the top loose sand layer. The efficiencies of the base resistance are almost constant when t_{top} is between 0 and the pile length L of 10 m (32.8 ft). When t_{top} is slightly greater than the pile length, the base efficiencies increase because of the embedment of the pile base into the dense sand layer. The efficiencies for the shaft resistance increase slightly as t_{top} increases up to the pile length of 10 m (32.8 ft) and then become constant for $t_{top} > 10$ m (32.8 ft).

2.3 Summary and Conclusions

A series of realistic, advanced finite-element analyses were performed for 1×5, 2×5, and 3×5 pile groups with soil-supported pile caps to have a better understanding of (1) the contribution of the cap towards the total foundation capacity and (2) the effect of the pile cap on the mobilization of resistance of the individual piles in the group. Through a parametric study, the effects of soil layering, pile cap size, pile group layout, and pile-to-pile spacing on the resistance mobilization of the pile cap and of the individual piles in the pile groups are evaluated.

Based on the analyses results, the pile cap contribution towards the total capacity of the pile-supported foundation in sand is significant. It ranges from approximately 12% to 80% depending on the type and the state of the soil in which the foundations were constructed, the pile spacing, the length of the piles, and the settlement level for the pile groups considered in this study. For uniform sand, the cap contribution towards resistance in dense sand is greater than that in loose sand by up to 21%. For loose-over-dense sand, the cap contributions of the 1×5, 2×5, and 3×5 pile groups decrease as the thickness t_{top} of the loose sand layer increases up to the pile length L of 10 m (32.8 ft). The cap contribution of the 1×5 pile group decreases at the fastest rate and the cap contribution of the 3×5 pile group decreases at the slowest rate as t_{top} of loose-over-dense sand increases from 0 to 10 m (32.8 ft). The cap contribution of the pile groups does not vary meaningfully for t_{top} greater than the pile length L. A layer of dense sand as thin as 2–3 m (6.6–9.8 ft) at the top of the soil profile can increase the cap contribution by up to 55%. The pile cap contribution in clay is quite small when compared to that in sand.

For the same pile geometry (pile diameter B = 0.36 m = 14 inches and pile length L = 10 m = 32.8 ft), pile-to-pile spacing s_p of 3B, pile-to-cap edge distance s_{edg} of 2B, and soil profile (uniform loose or dense sands), the 1×5 pile group provides the largest cap contribution, ranging from 33% to 42%, and the 3×5 pile group provides the smallest cap contribution, ranging from 16% to 25%. The cap contribution increases as the pile cap settlement increases due to continuous mobilization

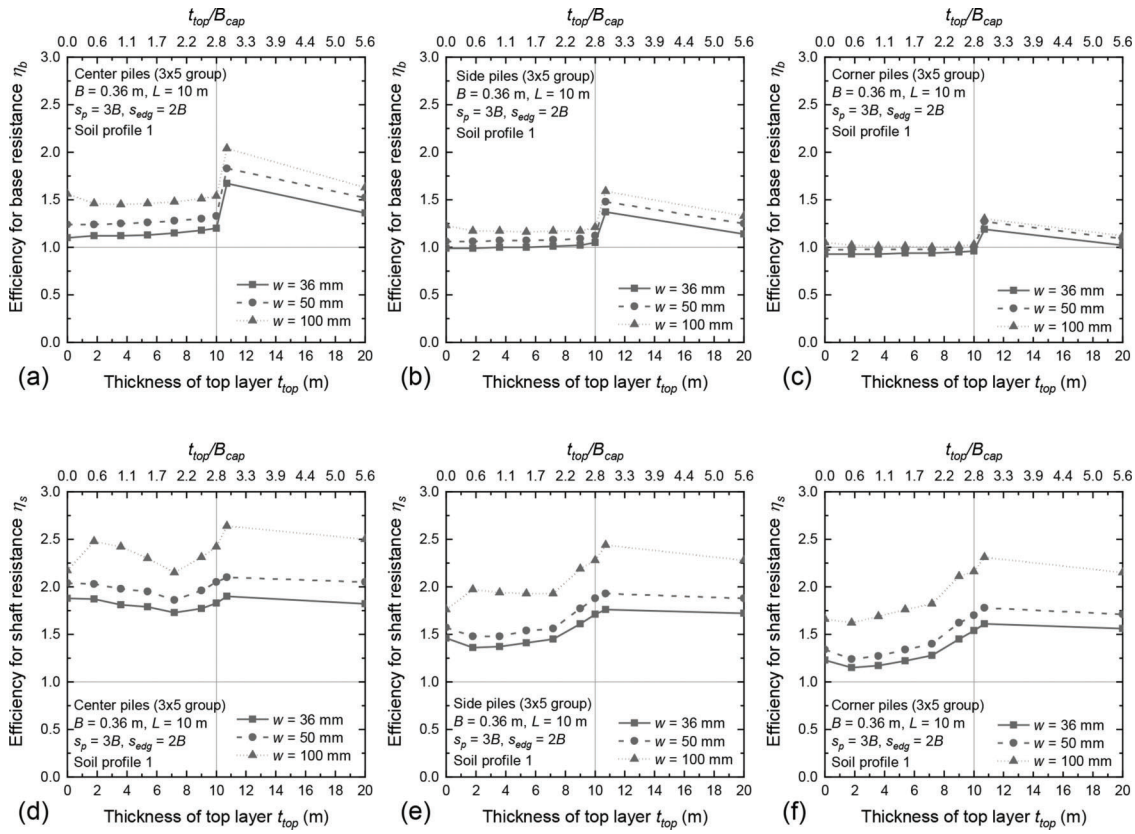

Figure 2.33 Efficiencies of individual piles in 3×5 pile groups in loose-over-dense sand (profile 1) with various thicknesses t_{top} of the top loose-sand layer: (a) base efficiency η_b of center pile, (b) base efficiency η_b of side pile, (c) base efficiency η_b of corner pile, (d) shaft efficiency η_s of center pile, (e) shaft efficiency η_s of side pile, and (f) shaft efficiency η_s of corner pile.

of the cap capacity. The cap contribution increases with increasing pile cap size. A larger size of the pile cap may result from use of piles with greater diameter B for given values of s_p/B and s_{edg}/B or from larger values of s_p/B and s_{edg}/B for a given pile diameter B.

The individual piles in pile groups can be grouped into two or three pile categories depending on the location of the piles: center and side piles for the 1×5 and 2×5 pile groups; and center, side and corner piles for the 3×5 pile group. The efficiencies of individual piles in the pile group increase as the pile cap settlement increases. At the beginning of the loading, the efficiencies are lower than 1 but, in general, become higher than 1 as the settlement increases. The efficiencies for the shaft resistance typically increase at higher rates than the efficiencies for the base resistance as the settlement increases from 0 mm to 100 mm (4 inches).

The amount and rate of change of shaft and base efficiencies at different settlement levels considered in this study depend on group layout, soil profile and the location of the pile in a group. In both base and shaft efficiencies, the 1×5 pile group has the least change and the 3×5 pile group has the most change. This can be because a larger size of the pile cap of the 3×5 pile group than that of the 1×5 pile group has more effect on the mobilization of base and shaft resistances of the piles in a group. The change in both base and shaft efficiencies of the piles in a group in dense sand is, in general, less than that in loose sand by up to about 23% for the cases considered in this study. A possible reason for this the more intense strain localization in dense sand, which narrows the influence zone of the pile-soil-pile interaction and the pile cap-soil contact. In the 1×5 and 2×5 pile groups, both the base and the shaft efficiencies of the center piles are lower than those of side piles at the beginning of loading, but they increase at a faster rate and become greater than those of side piles as the settlement increases from 0 mm to 100 mm (4 inches). This shows that, at the beginning of loading, side piles carry greater loads than center piles but, as the settlement increases, center piles carry greater loads than side piles in the 1×5 and 2×5 pile groups. In the 3×5 pile group, the center piles have the lowest base and shaft efficiencies, and the corner piles have the highest base and shaft efficiencies at the beginning of the loading, but, as the settlement increases, the base and shaft efficiencies of the center piles increase at the fastest rate, exceeding those of side and corner piles, while the efficiencies of corner piles increase at the slowest rate and become less than that of center and side piles. This shows that at the beginning of the loading, corner piles carry higher loads, and the center piles carry lower loads, but, as the settlement increases, these reverse.

Pile base and shaft efficiencies calculated at a settlement of 100 mm (4 inches) are similar in 1×5 pile groups with pile diameters of 0.36 m (14 inches) and 0.6 m (23.6 inches) for the same s_p of $3B$ and s_{edg} of $2B$. If a different comparison is now made of a 1×5 pile group with s_p of $5B$ and s_{edg} of $6B$ to the 1×5 pile group with s_p of $3B$ and s_{edg} of $2B$, we find that base and shaft efficiencies are then 29% and 52% greater for the pile group with larger spacings because of the greater size of the pile cap.

3. GUIDELINES FOR FOUNDATION REUSE

3.1 Consideration of Updated Design Loads

Bridge rehabilitation and replacement projects that rely on foundation reuse can have design loads—we will refer to this as updated design loads—that are different from the current loads applied on existing foundations because the superstructure or bridge may be replaced or widened, or because other types of loading are considered. Changes in design loads can also result from repurposing or retrofitting of the bridge foundations to accommodate the changes in bridge design. Even if there are no changes in the loads applied on existing foundations, the design loads need to be updated to account for current design specifications and to verify original design load calculations. Many old bridges considering foundation reuse were designed following ASD (allowable stress design) or LFD (load factor design) standards, which is different from the current design framework, LRFD (load and resistance factor design).

In the strength limit state design in the LRFD and LFD frameworks, factored design load should be less than the factored capacity (resistance) of foundations. The factored load Q is defined by

$$Q = \sum (LF_i) Q_{i,n} \qquad \text{(Eq. 3.1)}$$

where $Q_{i,n}$ is a nominal load—a dead load, live load or other source-linked load—and LF_i is the corresponding load factor. In the ASD framework, the factored load equals to the nominal load because uncertainties regarding the loads are considered in the factor of safety (FS). Table 3.1 compares load factors in the LRFD and LFD frameworks and equivalent load factor, which is 1 in the ASD framework, proposed by AASTHO (AASHTO, 2002, 2020) for dead and live loads. This comparison shows that different design specifications can provide different factored loads for the same nominal loads, which can lead to different results in design checks.

TABLE 3.1
Comparison of load factors for dead load and live load for different design specifications

	Load Factor		
Load Type	**ASD**	**LFD**	**LRFD**
Dead Load (DL)	1	0.9–1.3	1.0–1.95 (max) 0.25–1.0 (min)
Live Load (LL)	1	1.25–2.86	1.35–1.75

3.2 Inspection of Existing Foundations

Collecting detailed and reliable information of existing foundations through inspection is necessary for foundation reuse design. The existing foundations need to be inspected to assess the following two main things:

- the structural integrity of the existing foundations; and
- the as-built geometry of the existing foundations.

Assessment of the structural integrity of existing foundation elements needs to be performed at the very beginning of the reuse foundation design. Existing foundation elements that have undergone severe deterioration are not suitable for foundation reuse because the capacity of the existing foundations may have degraded, shortening their service life. The structural integrity of existing foundations can be evaluated by analyzing historical inspection records and performing visual inspection when foundation reuse is being considered and also by using destructive and/or nondestructive methods.

Accurate information on as-built geometry of existing foundations is essential for capacity estimation. The as-built geometry of existing foundations can be determined from the original plan drawings or construction records. Otherwise, destructive or nondestructive methods can be used to determine the as-built geometry of existing foundations.

Details on methods and procedures for the inspection of existing foundations can be found in Chapter 4.

3.3 Capacity Estimation of Existing Foundations

Capacity estimation of existing foundations is challenging for foundation reuse because it involves consideration of several factors that are not considered in the capacity estimation of new foundations (Davis et al., 2018; Hoomaan et al., 2021). The main factors in the estimation of the capacity of existing foundations are the following.

- The level of uncertainty in capacity estimation for existing foundations is highly dependent on the reliability of the inspection results and historical records.
- The level of deterioration of existing foundation elements and other time-related effects (e.g., pile setup) must be determined and considered in the capacity estimation of the existing foundations.
- The design checks using current LRFD design specifications can yield different results from those using the original (ASD or LFD) checks.

The current capacity of existing foundations can be estimated by considering of some of the following.

1. Historical records (original plan drawings, construction records, as-built plans showing the geometry of existing foundations or inspection records).

2. Results of inspections or structural integrity evaluations.
3. Site investigation data.
4. Load tests.

Details on methods and procedures used for the capacity estimation of existing foundations can be found in Chapter 5.

3.4 Design Checks and Selection of Foundation Reuse Solution

Based on the updated design loads, current soil profile and estimated current capacity of existing foundations, the design checks for foundation reuse can be performed. The minimum requirements for foundation reuse may be set as follows:

- factored foundation resistance > factored load,
- structurally sound foundation elements,
- no significant scour,
- no excessive total and differential settlements,
- no excavations or other work that might lead to loss of foundation support,
- no significant reconfiguration of loads, and
- ability to do construction work as needed for the existing and new foundation elements.

If the existing foundations do not pass design checks, they can be repaired or strengthened to increase their capacity, or the superstructure design loads can be revised (e.g., by using light-weight superstructure materials). If none of these methods work, the existing foundations can be completely replaced by new foundations, or the overstress may be accepted by the asset owner. The detailed methods and procedures addressing the selection of foundation reuse solutions are provided in Chapter 6.

3.5 Framework for Foundation Reuse

Figure 3.1 shows the proposed guidelines for foundation reuse. The first step is to determine the as-built geometry of the existing foundations. After the as-built geometry of the existing foundations is determined, the structural integrity of the existing foundations should be assessed. If the structural integrity of the existing foundations is not sufficient for potential reuse, the existing foundations should be completely replaced by new foundations. If the structural integrity of the existing foundations is sufficient for potential reuse with or without repairs, the available site investigation data should be collected and analyzed.

After the available site investigation data is analyzed, if necessary, additional site investigations should be performed. Initially, the site investigation data can be obtained from available geotechnical reports and other general INDOT foundation documents. The data that can be used for the analysis includes the following:

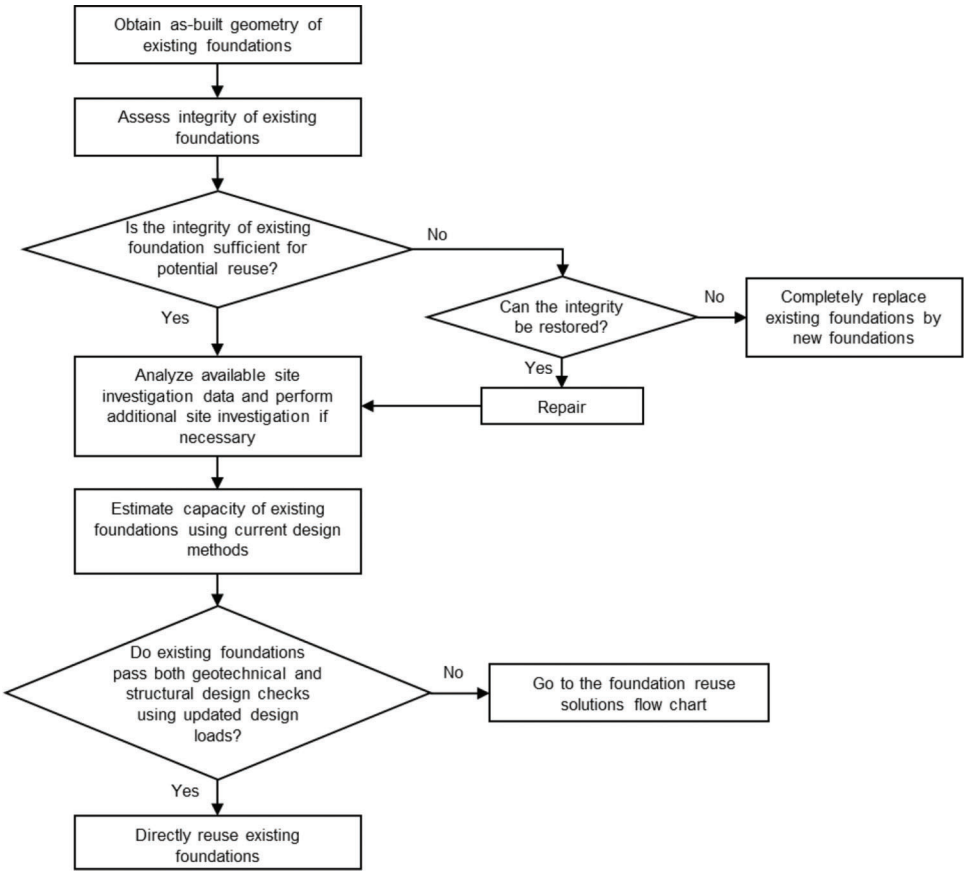

Figure 3.1 Framework of the foundation reuse strategy.

- geotechnical logs: soil description, layering, soil density, SPT and/or CPT, water content, groundwater level and flow pattern (i.e., hydrostatic, hydrodynamic, artesian conditions) and laboratory test results; and
- records of geohazard vulnerability assessments.

Geohazard vulnerability assessments includes vulnerability to scour and seismic and other hazards (including liquefaction, settlement, slope failure, and fault rupture). Records on corrosive soils, Karst formations, loss of soil foundation support and drainage during or after a rain event can also be considered in the data analysis.

If available historical records are incomplete and do not provide sufficient information, additional site investigation can be performed in the context of reuse decisions (including deciding which types of *in situ* or laboratory tests are more appropriate for the site conditions). Even when the original borings from the time of initial construction are available, further exploration can be done to confirm the available data. If only standard penetration test (SPT) data are available, more reliable tests, such as the cone penetration test (CPT), can be performed.

The next step is to estimate the geotechnical capacity of the existing foundations. The capacity of the existing foundations can be estimated from available original bridge project documentations; however, the estimation from the original bridge project documentation should be considered as a reference, or even as the minimum likely capacity, because the original bridge plans typically followed old design codes that are conservative and do not consider time effects on current soil profiles; current capacities of the existing foundations reflect factors such as pile setup and consolidation of the soil supporting shallow foundations. The current capacity of existing foundations can be estimated using the current design equations used by INDOT and their Geotechnical Consultants as recommended by FHWA, INDOT and AASHTO, in addition to methods developed over the years at Purdue University (Han et al., 2015; Han, Ganju, et al., 2019, 2020; Han, Prezzi, et al., 2017; Sakleshpur et al., 2021a and b; Salgado, 2008, 2022a; Salgado et al., 2017).

Once the design loads from the new superstructure and the capacity of existing foundations are determined, geotechnical and structural design checks can be performed. If the existing foundations pass the design checks, they can be directly reused without modification, but with the necessary care to properly connect them to the new or modified superstructure. Otherwise, modification or extension of the existing foundations or construction of new foundations may be needed.

Several factors need to be considered when making plans for foundation reuse: type, size and elevation of the existing and new foundations; constructability of the new foundations; integration of the new structure with the existing foundations and any retrofitting that may be needed; cost effectiveness of the foundation reuse plan; impact of new foundation construction on the existing foundations and structures (e.g., ground settlement, slope failures, heaving, artesian conditions, rotation or deflection of existing structures, load distribution, and effects on the capacity of the existing foundation due to new foundation construction); age of the existing structure; and the life expectancy of the reconstructed structure.

4. INSPECTION OF EXISTING FOUNDATIONS

4.1 Framework for the Inspection of Existing Foundations

In order to make informed decisions regarding foundation reuse, it is necessary to collect detailed information of the existing foundation elements. Such information includes the following.

- Type of foundation (e.g., driven piles, drilled shafts, footings), including material type.
- Location and elevation of the foundation elements (see Figure 4.1).
- Dimensions (e.g., width and length of footings, diameter and wall thickness of pipe piles, and size and thickness of a pile cap) of the foundation elements (see Figure 4.1).
- Structural integrity of the existing foundations.

In this chapter, we discuss different methods and techniques that INDOT may use to determine the geometry and assess the integrity of existing foundations. As summarized in Table 4.1, these methods can be divided into four categories: review of historical records, visual observation, destructive methods, and nondestructive methods. Table 4.1 summarizes the pros and cons of these methods, which will be discussed in detail later in this chapter.

4.2 Determination of As-Built Geometry of Existing Foundations

Determining as-built geometry of existing foundations is essential for accurate estimation of the capacity of existing foundations for reuse. The information on the geometry of existing foundations could be found from the original plan drawings or construction records if those records are available. Otherwise, destructive or nondestructive methods can be used to determine the as-built geometry of existing foundations. Table 4.2 summarizes the options that are available to determine a specific dimension of the unknown foundation element by using destructive and/or nondestructive methods.

When a decision is made regarding which method or technique to use, a number of factors should be considered, such as the cost and time it takes to perform the test, the site accessibility for the method to be applied, the target accuracy, and the suitability of the method for measuring a specific dimension. Figure 4.2 is a flow chart that can be used to plan a scheme to determine the geometry of any unknown foundation element.

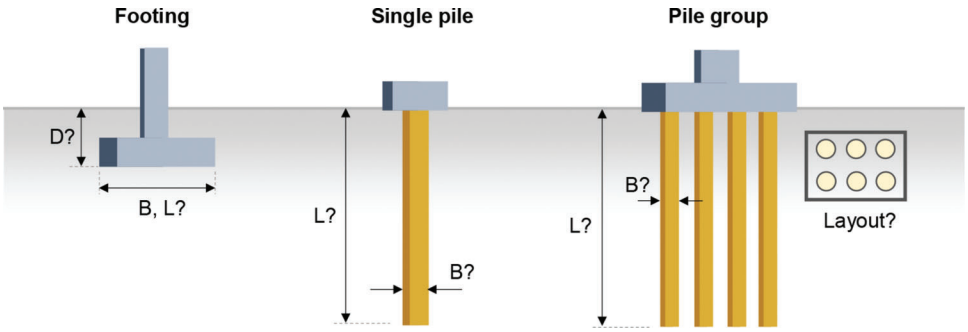

Figure 4.1 Geometry of foundation elements to be obtained for foundation reuse decisions.

TABLE 4.1
Methods that can be used to determine the dimensions and integrity of the existing foundations

Method Category	Methods		Advantages	Limitations
Review of Historical Records	Review of the following. Plan drawings Construction records Inspection records		Reliable, fast, and inexpensive	A set of records may be unavailable or incomplete
Visual Observation	Visual observation Dye penetrant testing		Fast, easy and inexpensive	It is applicable only to foundation elements above the ground
Destructive Methods	Sampling and lab testing		Reliable	Data is discontinuous and limited
	Partial or full excavation		Reliable	Excavation depth is limited due to safety or economic concerns
	Probing		Fast and inexpensive	Inspection range is limited to the top elevation of pile cap/footing
	Vertical coring with wireline logging		Accurate; continuous; providing samples for additional testing	It is relatively expensive and time-consuming, and limited by site accessibility
Nondestructive Methods	Pile integrity test methods	Sonic echo/impulse response (SE/IR) Ultra-seismic Impact echo (IE) Ultrasonic pulse velocity (UPV) Spectral analysis of surface waves (SASW) ER, radiography, cover meters, infrared thermography Magnetic particle testing, eddy current testing, ultrasonic testing (UT), phased array ultrasonic testing (PAUT), acoustic emission (AE)	Fast and relatively inexpensive	Exploration depth is limited due to energy attenuation; the upper part of foundation elements needs to be accessible
	Surface geophysical methods	Seismic methods Surface resistivity testing Ground penetration radar (GPR)	Fast and relatively inexpensive	Accuracy is low; it is applicable only for shallow depths (down to 50 ft)
	Borehole methods	Parallel seismic Cross-borehole tomography Induction field (IF) testing Borehole radar and sonic	Reliable	It is relatively expensive and limited by site accessibility

TABLE 4.2
Destructive and nondestructive methods that can be used to obtain specific dimensions of existing foundations

Unknown Dimension to Obtain	Methods/Techniques
Pile Length	Vertical coring, sonic echo/impulse response, bending wave method, ultra-seismic, seismic methods, cross-borehole tomography, parallel seismic, magnetometry, GPR, borehole radar and sonic, induction field (IF) testing
Thickness of Footing/Pile Cap	Excavation, vertical coring, seismic methods, impact echo, surface resistivity testing, GPR, borehole radar and sonic
Elevation of the Top of Pile Cap/Footing	Excavation, probing, seismic methods, GPR, surface resistivity testing, borehole radar and sonic
Width and Length of Footing/Pile Cap	Excavation, probing, seismic methods, GPR, surface resistivity testing
Layout of Pile Group	Partial excavation, seismic methods, impact echo, GPR

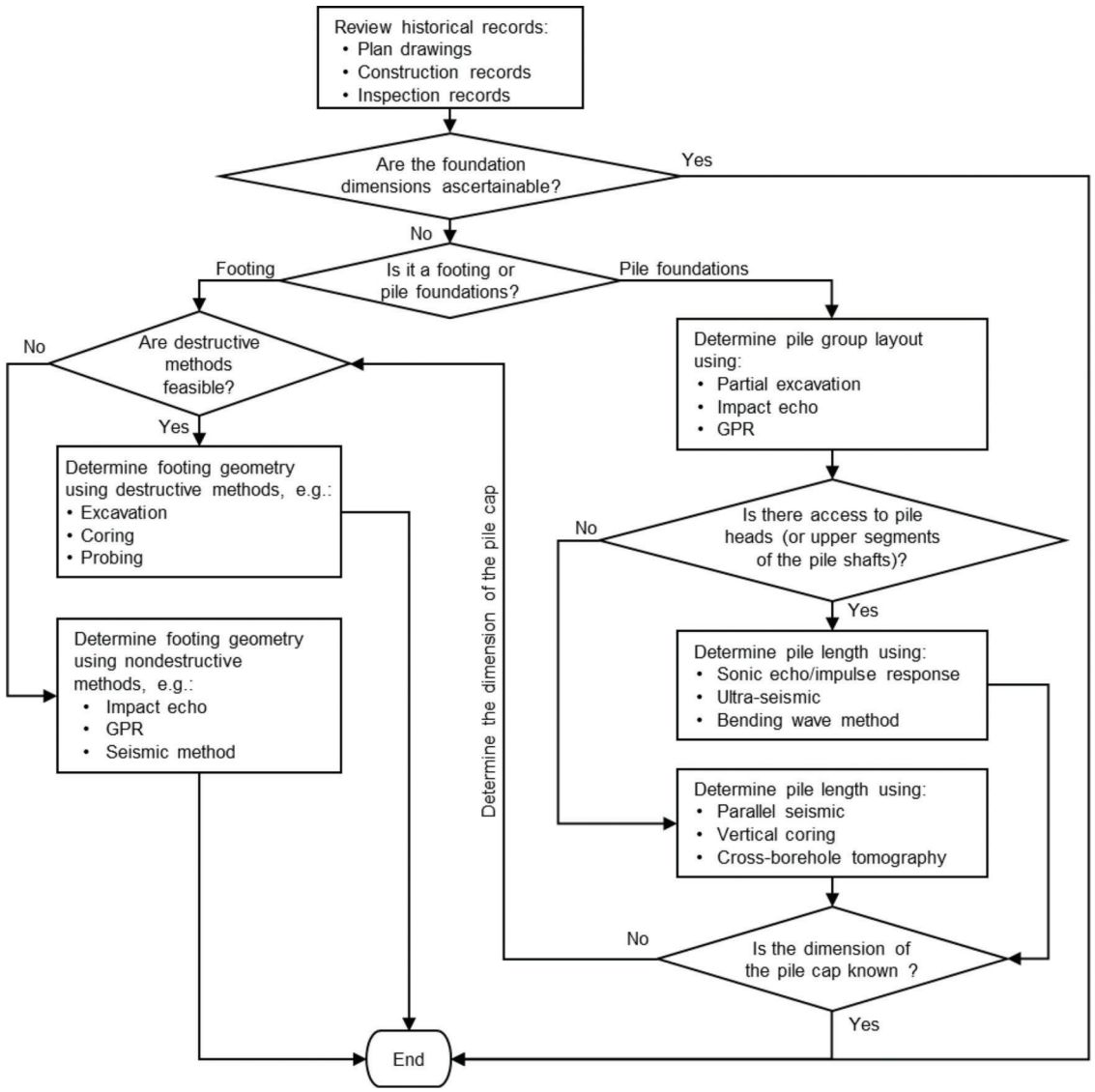

Figure 4.2 Flow chart to determine the geometry of the unknown foundation.

4.3 Inspection of Structural Integrity of Existing Foundations

Assessing the structural integrity of existing foundation elements is a crucial step in the initial decision on foundation reuse because severe deterioration in foundation elements can significantly lower the capacity of the foundation and reduce its remaining service life. For example, a concrete pile foundation after 20 years of wet-dry-freeze-thaw cycles was shown to

have a gradual decrease in its capacity, ending with a total reduction of 34.5% (Feng et al., 2021).

Different inspection methods can be chosen for different foundation material types. Table 4.3 and Table 4.4 show inspection items and the corresponding inspection methods (review of historical records, visual observations, destructive methods or nondestructive methods) for concrete and steel foundation elements, respectively. Various inspection items mentioned in Agrawal et al. (2018), MassDOT (2013), ODOT (2020) for concrete and steel can be categorized into material properties, defects and geometry. Material properties include strength of the material; defects include cracks or corrosion and section loss; and geometry includes discontinuities or breaks in the foundation. Each category can be inspected through different processes, as shown in Figure 4.3.

The durability of concrete foundation elements can be affected by temperature changes, freeze-thawing cycles, Alkali-Silica Reaction (ASR), Delayed Ettringite Formation (DEF), sulfate attack, calcium leaching, chloride intrusion, carbonation, concrete paste erosion, extreme events (e.g., fire, flooding, earthquakes), and foundation movements (total and differential settlements) (Agrawal et al., 2018). Damage resulting from these different processes produce different crack patterns in concrete elements. Through the inspection process and forensic evaluation of foundation elements, processes causing damage to concrete foundations can be identified and plans can be developed and implemented to restore integrity and to protect concrete from further deterioration.

Steel foundation elements can be damaged by corrosion in zones with fluctuating water levels (e.g., ocean, tide, river, or lake water levels), impact, seismic events, fatigue, tensile or shear loading on connections, and improper driving (Agrawal et al., 2018). Proper inspection of foundation elements helps not only with the understanding of critical factors affecting their integrity but also with the development of plans to improve their durability and increase their remaining service life.

4.4 Inspection Methods

4.4.1 Review of Historical Records

When available, the easiest and most reliable way to obtain information on existing foundations is by reviewing historical records of bridge projects. Historical records include but are not limited to plan drawings, construction records (including as-built plans or drawings and pile driving records or PDA data), and inspection records. Specifications or special provisions from the original construction, monitoring reports and

TABLE 4.3
Inspection items and corresponding inspection methods for existing concrete foundations

Item Category	Inspection Items	Methods/Techniques
Material Properties	Mixture properties, compressive strength, elastic modulus, rebar strength	Review of historical records, destructive methods (sampling and laboratory testing, and vertical coring with wireline logging)
Surface Defects	Cracking/crack density and width, spalling, delamination, patching, discoloration, efflorescence and rust/moist staining, cold joints, section loss	Visual observation, destructive methods (excavation)
Internal Defects	Cracking, voids, weak zones, honeycombing, delamination, presence of water, chloride and salts, presence and extent of corrosion of rebar, section loss	Destructive methods (excavation, vertical coring with wireline logging), nondestructive methods (GPR, ultrasonic pulse velocity, infrared thermography, electrical resistivity, radiography, sonic echo/impulse response method, ultra-seismic, impact echo, SASW, bending wave method)
Geometry	Discontinuities, breaks, rebar layout	Review of historical records, destructive methods (excavation), nondestructive methods (GPR, radiography, cover meters, parallel seismic, induction field testing)

TABLE 4.4
Inspection items and corresponding inspection methods for existing steel foundations

Item Category	Inspection Items	Methods/Techniques
Material Properties	Yield strength and tensile strength	Review of historical records, destructive methods (sampling and laboratory testing)
Defects	The location and extent of corrosion, cracks (especially near welds and bolts), surface flaws, condition of fatigue prone elements, condition of cover plate cutoffs, condition of connection details and fasteners, presence of lead paint, section loss	Visual observation, dye penetrant testing, destructive methods (sampling and laboratory testing), nondestructive methods (magnetic particle testing, Eddy current testing, ultrasonic testing and phased array ultrasonic testing, acoustic emission)
Geometry	Discontinuities, defects	Destructive methods (excavation), nondestructive methods (GPR, parallel seismic, induction field testing)

documentation of any extreme events, such as flooding, barge impacts, earthquakes, and fire, affecting the bridge performance are also included in historical records. Among these documents, construction records are more reliable than plan drawings because the as-built geometry of existing foundations may be different from what is in the plan drawings as a result of adjustments made during construction. A high degree of confidence that records are accurate need to exist for this method to be used.

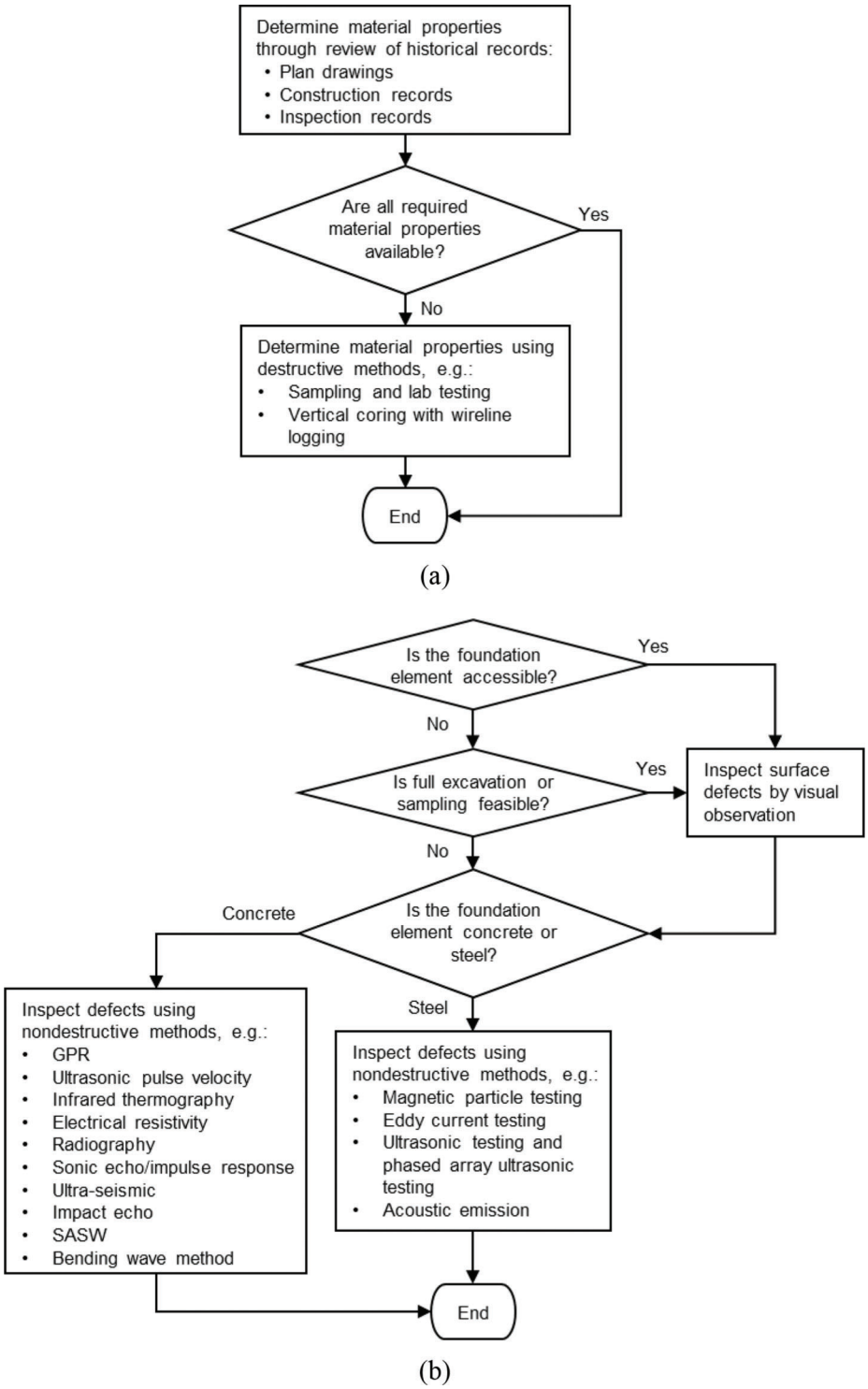

Figure 4.3 Continued.

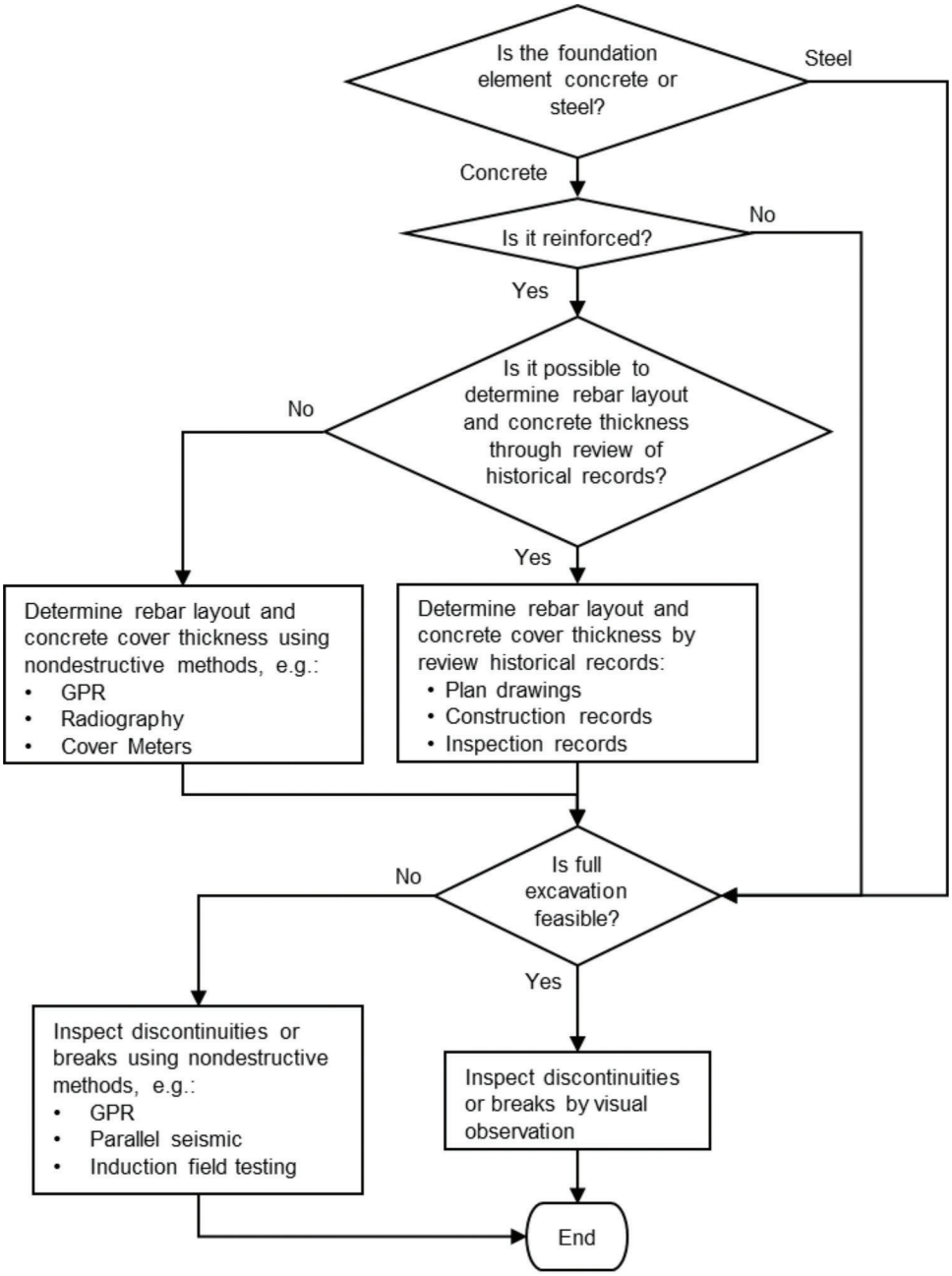

Figure 4.3 Flow chart to inspect three aspects of structural integrity of existing foundations: (a) material properties of foundation elements, (b) defects in existing foundations, and (c) a change in the geometry of existing foundations.

4.4.2 Visual Observation

Visual observation is one of the most basic and easiest ways to inspect existing foundation elements. For concrete elements, observable cracking, spalling, efflorescence, carbonation, rust staining, cold joints or other defects can be recorded during inspection. If reinforcements of concrete elements are exposed due to concrete deterioration, the presence and extent of corrosion of reinforcements can also be recorded. For steel elements, the extent of corrosion, connection deterioration, cracking (especially near welds and bolts) can be determined by visual inspection. To detect microcracks and small surface flaws in steel elements, dye penetrant testing can also be performed.

4.4.3 Destructive Methods

While detailed design and construction records are the most reliable source to inspect existing foundations, they are sometimes unavailable, more often so for older bridges. In these cases, destructive and/or nondestruc-

tive methods and techniques can be used to estimate the geometry of the unknown foundations and to assess the structural integrity of existing foundations. Destructive testing methods are intrusive and may affect the condition or integrity of the existing foundations. Commonly used destructive methods include sampling and laboratory testing, partial or full excavation, probing, and vertical coring and wireline logging.

4.4.3.1 Sampling and laboratory testing. If samples of materials from existing foundation elements can be obtained, visual inspection and various laboratory tests can be performed to determine material properties and to determine the degree of deterioration of existing foundation elements at most relevant locations. For concrete elements, petrography and unconfined compressive strength testing can be performed to ascertain the cause of concrete deterioration by examining the mineralogical and chemical characteristics of the material and to determine current material properties, respectively. If the concrete element is reinforced, rebar strength tests can also be performed to determine its current material properties. For steel elements, several tests can be performed, including the Brinell hardness test, the Charpy impact test, and tensile tests, to determine their current material properties. The number of samples collected from the existing foundations should be limited to prevent additional degradation of their strength and integrity. Visual inspection and nondestructive methods, such as ground penetration radar (GPR) or cover meter tests to determine the concrete cover over the reinforcement, can be performed before sample collection to determine the location and frequency of sampling.

4.4.3.2 Partial or full excavation. When deemed feasible, without compromising the performance of the existing foundations, the ground can be excavated to reveal a portion of the foundation because this is the most direct method to find out the exact location and dimensions of the existing foundations. The method can be used for footings to obtain their location and dimensions. Partial excavation can be done to expose the cap of a pile group and possibly the top portion of the piles to obtain their dimensions and pile group layout. The method is reliable, but often limited to the maximum depth of excavation due to cost and safety concerns. According to a survey performed by Boeckmann and Loehr (2017), about 51% of the DOTs have used this method to determine the geometry of unknown foundations, and the excavation depths that have been used were up to 10 ft. The excavation method becomes impractical when the ground water table is near the ground surface, (dewatering would be needed). In addition, excavations should be avoided when removal of soil undermines the support that the soil provides to the foundation elements and the structure.

4.4.3.3 Probing. Probing is a technique that introduces a small-diameter rod (such as the CPT cone) into the ground to reach the top of the footing or pile cap to determine the depth to the top of these foundation elements. The method is simple to implement, but the collected information is limited to the top elevation of these elements and the approximate horizontal extent of these elements when multiple probing tests are performed (Olson et al., 1998).

4.4.3.4 Vertical coring with wireline logging. If the foundation elements are made of concrete, vertical coring can be done through footings, pile caps, or drilled shafts to obtain their top and bottom elevations. Visual inspection of the collected samples enables the assessment of defects (e.g., cracking or corrosion) that may impact the structural integrity of these foundation elements. In addition, laboratory testing can be performed on the samples collected to obtain their strength and stiffness. Vertical coring is accurate and provides samples for additional testing, but the method is relatively expensive, time-consuming and often limited by site accessibility (Boeckmann & Loehr, 2017; Olson et al., 1998). Vertical coring can be performed with wireline logging, which allows recording continuous vertical logs of density and wave speed (Agrawal et al., 2018).

4.4.4 Nondestructive Methods

There are various nondestructive techniques that can be used to determine the dimensions and assess the integrity of existing foundations (Azari, 2020; Baker et al., 1991; Hertlein & Davis, 2007; O'Neil & Reese, 1999; Samtani & Nowatzki, 2006). These methods can be grouped into three categories: pile integrity test methods, surface geophysical methods, and borehole methods.

4.4.4.1 Pile integrity test methods. Pile integrity test methods typically involve generating an impact (e.g., ultrasonic wave or hammer blow) on foundation elements and then measuring the reflected waves at receiver sensors attached to the foundations. Only the signals within the foundation elements are involved. Commonly used impact wave methods are sonic echo (SE)/impulse response (IR) method, bending wave method, ultra-seismic method, impact echo (IE) method, ultrasonic pulse velocity (UPV) method, and spectral analysis of surface waves (SASW) method.

Sonic echo (SE)/impulse response (IR) methods are widely used pile integrity testing (PIT) methods to determine the length of a pile and to locate defects (e.g., cracks or corrosion) in a pile. In this method, a shock wave is generated by striking a hammer blow at the top of a pile, as shown in Figure 4.4(a). The compression wave travels down along the pile length, reflects at the pile bottom, and travels back to the pile top, where the acceleration of the reflected waves is measured by the sensors (e.g., accelerometer) attached to the pile head.

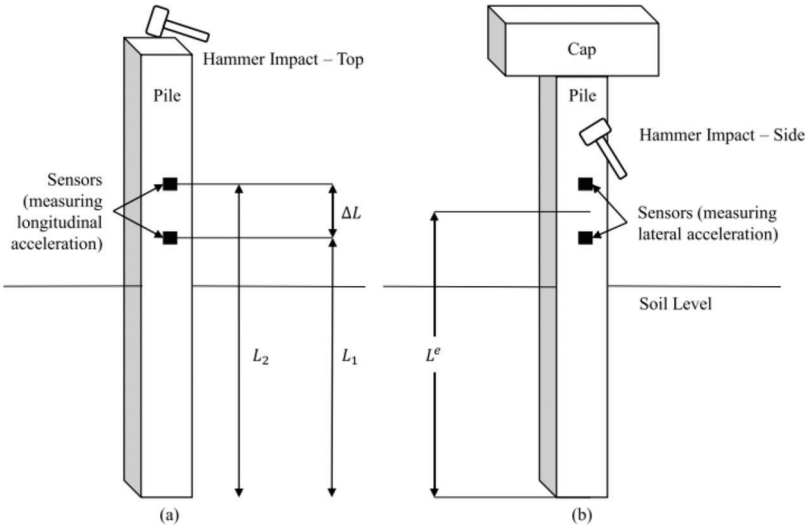

Figure 4.4 Testing methods that can be used to determine pile length and locate defects in piles using: (a) Sonic echo (SE)/impulse response (IR) with top hammer impact, and (b) bending wave method with side hammer impact (Samu & Guddati, 2020).

The difference between the sonic echo (SE) method and the impulse response (IR) method is related to the interpretation of the collected data: SE relies on the time domain analysis of the reflected waves, whereas IR focuses on the frequency domain analysis. The SE/IR methods are fast, easy, and inexpensive to perform, but are subject to two important limitations: (1) they cannot be performed when there is no access to the pile top, and (2) the accuracy of the interpretation drops as the pile length increases due to increased attenuation. The methods are limited to about 25 feet when the pile is installed in very stiff soils (Boeckmann & Loehr, 2017).

The *bending wave method* is very similar to the sonic echo (SE)/impulse response (IR) methods. Instead of relying on the generation of compression waves as is the case for the SE/IR methods, the bending wave method relies on bending (flexural) waves (Samu & Guddati, 2019, 2020) generated by striking the foundation with a hammer on its side near the top of the pile, as shown in Figure 4.4(b). The bending wave method does not require access to the top surface of the pile foundation (to generate the hammer blow), but it is subject to limitations such as the maximum pile length that can be detected due to severe attenuation of the bending waves: it severely underestimates the length of piles longer than 55 ft in the field (Samu & Guddati, 2020) without modification on the original method.

The *ultra-seismic method* was developed as an improvement on the SE/IR and bending wave methods. Unlike the SE/IR methods, which typically uses 1–2 receiver sensors, the ultra-seismic method relies on multiple (e.g., 4–5) triaxial sensors that measure movements in all three directions, improving the accuracy of the pile dimension estimates (Jalinoos et al., 2017; Tran et al., 2019).

The measurement principle for the *impact echo (IE) method* is similar to those for the SE/IR methods. As shown in Figure 4.5, the IE device travels along the top of a footing or a pile cap, generating stress or acoustic waves, which are reflected at the bottom of the foundation element and then captured by the receiver sensor embedded in the IE device. Based on the time it takes for the acoustic/stress wave to travel (for a round trip) in the foundation element, its thickness/length can be estimated. The IE method can be used to determine the thickness of a footing or a pile cap, the length of a pile and the layout of the pile group under the pile cap, as well as the location of defects (e.g., cracking or corrosion) or weak zones.

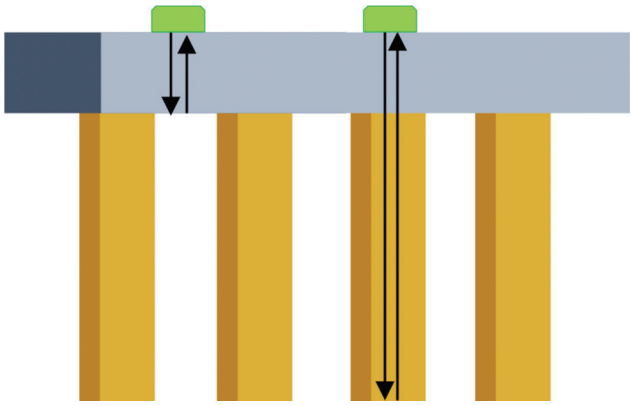

Figure 4.5 The impact echo method can be used to determine the thickness of pile cap and the pile group layout.

The *ultrasonic purse velocity (UPV) method* uses an ultrasonic pulse to detect the location of internal defects of foundation elements. A transducer attached on one side of the foundation element generates an ultrasonic pulse and an accelerometer attached on the other side of the foundation element receives the pulse. By measuring ultrasonic pulse velocities at different locations, the location and size of internal defects can be estimated.

The *spectral analysis of surface waves (SASW) method* uses the propagation of surface (Rayleigh) waves within the foundation element to determine the stiffness of concrete elements and locate internal defects such as voids and delamination (Wightman et al., 2004). The surface waves are generated by tapping the surface of the element using a small hammer and the acceleration of the waves are measured at multiple accelerometers located in a line from the hammer strike point.

Especially for concrete foundation elements, the following nondestructive methods can be used to determine internal defects of concrete elements: electrical resistivity (ER) test, radiography, cover meter tests, and infrared thermography. The *electrical resistivity (ER) test* measures the relative difference in electrical resistivities within the element to detect internal damages or cracks. The *radiography* uses X-rays to locate internal elements (e.g., rebars) and internal defects (e.g., cracks or voids) within concrete elements. The *cover meter test* measures magnetic field disturbance to estimate the concrete cover thickness, and the *infrared thermography* measures heat flow though the concrete element and detects areas having different heat conductions to determine delamination of concrete elements.

To assess the structural integrity of steel foundation elements, nondestructive methods such as magnetic particle testing, Eddy current method, ultrasonic testing (UT) and phased array ultrasonic testing (PAUT), and acoustic emission testing can be used. The *magnetic particle testing* uses a magnetic field to detect the presence of defects in steel elements. The *Eddy current method* uses electromagnetic induction to estimate surface flaws, material or coating thickness, and cracking of steel elements. The *ultrasonic testing (UT)* uses ultrasounds to estimate flaws, cracks, material thickness, geometry and section loss of steel elements. The *phased array ultrasonic testing (PAUT)* creates an ultrasound beam to image internal flaws, cracks and pit corrosion in steel elements and connection defects. The *acoustic emission (AE) testing* is commonly used to monitor crack growth in steel elements by detecting acoustic emissions (pressure waves) that are generated as cracks or discontinuities within steel elements actively grow.

4.4.4.2 Surface geophysical methods. Surface geophysical methods rely on the analysis of how signals (e.g., seismic waves, electrical current, and electromagnetic signals) propagate through soil and reflect at the boundaries of foundation elements. Depending on the type of signals used, the tests are known as the seismic method, surface resistivity testing, and ground penetration radar. These tests are fast and inexpensive to perform but are known for the relatively low measurement accuracy and precision.

For the *seismic method*, an array of geophones is placed on the ground surface on one side of the unknown foundation to receive the seismic waves generated from a hammer blow applied on the ground surface on the other side of the unknown foundation. As a seismic wave travels at different speeds depending on the stiffness of the medium through which it propagates, the signals captured by the geophone array will reflect the contrast in the stiffnesses of the foundation elements and the surrounding soil, generating an estimate of the location and dimensions of the unknown foundation elements (Agrawal et al., 2018).

Surface resistivity testing relies on the difference in the electrical resistivity (ER) values for different materials (e.g., concrete, steel, and soil). The method involves injecting electric current into the ground at two sources and measuring the electrical potential at two different receivers between the two sources. The method has been successfully used to identify foundation depths up to 30 feet (Tucker et al., 2015).

The *ground penetration radar (GPR)* method uses electromagnetic radiation in the microwave band of the radio spectrum and detects the reflected signals from material interfaces beneath the ground surface. Higher frequency radar provides higher measurement resolution but is limited to a small depth, whereas lower frequency radar can detect features at greater depths but with low resolution. GPR is typically used to determine the geometry and integrity of near surface foundation elements (e.g., footings).

4.4.4.3 Borehole methods. Borehole methods is a class of methods that involve drilling vertical borehole(s) close to the foundation elements and then lowering a logging device down the borehole to send and receive signals (e.g., seismic wave, radar, acoustic and magnetic) that are used to determine the geometry of the unknown foundation elements. Borehole methods are accurate and reliable, but they are relatively time-consuming, expensive, and subject to limitations of site accessibility. Commonly-used borehole methods include parallel seismic, cross-borehole tomography, induction field testing, and borehole radar and sonic testing.

As shown in Figure 4.6, *parallel seismic testing* starts by drilling a vertical borehole parallel to the unknown foundation. Then, a hammer blow is generated on the pile top, producing a seismic wave propagating down the foundation; the refracted wave is collected by a receiver sensor (e.g., geophone) placed in the borehole. This is repeated multiple times with the receiver sensor placed at different elevations. As the seismic wave travels at different speeds in the foundation and in soil, the elevation of the foundation bottom can be estimated by comparing the arrival times of the signal received by the sensor positioned at different elevations. The borehole is typically kept at a distance of 3–4 ft from the foundation to ensure high accuracy. In addition, signal processing techniques, such as the Automatic Gain Control technique and noise filtering techniques, can be used to help optimize the measured data from the parallel seismic tests by minimizing the impact of noise (Wightman et al., 2004). The parallel

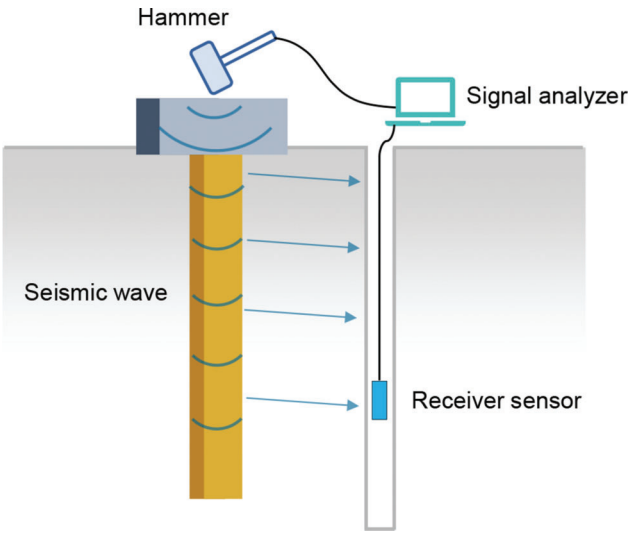

Figure 4.6 Parallel seismic testing that can be used to determine the length of unknown foundation.

seismic method is reliable and produces estimates of pile length with an accuracy of at least 95% (Wightman et al., 2004).

The *cross-borehole tomography* method uses a pair of vertical boreholes to create an image of the soil and foundation geometry between the boreholes by sending signals from a transmitter that travels vertically in one of the boreholes and measuring the arriving signals with a receiver placed in the other borehole at various elevations (Boeckmann et al., 2018; Olson et al., 1998).

Induction field (IF) testing deploys a magnetic sensor that travels down the borehole drilled next to the unknown foundation to detect metal (such as a steel pipe pile, or the reinforcement rebars in drilled shafts) in the foundation elements, providing an estimate of the foundation length (Agrawal et al., 2018).

Borehole radar and sonic testing works similarly to the parallel seismic testing. A transmitter and a receiver are simultaneously sent down the borehole. The radar or acoustic signals are reflected off the unknown foundation and then measured by the receiver sensor. This way, the length of the foundation element can be determined (Boeckmann & Loehr, 2017).

4.5 Examples of Inspection of Existing Foundations

4.5.1 Estimation of Footing Thicknesses by Using Ground Penetration Radar (GPR)

Ground penetration radar (GPR) is a nondestructive, surface geophysical method that can be used to determine the geometry of unknown foundations. This section provides an example of how GPR can be used to estimate the thicknesses of existing spread foundations (Grinč et al., 2015). At the site considered, destructive methods were not allowed to prevent damage to the water proofing of the basement of the structure. The GPR data was collected by a device, GSSI SIR-3000, with a ground coupled antenna of 400 MHz. The device is suggested to be used for a depth not deeper than 3 to 4 m (9.8–13.1 ft), so the test is performed up to a depth of 3 m (9.8 ft). The GPR test was performed in two profiles: the 11-m-long (36-ft-long) profile 1 including one spread footing; and the 32-m-long (105-ft-long) profile 2 including three spread footings. The data was collected at every 0.01 m (0.4 inches) in each profile, with the data recorded at every 60 ns. The GPR data was processed by the software, ReflexW. The frequencies outside the range between 100 to 800 MHz were filtered out during the data acquisition.

Figure 4.7 shows the GPR test results for profile 1. From the test data, three boundaries were identified, as shown in Figure 4.7a. Figure 4.7b shows the interpreted data with three different layers below the ground surface within a depth of 3 m (9.8 ft). The first layer (red area in Figure 4.7b) was interpreted as a top concrete layer, and the second layer (blue area in Figure 4.7b) was interpreted as a reinforced concrete layer. The last third layer (green area in Figure 4.7b) was interpreted as a base layer of the footing consisting of an aggregate or gravel layer. From the GPR test results, the thickness of the footing was estimated as 1 m (3.28 ft) and the shape of the footing below the ground surface was also estimated. The estimated thickness of the footing was very close to the data available in the technical documentation of the foundation construction (Grinč et al., 2015).

Figure 4.8 shows the GPR test results for profile 2. The obtained results were similar to those for profile 1: three boundaries and layers were identified within a depth of 3 m (9.8 ft). In this case, three concrete footings were detected, and the thicknesses of all the footings were estimated as 1 m (3.28 ft).

4.5.2 Estimation of Pile Length Using Bending Wave Method

The bending wave method is one of the nondestructive, impact wave methods. The bending wave method can be analyzed by using Effective Dispersion Analyses of Reflections (EDAR), which was developed by Samu and Guddati (2019). The bending wave method using EDAR underestimates the length of piles longer than 55 ft in the field due to severe attenuation of the bending waves (Samu & Guddati, 2020). To solve this problem, Samu and Guddati (2020) improved the original EDAR method and developed the modified EDAR method which can accurately estimate the length of relatively long piles in the field. This section provides an example of the estimation of lengths of existing pile foundations in the field by using the modified EDAR method (Samu & Guddati, 2020). The detailed procedure of the method can be found in Samu and Guddati (2019, 2020).

The bending wave method was performed for two square solid concrete piles embedded in Rodanthe, Outer Banks, NC. Figure 4.9(a) shows the test piles,

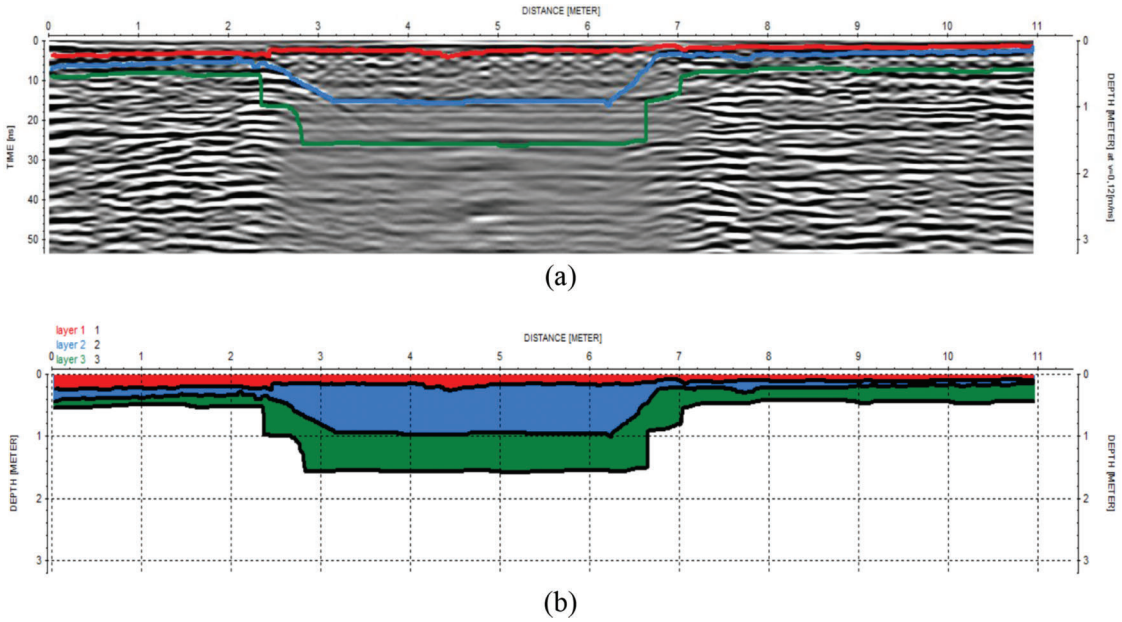

Figure 4.7 The GPR test results for profile 1: (a) the radagram result with the detected boundaries in colored lines, and (b) the interpreted results with three different layers below the ground surface (Grinč et al., 2015).

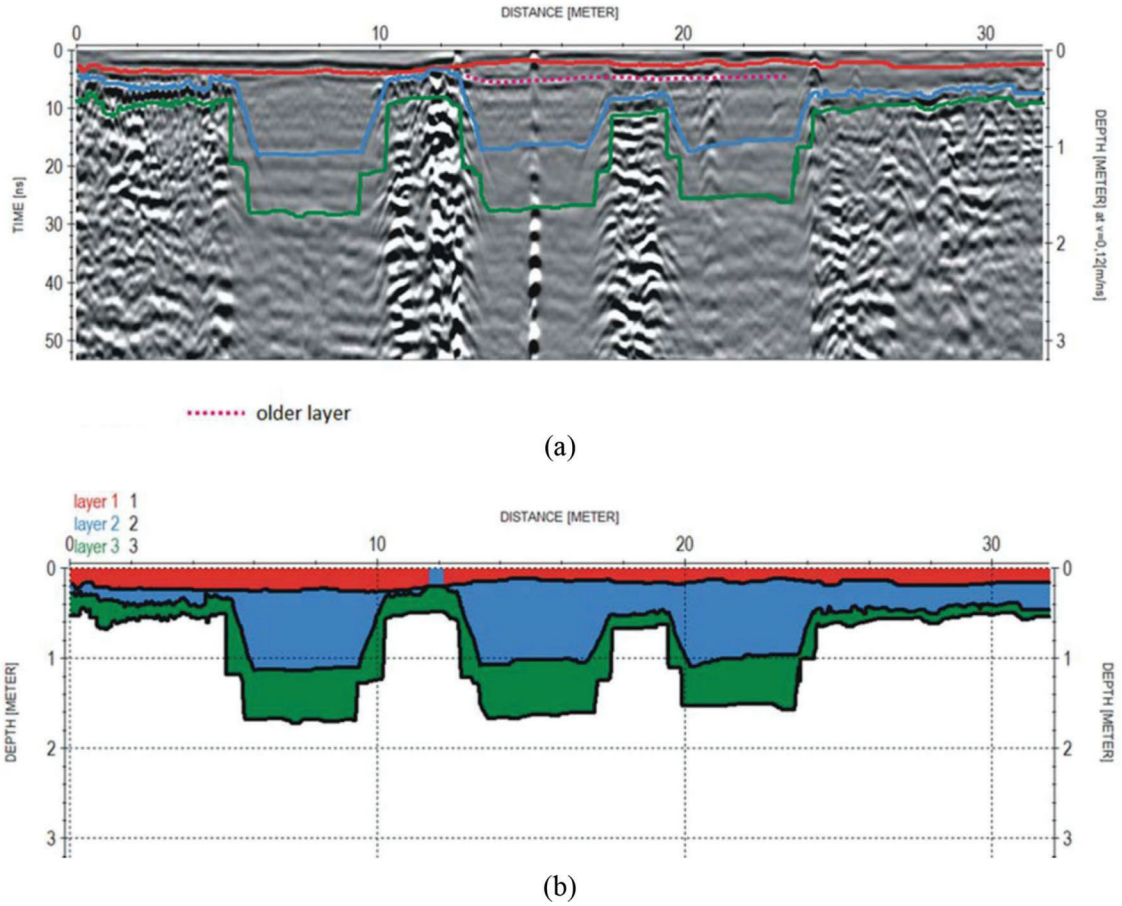

Figure 4.8 GPR test results for profile 2: (a) the radargram result with the detected boundaries in colored lines, and (b) the interpreted results with three different layers below the ground surface (Grinč et al., 2015).

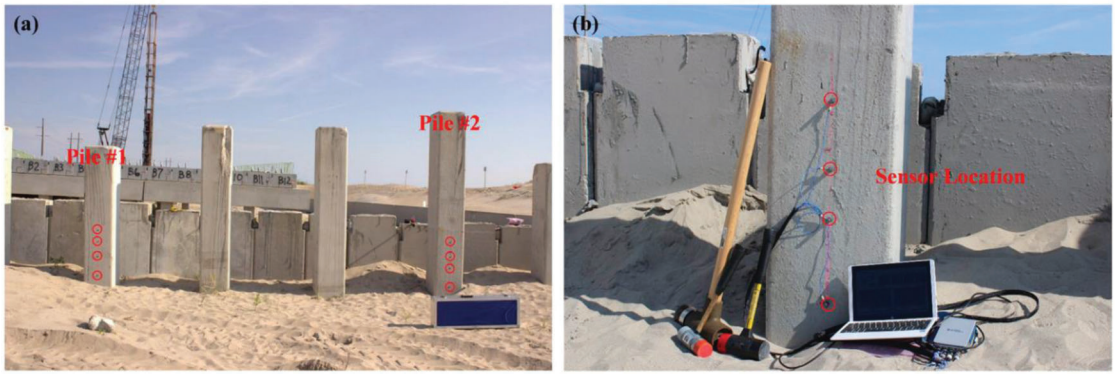

Figure 4.9 Test piles and the bending wave method equipment in the field: (a) embedded test piles (Pile #1 and Pile #2), and (b) data acquisition system, different types of hammers and sensors attached on the upper part of a test pile (Samu & Guddati, 2020).

TABLE 4.5
The estimated lengths of the piles and corresponding errors (Samu & Guddati, 2020)

Test Pile	Estimated Length from the Sensor Midpoint to the Pile Tip (ft)	Estimated Total Length of the Pile (ft)	Actual Length of the Pile (ft)	Error (%)
Pile #1	50.5	55.1	56	-1.6
Pile #2	50.2	57.1	56	2

named Pile #1 and Pile #2 in the field, and Figure 4.9b shows the equipment (data acquisition, hammers and sensors attached on the upper segment of the pile) used for testing. The test piles have the same dimensions: the width of the square cross section of the pile is 16 inches and the length of the pile is 56 ft. The distance from the head of Pile #1 to its bottommost sensor is 5.71 ft, and the distance from the head of Pile #2 to the bottommost sensor is 7.87 ft. Four sensors were attached at different vertical locations on the upper segment of each pile, as shown in Figure 4.9b, and different pairs of sensors were used for the tests. Different types of hammers were also used for each test. In the data analyses, the density and Poisson's ratio of the concrete were assumed to be 150 pcf (2,400 kg/m^3) and 0.15, respectively.

Table 4.5 shows the estimated lengths of the test piles by using the modified EDAR method, and the corresponding errors. The estimated lengths of Pile #1 and Pile #2 were 55.1 ft and 57.1 ft, respectively, and the corresponding errors were -1.6% and 2%, respectively. This example clearly shows that the bending wave method using the modified EDAR method can accurately estimate the lengths of existing pile foundations.

5. CAPACITY ESTIMATION OF REUSED AND NEW FOUNDATIONS

5.1 Framework for Capacity Estimation of Existing Foundations

Estimation of the current capacity of existing foundations is one of the major challenges for foundation reuse because estimating the capacity of existing foundations is different from doing so for new foundations for the following two main reasons.

- The level of uncertainty in capacity estimation is highly dependent on the reliability of inspection results and historical records. The reliability of the obtained as-built geometry of existing foundations from the inspection is highly dependent on inspection methods. The reliability of historical records also depends on the type of documentation. The estimated capacity from the original plan drawings and the estimated capacity from the historical records of applied loads and observed performance of existing foundations have different levels of uncertainties.
- The deterioration of existing foundation elements and other time-related effects (e.g., pile set-up and densification of soil near existing foundations) can decrease or increase the capacity of existing foundations over time. This needs to be explicitly accounted for.

The current capacity of existing foundations can be estimated from consideration of some of the following.

1. Historical records (original plan drawings, construction records, as-built plans showing the geometry of existing foundations or inspection records).
2. Results of inspection or structural integrity evaluations.
3. Site investigation data.
4. Load tests.

Historical records include original plan drawings, which typically have design bearing pressures for shallow foundations and design loads for deep foundation elements. Ultimate foundation resistances can be estimated by multiplying these loads by design factors of safety (or resistance factors) if the factors used in the original design calculations are known. The RuFUS handbook (Butcher et al., 2006) recommends checking

the original design calculations. If pile driving logs are available for driven pile foundations, pile dynamic formulas can be used to estimate the capacity of existing foundations. If previous load test data is available, the capacity of existing foundations at the time of testing can be directly determined. Possible decrease in capacity due to scour, down drag, loss of soils near the foundation or deterioration in the foundation, and possible increase in capacity due to set-up or consolidation of the soil supporting the foundation need to be considered. Capacity estimation following these approaches can be combined with existing foundation capacity estimation using current design methods with consideration of inspection results and site investigation data. Capacity estimation based on analyses of historical records is easy and inexpensive if the available data is complete. However, performing load tests on existing foundations and using current design equations (such as the methods of foundation design developed over the years at Purdue (Han et al., 2015; Han, Ganju, et al., 2019, 2020; Han, Prezzi, et al., 2017; Salgado, 2008, 2022a; Salgado et al., 2017) and other methods) can produce more reliable and accurate estimations of the current capacity of existing foundations. Historical records can be used for a preliminary estimation of the capacity of existing foundations.

Based on the results of inspections of the existing foundations and establishment of the current soil profile based on recently performed *in situ* tests, the capacity of existing foundations can be estimated using current design equations. In this case, reliable data from foundation inspection and site investigation is necessary. The uncertainty in capacity estimation depends on the reliability of the data from the inspection and site investigation. Numerical analyses can also be performed to accurately estimate the current capacity of existing foundations. Design equations and/or numerical analyses can account for the effects of foundation deterioration and/or time on the estimated capacity of existing foundations.

The most reliable method to predict the capacity of existing foundation is by performing static and/or dynamic load tests. If possible, the superstructure or other components of the foundation elements (e.g., pile cap and adjacent piles) can be used to provide the reaction forces for the static load tests. In this approach, the measured capacity of the existing foundations includes any effects due to deterioration or time, but access to the upper segments of the existing foundations and sufficient space for testing are necessary.

Table 5.1 summarizes the required data, and pros and cons of capacity estimation methods for existing foundations. Figure 5.1 shows a flow chart that can be used to estimate the capacity of existing foundations.

5.2 Nominal Capacity Estimation of Existing and New Foundations

5.2.1 Load Tests

5.2.1.1 Plate load tests. The bearing capacity of existing and new shallow foundations can be estimated by performing plate load tests, following ASTM D1194. The plate load tests should be performed near the shallow foundation of interest. Site investigation data should guarantee that the soil profile below which the plate load test is performed is similar to the one below the shallow foundation. When the plate load test results are used for the capacity estimation of shallow foundations, scale effects should also be considered (Loukidis & Salgado, 2011).

5.2.1.2 Static and dynamic load tests. The capacity of existing and new piles can be estimated by performing static and/or dynamic load tests on test piles that have the same dimensions and materials and are constructed in the same manner as the pile of interest. If possible, static and/or dynamic load tests can be performed directly on the pile of interest but, access to the upper segments of the pile and sufficient space for testing are necessary.

According to (AASHTO, 2020), a static pile load test should be performed following ASTM D1143 with the quick load test procedure. For driven piles, (AASHTO, 2020) recommends that the static pile load test be performed at least 5 days after driving unless it is approved by the engineer of record. Table 5.2 summarizes the methods of nominal pile capacity determination from static load test results suggested by (AASHTO, 2020).

TABLE 5.1
Methods that can be used to determine the capacity of existing foundations

Methods	Required Data	Advantages	Limitations
Analyzing Historical Records	Original plan drawings: Design guidelines and specifications considered during the initial construction Construction records (pile driving logs)	Easy and inexpensive	Data can be limited and incomplete; effects of deterioration and time on capacity need to be considered separately
Using Current Design Methods Based on Inspection Results and Site Investigation Data	Inspection results of existing foundations (type, as-built geometry and structural integrity) Information on current soil profile	Reasonably reliable	Reliable data are necessary
Performing Load Tests	Load test results	Reasonably reliable	It is relatively expensive and limited by site accessibility

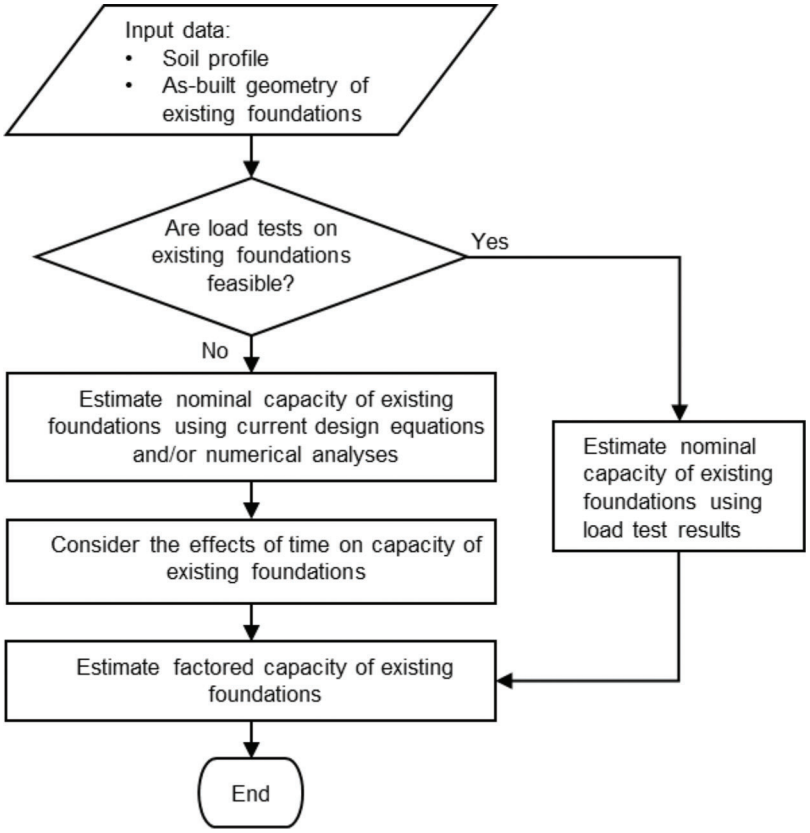

Figure 5.1 Flow chart to estimate the capacity of existing foundations.

TABLE 5.2
Nominal capacity determination from static load test results for piles (AASHTO, 2020)

Pile Type	Pile Diameter (or Length of Side for Square Piles)	Capacity Determination Method
Driven Piles	24.0 inches or less	Davisson method
	Greater than 24.0 inches and less than 36.0 inches	Linear interpolation between the criteria determined for diameters of 24.0 and 36.0 inches
	Larger than 36.0 inches	Capacity at the pile head settlement of s_f [inches] $= \frac{QL}{12AE} + \frac{B}{2.5}$
Drilled Shafts	–	Capacity at plunging; otherwise, the capacity at the gross settlement or uplift of $0.05B$

Note: Q = test load (kips), L = pile length (ft), A = cross-sectional area of the pile (ft^2), E = Young's modulus of the pile (ksi), and B = pile diameter (or the length of side for square piles) (ft).

It should be stressed that such methods are not linked by (AASHTO, 2020) to specific methods of determination of axial capacity. It is better to estimate capacity from load tests by using a definition consistent with the method of design that was or will be used to design the piles.

For existing piles, the hydraulic jack can be installed between the pile and the pile cap after removing a section of the pile to apply static loads. In this case, the superstructure and/or the other parts of foundation elements (e.g., pile cap and adjacent piles) can be used to provide the reaction forces after checking the structural stability of the superstructure and/or foundation elements.

According to AASHTO (2020), dynamic load tests should be performed following ASTM D4945 for restrike tests. The nominal capacity of the pile can be determined by performing a signal matching analysis based on the dynamic load test results.

5.2.1.3 Future load tests. The capacity of existing foundations can be estimated by performing a "future load test" (Agrawal et al., 2018), where the estimated additional future load is applied on the bridge deck.

The future load test does not require access to individual foundation elements; however, it can be performed only when the existing superstructure can handle loads large enough to transfer the desired additional loads to the foundations. From this type of test, the total capacity of the entire foundation system can be estimated but not the capacity of the individual piles, unless individual piles had been instrumented. The nominal capacity of the entire foundation system can be determined by the applied load under which one of the piles fails or the settlement of one of the piles reaches the settlement criteria. If possible, strain gauges can be installed on individual piles to monitor the loads transferred to the individual piles during the test. The steps in a future load test are as follows (Agrawal et al., 2018).

1. Estimate the maximum safe test load for the superstructure and the substructure elements to be tested. The maximum safe test load should be less than the load under which any one of the elements of the structure fails.
2. Determine the current load and estimate the additional load on the existing foundations.
3. Apply the test load on the bridge deck incrementally following standard static load test procedures.

5.2.2 Design Equations

5.2.2.1 Shallow foundations. The nominal capacity R_n of a shallow foundation can be expressed by the unit bearing capacity q_{bL} as

$$R_n = q_{bL} A \qquad \text{(Eq. 5.1)}$$

where A is the cross-sectional area of the footing. The unit bearing capacity q_{bL} can be determined by the bearing capacity equation (Meyerhof, 1951; Salgado, 2022a; Terzaghi, 1943) as

$$q_{bL} = cN_c(s_c d_c i_c b_c g_c) + q_0 N_q(s_q d_q i_q b_q g_q) + \frac{1}{2}\gamma B N_\gamma (s_\gamma d_\gamma i_\gamma b_\gamma g_\gamma) \qquad \text{(Eq. 5.2)}$$

where N_c, N_q, and N_γ are bearing capacity factors, respectively, corresponding to the cohesive intercept c, the surcharge q_0 acting at the base level of the footing and a representative unit weight γ of the soil below the base of the footing, respectively. The effects of footing shape, embedment depth, load inclination, base inclination, and ground inclination can be considered by multiplication of each bearing capacity factor by shape, depth, load inclination, base inclination, and ground inclination factors, which are denoted in Equation 5.2 by the letters s, d, i, b, and g with subscripts indicating whether they apply to the c, q_0 or γ term of the bearing capacity equation. Table 5.3 shows some design equations for the bearing capacity factors for sand and clay.

Table 5.4, Table 5.5, and Table 5.6 show commonly used expressions for the shape factor, depth factor, and load, base and ground inclination factors for sand, respectively. Table 5.7 shows commonly used expressions for the shape, depth, and load inclination factors for clay.

In AASHTO (2020), the recommended method to calculate the nominal bearing resistance of a footing, in ksf, is:

$$q_n = cN_{cm} + \gamma_q D_f N_{qm} C_{wq} + 0.5\gamma_f B N_{\gamma m} C_{wy} \qquad \text{(Eq. 5.3)}$$

in which,

$$N_{cm} = N_c s_c i_c$$
$$N_{qm} = N_q s_q d_q i_q$$
$$N_{\gamma m} = N_\gamma s_\gamma i_\gamma \qquad \text{(Eq. 5.4)}$$

In Equation 5.3 and Equation 5.4, c is the undrained shear strength in ksf; N_c is the cohesion term bearing capacity factor (used in undrained loading); N_q is the surcharge term bearing capacity factor; N_γ is the unit weight term factor; γ_q is the total unit weight of soil above the bearing depth of the footing (kcf); γ_f is the total unit weight of soil below the bearing depth of the footing (kcf); D_f is the footing embedment depth (ft), B is the footing width (ft); C_{wq} and $C_{w\gamma}$ are correction

TABLE 5.3
Bearing capacity factors used for sand and clay (Salgado, 2022a)

Soil/Analysis	Bearing Capacity Factor
Sand: effective stress analysis of purely frictional soil ($c = 0$, $\phi > 0$, $\psi = \phi$) Associated flow rule	$N_q = \frac{1+\sin\phi}{1-\sin\phi} e^{\pi \tan\phi}$ $N_\gamma = 1.5(N_q - 1)\tan\phi$ $N_\gamma = (N_q - 0.6)\tan(1.33\phi)$
Sand: effective stress analysis of purely frictional soil ($c = 0$, $\phi > 0$, $\psi < \phi$) Non-associated flow rule	$N_q = \frac{1+\sin\phi}{1-\sin\phi} e^{F(\phi,\psi)\pi \tan\phi}$ $F(\phi,\psi) = 1 - \tan\phi[\tan(0.8(\phi-\psi))]^{2.5}$ $N\gamma = (N_q - 0.6)\tan(1.33\phi)$
Sand: N_γ based on relative density	$N_\gamma = 2.82 \exp\left(3.64 \frac{D_R}{100\%}\right)\left(\frac{\gamma B}{p_A}\right)^{-0.4}$
Clay: total stress analysis with soil modeled as purely cohesive ($c = s_u$ and $\phi = 0$)	$N_c = 2 + \pi$

Note:
ϕ is the friction angle, ψ is the dilatancy angle, D_R is the relative density of sand, s_u is the undrained shear strength of clay, B is the width of footing, and p_A is a reference pressure (= 100 kPa).

TABLE 5.4
Commonly used expressions for shape factors of sand (Salgado, 2022a)

c term	q_0 term	γ term
(Meyerhof, 1963)		
$s_c = 1 + 0.2\left(\frac{1+\sin\phi}{1-\sin\phi}\right)\frac{B}{L}$	$s_q = 1 + 0.1\left(\frac{1+\sin\phi}{1-\sin\phi}\right)\frac{B}{L}$	$s_\gamma = 1 + 0.1\left(\frac{1+\sin\phi}{1-\sin\phi}\right)\frac{B}{L}$
(Hansen, 1970)		
$s_c = 1 + \cos\phi\frac{N_q}{N_c}\frac{B_{eff}}{L_{eff}}$	$s_q = 1 + \frac{B_{eff}}{L_{eff}}\sin\phi$	$s_\gamma = 1 - 0.4\frac{B_{eff}}{L_{eff}} \geq 0.6$
(Vesic, 1973)		
$s_c = 1 + \frac{N_q}{N_c}\frac{B}{L}$	$s_q = 1 + \frac{B}{L}\tan\phi$	$s_\gamma = 1 - 0.4\frac{B}{L} \geq 0.6$
(Lyamin et al., 2007)		
NA	$s_q = 1 + \left[(0.098\phi - 1.64) \times \left(\frac{D}{B_{eff}}\right)^{0.7-0.01\phi}\left(\frac{B_{eff}}{L_{eff}}\right)^{1-0.16\left(\frac{D}{B_{eff}}\right)}\right]$ $s_q^{circ} = (1 + 0.0025\phi)s_q$	$s_\gamma = 1 + (0.0336\phi - 1)\frac{B_{eff}}{L_{eff}}$ $s_\gamma^{circ} = (1 + 0.002\phi)s_\gamma$
(Loukidis & Salgado, 2009)		
NA	$s_q^{circ} = 1 + 2.9\tan^2\phi$	$s_\gamma^{circ} = 1 + \left(0.26\frac{1+\sin\phi}{1-\sin\phi} - 0.73\right)$

Note:
B is the footing width, L is the footing length, B_{eff} is the effective width, defined by $B - 2e_B$ where e_B is the load eccentricity in the B direction, L_{eff} is the effective length, defined by $L - 2e_L$ where e_L is the load eccentricity in the L direction, D is the embedment depth, ϕ is the friction angle, and s_q^{circ} and s_γ^{circ} are s_q and s_γ for circular footings, respectively. ϕ for Lyamin et al. (2007) factors is in degrees.

TABLE 5.5
Commonly used expressions for depth factors of sand (Salgado, 2022a)

c term	q_0 term	γ term
(Meyerhof, 1963)		
$d_c = 1 + 0.2\sqrt{\frac{1+\sin\phi}{1-\sin\phi}}\frac{D}{B}$	$d_q = 1 + 0.1\sqrt{\frac{1+\sin\phi}{1-\sin\phi}}\frac{D}{B}$	$d_\gamma = 1 + 0.1\sqrt{\frac{1+\sin\phi}{1-\sin\phi}}\frac{D}{B}$
(Hansen, 1970)		
$D/B_{eff} \leq 1$ $d_c = 1 + 2(1-\sin\phi)^2\frac{N_q}{N_c}\frac{D}{B_{eff}}$	$d_q = 1 + 2\tan\phi(1-\sin\phi)^2\frac{D}{B_{eff}}$	$d_\gamma = 1$
$D/B_{eff} > 1$ $d_c = 1 + 2(1-\sin\phi)^2\frac{N_q}{N_c}\tan^{-1}\frac{D}{B_{eff}}$	$d_q = 1 + 2\tan\phi(1-\sin\phi)^2\tan^{-1}\frac{D}{B_{eff}}$	$d_\gamma = 1$
(Vesic, 1973)		
$D/B \leq 1$ $d_c = 1 + 0.4\frac{D}{B}$	$d_q = 1 + 2\tan\phi(1-\sin\phi)^2\frac{D}{B}$	$d_\gamma = 1$
$D/B > 1$ $d_c = 1 + 0.4\tan^{-1}\frac{D}{B}$	$d_q = 1 + 2\tan\phi(1-\sin\phi)^2\tan^{-1}\frac{D}{B}$	$d_\gamma = 1$
(Lyamin et al., 2007)		
NA	$d_q = 1 + (0.0036\phi + 0.393)\left(\frac{D}{B_{eff}}\right)^{-0.27}$	$d_\gamma = 1$

Note:
B is the footing width, B_{eff} is the effective width, defined by $B - 2e_B$ where e_B is the load eccentricity in the B direction, D is the embedment depth, and ϕ is the friction angle. ϕ for Lyamin et al. (2007) factors is measured in degrees.

TABLE 5.6
Commonly used load, base, and ground inclination factors for sand (Salgado, 2022a)

c term	q_0 term	γ term
(Meyerhof, 1963)		
$i_c = \left[1 - \frac{\arctan\left(\frac{Q_{tr}}{Q_{ax}}\right)}{90^\circ}\right]^2$	$i_q = \left[1 - \frac{\arctan\left(\frac{Q_{tr}}{Q_{ax}}\right)}{90^\circ}\right]^2$	$i_\gamma = \left[1 - \frac{\arctan\left(\frac{Q_{tr}}{Q_{ax}}\right)}{\phi}\right]^2$
(Hansen, 1970)		
$i_c = i_q - \frac{1-i_q}{N_q - 1}$ $b_c = b_q - \frac{1-b_q}{N_q - 1}$ $g_c = g_q - \frac{1-g_q}{N_q - 1}$	$i_q = \max\left[\left(1 - \frac{0.5Q_{tr}}{Q_{ax} + Ac\cot\phi}\right)^5, 0\right]$ $b_q = \exp(-0.035\alpha_b \tan\phi)$ $g_q = (1 - 0.5\tan\alpha_g)^5$	$i_\gamma = \max\left[\left(1 - \frac{0.7Q_{tr}}{Q_{ax} + Ac\cot\phi}\right)^5, 0\right]$ $b_\gamma = \exp(-0.047\alpha_b \tan\phi)$ $g_\gamma = (1 - 0.5\tan\alpha_g)^5$
(Vesic, 1973)		
$i_c = i_q - \frac{1-i_q}{N_q - 1}$ $b_c = 1 - \frac{2\alpha_b}{(2+\pi)\tan\phi}$ $g_c = i_q - \frac{1-i_q}{(2+\pi)\tan\phi}$	$i_q = \max\left[\left(1 - \frac{Q_{tr}}{Q_{ax} + Ac\cot\phi}\right)^m, 0\right]$ $b_q = \left(1 - \frac{\alpha_b \tan\phi}{57^\circ}\right)^2$ $g_b = (1 - \tan\alpha_g)^2$ $m = \sqrt{m_B^2 + m_L^2}$	$i_\gamma = \max\left[\left(1 - \frac{Q_{tr}}{Q_{ax} + Ac\cot\phi}\right)^{1+m}, 0\right]$ $b_\gamma = \left(1 - \frac{\alpha_b \tan\phi}{57^\circ}\right)^2$ $g_\gamma = (1 - \tan\alpha_g)^2$ $m = \sqrt{m_B^2 + m_L^2}$
(Loukidis et al., 2008)		
NA	–	$i_\gamma = \left(1 - 0.94\frac{\tan\alpha}{\tan\phi}\right)^{(1.5\tan\phi + 0.4)^2}$

Note:
B is the footing width, L is the footing length, Q_{tr} and Q_{ax} are the transverse and axial components of load, respectively, ϕ is the friction angle, c is the cohesion, A is the area of footing base, α, α_b, and α_g are inclination angles of the load, footing base and the ground, respectively, m_B is $(2 + B/L)/(1 + B/L)$ if $Q_{tB} > 0$, otherwise, 0, and m_L is $(2 + L/B)/(1 + L/B)$ if $Q_{tL} > 0$, otherwise, 0 where Q_{tB} and Q_{tL} are the Q_{tr} components in the B and L directions, respectively. m values for Vesic factors may also be used for the Hansen factors if they fall in the $2 < m < 5$ range.

TABLE 5.7
Correction factors for the *c* term in the bearing capacity equation for clay (Salgado, 2022a)

(Meyerhof, 1953, 1963)	(Hansen, 1970)	(Salgado et al., 2004)
$s_c = 1 + 0.2\frac{B}{L}$ $d_c = 1 + 0.2\frac{D}{B}$ for $\frac{D}{B} < 2.5$ $i_c = 1 - 1.3\frac{Q_{tr}}{Q_{ax}}$ for $\frac{Q_{tr}}{Q_{ax}} \le 0.4$	$d_c = 1 + 0.4\frac{D}{B}$ for $\frac{D}{B} \le 1$ $d_c = 1 + 0.4\tan^{-1}\frac{D}{B}$ for $\frac{D}{B} > 1$	$s_c = 1 + C_1\frac{B}{L} + C_2\sqrt{\frac{D}{B}}$ $d_c = 1 + 0.27\sqrt{\frac{D}{B}}$

Note:
B is the footing width, L is the footing length, D is the embedment depth, Q_{tr} and Q_{ax} are the transverse and axial components of load, respectively, and C_1 and C_2 are functions of B/L, given in Table 5.8.

factors to account for the location of the groundwater table; d_q is the depth correction factor to account for the shearing resistance along the failure surface passing through cohesionless material above the bearing elevation; and i_c, i_γ, and i_q are load inclination factors. Equation 5.3 is the complete formula to calculate the bearing capacity of the footing. However, in practice, not all the terms and parameters are used for any given problem.

For $\phi_f = 0$ degrees,

$$i_c = 1 - nH/cBLN_c \qquad \text{(Eq. 5.5)}$$

For $\phi_f > 0$,

$$i_c = i_q - \left[(1 - i_q)/(N_q - 1)\right] \qquad \text{(Eq. 5.6)}$$

TABLE 5.8
Regression constants C_1 and C_2 (Salgado et al., 2004) in shape factor (Salgado, 2022a)

B/L	C_1	C_2
1 (circle)	0.163	0.210
1 (square)	0.125	0.219
0.50	0.156	0.173
0.33	0.159	0.137
0.25	0.172	0.110
0.20	0.190	0.090

Note:
B is the footing width, and L is the footing length.

in which,

$$i_q = \left[1 - \frac{H}{V + cBL\cot\phi_f}\right]^n$$
$$i_\gamma = \left[1 - \frac{H}{V + cBL\cot\phi_f}\right]^{n+1} \quad \text{(Eq. 5.7)}$$

and

$$n = [(2 + L/B)/(1 + L/B)]\cos^2\theta + [(2 + B/L)/(1 + B/L)]\sin^2\theta \quad \text{(Eq. 5.8)}$$

where B is the footing width in ft, L is the footing length in ft, H is the unfactored horizontal load in kips, V is the unfactored vertical load in kips, θ is the projected direction of the load in the plane of the footing, measured from the side of length L, in degrees, and ϕ_f is the internal friction angle of the soil.

The bearing capacity factors can be found in Table 5.9. The shape correction factors are shown in Table 5.11. The groundwater-related coefficients C_{wq} and $C_{w\gamma}$ are shown in Table 5.10.

The depth factor d_q can be written as:

$$d_q = 1 + 2\tan\phi_f(1 - \sin\phi_f)^2 \arctan\left(\frac{D_f}{B}\right) \quad \text{(Eq. 5.9)}$$

where $\arctan\frac{D_f}{B}$ is given in radians.

AASHTO (2020) also recommended semiempirical procedures to determine the bearing capacity for footings in sand based on SPT data and CPT data. The equations are summarized in Table 5.12.

5.2.2.2 Piles. The nominal capacity R_n of a single pile can be expressed by the sum of the nominal base capacity R_{bn} and the nominal shaft capacity R_{sn}, which can be expressed as

$$R_{bn} = Q_{b,ult} = q_{b,ult}A_b \quad \text{(Eq. 5.10)}$$

$$R_{sn} = Q_{sL} = \sum_{i=1}^{n} q_{sL,i}A_{s,i} \quad \text{(Eq. 5.11)}$$

where $Q_{b,ult}$ is the ultimate base resistance, Q_{sL} is the limit shaft resistance, $q_{b,ult}$ is the ultimate unit base resistance, A_b is the area of the pile base, $q_{sL,i}$ is the unit limit shaft resistance of layer i, $A_{s,i}$ is the area of pile shaft of layer i, and n is the number of layers along the pile shaft. The unit base and shaft resistances in Equation 5.10 and Equation 5.11 can be determined using a variety of design equations including both property-based and *in situ* test-based methods.

AASHTO (2020) suggests the use of some methods to estimate the shaft resistance and base resistance for both driven piles and drilled shafts. Table 5.13 summarizes the design equations for shaft resistance for driven piles suggested by AASHTO (2020) (note that q_s = unit shaft resistance in ksf).

Table 5.14 summarizes the design equations for base resistance for driven piles suggested by AASHTO (2020). The design equations suggested by AASHTO (2020) for drilled shafts can be found in Table 5.15.

Table 5.16 and Table 5.17 provides some recently proposed design equations for driven piles in sand and clay, respectively, and Table 5.18 and Table 5.19 provides design equations for drilled shafts in sand and clay, respectively.

TABLE 5.9
Bearing capacity factors (AASHTO (2020) Table 10.6.3.1.2a-1)

ϕ_f	N_c	N_q	N_γ	ϕ_f	N_c	N_q	N_γ
0	5.14	1	0	23	18.1	8.7	8.2
1	5.4	1.1	0.1	24	19.3	9.6	9.4
2	5.6	1.2	0.2	25	20.7	10.7	10.9
3	5.9	1.3	0.2	26	22.3	11.9	12.5
4	6.2	1.4	0.3	27	23.9	13.2	14.5
5	6.5	1.6	0.5	28	25.8	14.7	16.7
6	6.8	1.7	0.6	29	27.9	16.4	19.3
7	7.2	1.9	0.7	30	30.1	18.4	22.4
8	7.5	2.1	0.9	31	32.7	20.6	26
9	7.9	2.3	1	32	35.5	23.2	30.2
10	8.4	2.5	1.2	33	38.6	26.1	35.2
11	8.8	2.7	1.4	34	42.2	29.4	41.1
12	9.3	3	1.7	35	46.1	33.3	48
13	9.8	3.3	2	36	50.6	37.8	56.3
14	10.4	3.6	2.3	37	55.6	42.9	66.2
15	11	3.9	2.7	38	61.4	48.9	78
16	11.6	4.3	3.1	39	67.9	56	92.3
17	12.3	4.8	3.5	40	75.3	64.2	109.4
18	13.1	5.3	4.1	41	83.9	73.9	130.2
19	13.9	5.8	4.7	42	93.7	85.4	155.6
20	14.8	6.4	5.4	43	105.1	99	186.5
21	15.8	7.1	6.2	44	118.4	115.3	224.6
22	16.9	7.8	7.1	45	133.9	134.9	271.8

TABLE 5.10
Coefficients C_{wq} and $C_{w\gamma}$ for various groundwater depths (AASHTO (2020) Table 10.6.3.1.2a-2)

Ground Water Table Depth D_w	C_{wq}	$C_{w\gamma}$
0	0.5	0.5
D_f	1	0.5
$>1.5B + D_f$	1	1

TABLE 5.11
Shape correction factors (AASHTO (2020) Table 10.6.3.1.2a-3)

Factor	Friction Angle	Cohesion Term (s_c)	Unit Weight Term (s_γ)	Surcharge Term (s_q)
Shape Factors s_c, s_γ, s_q	$\phi_f = 0$	$1+\left(\frac{B}{5L}\right)$	1.0	1.0
	$\phi_f > 0$	$1+\left(\frac{B}{L}\right)\left(\frac{N_q}{N_c}\right)$	$1-0.4\left(\frac{B}{L}\right)$	$1+\left(\frac{B}{L}\tan\phi_f\right)$

TABLE 5.12
Semi-empirical procedures to determine the bearing resistance of spread footings in sand suggested by AASHTO (2020)

Method	Equations
Based on SPT Data	$q_n = \frac{\overline{N1_{60}}B}{5}\left(C_{wq}\frac{D_f}{B}+C_{w\gamma}\right)$ $\overline{N1_{60}}$ q_n is the nominal bearing resistance of sand in ksf. $\overline{N1_{60}}$ q_n is the average corrected SPT blow counts over a depth ranging from the bottom of the footing to 1.5B below the bottom of the footing. B is the footing width in ft. C_{wq} and $C_{w\gamma}$ are correction factors to account for the location of the groundwater table as specified in Table 5.10. D_f is the footing embedment depth taken to the bottom of the footing (ft).
Based on CPT Data	$q_n = \frac{\overline{q_c}B}{40}\left(C_{wq}\frac{D_f}{B}+C_{w\gamma}\right)$ $\overline{q_c}$ is the average cone tip resistance within a depth range B below the bottom of the footing (ksf). C_{wq} and $C_{w\gamma}$ are correction factors to account for the location of the groundwater table as specified in Table 5.10. D_f is the footing embedment depth taken to the bottom of the footing (ft).

For individual piles in pile groups, group efficiency should be multiplied to the nominal capacity R_n of individual piles to consider the interaction between adjacent piles within a group. Table 5.20 provides the group efficiencies suggested by (AASHTO, 2020).

5.2.2.3 Pile cap capacity. If the pile cap is in solid contact with sand, the contribution of the pile cap capacity can be considered in capacity estimation for the pile group. Although no state DOT has decided to consider the contribution of cap capacity towards total foundation capacity, it is important to study what it might be so that, in the future, it may be considered in substructure design. In this report, the pile cap capacity Q_{cap} is proposed based on a series of rigorous numerical simulation results shown in Chapter 2 as

$$Q_{cap} = q_{cap}A_{net} \qquad \text{(Eq. 5.12)}$$

where A_{net} is the net area of contact between the pile cap and the soil, which can be determined from $[A_{cap} - \sum_{i=1}^{n} A_{b,i}]$ with the cross-sectional area A_{cap} of the pile cap, area of the i^{th} pile base $A_{b,i}$, and the total number n of piles in a pile group; and q_{cap} is the unit bearing capacity of the pile cap, given by

$$q_{cap} = \frac{1}{2}\gamma' B_{cap} N_\gamma^{cap} S_\gamma^{cap} \qquad \text{(Eq. 5.13)}$$

where γ' is the effective unit weight of the soil (= buoyant unit weight of the soil), B_{cap} is the width of the pile cap, N_γ^{cap} is the bearing capacity factor for the pile cap and s_γ^{cap} is the shape factor for the pile cap. The bearing capacity factor N_γ^{cap} and the shape factor s_γ^{cap} can be determined by

$$N_\gamma^{cap} = a\ \exp\left(2.33\frac{D_R}{100\%}\right)\left(\frac{\gamma' B_{cap}}{p_A}\right)^{-0.6} \qquad \text{(Eq. 5.14)}$$

$$S_\gamma^{cap} = \exp\left(-2.58\frac{B_{cap}}{L_{cap}}\right) \qquad \text{(Eq. 5.15)}$$

where the constant a is equal to 3.5 for a settlement of 2 inches and 5.9 for a settlement of 4 inches, and L_{cap} is the length of the pile cap.

Table 5.21 and Table 5.22 show comparisons of unit cap capacities in uniform loose and dense sands from the simulation results and the proposed design equations (Equation 5.13–Equation 5.15). The considered relative densities for loose and dense sands are 40% and 80%, respectively. Different group configurations (1×5, 2×5, and 3×5), pile diameters B (14 and 23.6 inches), pile-to-pile spacings (3B and 5B), pile-to-cap edge distances (2B and 6B) and settlements (2 and 4 inches) were considered for comparison. For pile groups with various group configurations, pile diameters, pile spacings and pile-to-cap edge distances in loose sand,

TABLE 5.13
Design equations for shaft resistance q_s for driven piles suggested by AASHTO (2020)

Method	Equations	Comments
α-Method	$q_s = \alpha s_u$ Where, s_u is the undrained shear strength of clay in ksf, and α can be found in Figure 10.7.3.8.6b-1 in AASHTO (2020).	–
β-Method	$q_s = \beta \sigma'_{v0}$ Where, σ'_{v0} is the vertical effective stress in ksf, and β can be found in Figure 10.7.3.8.6c-1 in AASHTO (2020).	β-method works best for piles in normally consolidated soil and slightly over consolidated soil.
λ-Method	$q_s = \lambda(\sigma'_v + 2s_u)$ Where, $\sigma'_v + 2s_u$ is the passive earth pressure in ksf, and λ can be found in Figure 10.7.3.8.6d-1 in AASHTO (2020).	
Nordlund/Thurman Method	$q_s = K_\delta C_F \sigma'_v \frac{\sin(\delta+\omega)}{\cos(\omega)}$ Where, K_δ is the coefficient of lateral earth pressure at mid-point of soil layer, which can be obtained from Figures 10.7.3.8.6f-1 through 10.7.3.8.6f-4 in AASHTO (2020). C_F is the correction factor for K_δ when $\delta \neq \phi_f$ with ϕ_f being the internal friction angle, which can be obtained from Figure 10.7.3.8.6f-5 in AASHTO (2020). σ'_v is the effective overburden stress at midpoint of soil layer under consideration in ksf; $_\delta$ is the friction angle between the soil and the pile in degrees, which can be obtained from Figure 10.7.3.8.6f-6 in AASHTO (2020). $_\omega$ is the angle of pile taper from vertical in degrees.	Nordlund/Thurman Method is mainly used for sandy ("cohesionless") soils and gravelly soils.
Using SPT in Sandy ("cohesionless") Soils	For displacement piles: $q_s = \frac{N_{1,60}}{25}$ For non-displacement piles: $q_s = \frac{N_{1,60}}{50}$ where $N_{1,60}$ is the averaged corrected SPT blow count through the pile side.	–
Using CPT in Sandy ("cohesionless") Soils	$R_{sn} = K_{s,c}\left[\sum_{i=1}^{N_1}\left(\frac{L_i}{8D_i}\right) f_{si} a_{si} h_i + \sum_{i=1}^{N_2} f_{si} a_{si} h_i\right]$ Where, $K_{s,c}$ are the correction factors for sand and clay, respectively, which can be obtained from Figure 10.7.3.8.6g-2 in AASHTO (2020). L_i is the depth to middle of length interval at point considered in ft. D_i is the pile width or diameter at the point considered in ft. f_{si} is the unit local sleeve friction resistance from CPT at the point considered in ksf. α_{si} is the pile perimeter at the point considered in ft. h_i is the length interval at the point considered. N_1 is the number of intervals between the ground surface and a point $8D$ below the ground surface; and N_2 is the number of intervals between $8D$ below the ground surface and the tip of the pile.	

Note: q_s = unit shaft resistance in ksf.

the relative error of the proposed equations for the unit cap capacity was in the 0.1%–15% range for a settlement of 2 inches and in the 0.7%–38% range for a settlement of 4 inches. For pile groups in dense sand, the relative error of the unit cap capacity was in the 0.1%–22% range for a settlement of 2 inches, and in the 0%–28% range for a settlement of 4 inches.

5.2.2.4 Consideration of time effects on capacity. The capacity of existing foundations can decrease due to foundation deterioration or damage. The current capacity of existing foundations can be estimated by considering the possible effects of changes in material properties and estimating the extent, level and main causes of any deterioration or damage of the existing

TABLE 5.14
Design equations for tip resistance for driven piles suggested by AASHTO (2020)

Method	Equations	Comments
Tip Resistance in Clayey ("cohesive") Soils	$q_p = 9s_u$ where s_u is the undrained shear strength.	This method suitable for piles in clay.
Nordlund/Thurman Method	$q_p = \alpha_t N'_q \sigma'_v \leq q_L$ Where, α_t is a dimensionless coefficient. N'_q is the bearing capacity factor. σ'_v is the effective overburden stress at pile tip in ksf; and q_L is the limiting unit tip resistance. The value of α_t, N'_q and q_L can be found in Figure 10.7.3.8.6f-7 through Figure 10.7.3.8.6f-9 in AASHTO (2020).	Nordlund/Thurman Method is mainly used for sandy ("cohesionless") soils and gravelly soils.
Using SPT in Sandy ("cohesionless") Soil	$q_p = \frac{0.8(N_{1,60})D_b}{D} \leq q_t$ Where, $N_{1,60}$ is the representative SPT blow count near the pile tip corrected for overburden pressure. D is the pile width or diameter in ft. D_b is the depth of penetration into bearing strata in ft. $q_t = 8N_{1,60}$ for sands in ksf, and $q_t = 6N_{1,60}$ for nonplastic silts in ksf.	
Using CPT in Sandy ("cohesionless") Soil	$q_p = \frac{q_{c1} + q_{c2}}{2}$ q_{c1} and q_{c2} are shown in Figure 10.7.3.86g-1 in AASHTO (2020).	

Note: q_p = unit tip resistance in ksf.

TABLE 5.15
Design equations for drilled shafts from AASHTO (2020)

Soil Type	Equations for Shaft Resistance	Equations for Base Resistance
Clayey ("cohesive") Soil	$q_s = \alpha s_u$ $\alpha = 0.55$ for $\frac{s_u}{p_A} \leq 1.5$ $\alpha = 0.55 - 0.1\left(\frac{s_u}{p_A} - 1.5\right)$ for $1.5 \leq \frac{s_u}{p_A} \leq 2.5$ Where, s_u is the undrained shear strength. p_A is the atmospheric pressure (= 2.12 ksf).	$q_p = N_c s_u \leq 80.0$ ksf $N_c = 6\left[1 + 0.2\left(\frac{Z}{D}\right)\right] \leq 9$ Where, D is the diameter of drilled shaft in ft. Z is the penetration of shaft in ft. s_u is the undrained shear strength in ksf.
Sandy ("cohesionless") Soil	$q_s = \beta\sigma'_v$ $\beta = (1 - \sin\phi'_f)\left(\frac{\sigma'_p}{\sigma'_v}\right)^{\sin\phi'_f} \tan\phi'_f$ $\phi'_f = 27.5 + 9.2\log(N_{1,60})$ $\frac{\sigma'_p}{p_A} = 0.47(N_{60})^m$ where, m = 0.6 for clean quartzitic sands, and 0.8 for silty sand to sandy silts; p_A is the atmospheric pressure; σ'_p is the effective vertical preconsolidation stress; σ'_v is the effective vertical stress at soil layer mid-depth; N_{60} is the SPT N-values; and $N_{1,60}$ is the SPT N-value corrected for effective overburden stress.	$q_p = 1.2N_{60} \leq 60$ ksf where N_{60} is the average SPT blow count in the design zone.

Note: q_s = unit shaft resistance in ksf; and q_p = unit tip resistance in ksf.

TABLE 5.16
State-of-the-art design equations for driven piles in sand

Method and Key References	Limit Unit Shaft Resistance q_{sL}	Ultimate Unit Base Resistance $q_{b,ult}$	Comments
Purdue Method (Han, Ganju, et al., 2019; Salgado, 2022a)	$q_{sL} = (K\sigma'_{v0})\tan\delta_c$ $K = K_{\min} + (K_{\max} - K_{\min})\exp(-\alpha\frac{h}{B})$ $K_{\max} = 0.01\frac{(q_c/p_A)}{\sqrt{\sigma'_{h0}/p_A}}$ h is the distance from the depth being considered to the pile base; $K_{\min} = 0.2$; $\alpha = 0.05$	$q_{b,ult} = (1–0.0058D_R)\ q_{cb,avg}$ $q_{cb,avg}$ is q_c averaged from $1B$ above to $2B$ below the pile base	
ICP Method (Jardine et al., 2005)	$q_{sL} = (\sigma'_{rc} + \Delta\sigma'_{rd})\tan\delta_c$ $\sigma'_{rc} = 0.029q_c\left(\frac{\sigma'_{v0}}{p_A}\right)^{0.13}\left(\max\left[\frac{h}{R},8\right]\right)^{-0.38}$ $\Delta\sigma'_{rd} = 2G\Delta r/R$ $G = q_c\,[0.0203 + 0.00125\eta - 1.216 \times 10^{-6}\eta^2]^{-1}$ $\eta = q_c(p_A\sigma'_{v0})^{-0.5}$ $\Delta r = 0.02$ mm for lightly rusted steel piles; h is the distance from the depth being considered to the pile base.	$q_{b,ult} = \max[0.3,\ 1 - 0.5\log(B/B_{CPT})]q_{cb,avg}$ B_{CPT} is cone diameter = 0.036 m	Intended to predict the pile bearing capacity 10 days after driving for “virgin” piles.
UWA Method (Lehane et al., 2005)	$q_{sL} = \frac{f}{f_c}\left(\sigma'_{rc} + \frac{4G\Delta r}{B}\right)\tan\delta_c$ $\sigma'_{rc} = 0.03q_c\left[\max\left(\frac{h}{B},2\right)\right]^{-0.5}$ $G/q_c = 185\left[\frac{q_c/p_A}{(\sigma'_{v0}/p_A)^{0.5}}\right]^{-0.75}$ $\Delta r = 0.02$ mm $f/f_c = 1$ for compression and 0.75 for tension.	$q_{b,ult} = 0.6\ q_{cb,avg}$	The method is intended to predict the pile bearing capacity measured 10–20 days after driving.
NGI Method (Clausen et al., 2005)	$q_{sL} = \max\left[p_A\left(\frac{z}{z_{base}}\right)\left(\frac{\sigma'_{v0}}{p_A}\right)^{0.25}F_{DR}F_{tip}F_{load}F_{mat}, 0.1\sigma'_{v0}\right]$ $F_{D_R} = 2.1[D^*_R - 0.1]^{1.7}$ $D^*_R = 0.4\ln\left\{\frac{q_c}{22(\sigma'_{v0}p_A)^{0.5}}\right\}$ where z is the depth below the ground surface; z_{base} is the pile base depth; $F_{tip} = 1.6$; $F_{load} = 1.3$ for compression; $F_{mat} = 1.0$ for steel and 1.2 for concrete pile; D^*_R is the nominal relative density, which may be greater than 100%.	$q_{b,ult} = \frac{0.8q_{cb,avg}}{1 + \left\{0.4\ln\left[\frac{q_{cb,avg}}{22(\sigma'_{vb}p_A)^{0.5}}\right]\right\}^2}$ σ'_{vb} is the vertical effective stress at the depth of the pile base.	–
Fugro Method (Kolk et al., 2005)	$q_{sL} = 0.08q_c\left(\frac{\sigma'_{v0}}{p_A}\right)^{0.05}\left(\frac{h}{R}\right)^{-0.9}$ *if* $\frac{h}{R} \geq 4$ $q_{sL} = 0.08q_c\left(\frac{\sigma'_{v0}}{p_A}\right)^{0.05}(4)^{-0.9}\left(\frac{h}{4R}\right)$ *if* $\frac{h}{R} < 4$ h is the distance from the depth being considered to the pile base.	$q_{b,ult} = 8.5p_A\left(\frac{q_{cb,avg}}{p_A}\right)^{0.5}$	The method is intended to predict the pile bearing capacity measured about 10 days after driving.

Note: ϕ_c = critical-state friction angle; σ'_{h0} = initial horizontal effective stress at the depth being considered; B = pile diameter; R = pile radius; p_A = reference stress = 100 kPa; q_c = representative cone resistance of the soil layer; σ'_{v0} = initial vertical effective stress at the depth being considered; δ_c = interface friction angle (ICP and UWA suggest using interface shear tests to determine the value of δ_c; if not feasible, it can also be estimated from the mean particle size (Jardine et al., 2005; Lehane et al., 2005). δ_c can also be determined from the critical-state friction angle in sand by: $\delta_c = 0.9\phi_c$ (Foye et al., 2009; Salgado et al., 2011)); $q_{cb,avg}$ = representative cone resistance at the pile base level.

TABLE 5.17
State-of-the-art design equations for driven piles in clay

Method and Key References	Limit Unit Shaft Resistance q_{sL}	Ultimate Unit Base Resistance $q_{b,ult}$	Comments
Purdue Method (Salgado et al., 2011)	$q_{sL} = \alpha s_u$ $\alpha = 1.28\left(\frac{s_u}{\sigma'_{v0}}\right)^{-0.05}$ $\left[A_1 + (1-A_1)e^{-\left(\frac{\sigma'_{v0}}{p_A}\right)(\phi_c - \phi_{r,\min})A_2}\right]$ A_1 = 0.75 for $\phi_c - \phi_{r,\min} \le 5^\circ$, 0.43 for $\phi_c - \phi_{r,\min} \ge 12^\circ$ and a linearly interpolated value for $5^\circ \le \phi_c - \phi_{r,\min} \le 12^\circ$ $A_2 = 0.64 + 0.4\ ln\left(\frac{s_u}{\sigma'_{v0}}\right)$	$10 s_u$	The method is intended to estimate the shaft resistance after dissipation of the excess pore pressure generated during pile installation.
Purdue Method (Salgado et al., 2011)	$q_{sL} = \alpha s_u$ $\alpha = 1.03\left[A_1 + (1-A_1)e^{-\left(\frac{\sigma'_{v0}}{p_A}\right)(\phi_c - \phi_{r,\min})A_2}\right]$ A_1 = 0.75 for $\phi_c - \phi_{r,\min} \le 5^\circ$, 0.43 for $\phi_c - \phi_{r,\min} \ge 12^\circ$ and a linearly interpolated value for $5^\circ \le \phi_c - \phi_{r,\min} \le 12^\circ$ $A_2 = 0.55 + 0.43\ ln\left(\frac{s_u}{\sigma'_{v0}}\right)$	$10 s_u$	The method is intended to estimate the shaft resistance within a short term (the excess pore pressure generated during pile installation is not fully dissipated).
ICP Method (Jardine et al., 2005)	$q_{sL} = 0.8 K_c \sigma'_{v0} \tan\delta_c$ $K_c = \left[2.2 + 0.016\,OCR - 0.870\,\Delta I_{vy}\right] OCR^{0.42}\left(\max\left[\frac{h}{R}, 8\right]\right)^{-0.20}$ $\Delta I_{vy} = \log_{10} S_t$ where OCR is the overconsolidation ratio; h is the distance from the depth being considered to the pile base and S_t is the sensitivity of clay = s_u/s_{ur}, s_{ur} being the undrained shear strength of disturbed samples.	For undrained loading: $q_{b,ult} = 0.8\ q_{cb,avg}$ For drained loading: $q_{b,ult} = 1.3\ q_{cb,avg}$	The method is intended to estimate the shaft resistance after dissipation of the excess pore pressure generated during pile installation. Ring shear interface tests are recommended to determine the interface friction angle δ_c.
UWA (Lehane et al., 2013)	$q_{sL} = 0.055 q_t \left[\max\left(\frac{h}{R}, 1\right)\right]^{-0.2}$ or $q_{sL} = \frac{0.23 q_t \left[\max\left(\frac{h}{R}, 1\right)\right]^{-0.2}}{\left(\frac{q_t}{\sigma'_{v0}}\right)^{0.15}} \tan\delta_c$ h is the distance from the depth being considered to the pile base.	N/A	Two equations were proposed for the shaft resistance and the first one is more reliable. Time effects were not mentioned.
NGI (Karlsrud et al., 2005)	For NC clays with $(s_u/\sigma'_{v0}) < 0.25$: $q_{sL} = \alpha^{NC} s_u$ $\alpha^{NC} = 0.32\ (PI–10)^{0.3}$ $(0.20 \le \alpha^{NC} \le 1.0)$ For OC clays with $(s_u/\sigma'_{v0}) > 1.0$: $q_{sL} = \alpha\ s_u\ F_{tip}$ $\alpha = 0.5\ (s_u/\sigma'_{v0})^{-0.3}$ $F_{tip} = 0.8 + 0.2\ (s_u/\sigma'_{v0})^{0.5}$ for closed-ended pipe piles $(1.0 \le F_{tip} \le 1.25)$ For clays with $0.25 < (s_u/\sigma'_{v0}) < 1.0$: α is determined by linear interpolation between the above two cases.	$9 s_u$	The calculated shaft resistance corresponds to a time of 100 days after the initial driving. s_u is recommended to be determined from unconsolidated undrained (UU) compression tests.
Fugro (Van Dijk & Kolk, 2011; Kolk & der Velde, 1996)	$q_{sL} = \alpha s_u$ $\alpha = 0.9\left(\frac{L-z}{B}\right)^{-0.2}(s_u/\sigma'_{v0})^{-0.3} \le 1$	$q_{b,ult} = 0.7\ (q_t - \sigma_{v0})$	The method for shaft resistance generally predicts long-term resistance.

Note: ϕ_c = critical-state friction angle; $\phi_{r,min}$ = minimum residual-state friction angle; PI = plasticity index; σ'_{h0} = initial horizontal effective stress at the depth being considered; σ'_{v0} = initial vertical effective stress at the depth being considered; σ_{v0} = initial vertical total stress at the depth being considered; L = pile length; z = depth being considered; B = pile diameter; R = pile radius; q_c = cone resistance at the depth being considered; $q_t = q_c + (1\text{-}a)u_2$, where a = cone area ratio and u_2 = pore pressure measured behind the cone tip; s_u = undrained shear strength of clay; δ_c = interface friction angle.

TABLE 5.18
State-of-the-art design equations for drilled shafts in sand

Method and Key References	Limit Unit Shaft Resistance q_{sL}	Ultimate Unit Base Resistance $q_{b,ult}$	Comments
Purdue Method (Han, Salgado, et al., 2017; Loukidis & Salgado, 2008; Salgado, 2006; Salgado et al., 2011; Salgado & Prezzi, 2007)	$q_{sL} = K\,\sigma'_{v0}\tan\phi_c$ (1) $K = K_0 0.7\exp\left[\left\{0.0114-0.0022\ln\left(\frac{\sigma'_{v0}}{p_A}\right)\right\}D_R\right]$ or (2) $K = \frac{K_0}{e^{0.2\sqrt{K_0-0.4}}}C_1 \exp\left[\frac{D_R}{100}\left\{1.3-0.2\ln\left(\frac{\sigma'_{v0}}{p_A}\right)\right\}\right]$ or (3) $K = \frac{K_0}{e^{0.3\sqrt{K_0-0.4}}}0.67 \exp\left\{\frac{D_R}{100}\left[1.5-0.35\ln\left(\frac{\sigma'_{v0}}{p_A}\right)\right]\right\}$ $D_R(\%) = \frac{\ln\left(\frac{q_c}{p_A}\right)-0.4947-0.1041\phi_c-0.841\ln\left(\frac{\sigma'_{h0}}{p_A}\right)}{0.0264-0.0002\phi_c-0.0047\ln\left(\frac{\sigma'_{h0}}{p_A}\right)} \le 100\%$ C_1 = 0.7 for clean sand.	(1) $q_{b,ult} = 0.23e^{-0.0066D_R}q_{cb,avg}$ or (2) $\frac{q_{b,ult}}{p_A} = 62\left(\frac{D_R}{100\%}\right)^{1.83}\left(\frac{\sigma'_{h0}}{p_A}\right)^{0.4}$ Second equation is applicable for $L/B < 50$.	Third K is used. First $q_{b,ult}$ is used when CPT is available; otherwise, second $q_{b,ult}$ is used.

Note: L = pile length; B = pile diameter; ϕ_c = critical-state friction angle; σ'_{h0} = initial horizontal effective stress at the depth being considered; p_A = reference stress = 100 kPa; q_c = representative cone resistance of the soil layer; σ'_{v0} = initial vertical effective stress at the depth being considered; $q_{cb,avg}$ = representative cone resistance at the pile base level; K_0 = coefficient of lateral earth pressure at-rest; D_R = relative density of sand.

TABLE 5.19
State-of-the-art design equations for drilled shafts in clay

Method and Key References	Limit Unit Shaft Resistance q_{sL}	Ultimate Unit Base Resistance $q_{b,ult}$	Comments
Purdue Method (Chakraborty et al., 2013; Salgado, 2006)	(1) $q_{sL} = 0.4\left[1-0.12\ln\left(\frac{s_u}{p_A}\right)\right]s_u$ or (2) $q_{sL} = \left(\frac{s_u}{\sigma'_{v0}}\right)^{-0.05}\left[A_1+(1-A_1)e^{-\left(\frac{\sigma'_{v0}}{p_A}\right)\left(\phi_c-\phi_{r,\min}\right)^{A_2}}\right]s_u$ A_1 = 0.75 for $\phi_c - \phi_{r,\min} \le 5^\circ$ A_1 = 0.4 for $\phi_c - \phi_{r,\min} \ge 12^\circ$ A_1 = a linearly interpolated value for $5^\circ < \phi_c - \phi_{r,\min} < 12^\circ$ $A_2 = 0.4+0.3\ln\left(\frac{s_u}{\sigma'_0}\right)$ First equation is valid for 3 < OCR < 5.	$q_{b,ult}$ = 9.6 s_u	Second q_{sL} is used

Note: ϕ_c = critical-state friction angle; $\phi_{r,\min}$ = minimum residual-state friction angle; σ'_{v0} = initial vertical effective stress at the depth being considered; s_u = undrained shear strength of clay; p_A = reference stress = 100 kPa.

foundations. Severely deteriorated foundation elements cannot be reused.

Depending on the site conditions, the capacity of existing foundations can be affected by scour, down drag and/or pile set-up. Scour can reduce the capacity of existing foundations by removing the soil supporting the foundation from beneath it. Down drag can decrease the available capacity of existing foundations by applying additional axial down drag forces to the piles. Pile setup, if not considered at design time, can provide some reserve geotechnical capacity to existing foundations. Traditionally, pile setup has not been considered in foundation designs, but, in a recent I-480 Valley View Bridge construction in Ohio, driven pile foundations were designed considering the reserve capacity from pile setup, and the design resulted in savings of 106,000 ft of piling (approximately 7,000 cubic yards of concrete) for the project (Winter & Maday, 2022).

TABLE 5.20
Group efficiency suggested by AASHTO (2020)

Soil Type	Pile Cap-Soil Contact	Pile Spacing	Group Efficiency
Sand	Free-standing or soil-supported pile cap	≥2.5*B*	1.0
Clay	Free-standing pile cap with soft soil at the surface	2.5*B*	0.65
		2.5*B*–6*B*	Linear interpolation
		6*B*	1.0
	Free-standing pile cap with stiff soil	–	1.0
	Soil-supported pile cap	–	1.0

Note: *B* = pile diameter.

TABLE 5.21
Comparison of unit cap capacities in uniform loose sand from the simulation results and the proposed design equations

Group Configuration	Pile Diameter *B* (inches)	Pile-to-Pile Spacing s_p	Pile-to-Cap Edge Distance s_{edg}	Unit Cap Capacity at *w* = 2 inches (ksf)			Unit Cap Capacity at *w* = 4 inches (ksf)		
				Simulation Results in Table 2.5	Design Equation	Error (%)	Simulation Results in Table 2.5	Design Equation	Error (%)
1 × 5	14	3*B*	2*B*	2.21	2.23	1.0	2.98	3.77	26.5
2 × 5	14	3*B*	2*B*	1.72	1.72	0.1	2.69	2.90	8.0
3 × 5	14	3*B*	2*B*	1.25	1.22	1.9	2.13	2.06	3.0
1 × 5	23.6	3*B*	2*B*	2.41	2.74	13.6	3.33	4.61	38.4
1 × 5	14	5*B*	6*B*	2.95	2.51	15.0	4.19	4.22	0.7

Note: *w* = settlement.

TABLE 5.22
Comparison of unit cap capacities in uniform dense sand from the simulation results and the proposed design equation

Group Configuration	Pile Diameter *B* (inches)	Pile-to-Pile Spacing s_p	Pile-to-Cap Edge Distance s_{edg}	Unit Cap Capacity at *w* = 2 inches (ksf)			Unit Cap Capacity at *w* = 4 inches (ksf)		
				Simulation Results in Table 2.6	Design Equation	Error (%)	Simulation Results in Table 2.6	Design Equation	Error (%)
1 × 5	14	3*B*	2*B*	7.50	5.85	22.0	9.86	9.86	0.0
2 × 5	14	3*B*	2*B*	4.64	4.51	2.8	8.28	7.60	8.2
3 × 5	14	3*B*	2*B*	2.93	3.21	9.5	6.04	5.40	10.6
1 × 5	23.6	3*B*	2*B*	2.91	7.17	21.4	9.43	12.08	28.2
1 × 5	14	5*B*	6*B*	6.57	6.56	0.1	10.92	11.06	1.3

Note: *w* = settlement.

5.3 Factored Capacity Estimation of Existing and New Foundations

The factored capacity *R* of a foundation in LRFD and LFD frameworks is obtained from

$$R = \sum (RF_i) R_{i,n} \qquad \text{(Eq. 5.16)}$$

where $R_{i,n}$ are different types of nominal resistances that the foundation have (e.g., shaft and base resistances for piles), which are identified by a different value of *i*, and RF_i are the corresponding resistance factors.

In the ASD framework, the allowable capacity R_{all} is defined by

$$R_{all} = \frac{\sum R_{i,n}}{FS} \qquad \text{(Eq. 5.17)}$$

where *FS* is the factor of safety. When the allowable capacity is assumed to be equal to the factored capacity, an equivalent resistance factor RF_{eq} can be estimated from the factor of safety as

$$RF_{eq} = \frac{1}{FS} \qquad \text{(Eq. 5.18)}$$

TABLE 5.23
Comparison of resistance factors for the bearing resistance of shallow foundations for different design specifications (ASD and LFD from AASHTO, 2002 and LRFD from AASHTO, 2020)

Method/Soil/Condition	Resistance Factor		
	ASD	LFD	LRFD
Theoretical method (Munfakh et al., 2001) in clay:	0.33		0.50
using shear strength measured in lab tests,	(max)	0.60	
using shear strength measured in field vane tests, and		0.60	
using shear strength estimated from CPT.		0.50	
Theoretical method (Munfakh et al., 2001) in sand:			
using CPT, and		0.45	0.50
using SPT.		0.35	0.45
Semi-empirical methods:			
for all soils (Meyerhof, 1976),		–	0.45
in sand using SPT,		0.45	–
in sand using CPT, and		0.55	–
in clay using CPT.		0.50	–
Footings on rock:			
for all types, and		–	–
using semi-empirical procedure (Carter & Kulhawy, 1988).		0.60	0.45
Plate load test			0.55

Note: ASD refers to allowable stress design, LFD refers to load factor design, and LRFD refers to load-and-resistance factor design.

Table 5.23, Table 5.24, and Table 5.25 summarize resistance factors in the LRFD and LFD frameworks and the equivalent resistance factors in ASD framework proposed by AASTHO (AASHTO, 2002, 2020) for shallow foundations, driven piles and drilled shafts, respectively. The comparisons show that different design specifications provide different factored resistances and lead to different design requirements.

Resistance factors represent in large measure the reliability of corresponding nominal resistances, so they depend on the method used to estimate the nominal resistance, and soil type and other factors considered in the estimation. As shown in Table 5.23, Table 5.24, and Table 5.25, AASHTO (2020) proposes resistance factors that can be used in LRFD framework for certain conditions in which the nominal resistance of the foundation is estimated, but it does not cover all types of estimation methods, including modern design equations that consider time-related effects on the capacity of existing foundations. In order to accurately estimate the factored capacity of existing foundations, additional reliability analyses are necessary to determine appropriate resistance factors for such methods, unless static and/or dynamic load tests are performed on existing foundations for capacity estimation.

5.4 Example of Capacity Estimation

5.4.1 Estimation of Pile Group Capacity Using Different Design Methods

Consider a 3×5 pile group with a soil-supported pile cap in a uniform sand layer. The pile diameter B is 14 inches, the pile length L is 60 ft, and the pile spacing s_{cc} is $3B$. The unit weight of the soil is 109 pcf, and the relative density of the sand is 70%. A CPT was performed at the site, and the obtained cone resistance q_c and sleeve friction f_s profiles are shown in Figure 5.2.

The nominal capacity of the pile group can be determined by the following:

1. calculating the nominal capacity R_n of a single pile using Equation 5.10 and Equation 5.11;
2. calculating the nominal capacity $R_{n,i}$ of the i^{th} pile in the group by multiplying the group efficiency in Table 5.20 to R_n;
3. for a soil-supported pile cap, calculating the pile cap capacity Q_{cap} using Equation 5.12–Equation 5.15, if needed; and
4. calculating the nominal capacity of the pile group by summing up the capacities of the individual piles in the group and the pile cap capacity.

Table 5.27 shows the estimated pile group capacities using different design methods.

When calculating the pile capacities using the Nordlund/Thurman method (AASHTO, 2020), we need to know the value of the internal friction angle ϕ_f of soil, which is not given in this problem. According to AASHTO (2020), we can estimate the internal friction angle based on the CPT cone resistance value using Sabatini et al. (2002):

$$\phi_f = \arctan\left(0.1 + 0.35 \log \frac{q_t}{\sigma'_{v0}}\right) \qquad \text{(Eq. 5.19)}$$

where q_t is the corrected total cone resistance, which is the same as q_c in this case, because we have a uniform sand layer, and σ'_{v0} is the vertical effective stress.

Since this pile group is in uniform sand, we will use a single layer to sand for the entire soil domain. The layer thickness is 60 ft and the middle point of the layer is at a

TABLE 5.24
Comparison of resistance factors for nominal bearing resistance of single driven piles for different design specifications (ASD and LFD from AASHTO, 2002; LRFD from AASHTO, 2020; and INDOT LRFD from INDOT, 2018)

Method/Soil/Condition	Resistance Factor			
	ASD	LFD	LRFD	INDOT LRFD
Driving criteria established by successful static load test of at least one pile per site condition and dynamic testing[1] of at least two piles per site condition, but no less than 2% of the production piles	0.53	0.80	0.80	0.80
Driving criteria established by static load test in combination with INDOT dynamic pile load test, PDA with CAPWAP	–	–	–	0.80
Driving criteria established by successful static load test of at least one pile per site condition without dynamic testing	0.50	0.80	0.75	0.75
Driving criteria established by dynamic testing[1] conducted on 100% of production piles	0.44	0.70	0.75	0.75
Driving criteria established by dynamic testing[1], quality control by dynamic testing[1] of at least two piles per site condition, but no less than 2% of the production piles	0.44	0.70	0.65	0.65
Driving criteria established by dynamic test with signal matching at the beginning of re-drive (BOR) INDOT dynamic pile load test, PDA with CAPWAP	–	–	–	0.70
Driving criteria established by INDOT dynamic formula at the end of initial drive condition (EOID) only	–	–	–	0.55
Wave equation analysis, without pile dynamic measurements or load test but with field confirmation of hammer performance	0.36	–	0.50	0.50
FHWA-modified Gates dynamic pile formula (end of drive condition only)	0.29	–	0.40	0.40
Engineering News dynamic pile formula (end of drive condition only)	0.29	–	0.10	0.10
Side Resistance in Clay and Mixed Soils:	–	–	–	–
Clay and mixed soils (Skempton, 1951)	0.29	–	–	–
α-method (Tomlinson & Woodward, 2007)	–	0.70	0.35	0.35
β-method (Esrig et al., 1981)	–	0.50	0.25	0.25
λ-method (Focht & Vijayvergiya, 1972)	–	0.55	0.40	0.40
End Bearing in Clay and Mixed Soils:	–	–	–	–
Clay and mixed soils (Skempton, 1951)	0.29	0.70	–	–
α-method (Tomlinson & Woodward, 2007)	–	–	0.35	0.35
β-method (Esrig et al., 1981)	–	–	0.25	0.25
λ-method (Focht & Vijayvergiya, 1972)	–	–	0.40	0.40
Side Resistance in Sand:	0.29	–	–	–
Nordlund/Thurman Method (Hannigan et al., 2006)	–	–	0.45	0.45
SPT-method (Meyerhof, 1963)	–	0.35	0.30	0.30
End Bearing in Sand:	0.29	–	–	–
Nordlund/Thurman Method (Hannigan et al., 2006)	–	–	0.45	0.45
SPT-method (Meyerhof, 1963)	–	–	0.30	0.30
Friction angle ϕ_f from CPT (Kulhawy, 1983)	–	0.45	–	–
Friction angle ϕ_f from SPT (Kulhawy, 1983)	–	0.30	–	–
CPT-method (Schmertmann, 1970).	0.29	0.55	0.50	0.50
SPT-method	–	0.45	–	–
End bearing in rock Canadian Geotechnical Society (1985)	–	0.50	0.45	0.45

[1]Dynamic testing requires signal matching, and best estimates of nominal resistance are made from a restrike. Dynamic tests are calibrated to the static load test, when available.

depth of 30 ft. The value of q_t at 30 ft is 290 ksf, according to Figure 5.2. The effective vertical stress σ'_v at 30 ft is 3.27 ksf. The internal friction angle ϕ_f of the soil is 40°. The equations for the unit shaft resistance of the piles and the unit base resistance of the piles are summarized in Table 5.13 and Table 5.14. The volume V of soil displaced per unit length of pile is taken as the area of the cross section of the pile. The coefficient of lateral earth pressure K_δ, the correction factor C_F and the value of $\frac{\delta}{\phi_f}$, where δ is the friction angle between the soil and the pile, can be obtained from Figure 10.7.3.8.6f-1 to Figure 10.7.3.8.6f-6 in AASHTO (2020). The coefficient α_t, the bearing capacity factor N'_q and the limit unit tip resistance can be found in Figure 10.7.3.8.6f-7 to Figure 10.7.3.8.6f-9 in AASHTO (2020). The values used in the calculations are summarized in Table 5.26.

For the "CPT method" (AASHTO, 2020), CPT data is directly used. The equations for the unit shaft resistance of the piles and the unit base resistance of the piles are summarized in Table 5.13 and Table 5.14.

For the Purdue method (Salgado, 2022a), the critical-state friction angle of the soil is taken as 31°, the coefficient of earth pressure at rest is taken as 0.45, and the pile-soil interface friction angle is taken as

TABLE 5.25
Comparison of resistance factors for nominal axial compressive resistance of single drilled shafts for different design specifications (ASD and LFD from AASHTO, 2002 and LRFD from AASHTO, 2020)

Method/Soil/Condition	Resistance Factor		
	ASD	LFD	LRFD
Static load test, all materials	0.50 (max)	0.80	0.70
Side resistance in clay: α-method (Brown et al., 2010)	0.40 (max)	0.65	0.45
Tip resistance in clay: Total Stress (Brown et al., 2010)	0.40 (max)	0.55	0.40
Side resistance in sand: β-method (Brown et al., 2010)	0.40 (max)	–	0.55
Tip resistance in sand (Brown et al., 2010)	0.40 (max)	–	0.50
Side resistance in cohesive IGMs:[1] (Brown et al., 2010)	0.40 (max)	–	0.60
Tip resistance in cohesive IGMs:[1] (Brown et al., 2010)	0.40 (max)	–	0.55
Side resistance in rock:			
Kulhawy et al. (2005)	0.40 (max)	–	0.55
Brown et al. (2010)		–	0.55
Carter and Kulhawy (1988)		0.55	–
Horvath and Kenney (1983)		0.65	–
Tip resistance in rock:			
Canadian Geotechnical Society (1985)	0.40 (max)	0.50	0.50
Pressuremeter Method (Canadian Geotechnical Society, 1985)		0.50	0.50
Brown et al. (2010)		–	0.50

[1]IGM refers to the intermediate geo-materials.

TABLE 5.26
The value of the coefficients and factors used in Nordlund/Thurman method in the design example

Coefficient/Factor in the Equation	Value Used
K_δ	3.0
C_F	0.8
$\frac{\delta}{\phi_f}$	0.65
V	1.07 ft^3/ft
ϕ_f	40°
ω	0°
α_t	0.73
N'_q	150
q_L	400 ksf
σ'_v at the center of the soil layer	3.27 ksf
σ'_v at the level of the base of the pile[1]	3.2 ksf

[1]σ'_v at the base of the pile is the taken as 3.2 ksf if the actual effective vertical stress at the base of the pile exceeds 3.2 ksf.

27.9°. The equations for the unit shaft and base resistances of the pile are summarized in Table 5.16.

As shown in Table 5.27, the estimated nominal capacities of a single pile using the Nordlund/Thurman method (AASHTO, 2020), the "CPT method" (AASHTO, 2020), and the Purdue method (Salgado, 2022a) are 1,131 kips, 680 kips, and 632 kips, respectively. The Nordlund/Thurman method provides the highest estimate, and the Purdue method provides the lowest estimate of the pile capacity. An engineer using the Nordlund/Thurman method must have confidence that the capacity that the method provides, which is about 80% higher than the Purdue design method, will indeed be available. This comparison shows the importance of choosing the most reliable design methods for capacity estimation considering site conditions.

When group efficiencies and pile cap capacity are considered in the capacity estimation of the 3×5 pile group, the estimated nominal capacities of the pile group using Nordlund/Thurman method (AASHTO, 2020), "CPT method" (AASHTO, 2020), and Purdue method (Salgado, 2022a) are 16,960 kips, 10,204 kips, and 12,570 kips, respectively. In this case, the Nordlund/Thurman method provides the highest estimate and the "CPT method" provides the lowest estimate of total capacity. The capacity estimation for the pile group indicates that there is some reserve in capacity according to the Purdue method because it considers pile cap capacity (which the other two methods do not) and its group efficiency is different from that used in AASHTO (2020). The group efficiencies used in the Purdue method were determined from realistic, advanced finite-element simulation results for the 3×5 pile groups in uniform loose and dense sands, as shown in Figure 2.19. In addition, the relationship (Equation 5.12–Equation 5.15) used in the Purdue method for the pile cap capacity was derived from the results of the FEA performed in this study. In calculation of the pile cap capacity, the pile-to-pile cap edge distance s_{edge} is assumed to be $2B$. The consideration of the FEA-derived group efficiencies provides

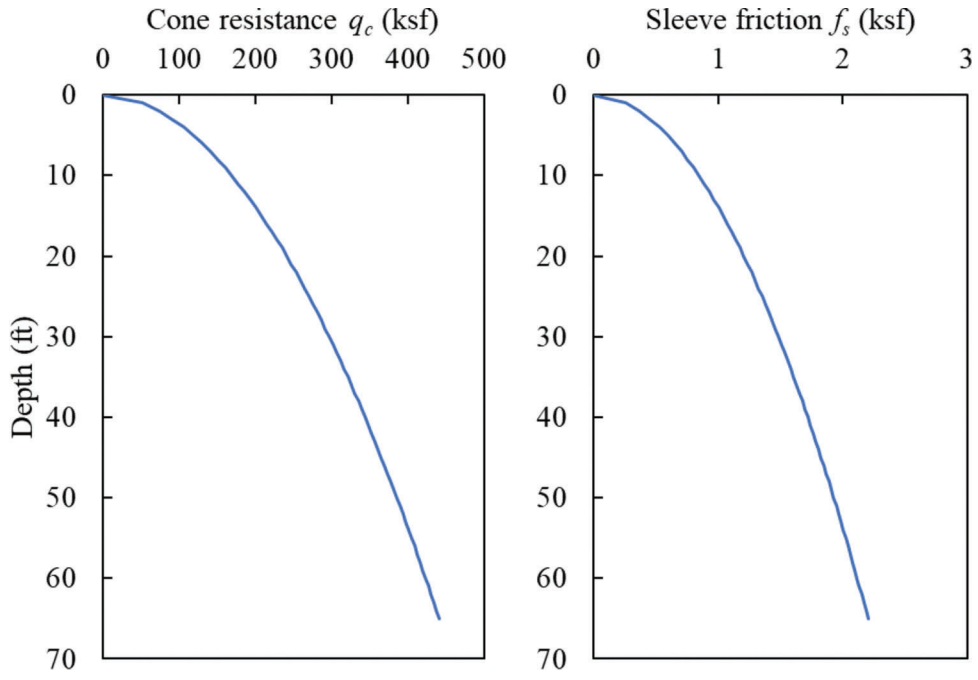

Figure 5.2 Cone resistance q_c and sleeve friction f_s profiles for the design example.

TABLE 5.27
Estimated pile group capacities using different design methods

Design Method	Nominal Capacity of Individual Pile (kips)				Pile Cap Capacity (kips)	Pile Group Capacity (kips)
	Base	Shaft	Group Efficiency	Total Capacity per Pile		
Nordlund/Thurman Method in Table 5.13 and Note: q_s = Unit Shaft Resistance in ksf. Table 5.14	374	756	1.0	1,131	0[2]	16,960
CPT Method in Table 5.13 and Note: q_s = Unit Shaft Resistance in ksf. Table 5.14	447	233	1.0	680	0[2]	10,204
Purdue Method in Table 5.16	270	362	Center piles[1]: 1.1 (base), 1.9 (shaft); Side piles[1]: 1.0 (base), 1.5 (shaft); Corner piles[1]: 0.9 (base), 1.2 (shaft)	805	493	12,570

[1]Interpolated values for a relative density of 70% at a settlement of 10% B in Figure 2.19, where B is the pile diameter.
[2]Pile cap capacity is not considered in AASHTO manual (AASHTO, 2020).

about 27% reserve in capacity and the consideration of pile cap capacity (estimated using Equation 5.12–Equation 5.15 proposed in this study) provides about 4% reserve in capacity of the pile group, as estimated using the Purdue method. This shows that capacity estimation considering the most current cutting-edge methods can be useful in estimating the reserve capacity of existing foundations.

6. GUIDELINES FOR THE SELECTION OF FOUNDATION REUSE SOLUTION

6.1 Framework for Selection of Foundation Reuse Solution

Given the updated design load, current soil profile, confirmed structural integrity of existing foundations and estimated current capacity of existing foundations, the suitability of existing foundations for reuse can be determined through both geotechnical and structural design checks following the current LRFD design specifications. When the design checks fail, the reuse solutions in Table 6.1 can be considered. Possible foundation reuse solutions can be compared and selected by considering several factors listed in Table 6.2. Figure 6.1 shows a flow chart that can be used to select foundation reuse solutions.

TABLE 6.1
Foundation reuse solutions

Category	Technique
Repair of Foundation Elements (Agrawal et al., 2018)	*For concrete elements:* Patching spalled and cracked concrete, cover replacement and encasement, fiber-reinforced polymer (FRP) wrapping, doweling, cathodic protection, and electrochemical chloride extraction and re-alkalisation of concrete *For steel elements:* Encasement or jacking in concrete, wrapping with a waterproof membrane, cathodic protection and application or reapplication of paint or protection coatings
Strengthening of Foundations	Addition of new deep foundation elements (micropiles, drilled shafts, driven piles, ground anchors, stone columns, and other deep foundation elements), widening of footings or pile cap, and ground improvement (compaction, grouting, soil mixing and stone columns)
Reduction of the Updated Design Loads (Agrawal et al., 2018)	Use of lightweight concrete, lightweight backfill or composite fiber-reinforced polymer (FRP) decks
Complete Replacement of Existing Foundations by New Foundations	Use of shallow foundations, drilled shafts, driven piles, micropiles, ground anchors, stone columns, and other deep foundation elements

TABLE 6.2
Factors to be considered for the selection of foundation reuse solutions

Factors to be Considered	References
Historical Aspects	Agrawal et al., 2018; MassDOT, 2013
Level of Risk, Including Life Cycle Risks	
Constructability	
Environmental Impact	
Sustainability	
Impact of New Foundation Construction on Existing Foundations and Structures (e.g., ground settlement, slope failures, heaving, artesian conditions, rotation or deflection of existing structures, and effects on the capacity of the existing foundation due to new foundation construction)	
Cost Effectiveness	

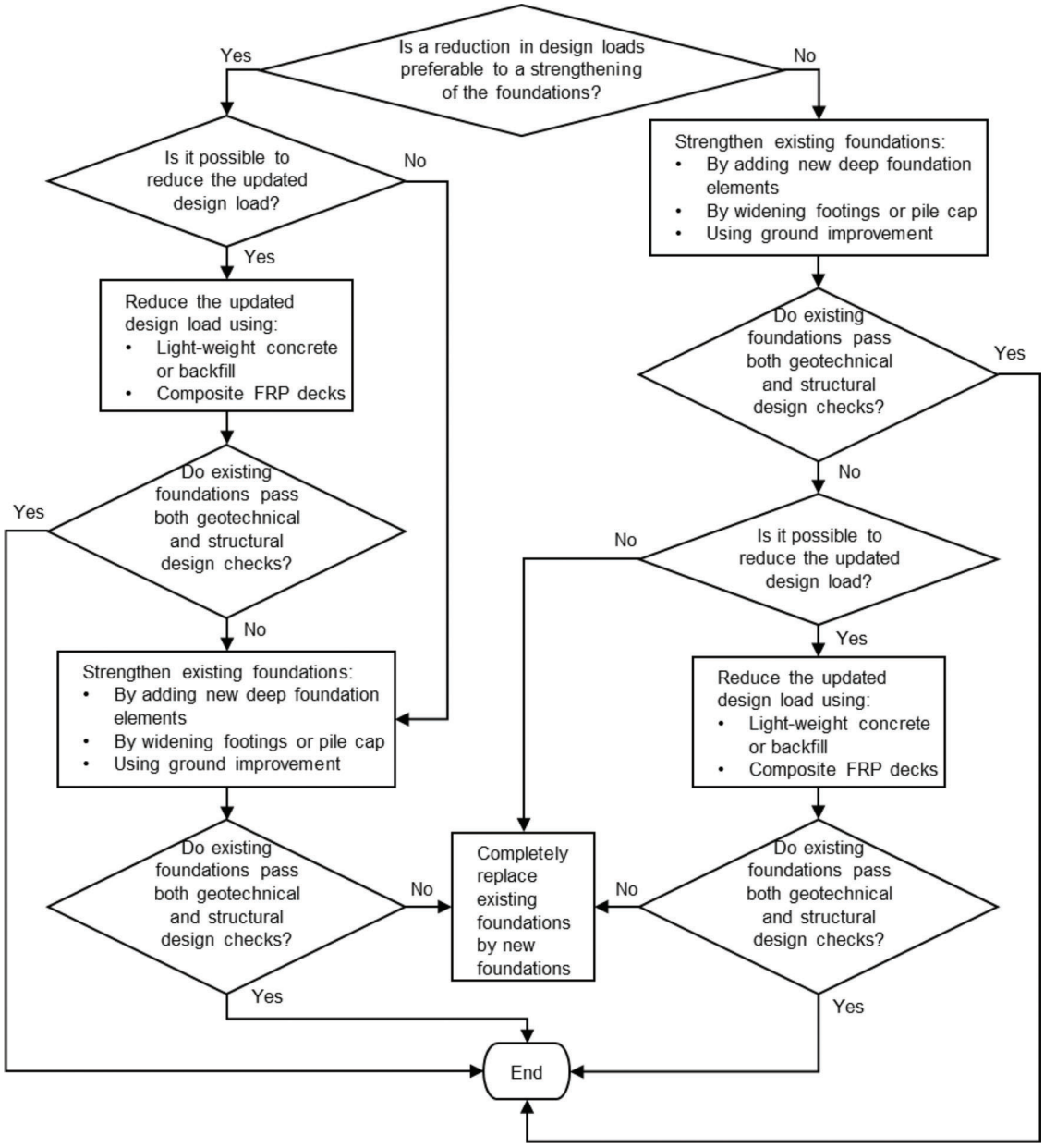

Figure 6.1 Flow chart to select foundation reuse solutions.

7. IMPLEMENTATION PROJECT: BRIDGE REHABILITATION AND WIDENING PROJECT ON I-465 OVER 71st STREET

7.1 Project Description

A bridge rehabilitation and widening project was planned for the bridge located on I-465 over 71st street, Marion County, IN. Figure 7.1 shows the location of the bridge.

The length of the bridge is 116 ft. Figure 7.2 shows the bridge construction site. Figure 7.2(a) shows the I-465 southbound side of the bridge, Figure 7.2(b) shows the I-465 northbound side of the bridge, and Figure 7.2(c) shows the interior piers of the bridge.

The bridge was originally built as two-span twin bridges supported by driven piles at the end bents and a shallow foundation at the interior pier. The original two-span bridges were planned in 1966. According to the bridge plan in 1966, about half of the driven piles at the end bents were battered towards the interior pier, the shallow foundation at the interior pier was 6 ft wide, the elevation level of the base of the shallow foundation was 814.88 ft, and the shallow foundation was designed for a maximum soil pressure of 5.0 ksf.

In the early 2000s, the two-span bridges were widened to both the inside and outside of the bridges. In this widening plan, additional battered driven piles were installed at the end bents, and the shallow foundation at the interior pier was widened. The base of the widened portion of the shallow foundation was located at El. 814.88 ft, and the width of the footing was 1,829 mm (about 6 ft). The widened portions of the shallow foundation were doweled into the existing foundations. Figure 7.3 shows the newly constructed interior piers of the bridge during the widening plan in 2000.

In 2021, further widening of the bridge to the outside and replacement of the existing decks were planned. During the widening project, additional steel encased concrete (SEC) piles were installed at the end bents, and the shallow foundation at the interior pier was widened with steel encased concrete (SEC) piles with a pile cap. The new foundations were designed following the load factor design (LFD) outlined in the *2002 AASHTO Standard Specifications for Highway Bridges*, 17th edition (AASHTO, 2002).

7.2 Foundation Overview

Figure 7.4 shows an overview of the existing and new foundations of the bridge in this project. In the figure, yellow boxes indicate the existing foundations designed during the original plan in 1966, orange boxes indicate the existing foundations designed during the widening plan in 2000, and green boxes indicate the new foundations designed during the widening plan in 2021. Pile numbers are also marked in the figure.

According to the original 1966 plan, each two-span bridge were supported by 9 driven piles (piles 10–18 at the southbound end bents 1 and 3, and piles 8–16 at the northbound end bents 1 and 3) with a pile cap at the end bents, and a shallow foundation at the interior pier. The locations of the existing foundations of the two-span twin bridges are identified using yellow boxes in Figure 7.4. During the widening plan in 2000, three additional driven piles (piles 7–9 at the southbound end bents 1 and 3) were installed on the outside of the southbound end bents, three additional driven piles (piles 5–7 on the northbound end bents 1 and 3) were installed on the outside of the northbound end bents, and three additional driven piles (piles 19–20 at the southbound end bents 1 and 3 and piles 17 at the northbound end bents 1 and 3) were installed inside the end bents. The existing shallow foundations for the interior pier of the two-span bridges were extended. The locations of the additionally added piles at each end bent and extended shallow foundation at the interior pier during the widening

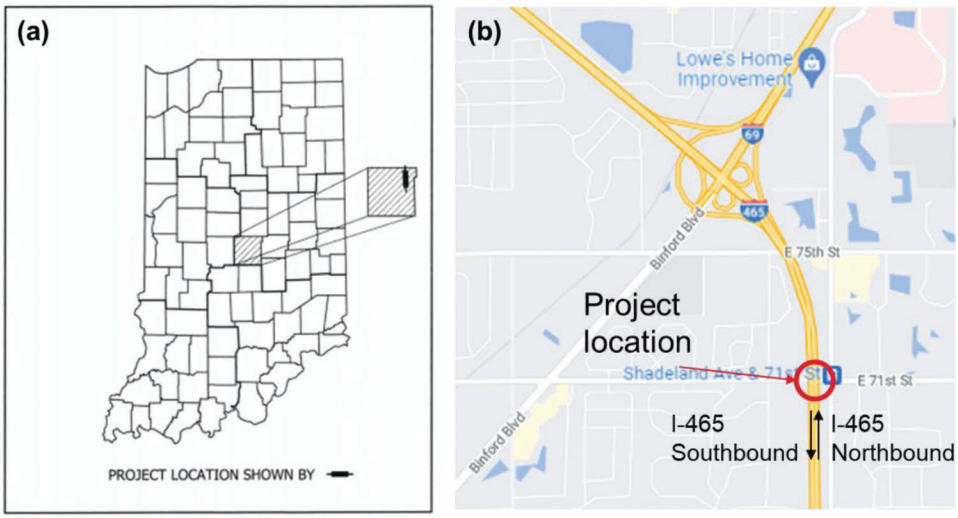

Figure 7.1 Location of the bridge rehabilitation and widening project on I-465 over 71st street: (a) location of the bridge in Indiana (figure is from the drawing plan of the project), and (b) a closer view of the project location (Google, 2022).

Figure 7.2 Bridge construction site: (a) I-465 Southbound side, (b) I-465 Northbound side, and (c) interior piers.

plan in 2000 are marked as pink boxes in Figure 7.4. For the widening project in 2021, four additional driven piles (piles 1–4 at the northbound end bents 1 and 3) were installed on the northbound side end bents, and 6 driven piles (piles 1–6 at the southbound end bents 1 and 3) were installed on the southbound side end bents. At the interior pier, 2×3 driven piles (piles 1–6 at the northbound interior pier) were installed and a pile cap constructed at the northbound side, and 2×4 driven piles (piles 1–8 at the southbound interior pier) were installed and a pile cap constructed at the southbound side of the bridge. The locations of the newly added foundations during the widening plan in 2021 are marked as green boxes in Figure 7.4.

7.3 Foundation Reuse Design

7.3.1 As-Built Geometry of Existing Foundations

The first step of the foundation reuse design is the determination of the as-built geometry of the existing foundations, as shown in Figure 3.1. According to Table 4.1, the dimensions of the existing foundations can be determined by the following:

- review of historical records,
- visual observation,
- destructive methods, and
- nondestructive methods.

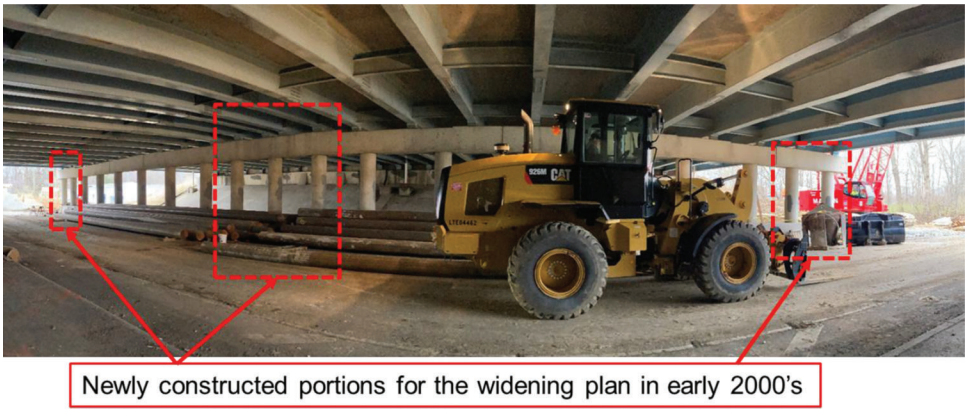

Figure 7.3 Newly constructed interior piers for the widening plan in 2000.

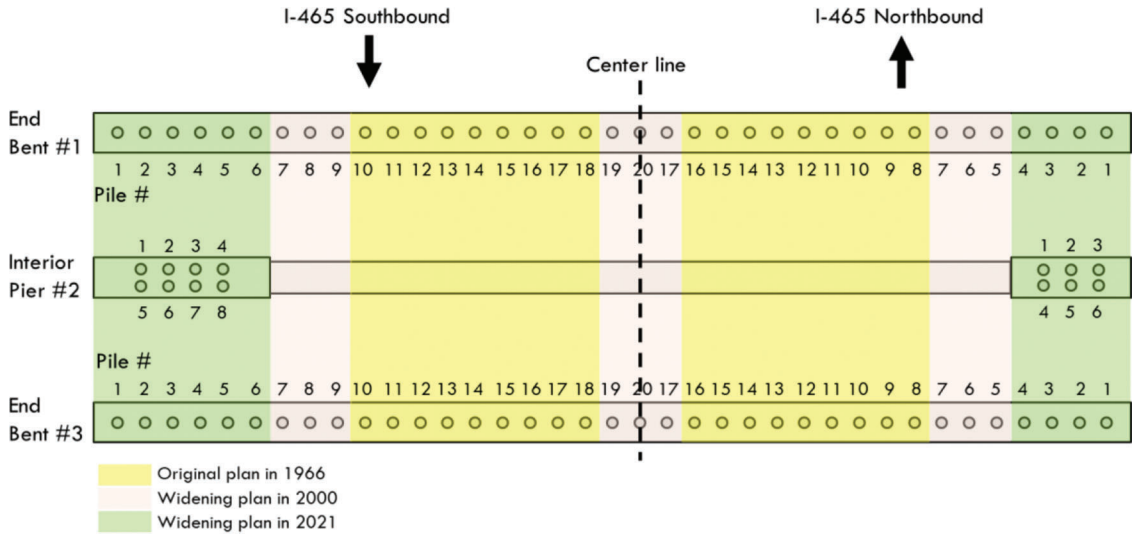

Figure 7.4 Overview of the existing and new foundations of the bridge.

Figure 4.2 shows the flow chart to determine the as-built geometry of existing foundations. In this project, the geometry of all existing foundations was determined from the original plan drawings and construction records. Based on visual inspection results, all existing foundations are assumed not to have experienced severe deterioration over time, and their as-built geometry is assumed to be the same as the geometry originally planned or initially constructed.

According to the original plan drawings, the geometry of the existing shallow foundation at the interior pier is as follows.

- Width B: 6 ft
- Length L: 155.66 ft
- Embedment depth D: 7.82 ft
- Elevation of the base: 814.88 ft

Pile driving records were available for all existing piles. Table 7.1 shows the as-built geometry of the existing piles at the end bents. The pile tip elevation in the table is calculated using the pile length below cut off obtained from the pile driving records and the elevation of the pile cap base obtained from the original plan drawings. The cutoff elevation is assumed to be equal to the elevation of the pile cap base.

7.3.2 Assessment of the Structural Integrity of Existing Foundations

According to the flowchart for the foundation reuse design, proposed in this study and shown in Figure 3.1, assessment of the structural integrity of existing foundations is the second step of the foundation reuse design. As shown in Table 4.1, the structural integrity of the existing foundations can be determined by the following:

- review of historical records,
- visual observation,
- destructive methods, and
- nondestructive methods

TABLE 7.1
As-built geometry of existing piles at the end bents

Location of the Pile	Pile #	Pile Type	Pile Diameter (inches)	Pile tip Elevation (ft)[1]	Source of Information	Year of Pile Driving
Southbound Bent #1	7	Steel encased concrete (SEC) pile	14	800.91	Original plan drawings and pile driving records	2002
	8			805.18		2002
	9			806.16		2002
	10			801.19		1969
	11			801.09		1969
	12			794.39		1969
	13			801.29		1969
	14			800.69		1969
	15			800.69		1969
	16			797.19		1969
	17			796.39		1969
	18			797.59		1969
	19			796.06		2002
Bent #1 Center	20			795.76		2002
Northbound Bent #1	5	Steel encased concrete (SEC) pile		808.79	Original plan drawings and pile driving records	2002
	6			809.11		2002
	7			808.79		2002
	8			797.59		1969
	9			791.39		1969
	10			802.19		1969
	11			802.29		1969
	12			803.09		1969
	13			808.29		1969
	14			802.99		1969
	15			810.09		1969
	16			811.09		1969
	17			794.68		2002
Southbound Bent #3	7	Steel encased concrete (SEC) pile	14	808.79	Original plan drawings and pile driving records	2002
	8			808.79		2002
	9			806.82		2002
	10			800.69		1969
	11			802.39		1969
	12			793.79		1969
	13			797.39		1969
	14			796.79		1969
	15			796.09		1969
	16			795.79		1969
	17			801.09		1969
	18			796.19		1969
	19			809.11		2002
Bent #3 Center	20			801.24		2002
Northbound Bent #3	5	Steel encased concrete (SEC) pile		803.54	Original plan drawings and pile driving records	2002
	6			803.87		2002
	7			804.52		2002
	8			795.19		1969
	9			796.99		1969
	10			796.99		1969
	11			796.39		1969
	12			801.49		1969
	13			801.19		1969
	14			796.59		1969
	15			797.09		1969
	16			794.89		1969
	17			801.90		2002

[1]Pile tip elevation = the elevation of the pile cap base (831.09 ft)—pile length below cut off.

The structural integrity of the existing foundations can be evaluated by inspecting material properties, surface and/or internal defects and geometry changes of existing foundations, as shown in Table 4.3 and Table 4.4. Figure 4.3 shows the flow charts to inspect material properties, defects and geometry changes of existing foundations using the corresponding methods.

Figure 7.5 Photo of the crack in the joint connecting the original and widened portions of the interior pier (photo from United Consulting, personal communication, April 28, 2022).

In this project, there were no historical records mentioning possible issues regarding the structural integrity of the existing foundations. The existing structures above the ground surface indicated no signs of loss of structural integrity of the existing foundations. All existing foundations were assumed to be in adequate condition and to have the same dimensions as in the original plan.

Small cracks near the joint connecting the original and widened portions of the existing pier were observed, as shown in Figure 7.5. The pattern of the cracks was interpreted as a sign of differential settlement between the original and widened portions of the shallow foundation at the interior pier.

7.3.3 Site Investigation

7.3.3.1 Boring logs. At the site, 90-ft long borings were performed in 2008, and 10-ft long borings were performed in 2018. Figure 7.6 shows the locations of boring logs available at the beginning of the widening project in 2021.

According to the 90-ft long boring log data, the subsurface profile consists mainly of loam, low-plasticity silty soils, classified as A-4 using the AASHTO soil classification system. A-4 soil represents silty soils that have more than 35% of fines passing the No. 200 sieve with maximum liquid limit and plasticity index equal to 40 and 10. The loam layer is located above the elevations 768 to 778 ft. Below the loam layer, the profile consists mainly of sandy soil. The loam layer typically contains frequent thin layers of "granular" soils (gravelly sand, sand and gravel). A few boulders were also observed within the loam layer.

All existing foundations are located within the loam layer. The average dry unit weight of the loam layer is 127 pcf, its gravel fraction is in the 1.2%–38.8% range, and its clay fraction is in the 8.6%–25.3%. The profiles

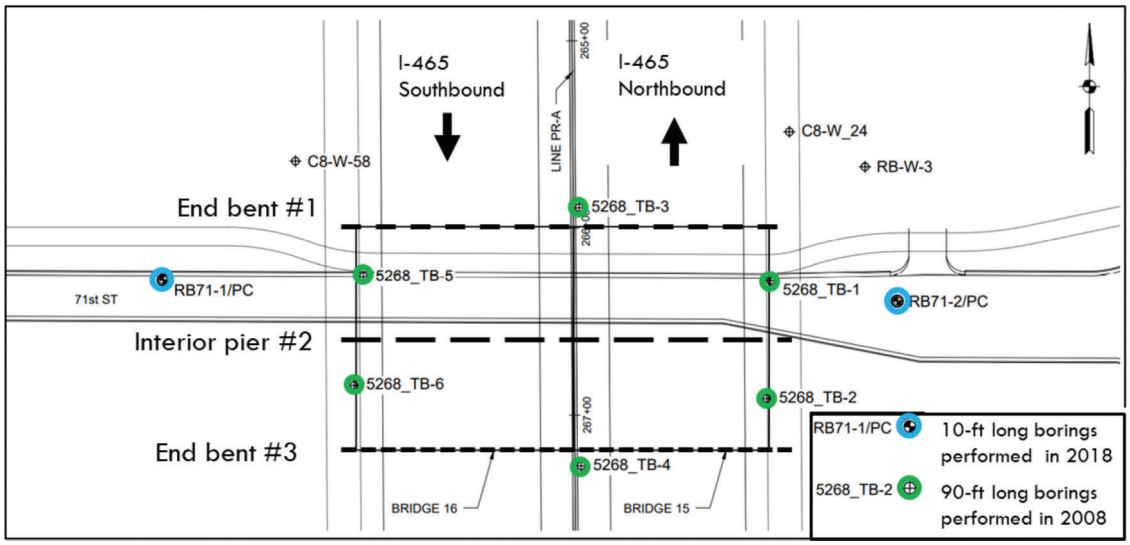

Figure 7.6 Locations of available boring log data

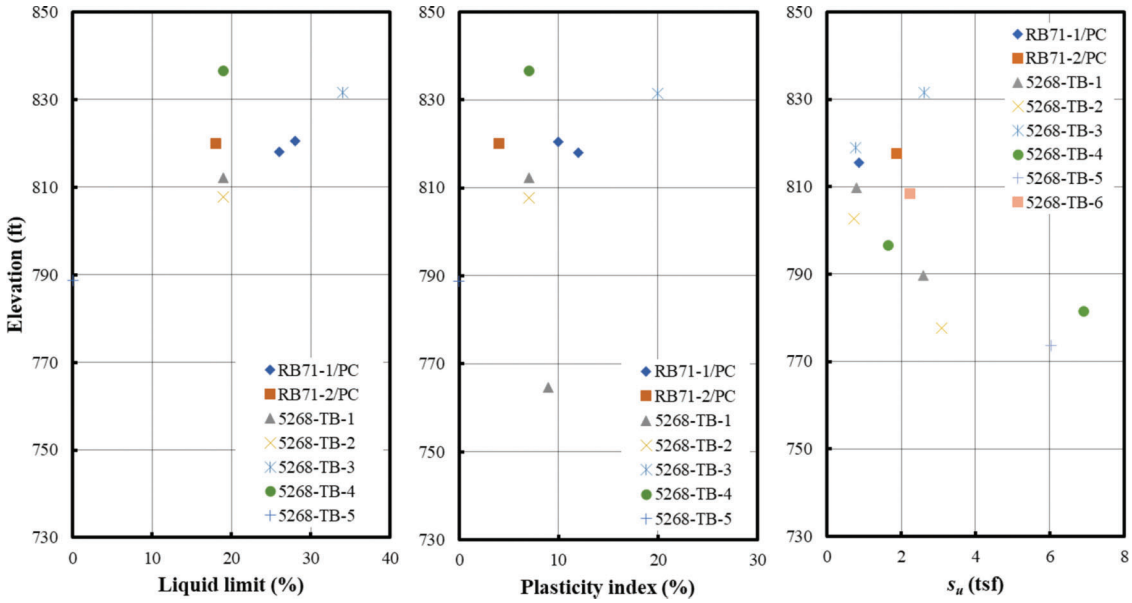

Figure 7.7 Profiles of liquid limit, plasticity index, and undrained shear strength s_u from unconfined compression tests.

TABLE 7.2
Observed groundwater level elevations from test borings

Observed Water Level Elevations (ft)	RB71-1/PC	RB71-2/PC	5268_TB-1	5268_TB-2	5268_TB-3	5268_TB-4	5268_TB-5	5268_TB-6
While Drilling	NW	NW	811.7	NW	805.5	NW	796.7	806.4
Upon Completion	NW	NW	807.2	813.7	802	NW	797.7	812.4
After Drilling	–	–	BF	BF	BF	816.5	BF	809.9

Note:
NW = no water.
BF = backfilled upon completion.

of the liquid limit, plasticity index and undrained shear strength measured from samples collected from the field are shown in Figure 7.7. In the figure, the undrained shear strength s_u is measured from unconfined compression tests. According to the test results, the measured undrained shear strength s_u of the loam is in the 0.7–6.9 tsf range and increasing with depth. The results of the 10-ft long shallow borings were consistent with the previous 90-ft long borings performed in 2008.

Table 7.2 shows the observed groundwater level elevations from the test borings. Groundwater readings were taken during and upon completion of the test borings, and delayed groundwater level readings were taken when feasible. The observed groundwater level is in the range of El. 796 ft to 816 ft. Observations during drilling were commonly in areas where "granular" soil seams were observed.

7.3.3.2 SPT data. Test borings performed in 2008 used 2-inch inner diameter split barrel sampler and a 140-lb hammer with a free fall height of 30 inches to obtain the SPT data. The hammer type used for the SPT borings performed in 2008 is unknown. Test borings performed in 2018 used an automatic hammer. From the SPT data N_{SPT} obtained from test borings, N_{60} profiles were obtained using (Salgado, 2022a):

$$N_{60} = C_h C_r C_s C_d N_{SPT} \qquad \text{(Eq. 5.20)}$$

where C_h, C_r, C_s, and C_d are correction factors for the hammer type, rod length, sampler type and borehole diameter, respectively. For the automatic hammer, $C_h = 1.33$ is used. For the test borings performed in 2008, $C_h = 1.33$ is assumed. Different values of C_r were used depending on the rod length: $C_r = 0.75$ if rod length is less than 4 m (13.1 ft), 0.85 if rod length is in between 4 m (13 ft) and 6 m (19.7 ft), 0.95 if rod length is in between 6 m (19.7 ft) and 10 m (32.8 ft), and 1 if rod length is larger than 10 m (32.8 ft). $C_s = 1$ for the standard ISSMGE sampler and $C_d = 1$ for the bore hole diameter in the 2.5–4.5 inches range were used. The upper limit of N_{SPT} is 100.

Figure 7.8 shows N_{60} profiles for the test borings. In general, N_{60} increases with depth within the loam layer. As shown in the figure, N_{60} within the loam layer varies considerably. For example, at the elevation 790 ft, the minimum N_{60} is about 27 measured from the 5268_TB-5

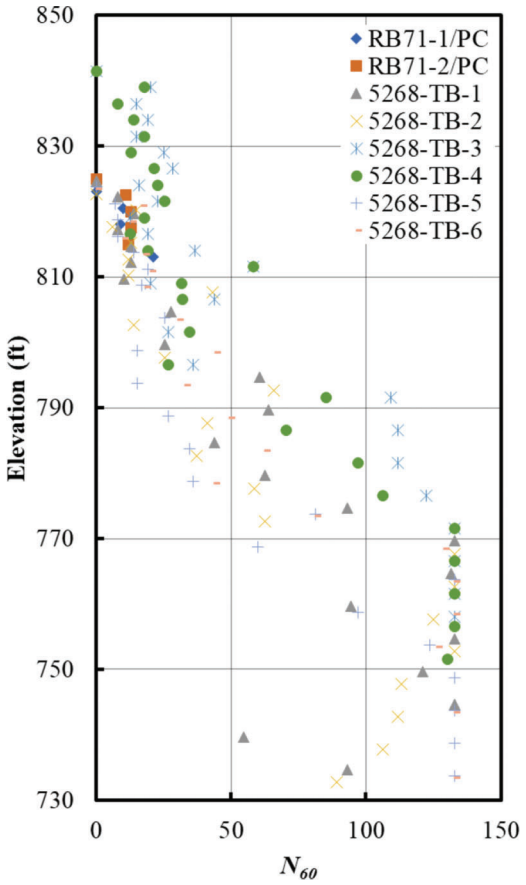

Figure 7.8 N_{60} profile

boring, and the maximum N_{60} is about 109 measured from the 5268_TB-3.

7.3.3.3 Additional CPT data. It is very important to classify the soil profiles into sandy ("cohesionless") or clayey ("cohesive") soils, because most of the design methods, including traditional ones described in AASHTO (AASHTO, 2020) and current ones, are developed for sand and clay, separately. Depending on the classification, the estimated capacities can be quite different, even for the same SPT or CPT data.

For example, when the "theoretical method" suggested by the AASHTO LRFD design manual (AASHTO, 2020) is used to estimate the capacity of the existing shallow foundation at the interior pier using the SPT data, the estimated capacities can be very different for sand and clay, even for the same value of N_{60}. Table 7.3 shows an example calculation of capacity estimations for the existing shallow foundation at the interior pier using the SPT data. When the loam layer is considered to be a sandy soil, using an average value of N_{60} below the footing base, which is about 19, the friction angle can be estimated to be 35° according to the table 10.4.6.2.4-1 in the AASHTO manual (AASHTO, 2020), and zero cohesion is assumed. When the loam layer is considered to be a clayey soil, the undrained shear strength of the soil can be estimated from the average value of N_{60} using the Brown method (Brown & Hettiarachchi, 2008) as about 1.7 ksf, and zero friction angle can be considered for the capacity estimation. When the same equations for the theoretical method in AASHTO LRFD design manual (AASHTO, 2020) were used for sandy soil, the estimated nominal and factored capacities were 53 ksf and 24 ksf, respectively, while the estimated nominal and factored capacities for clayey soil were about 10 ksf and 5 ksf, respectively. The estimated capacity for sandy soil was about 5 times greater than the one for clayey soil even though the same value of N_{60} was used in the calculations.

It can be challenging to classify a silty soil like the loam layer at this site as a sand or a clay. According to the available boring log data, the loam layer could be considered to behave like sandy soils because (1) the clay fraction is mostly lower than 20%, and (2) the N_{60} values are relatively high. However, the Purdue research team recommended the performance of additional site investigations to decrease the uncertainties regarding site investigation data. The research team pointed out that (1) the obtained N_{60} profiles from test borings varied considerably within the loam layer, and (2) the soil samples from the test borings were plastic with non-zero plasticity index and undrained shear strengths, which could be inconsistent with a sandy soil classification. INDOT performed an additional CPT test at the site in October 2022. In comparison with the SPT, CPT provides more reliable data (Salgado, 2022a) and, using the CPT data, current design equations, such as the methods of foundation design developed over the years at Purdue (Han et al., 2015; Han, Ganju, et al., 2019, 2020; Han, Prezzi, et al., 2017; Salgado, 2008, 2022; Salgado et al., 2017)) can be used for comparison when the capacities of existing foundations are estimated. The location of the CPT, which is referred to as CPT-1, is shown in Figure 7.9. A digital cone with five channels (tip, friction, pore pressure, inclination and seismic) with cone serial number 1169 was used in the CPT.

CPT-1 was performed within the loam layer and stopped at the depth of 57 ft because the CPT truck started lifting. Figure 7.10 shows the CPT results. In the figure, q_t refers to the corrected cone tip resistance, f_s refers to the sleeve friction, and u refers to the pore-water pressure. As shown in the figure, within the loam layer, there are clayey soil layers at elevations 822–815 ft, 814–808 ft, and 798.5–796.5 ft, which has a low q_t and high pore-water pressure u.

Using the CPT data at each depth, the soil behavior types were classified using the modified soil behavior chart in Ganju et al. (2017), which is modified from the original Tumay chart (Tumay, 1985). Figure 7.11 shows the results of the soil behavior type classification. Figure 7.11(a) shows the soil behavior type classification using the modified soil behavior chart in Ganju et al. (2017) and Figure 7.11(b) shows the classified soil behavior type using the modified soil behavior chart in Ganju et al. (2017) at each elevation. As shown in Figure 7.11(b), most of the layers within the loam layer

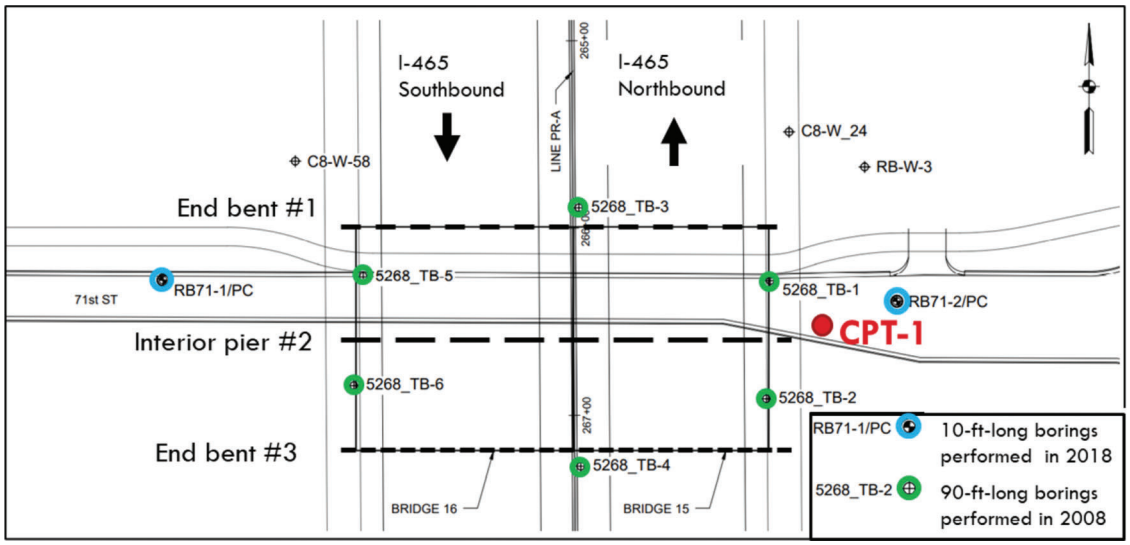

Figure 7.9 Location of additionally performed CPT, referred to as CPT-1, at the site.

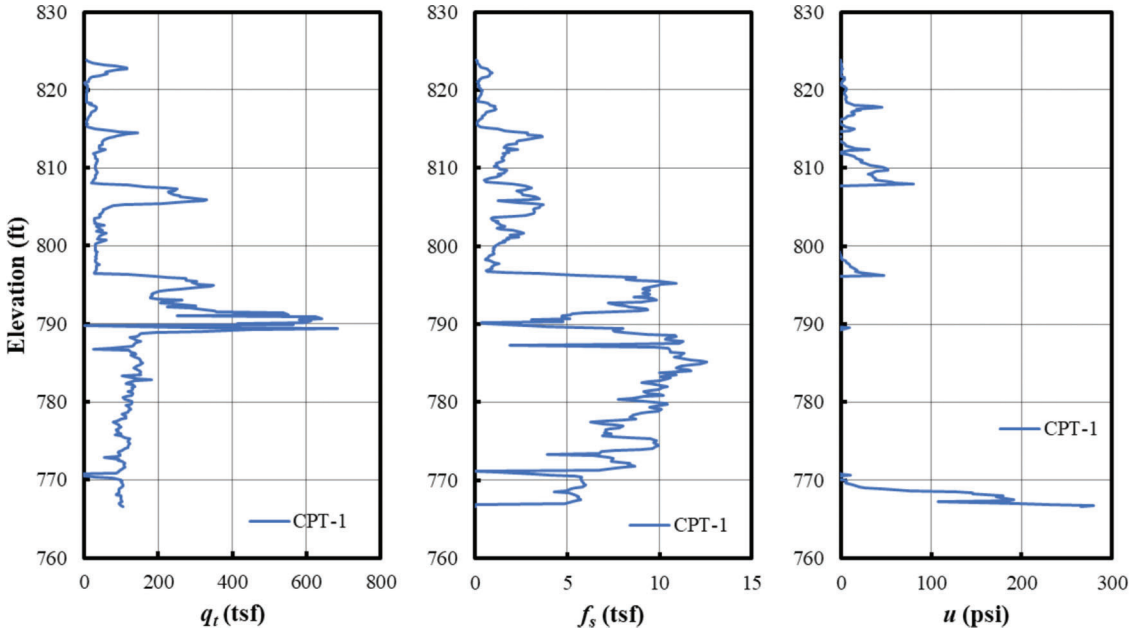

Figure 7.10 Additional CPT data

can be interpreted as a clayey soil, which is inconsistent with the SPT data.

In conclusion, the loam layer is considered to be multilayered with both sandy soil and clayey soil layers, and the soil type at each depth is determined using both SPT and CPT data. For the capacity estimation of existing foundations, CPT data was primarily used in the calculations.

7.3.4 Capacity Estimation of Existing Foundations

7.3.4.1 Capacity estimation of existing shallow foundation. Using the analyzed site investigation data and the obtained as-built geometry of the existing foundations, the capacities of the existing foundations were estimated.

To estimate the capacity of the shallow foundation at the interior pier, boring logs near the interior pier (5268_TB-1, 5268_TB-2, 5268_TB-5, and 5268_TB-6) and CPT-1 data were considered. Figure 7.12 shows a comparison between SPT and CPT data with the soil type classification using the CPT data within a depth of $1.5B$ below the elevation level of the footing base, where B is the footing width. Based on the comparison, the loam layer below the footing base is considered as a clayey soil layer sandwiched by sandy soil layers, as shown in Figure 7.12.

TABLE 7.3
Example calculation of capacity estimation for existing shallow foundation at the interior pier using SPT data

Design Methods	Nominal Bearing Capacity (ksf)	Resistance Factor	Factored Bearing Capacity (ksf)
Theoretical Method in Sand Using SPT (AASHTO, 2020)	53	0.45 (AASHTO, 2020)	24
Theoretical Method in Clay (AASHTO, 2020)	10	0.5 (AASHTO, 2020)	5

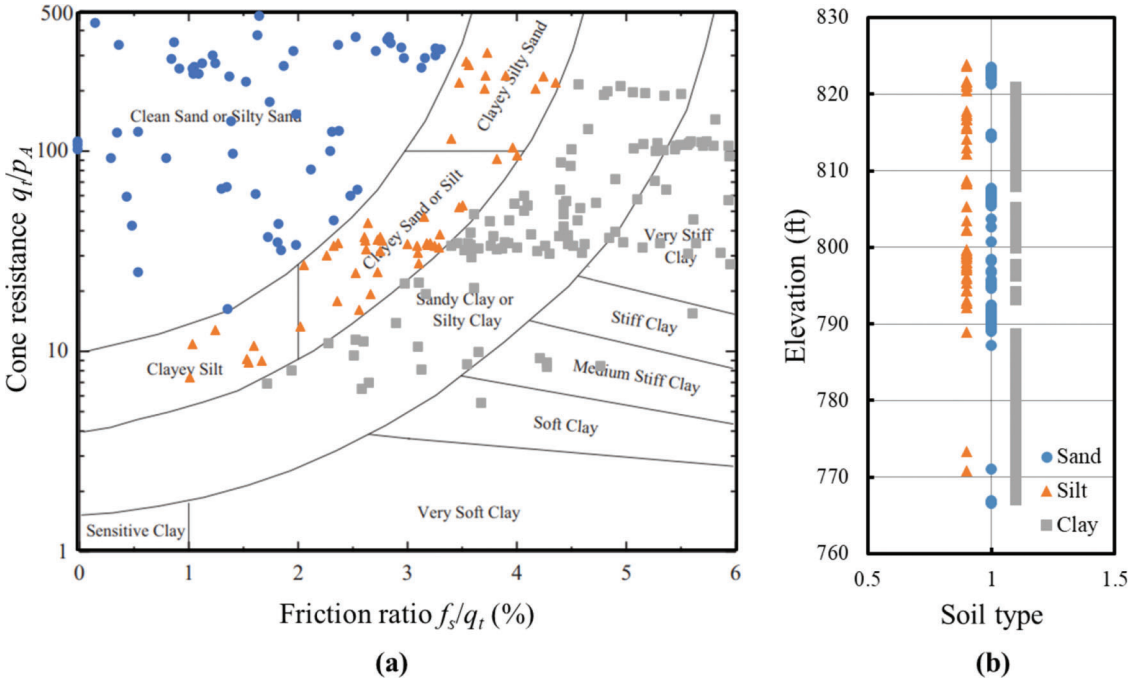

Figure 7.11 Soil behavior type classification using CPT data: (a) soil type classification using the chart provided in Ganju et al. (2017), and (b) soil type classification at each elevation.

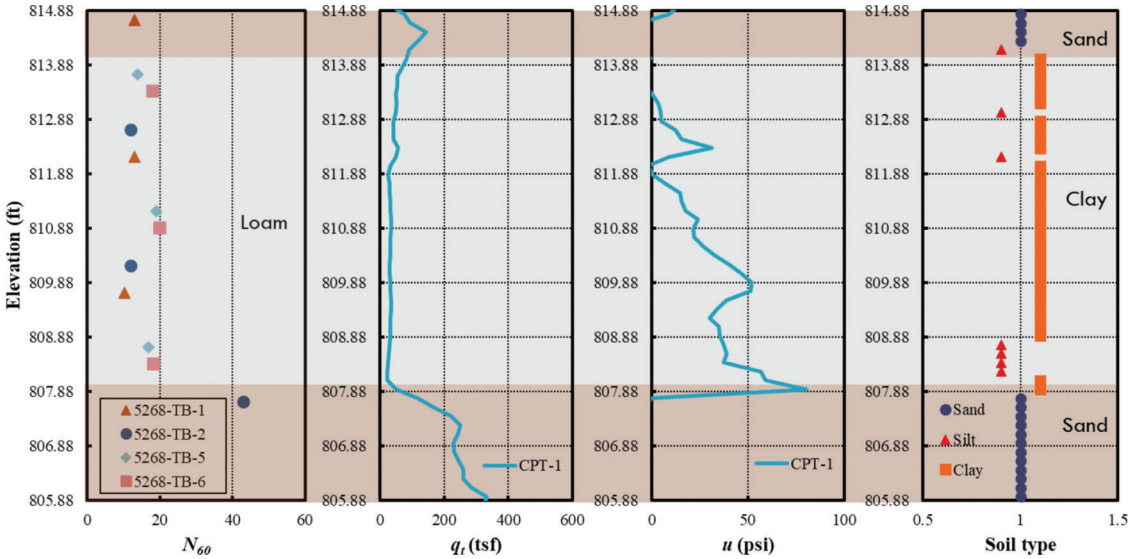

Figure 7.12 Comparison between SPT and CPT data within a depth of 1.5B below the footing base, where B is the footing width.

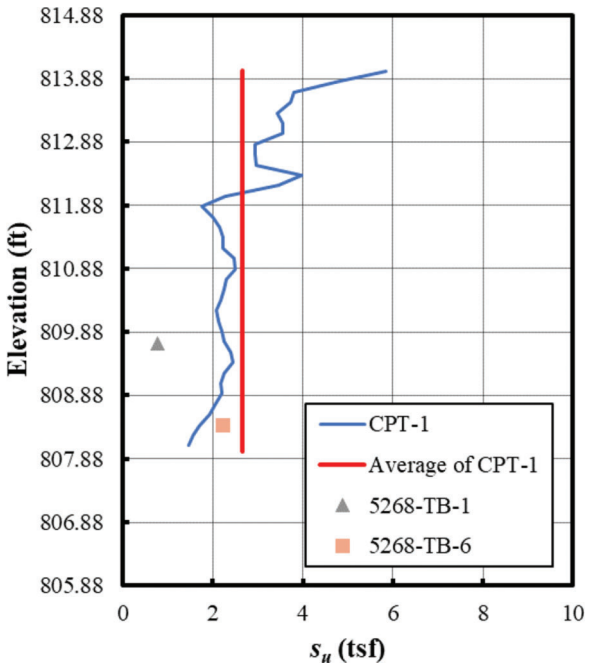

Figure 7.13 Estimated undrained shear strength s_u profile of the clay layer below the footing base.

The capacity of the existing shallow foundation is estimated using (1) the "theoretical method" for clay suggested by the AASHTO LRFD design manual (AASHTO, 2020) and (2) the Purdue method for clay (Salgado, 2022a).

The theoretical method in clay suggested by AASHTO LRFD design manual (AASHTO, 2020) is defined by Equations 10.6.3.1.2a-1–10.6.3.1.2a-4, and the bearing capacity factors, shape correction factors, depth factor and coefficients for various groundwater depths can be found in Tables 10.6.3.1.2a-1–10.6.3.1.2a-3 and Equation 10.6.3.1.2a-10 in the AASHTO manual. For the clay layer, the undrained shear strength s_u is determined from the CPT data using

$$s_u = \frac{q_t - \sigma_v}{N_k} \qquad \text{(Eq. 5.21)}$$

where σ_v is total vertical stress and N_k is the cone factor. The clay layer is considered to be overconsolidated because it has higher values of N_{60} and q_t than typical values for normally consolidated clays, so the higher end value for N_k, equal to 14, is used for the estimation of the undrained shear strength.

Figure 7.13 shows a comparison between the undrained shear strengths obtained from the samples from the test borings and the estimated undrained shear strength from the CPT data within the clay layer below the footing base. The average value of the estimated s_u from the CPT data, which is 2.65 tsf, is used in the capacity estimation, and zero friction angle is considered for the clay layer.

The top sand layer below the footing base is considered using the 2:1 method. First of all, the nominal bearing capacity q_n* acting on top of the clay layer is estimated using the design methods with the enlarged footing width B^* and length L^* calculated based on the 2:1 method, and the nominal bearing capacity q_n acting on top of the sand layer is estimated using

$$q_n = \frac{q_n^* B^* L^*}{BL} \qquad \text{(Eq. 5.22)}$$

where B^* = 6.88 ft and L^* = 156.88 ft.

Table 7.4 shows the capacity estimation of the shallow foundation using the two different design methods. As shown in the table, the Purdue method provides 29% higher nominal bearing capacity and 88% higher factored bearing capacity than the AASHTO method. Given that some recent methods may be more reliable, this comparison shows that there may be reserve in the capacity of the existing foundations.

In the original design plan, the factored maximum soil pressure is 5 ksf, which is similar to the capacity estimated based on the SPT data in clay, as shown in Table 7.3. However, when the factored bearing capacities were estimated using the currently performed CPT data, the estimated values are about 2–3 times greater than 5 ksf. This shows that a quality site investigation can also help establish whether there is reserve in capacity of the existing foundations.

7.3.4.2 Capacity estimation of existing piles. To estimate the capacities of the existing driven piles at each end bents, 90-ft long boring logs (5268_TB-1, 5268_TB-2, 5268_TB-3, 5268_TB-4, 5268_TB-5, and 5268_TB-6) and CPT-1 data were considered. The existing piles were assumed to be predrilled to the elevation of 822 ft, so shaft capacities were considered only from the 822 ft elevation. Figure 7.14 shows a comparison between SPT and CPT data with the soil type classification using the CPT data of the loam layer below the elevation of 822 ft. As discussed in Section 7.3.3.3, the SPT data varies substantially within the loam layer and, in general, the SPT profile is inconsistent with the CPT profile. Most of the pile tips are located within the layer at elevations 796.5–769 ft, so it is important to properly determine the soil type for this layer. However, as shown in Figure 7.14, especially within this layer, the SPT data varies the most, and relatively high N_{60} values would indicate that the soil is a sandy soil, but, in contrast, the relatively low q_t values indicate the soil to be clayey instead. The inconsistency between SPT and CPT data can be because of (1) thin gravelly sand or sand seams exist within the loam layer or (2) the soil profile at the site has high horizontal variability. In this study, soil types within the loam layer were decided based on both SPT and CPT data. The layers where nonnegligible excess pore pressure was observed during cone penetration were considered to be clayey soils. Ideally, more extensive site investigation data, such as from additional CPTs, would have been very helpful for an accurate capacity estimation of the existing foundations.

TABLE 7.4
Capacity estimation of existing shallow foundation at the interior pier

Design Methods	Nominal Bearing Capacity (ksf)	Resistance Factor	Factored Bearing Capacity Calculated Using CPT Data (ksf)
Theoretical Method in Clay (AASHTO, 2020)	17	0.5 (AASHTO, 2020)	8.5
Purdue Method in Clay (Salgado, 2022a)	22	0.73 (Foye et al., 2006)	16

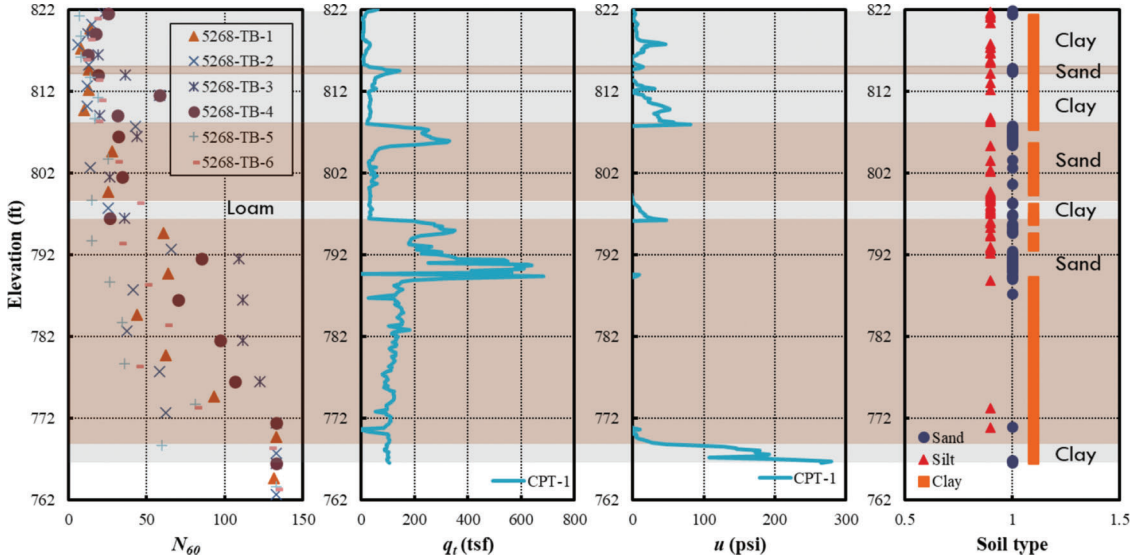

Figure 7.14 Comparison between SPT and CPT data of the loam layer below the elevation 822 ft where existing driven piles are located.

The capacities of the existing driven piles are estimated using the following.

1. AASHTO LRFD design methods (AASHTO, 2020).
   a. Dynamic formula (10.7.3.8.5 in the AASHTO design manual).
      i. FHWA modified Gates formula.
      ii. Engineering News Record formula.
   b. CPT-method (Nottingham and Schmertmann method) (Equations 10.7.3.8.6g-4 and 10.7.3.8.6g-5 and Figures 10.7.3.8.6g-1 and 10.7.3.8.6g-2 in the AASHTO design manual).

2. Purdue method (Salgado, 2022a).
   a. CPT-based method in sand (Han, Ganju, et al., 2019) and CPT-based method in clay (Salgado et al., 2011) modified with the degradation term $[\max(h/B, 1)]^{-0.25}$ in the unit shaft resistance for clay. In the degradation term, h is the distance from the depth being considered to the pile base, and B is the pile diameter.

There are driving records for all existing piles. The existing piles driven in 1969 were driven using a Vulcan #1 air hammer, and the existing piles driven in 2002 were driven using a Delmag D12-32 hammer. Based on driving records, the capacities of the existing piles were estimated using the dynamic formulas, as shown in Table 7.5. The estimated nominal capacities of the piles using the FHWA Gates formula are in the range of 220–372 kips with the average value of 268 kips. When the resistance factor of 0.55 is applied, the average value of the factored capacity is 147 kips. The estimated nominal capacities of the piles using the Engineering News Record formula are in the range of 417–1,108 kips, with an average value of 619 kips. When the resistance factor of 0.10 is applied, the average value of the factored capacity is 62 kips.

The capacities of the existing piles were also estimated using the site investigation data, as shown in Table 7.6. When the capacities were estimated using the CPT method in the AASHTO LRFD design manual (AASHTO, 2020), the estimated nominal shaft and base capacities resulted in the range of 45–407 kips and 121–459 kips, respectively. The estimated total nominal capacities are in the range of 180–812 kips, with an average value of 379 kips. When the resistance factor of 0.50 is applied, the average value of the factored capacity is 189 kips. When the capacities were estimated using the Purdue CPT-based method (Salgado, 2022a), the estimated nominal shaft and base capacities are in the range of 116–196 kips, and 47–372 kips, respectively. The estimated total nominal capacities are in the range of 163–568 kips, with an average value

TABLE 7.5
Estimated capacities of the existing piles at the end bents using dynamic formulae in the AASHTO LRFD design manual (AASHTO, 2020)

		FHWA Gates Formula			Engineering News Record Formula		
Location of the Pile	**Pile #**	**Nominal Capacity (kips)**	**Resistance Factor**	**Factored Capacity (kips)**	**Nominal Capacity (kips)**	**Resistance Factor**	**Factored Capacity (kips)**
Southbound	7	221	0.55	122	426	0.10	43
Bent #1	8	221	(INDOT, 2013)	122	426	(AASHTO, 2020)	43
	9	221		122	426		43
	10	291		160	720		72
	11	277		152	655		65
	12	277		152	655		65
	13	277		152	655		65
	14	277		152	655		65
	15	264		145	600		60
	16	264		145	600		60
	17	270		149	626		63
	18	264		145	600		60
	19	220		121	435		44
Bent #1 Center	20	241		133	469		47
Northbound	5	239	0.55	131	478	0.10	48
Bent #1	6	243	(INDOT, 2013)	134	493	(AASHTO, 2020)	49
	7	239		131	478		48
	8	264		145	600		60
	9	277		152	655		65
	10	308		169	800		80
	11	372		205	1,108		111
	12	329		181	900		90
	13	329		181	900		90
	14	299		164	758		76
	15	355		195	1,029		103
	16	355		195	1,029		103
	17	238		131	463		46
Southbound	7	221	0.55	121	420	0.10	42
Bent #3	8	221	(INDOT, 2013)	122	426	(AASHTO, 2020)	43
	9	221		122	417		42
	10	264		145	600		60
	11	277		152	655		65
	12	270		149	626		63
	13	264		145	600		60
	14	264		145	600		60
	15	277		152	655		65
	16	258		142	576		58
	17	299		164	758		76
	18	264		145	600		60
	19	224		123	438		44
Bent #3 Center	20	220		121	431		43
Northbound	5	260	0.55	143	560	0.10	56
Bent #3	6	275	(INDOT, 2013)	151	625	(AASHTO, 2020)	63
	7	265		146	580		58
	8	277		152	655		65
	9	270		149	626		63
	10	270		149	626		63
	11	277		152	655		65
	12	264		145	600		60
	13	270		149	626		63
	14	264		145	600		60
	15	264		145	600		60
	16	270		149	626		63
	17	270		149	620		62

TABLE 7.6
Estimated capacities of existing piles at the end bents using CPT-based methods

Location of the Pile	Pile #	AASHTO LRFD CPT Method (AASHTO, 2020)				Purdue CPT-Based Method (Salgado, 2022a)			
		Nominal Capacity (kips)		Resistance Factor	Factored Capacity (kips)	Nominal Capacity (kips)		Resistance Factor	Factored Capacity (kips)
		Shaft	Base			Shaft	Base		
Southbound Bent #1	7	161	128	0.50 (AASHTO, 2020)	144	138	80	0.45 (shaft) 0.59 (base) (Foye et al., 2009)[1]	110
	8	106	133		120	150	137		148
	9	89	121		105	147	181		173
	10	158	124		141	139	81		110
	11	159	124		141	139	81		110
	12	275	410		343	178	253		229
	13	156	124		140	139	81		111
	14	163	136		149	138	78		108
	15	163	136		149	138	78		108
	16	180	314		247	158	136		151
	17	184	299		241	168	187		186
	18	178	298		238	150	113		134
	19	194	295		245	168	204		196
Bent #1 Center	20	207	308		258	170	221		207
Northbound Bent #1	5	52	217	0.50 (AASHTO, 2020)	135	144	108	0.45 (shaft) 0.59 (base) (Foye et al., 2009)[1]	129
	6	51	214		133	140	91		117
	7	52	217		135	144	108		129
	8	178	298		238	150	113		134
	9	407	405		406	196	372		307
	10	145	126		136	141	81		111
	11	144	125		135	141	81		111
	12	138	127		133	143	81		112
	13	53	208		131	148	136		147
	14	139	127		133	143	82		113
	15	48	201		124	128	51		88
	16	45	135		90	116	47		80
	17	262	383		322	177	253		229
Southbound Bent #3	7	52	217	0.50 (AASHTO, 2020)	135	144	108	0.45 (shaft) 0.59 (base) (Foye et al., 2009)[1]	129
	8	52	217		135	144	108		129
	9	76	144		110	147	195		181
	10	163	136		149	138	78		108
	11	144	125		134	141	81		111
	12	304	459		381	180	255		232
	13	179	309		244	155	124		143
	14	181	312		246	165	164		171
	15	193	295		244	168	204		196
	16	206	307		257	169	214		202
	17	159	124		141	139	81		110
	18	190	296		243	168	196		191
	19	51	214		133	140	91		117
Bent #3 Center	20	157	124		140	139	81		110
Northbound Bent #3	5	135	129	0.50 (AASHTO, 2020)	132	144	83	0.45 (shaft) 0.59 (base) (Foye et al., 2009)[1]	114
	6	132	129		131	145	84		115
	7	120	130		125	148	102		127
	8	236	340		288	173	248		224
	9	180	315		248	162	148		160
	10	180	315		248	162	148		160
	11	184	299		241	168	187		186
	12	154	124		139	139	91		111
	13	158	124		141	139	81		110
	14	181	303		242	168	174		178
	15	180	314		247	160	144		157
	16	251	362		306	175	252		227
	17	148	125		136	140	82		111

[1]Resistance factors are for the closed-ended pipe piles.

TABLE 7.7
Average values of the estimated capacities of the existing piles at the end bents

Design Methods	Nominal Capacity (kips/pile)	Resistance Factor	Factored Capacity (kips/pile)
FHWA Gates Formula (AASHTO, 2020)	268 (220–372)	0.55 (INDOT, 2013)	147
Engineering News Formula (AASHTO, 2020)	619 (417–1,108)	0.10 (AASHTO, 2020)	62
CPT Method (AASHTO, 2020)	Shaft: 156 Base: 223 Total: 379 (180–812)	0.50 (AASHTO, 2020)	189
CPT-based Method (Salgado, 2022a)	Shaft: 152 Base: 136 Total: 287 (163–568)	Shaft: 0.45 Base: 0.59 (Foye et al., 2009)[1]	148

[1]Resistance factors are for the closed-ended pipe piles.

of 287 kips. When the resistance factors 0.45 and 0.59 are applied for the shaft and base resistances, the average value of the factored capacity is 148 kips.

Table 7.7 summarizes the average values of the estimated capacities of the existing piles at the end bents using different design methods. In the table, the ranges of estimated total nominal capacities using different methods are also noted within the parentheses to highlight the variability of estimated capacities from mean values. As shown in the table, the FHWA Gates formula has the narrowest capacity range. Even though the same driving records were used for the Engineering News formula, it has a wider capacity range than the FHWA Gates formula. Both the AASHTO CPT method and Purdue CPT-based methods provide relatively high variability in the estimated capacities. This can be because of the high horizontal variability of the soil profile at the site, as we discussed earlier in this chapter.

7.3.5 Design Checks

According to the flowchart for foundation reuse design proposed in this study and provided in Figure 3.1, the design checks for foundation reuse can be performed using the estimated capacities of existing foundations and the updated design loads. The minimum requirements for foundation reuse, described in Chapter 3.4, can be checked for this project as shown below.

1. Factored foundation resistance > factored load.
   a. Table 7.8 and Table 7.9 show the factored resistances of the existing foundations and the updated factored loads, respectively. Factored resistances and loads are calculated using different design codes: AASHTO ASD method (AASHTO, 2002), AASHTO LFD method (AASHTO, 2002), and AASHTO LRFD method (AASHTO, 2020). In Table 7.9, the updated factored loads are also compared with the corresponding factored resistances. As shown in the table, none of the existing foundations, except the piles on the northbound side when the AASHTO LRFD method is used, passes this criterion.
2. No significant foundation element deterioration.
   a. The existing foundations pass the structural integrity check according to inspection done by INDOT personnel or contractors.
3. Structurally sound foundation elements.
   a. The existing foundations pass the structural integrity check according to inspection done by INDOT personnel or contractors.
4. No significant scour.
   a. A significant scour was not observed during inspection by INDOT personnel or contractors.
5. No excessive total and differential settlements.
   a. Excessive total and differential settlements were not observed during inspection by INDOT personnel or contractors.
6. No excavations or other work that might lead to loss of foundation support.
   a. Any work that might lead to loss of existing foundation support is not expected during the bridge widening project.
7. No significant reconfiguration of loads.
   a. The total nominal load on the southbound end bent increases from 1,010 kips to 1,601 kips; the total nominal load on the northbound end bent increases from 1,010 kips to 1,461 kips; total nominal load on the southbound interior pier increases from 2,335 kips to 3,924 kips, and total nominal load on the northbound interior pier increases from 2,335 kips to 3,460 kips. The updated loads are about 45%–68% higher than the original loads, so there is a significant increase in the updated loads.
8. Lack of ability to perform construction as needed for the existing and new foundation elements.
   a. New foundations can be constructed.

For this bridge widening project, the updated loads are significantly higher than the original loads, so, as

TABLE 7.8
The factored resistances of existing foundations

Location of the Foundation	Foundation Type	Nominal Capacity of Existing Foundation[2] (kips)	AASHTO ASD Design Specification (AASHTO, 2002)		AASHTO LFD Design Specification (AASHTO, 2002)		AASHTO LRFD Design Specification (AASHTO, 2020)	
			FS	*R* (kips)	ϕ	*R* (kips)	RF	*R* (kips)
Southbound Bent #1	19+1/2 piles[1]	3,465	3.5	990	0.4[3]	1,386	0.55	1,905
Northbound Bent #1	17+1/2 piles[1]	3,968		1,134		1,587	(INDOT, 2013)	2,182
Southbound Bent #3	19+1/2 piles[1]	3,434		981		1,374		1,889
Northbound Bent #3	17+1/2 piles[1]	3,606		1,030		1,442		1,983
Southbound Interior Pier	8 piles + shallow foundation	7,939	3.0	2,646	0.5	3,970	0.5	3,970
Northbound Interior Pier	6 piles + shallow foundation	7,939		2,646		3,970		3,970

Note:
FS = factor of safety, *R* = factored resistance, ϕ = performance factor, RF = resistance factor.
[1]Half of nominal capacities of center piles are added to both nominal capacities of northbound and southbound piles.
[2]Nominal capacities of driven piles are estimated using FHWA Gates formula, and nominal capacities of shallow foundation is estimated using the theoretical method in clay (AASHTO, 2020).
[3]No information on the performance factor for FHWA Gates formula. 0.4 is assumed.

TABLE 7.9
The updated factored loads

Location of the Foundation	Foundation Type	Nominal Load Acting on Existing Foundation (Kips)	AASHTO ASD Design Specification (AASHTO, 2002)		AASHTO LFD Design Specification (AASHTO, 2002)		AASHTO LRFD Design Specification (AASHTO, 2020)	
			Load Factor	Factored Load (kips)	Load Factor	Factored Load (kips)	Load Factor	Factored Load (kips)
Southbound Bent #1	19+1/2 piles[1]	Dead: 1,291 Live: 310 Total: 1,601	Dead: 1.0 Live: 1.0 Vertical earth pressure: 1.0	1,601>990	Dead: 1.3 Live: 2.17 Vertical earth pressure: 1.0	2,352>1,386	Dead: 1.25 Live: 1.75 Vertical earth pressure: 1.3	2,157>1,905
Northbound Bent #1	17+1/2 piles[1]	Dead: 1,152 Live: 310 Total: 1,461		1,461>1,134		2,170>1,587		1,982<2,182
Southbound Bent #3	19+1/2 piles[1]	Dead: 1,291 Live: 310 Total: 1,601		1,601>981		2,352>1,374		2,157>1,889
Northbound Bent #3	17+1/2 piles[1]	Dead: 1,152 Live: 310 Total: 1,461		1,461>1,030		2,170>1,442		1,982<1,983
Southbound Interior Pier	8 piles + shallow foundation	Dead: 3,834 Live: 73 Earth pressure: 17 Total: 3,924		3,924>2,646		5,159>3,970		4,942>3,970
Northbound Interior Pier	6 piles + shallow foundation	Dead: 3,373 Live: 73 Earth pressure: 14 Total: 3,460		3,460>2,646		4,557>3,970		4,362>3,970

[1]Half of nominal capacities of center piles are added to both nominal capacities of northbound and southbound piles.

TABLE 7.10
As-built geometry and estimated nominal capacities of new piles at the end bents and the interior pier

Location of the Pile	Pile #	Pile Tip Elevation (ft)	Capacity Estimation Using FHWA Gates Formula		PDA Test Result at BOR	
			Nominal Capacity (kips)	Factored Capacity[1] (kips)	Nominal Capacity (kips)	Factored Capacity[1] (kips)
Southbound Bent #1	1	794.26	484	266	–	–
	2	793.42	521	286	–	–
	3	793.51	521	286	–	–
	4	794.51	539	296	–	–
	5	795.42	521	286	–	–
	6 (test)	792.01	505	278	384	269
Northbound Bent #1	1	793.17	487	268	–	–
	2	794.51	493	271	–	–
	3	793.17	464	255	–	–
	4 (test)	793.26	493	271	355	249
Southbound Bent #3	1	792.76	499	274	–	–
	2	793.42	485	267	–	–
	3	793.51	459	253	–	–
	4	794.51	478	263	–	–
	5	795.42	485	267	–	–
	6 (test)	795.67	471	259	369	258
Northbound Bent #3	1	797.17	440	242	–	–
	2	794.76	440	242	–	–
	3	794.42	440	242	–	–
	4 (test)	792.92	470	258	314	220
Southbound Interior Pier #2	1	779.03	532	292	–	–
	2	777.20	562	309	–	–
	3	777.62	553	304	–	–
	4	781.28	524	288	–	–
	5	776.78	566	311	–	–
	6	781.03	540	297	–	–
	7	778.70	517	284	–	–
	8 (test)	780.78	536	295	523	366
Northbound Interior Pier #2	1	773.03	661	364	–	–
	2	772.53	641	352	–	–
	3	775.20	649	357	–	–
	4 (test)	771.78	607	334	595	417
	5	775.12	605	333	–	–
	6	776.70	668	367	–	–

[1]Resistance factors for FHWA Gates formula and the PDA test results at BOR (the beginning of restrike) are 0.55 and 0.70, respectively (INDOT, 2013).

shown in Table 7.9, the existing foundations cannot bear the estimated updated loads with the required level of reliability. Therefore, foundation reuse solutions are required.

7.3.6 Selection of Foundation Reuse Solution

7.3.6.1 Foundation reuse solution. As described in Chapter 7.3.5, the existing foundations do not pass the design checks, so there is a need for foundation reuse solutions. Foundation reuse solutions can be determined by using the flow chart shown in Figure 6.1. For this project, reducing the updated design loads was not preferable or possible, so the existing foundations were strengthened by the following:

- adding new piles at the end bents and interior pier, and
- widening the shallow foundation and constructing a pile cap at the interior pier.

As we discussed in Chapter 7.3.2, during the inspection, small cracks near the join connecting the original and widened portions of the existing pier on shallow foundations were observed, and the pattern of the cracks was interpreted as a sign of differential settlements. Therefore, the foundation at the interior pier was widened and placed on piles to minimize any

TABLE 7.11
Design checks with the increased factored resistances

Location of the Foundation	AASHTO ASD Design Specification (AASHTO, 2002)		AASHTO LFD Design Specification (AASHTO, 2002)		AASHTO LRFD Design Specification (AASHTO, 2020)	
	Factored Resistance (kips)	Factored Load (kips)	Factored Resistance (kips)	Factored Load (kips)	Factored Resistance (kips)	Factored Load (kips)
Southbound Bent #1	1,873>	1,601	2,622>	2,352	3,604>	2,157
Northbound Bent #1	1,688>	1,461	2,362>	2,170	3,248>	1,982
Southbound Bent #3	1,803>	1,601	2,525>	2,352	3,471>	2,157
Northbound Bent #3	1,542>	1,461	2,158<	2,170	2,968>	1,982
Southbound Interior Pier	3,883<	3,924	5,702>	5,159	6,351>	4,942
Northbound Interior Pier	3,740>	3,460	5,502>	4,557	6,076>	4,362

differential settlements between the existing and new foundations.

7.3.6.2 Capacity estimation of new foundations. The newly added piles at each end bent and at the interior pier location are steel encased concrete (SEC) piles with 14-inch pile diameters. The piles were driven using an APE D19-52 hammer in 2022. Table 7.10 shows the pile tip elevations and the estimated capacity of each pile using the FHWA Gates formula (AASHTO, 2020). PDA tests were performed only for the test piles that are noted in parentheses next to the pile number in the table. For the test piles, the estimated nominal capacities using the PDA results at the beginning of restrike 3 to 5 days after driving were also calculated. Factored capacities for the FHWA Gates formula and PDA test results were calculated with resistance factors of 0.55 and 0.70, respectively (INDOT, 2013).

7.3.6.3 Design checks. Design checks were performed again using the increased factored resistances of the foundations after adding additional piles at each end bent and at the interior pier to strengthen the foundations. Table 7.11 shows the comparisons between the factored resistances and the factored loads using different design codes: AASHTO ASD method (AASHTO, 2002), AASHTO LFD method (AASHTO, 2002), and AASHTO LRFD method (AASHTO, 2020). As shown in the table, when the LRFD design framework is used, all foundations have higher factored resistances than the factored loads, but when the ASD design framework is used, the foundation at the southbound interior pier has lower factored resistance than the factored load and when the LFD design framework is used, the piles at the northbound end bent #3 has lower factored resistance than the factored load.

7.4 Lessons Learned from the Implementation Project

The following lessons were learned from the implementation project.

- Loam layers, which are typical in Indiana, may be hard to classify as a sandy soil or clayey soil. However, a correct classification is very important, because most of the design methods, including traditional ones contained in AASHTO (AASHTO, 2020) and current methods, are developed for sand and clay, separately; therefore, depending on the classification, the estimated capacities can be very different even for the same SPT or CPT values.
- Accurate site investigation is essential to estimate whether there is reserve capacity in existing foundations, and additional site investigation is generally worth doing, not only to account for any strengthening of the soil that may have occurred in time, but also because of the greater accuracy in interpretation and analysis that results.
- Capacity estimation using the most current, state-of-the-art methods can be useful in estimating the reserve capacity of existing foundations.
- Design checks using different design codes can produce contrasting results.

REFERENCES

AASHTO. (2002). *AASHTO standard specifications for highway bridges* (17th ed.). American Association of State Highway and Transportation Officials.

AASHTO. (2020). *AASHTO LRFD bridge design specifications* (9th ed.). American Association of State Highway and Transportation Officials.

Agrawal, A. K., Jalinoos, F., Davis, N., Hoomaan, E., & Sanayei, M. (2018). *Foundation reuse for highway bridges* (Report No. FHWA-HIF-18-055). Federal Highway Administration.

Aktan, H., & Attanayake, U. (2015). *Research on evaluation and standardization of accelerated bridge construction techniques* (Report No. MDOT RC-1618A). Western Michigan University.

Azari, H. (2020, August). *FHWA nondestructive evaluation program: Strategic plan for FY 2019-2022* (Publication No. FHWA-HRT-20-045). Federal Highway Administration. https://highways.dot.gov/sites/fhwa.dot.gov/files/FHWA-HRT-20-045.pdf

Baker, C. N., Jr., Drumright, E. E., Mensah, F. D., Parikh, G., & Ealy, C. D. (1991). Use of nondestructive testing to evaluate defects in drilled shafts: Results of FHWA research. *Transportation Research Record*, *1331*, 28–35.

Boeckmann, A. Z. (2019). Estimating capacity and reliability of existing foundations for evaluation of reuse. *DFI Journal: The Journal of the Deep Foundations Institute*, *13*(1), 11–24.

Boeckmann, A. Z., & Loehr, J. E. (2017). Current practices and guidelines for the reuse of bridge foundations. In *Current Practices and Guidelines for the Reuse of Bridge Foundations* (NCHRP Synthesis 505). Transportation Research Board of the National Academies.

Boeckmann, A., & Shields, H. (2022, Jan/Feb). DFI46 panel on foundation reuse. In *Deep Foundations: The Magazine of the Deep Foundation Institute* (pp. 93–97). Deep Foundations Institute. https://www.nxtbook.com/dfi/DEEP-FOUNDATIONS/january-february-2022/index.php#/p/Intro

Boeckmann, A. Z., Rosenblad, B. L., & Bowders, J. J. (2018, May). *Foundation reuse: Length, condition, and capacity of existing driven piles* (Report No. CMR 18-008). University of Missouri-Columbia.

Bozozuk, M. (1978). Bridge foundations move. *Transportation Research Record*, *678*, 17–21. Transportation Research Board.

Brown, D. A., Turner, J. P., & Castelli, R. J. (2010). *Drilled shafts: Construction procedures and LRFD design methods* (Report No. FHWA-NHI-10-016). Federal Highway Administration.

Brown, T., & Hettiarachchi, H. (2008). Estimating shear strength properties of soils using SPT blow counts: An energy balance approach. *GeoCongress 2008: Characterization, Monitoring, and Modeling of GeoSystems* (pp. 364–371).

Butcher, A. P., Powell, J. J. M., & Skinner, H. D. (2006). *Reuse of foundations for urban sites: a best practice handbook*. Building Research Establishment Press.

Butterfield, R., & Banerjee, P. K. (1971). The problem of pile group–pile cap interaction. *Géotechnique*, *21*(2), 135–142.

Canadian Geotechnical Society. (1985). *Canadian foundation engineering manual* (2nd ed.). Bitech Publishers.

Carter, J. P., & Kulhawy, F. H. (1988). *Analysis and design of drilled shaft foundations socketed into rock* (Research Project EL-5918). Cornell University Geotechnical Engineering Group.

Chakraborty, T., Salgado, R., Basu, P., & Prezzi, M. (2013). Shaft resistance of drilled shafts in clay. *Journal of Geotechnical and Geoenvironmental Engineering*, *139*(4), 548–563. American Society of Civil Engineers.

Chakraborty, T., Salgado, R., & Loukidis, D. (2013). A two-surface plasticity model for clay. *Computers and Geotechnics*, *49*, 170–190.

Chow, Y. K., & Teh, C. I. (1991). Pile-cap-pile-group interaction in nonhomogeneous soil. *Journal of Geotechnical Engineering*, *117*(11), 1655–1668.

Clausen, C. J. F., Aas, P. M., & Karlsrud, K. (2005). Bearing capacity of driven piles in sand, the NGI approach. *Frontiers in Offshore Geotechnics, ISFOG 2005 - Proceedings of the 1st International Symposium on Frontiers in Offshore Geotechnics* (pp. 677–681).

Collin, J. G., & Jalinoos, F. (2014). *Foundation characterization program (FCP): TechBrief # 1—Workshop Report on the Reuse of Bridge Foundations* (FHWA Publication No. FHWA-HRT-14-072). Federal Highway Administration.

Davis, N. T., Hoomaan, E., Agrawal, A. K., Sanayei, M., & Jalinoos, F. (2019). Foundation reuse in accelerated bridge construction. *Journal of Bridge Engineering*, *24*(10), 05019010.

Davis, N. T., Hoomaan, E., Sanayei, M., Agrawal, A. K., & Jalinoos, F. (2018). Integrated superstructure-substructure load rating for bridges with foundation movements. *Journal of Bridge Engineering*, *23*(5), 04018022.

Esrig, M. I., Kirby, R. C., & Murphy, B. S. (1981). Advances in general effective stress method for prediction of axial capacity for driven piles in clay. *Journal of Petroleum Technology*, *33*(9), 1793–1802.

Feng, Z., Huo, J., Hu, H., Zhao, R., Wang, F., Jiang, G., Yao, X. H., Li, T., & Song, Z. (2021). Research on corrosion damage and bearing characteristics of bridge pile foundation concrete under a dry-wet-freeze-thaw cycle. *Advances in Civil Engineering*, *2021*(6), 1–13. https://doi.org/10.1155/2021/8884396

Focht, J. A., & Vijayvergiya, V. N. (1972). A new way to predict capacity of piles in clay. In *4th Annual Offshore Technology Conference* (Paper No. OTC-1718-MS) (pp. 865–874). https://doi.org/10.4043/1718-MS

Foye, K. C., Abou-Jaoude, G., Prezzi, M., & Salgado, R. (2009). Resistance factors for use in load and resistance factor design of driven pipe piles in sands. *Journal of Geotechnical and Geoenvironmental Engineering*, *135*(1), 1–13.

Foye, K. C., Salgado, R., & Scott, B. (2006). Resistance factors for use in shallow foundation LRFD. *Journal of Geotechnical and Geoenvironmental Engineering*, *132*(9), 1208–1218.

Ganju, E., Prezzi, M., & Salgado, R. (2017). Algorithm for generation of stratigraphic profiles using cone penetration test data. *Computers and Geotechnics*, *90*, 73–84.

Google. (2022). [*Google Maps Shadeland Avenue and 71st street, Indianapolis, IN, US*]. Retrieved in December 2022 from https://www.Google.Com/Maps/Place/Shadeland+Ave+%26+71st+St/@39.8837121,-86.0486193,17z/Data=!3m1!4b1!4m6!3m5!1s0x886b4ce4d2039c75:0x619e54bebb5d0a30!8m2!3d39.883708!4d-86.046039!16s%2Fg%2F1tgxjt63

Grinč, M., Vondráčková, T., Vlček, J., Myslivečková, M., Nývlt, V., & Kovalčík, L′. (2015). Non–invasive GPR investigation of spread footings. *Procedia Earth and Planetary Science*, *15*, 31–36.

Han, F., Ganju, E., Prezzi, M., Salgado, R., & Zaheer, M. (2020). Axial resistance of open-ended pipe pile driven in gravelly sand. *Géotechnique*, *70*(2), 138–152.

Han, F., Ganju, E., Salgado, R., & Prezzi, M. (2019). Comparison of the load response of closed-ended and open-ended pipe piles driven in gravelly sand. *Acta Géotechnica*, *14*(6), 1785–1803.

Han, F., Lim, J., Salgado, R., Prezzi, M., & Zaheer, M. (2015). *Load and resistance factor design of bridge foundations accounting for pile group–Soil interaction* (Joint Transportation Research Program Publication No. FHWA/IN/JTRP-2015/24). West Lafayette, IN: Purdue University. https://doi.org/10.5703/1288284316009

Han, F., Marashi, M., Prezzi, M., Salgado, R., Wells, T., & Zaheer, M. (2020). Monitoring of the response of the Sagamore Parkway Bridge and its foundations during a live load test. *Transportation Research Record*, *2675*(3), 358–366. https://doi.org/10.1177/036119812097126

Han, F., Prezzi, M., Salgado, R., Marashi, M., Wells, T., & Zaheer, M. (2020). *Verification of bridge foundation design assumptions and calculations* (Joint Transportation Research Program Publication No. FHWA/IN/JTRP-2020/18). West Lafayette, IN: Purdue University. https://doi.org/10.5703/1288284317084

Han, F., Prezzi, M., Salgado, R., & Zaheer, M. (2017). Axial resistance of closed-ended steel-pipe piles driven in multi-layered soil. *Journal of Geotechnical and Geoenvironmental Engineering*, *143*(3), 04016102.

Han, F., Salgado, R., Prezzi, M., & Lim, J. (2017). Shaft and base resistance of non-displacement piles in sand. *Computers and Geotechnics*, *83*, 184–197.

Han, F., Salgado, R., Prezzi, M., & Lim, J. (2019). Axial resistance of nondisplacement pile groups in sand. *Journal of Geotechnical and Geoenvironmental Engineering*, *145*(7).

Hannigan, P. J., Goble, G. G., Thendean, G., Likins, G. E., & Rausche, F. (2006). *Design and construction of driven pile foundations-volume I and II* (Report No. FHWA-NHI-16-009). National Highway Institute.

Hansen, J. B. (1970). A revised and extended formula for bearing capacity. *Bulletin of the Danish Geotechnical Institute*, *28*, 5–11.

Hertlein, B., & Davis, A. G. (2007). *Nondestructive testing of deep foundations*. John Wiley & Sons.

Hoomaan, E., Agrawal, A., Davis, N., & Jalinoos, F. (2021). Risks in reuse of highway bridge foundations. *Journal of Infrastructure Systems*, *27*(4), 04021043.

Horvath, R. G., Kenney, T. C., & Kozicki, P. (1983). Methods of improving the performance of drilled piers in weak rock. *Canadian Geotechnical Journal*, *20*(4), 758–772.

Huang, M., Liang, F., & Jiang, J. (2011). A simplified nonlinear analysis method for piled raft foundation in layered soils under vertical loading. *Computers and Geotechnics*, *38*(7), 875–882.

IDOT. (2011). *Bridge condition report procedures and practices*. Illinois Department of Transportation.

INDOT. (2013). *Indiana design manual*. Indiana Department of Transportation.

INDOT. (2018). *Indiana design manual*. Indiana Department of Transportation.

Jalinoos, F. (2015, November/December). Reusing bridge foundations. *Public Roads*, *79*(3).

Jalinoos, F., Mulla, M. A., & Schaefer, V. R. (2016). Foundation reuse and enhancement: A viable option for bridge widening and replacement projects. *GeoStrata Magazine Archive*, *20*(3), 52–57.

Jalinoos, F., Tran, K. T., Nguyen, T. D., & Agrawal, A. K. (2017). Evaluation of bridge abutments and bounded wall type structures with ultraseismic waveform tomography. *Journal of Bridge Engineering*, *22*(12).

Janabi, F. H., Prezzi, M., Salgado, R., & Lim, J. (2022). *Limit bearing capacity of footings in sand from half-model footing tests performed in a calibration chamber with a viewing window* [Manuscript in preparation].

Jardine, R., Chow, F., Overy, R., & Standing, J. (2005). ICP design methods for driven piles in sand and clays. In *Heron* (Vol. 106). Thomas Telford.

Karlsrud, K., Clausen, C. J. F., & Aas, P. M. (2005). Bearing capacity of driven piles in clay, the NGI approach. In *Proceedings of the 1st International Symposium on Frontiers in Offshore Geotechnics*, *1*, 775–782.

Kolk, H. J., Baaijens, A. E., & Senders, M. (2005). Design criteria for pipe piles in silica sands. In *Design Criteria For Pipe Piles in Silica Sands* (pp. 711–716). CRC Press/ Balkema.

Kolk, H. J., & der Velde, E. (1996, April). *A reliable method to determine friction capacity of piles driven into clays* [Paper presentation]. Offshore Technology Conference, Houston, Texas. https://doi.org/10.4043/7993-MS

Kulhawy, F. H., Akbas, S. O., & Prakoso, W. A. (2005). Evaluation of capacity of rock foundation sockets. *American Rock Mechanics Association - 40th US Rock Mechanics Symposium, ALASKA ROCKS 2005: Rock Mechanics for Energy, Mineral and Infrastructure Development in the Northern Regions*. American Rock Mechanics Association.

Kulhawy, F. H., Trautmann, C. H., Beech, J. F., O'Rourke, T. D., McGuire, W. (1983). *Transmission line structure foundation for uplift-compression loading* (Report No. EPRI-EL-2870). Electric Power Research Institute.

LeGrand, L. (2015). Keeping Virginia moving (Publication No. FHWA-HRT-15-005). *Public Roads*, *79*(1). Federal Highway Administration.

Lehane, B. M., Li, Y., & Williams, R. (2013). Shaft capacity of displacement piles in clay using the cone penetration test. *Journal of Geotechnical and Geoenvironmental Engineering*, *139*(2), 253–266.

Lehane, B. M., Schneider, J. A., & Xu, X. (2005). The UWA-05 method for prediction of axial capacity of driven piles in sand. In M. J. Cassidy and S. Gourvenec (Eds.), *Proceedings of the International Symposium on Frontiers in Offshore Geotechnics* (pp. 683–689). CRC Press.

Loukidis, D., Chakraborty, T., & Salgado, R. (2008). Bearing capacity of strip footings on purely frictional soil under eccentric and inclined loads. *Canadian Geotechnical Journal*, *45*(6), 768–787.

Loukidis, D., & Salgado, R. (2008). Analysis of the shaft resistance of non-displacement piles in sand. *Géotechnique*, *58*(4), 283–296.

Loukidis, D., & Salgado, R. (2009). Bearing capacity of strip and circular footings in sand using finite elements. *Computers and Geotechnics*, *36*(5), 871–879.

Loukidis, D., & Salgado, R. (2011). Effect of relative density and stress level on the bearing capacity of footings on sand. *Géotechnique*, *61*(2), 107–119.

Lyamin, A. V., Salgado, R., Sloan, S. W., & Prezzi, M. (2007). Two-and three-dimensional bearing capacity of footings in sand. *Géotechnique*, *57*(8), 647–662.

MaineDOT. (2018). *Bridge design guide*. Maine Department of Transportation.

MassDOT. (2013). *LRFD bridge manual*. Massachusetts Department of Transportation.

McCabe, B. A., & Lehane, B. M. (2006). Behavior of axially loaded pile groups driven in clayey silt. *Journal of Geotechnical and Geoenvironmental Engineering*, *132*(3), 401–410.

Meyerhof, G. G. (1951). The ultimate bearing capacity of foundations. *Géotechnique*, *2*(4), 301–332. https://doi.org/10.1680/geot.1951.2.4.301

Meyerhof, G. G. (1953). The bearing capacity of foundations under eccentric and inclined loads. *Proceedings of 3rd International Conference on Soil Mechanics and Foundation Engineering* (pp. 440–445). International Society for Soil Mechanics and Geotechnical Engineering.

Meyerhof, G. G. (1963). Some recent research on the bearing capacity of foundations. *Canadian Geotechnical Journal*, *1*(1), 16–26.

Meyerhof, G. G. (1976). Bearing capacity and settlement of pile foundations. *Journal of the Geotechnical Engineering Division*, *102*(3), 197–228. https://doi.org/10.1061/AJGEB6.0000243

Morgenstern, N. R., & Tchalenko, J. S. (1969). Microscopic structures in kaolin subjected to direct shear. *Géotechnique*, *19*(3), 426–427. https://doi.org/10.1680/geot.1969.19.3.426

Munfakh, G. A., Arman, A., Collin, J. G., Hung, J. C.-J., & Brouillette, R. P. (2001). *Shallow foundations reference manual* (FHWA-NHI-01-23). U.S. Department of Transportation, Federal Highway Administration

ODOT. (2020). *Bridge design manual*. Ohio Department of Transportation. https://www.transportation.ohio.gov/wps/wcm/connect/gov/500258d3-ee36-462f-b7d6-422c9caba872/2020_BDM_07-21-23.pdf?MOD=AJPERES&CONVERT_TO=url&CACHEID=ROOTWORKSPACE.Z18_M1HGG

IK0N0JO00QO9DDDDM3000-500258d3-ee36-462f-b7d6-422c9caba872-oBUkbBJ

Olson, L. D., Jalinoos, F., & Aouad, M. F. (1998). *Determination of unknown subsurface bridge foundations: A summary of the NCHRP 21-5 interim report*. U.S. Department of Transportation, Federal Highway Administration.

O'Neil, M. W., & Reese, L. C. (1999, August). *Drilled shafts: Construction procedures and design methods* (Report No. FHWA-IF-99-025). All American Soils.

Ottaviani, M. (1976, March). Discussion: Three-dimensional finite element analysis of vertically loaded pile groups. *Géotechnique*, *26*(1), 238–241.

Park, D., Choi, K.-C., & Lee, J. (2012). Analysis of piled raft interactions in sand with centrifuge test. *Journal of the Korean Geotechnical Society*, *28*(10), 27–40.

Sabatini, P. J., Bachus, R. C., Mayne, P. W., Schneider, J. A., & Zettler, T. E. (2002). *Evaluation of soil and rock properties* (Report No. FHWA-IF-02-034). Federal Highway Administration.

Sakleshpur, V. A., Prezzi, M., Salgado, R., & Zaheer, M. (2021a). *CPT-based geotechnical design manual, Volume 2: CPT-based design of foundations—Methods* (Joint Transportation Research Program Publication No. FHWA/IN/JTRP-2021/23). West Lafayette, IN: Purdue University. https://doi.org/10.5703/1288284317347

Sakleshpur, V. A., Prezzi, M., Salgado, R., & Zaheer, M. (2021b). *CPT-based geotechnical design manual, Volume 3: CPT-based design of foundations—Example problems* (Joint Transportation Research Program Publication No. FHWA/IN/JTRP-2021/24). West Lafayette, IN: Purdue University. https://doi.org/10.5703/1288284317348

Salgado, R. (2006). The role of analysis in non-displacement pile design. In *Modern Trends in Geomechanics* (pp. 521–540). Springer Berlin Heidelberg.

Salgado, R. (2008). *The engineering of foundations* (1st ed.). McGraw-Hill.

Salgado, R. (2022a). *The engineering of foundations, slopes and retaining structures*. CRC Press.

Salgado, R. (2022b). Risk runs through it: The legal framework for dam breach failures. *University of Louisville Law Review*, *61*(1), 1–53.

Salgado, R., Han, F., & Prezzi, M. (2017). Axial resistance of non-displacement piles and pile groups in sand. *Rivista Italiana Di Geotecnica*, *51*(4), 35–46.

Salgado, R., Lyamin, A. V., Sloan, S. W., & Yu, H. S. (2004). Two- and three-dimensional bearing capacity of foundations in clay. *Géotechnique*, *54*(5), 297–306.

Salgado, R., & Prezzi, M. (2007). Computation of cavity expansion pressure and penetration resistance in sands. *International Journal of Geomechanics*, *7*(4), 251–265.

Salgado, R., Woo, S. I., & Kim, D. (2011). *Development of load and resistance factor design for ultimate and serviceability limit states of transportation structure foundations* (Joint Transportation Research Program Publication No. FHWA/IN/JTRP-2011/03). West Lafayette, IN: Purdue University. https://doi.org/10.5703/1288284314618

Samtani, N. C., & Nowatzki, E. A. (2006). *Soils and foundations reference manual–Volume II*. Federal Highway Administration.

Samu, V., & Guddati, M. (2019). Nondestructive method for length estimation of pile foundations through effective dispersion analysis of reflections. *Journal of Nondestructive Evaluation*, *38*(2), 1–11.

Samu, V., & Guddati, M. (2020). Nondestructive length estimation of an embedded pile through combined analysis of transverse and longitudinal waves. *NDT and E International*, *110*, 102203.

Schmertmann, J. H. (1970). Static cone to compute static settlement over sand. *Journal of the Soil Mechanics and Foundations Division*, *96*(3), 1011–1043.

Senna, R. S., Cintra, J. C. A., Rezende, M. E. B., & Carvalho, D. (1993). Load distribution in bored pile groups. *Proceedings of the 2nd International Geotechnical Seminar on Deep Foundations on Bored and Auger Piles* (pp. 151–154).

Shen, W. Y., Chow, Y. K., & Yong, K. Y. (2000). A variational approach for the analysis of pile group–pile cap interaction. *Géotechnique*, *50*(4), 349–357. https://doi.org/10.1680/geot.2000.50.4.349

SIMULIA. (2017). *Abaqus/CAE*. Dassault Systèmes.

SIMULIA. (2021). *Abaqus/CAE*. Dassault Systèmes.

Skempton, A. W. (1951). The bearing capacity of clays. *Selected Papers on Soil Mechanics* (pp. 50–59).

Tehrani, F. S., Han, F., Salgado, R., Prezzi, M., Tovar, R. D., & Castro, A. G. (2015). Effect of surface roughness on the shaft resistance of non-displacement piles embedded in sand. *Géotechnique*, *66*(5), 386–400. https://doi.org/10.1680/jgeot.15.P.007

Terzaghi, K. (1943). *Theoretical soil mechanics*. Wiley. https://onlinelibrary.wiley.com/doi/epdf/10.1002/9780470172766

Thakur, V. (2007). *Strain localization in sensitive soft clays* [Doctoral dissertation, Norwegian University of Science and Technology].

Thakur, V. (2011). Numerically observed shear bands in soft sensitive clays. *Geomechanics and Geoengineering: An International Journal*, *6*(2), 131–146.

Tiberio, T. (2015). Reuse of Milton Madison bridge piers. *Proceedings of the 94th Annual Meeting of the Transportation Research Board*. Transportation Research Board.

Tomlinson, M., & Woodward, J. (2007). *Pile design and construction practice* (5th ed.). CRC Press.

Tovar-Valencia, R. D., Galvis-Castro, A. C., Salgado, R., & Prezzi, M. (2018). Effect of surface roughness on the shaft resistance of displacement model piles in sand. *Journal of Geotechnical and Geoenvironmental Engineering*, *144*(3), 04017120.

Tran, K. T., Jalinoos, F., Nguyen, T. D., & Agrawal, A. K. (2019). Evaluation of bridge abutment with ultraseismic waveform tomography: Field data application. *Journal of Nondestructive Evaluation*, *38*(4), 95.

Tucker, S. E., Briaud, J.-L., Hurlebaus, S., Everett, M. E., & Arjwech, R. (2015). Electrical resistivity and induced polarization imaging for unknown bridge foundations. *Journal of Geotechnical and Geoenvironmental Engineering*, *141*(5), 04015008.

Tumay, M. T. (1985). *Field calibration of electric cone penetrometers in soft soil*. Federal Highway Administration.

Van Dijk, B. F. J., & Kolk, H. J. (2011). CPT-based design method for axial capacity of offshore piles in clays. *Frontiers in Offshore Geotechnics II* (pp. 555–560). CRC Press.

Vesic, A. S. (1973). Analysis of ultimate loads of shallow foundations. *Journal of the Soil Mechanics and Foundations Division*, *99*(1), 45–73.

Wightman, W. E., Jalinoos, F., Sirles, P., & Hanna, K. (2004). *Application of geophysical methods to highway related problems*. Federal Highway Administration. https://rosap.ntl.bts.gov/view/dot/49856/dot_49856_DS1.pdf

Winter, C., & Maday, M. (2022). Pile set-up to optimize high-rise bridge design. *The Magazine of the Deep Foundation Institute*, 84–88.

APPENDICES

Appendix A. Summary of Protocols for Foundation Reuse

APPENDIX A. SUMMARY OF PROTOCOLS FOR FOUNDATION REUSE

Figure A.1 shows the proposed framework for foundation reuse analysis. The detailed information can be found in Section 3 of the report.

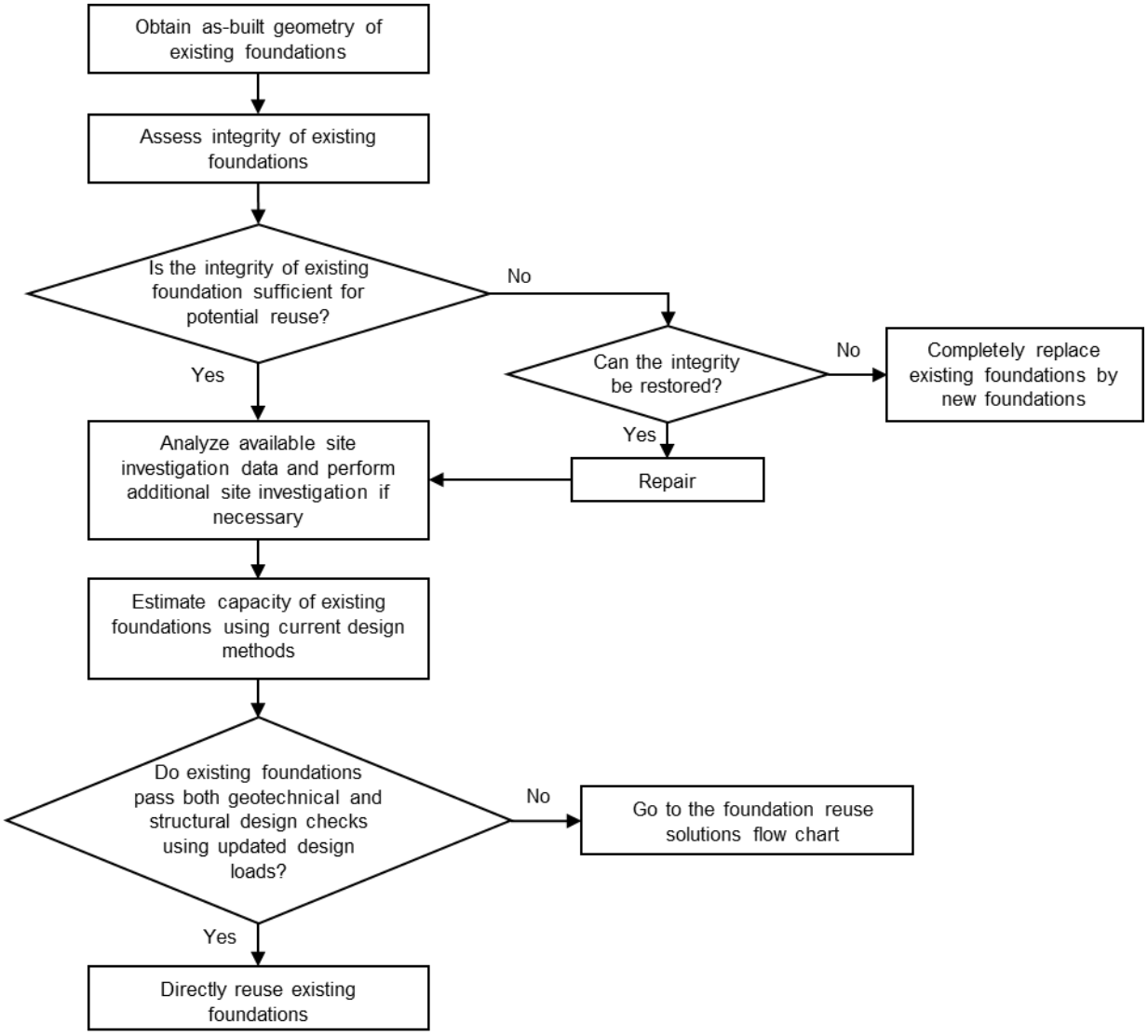

Figure A.1 Framework of the foundation reuse strategy.

A.1 Inspection of Existing Foundations

A.1.1 Determination of As-Built Geometry of Existing Foundations

Determination of the as-built geometry of existing foundations is the first step of the foundation reuse. Table A.1 shows destructive and nondestructive inspection methods that can be used to obtain specific dimensions of existing foundations. The detailed inspection methods can be found in Section 4.4 of the report. Figure A.2 shows the flow chart to determine the geometry of unknown foundations.

Table A.1 Destructive and nondestructive methods that can be used to obtain specific dimensions of existing foundations.

Unknown Dimension To Obtain	**Methods/Techniques**
Pile length	Vertical coring, sonic echo/impulse response, bending wave method, ultra-seismic, seismic methods, cross-borehole tomography, parallel seismic, magnetometry, GPR, borehole radar and sonic, induction field (IF) testing
Thickness of footing/pile cap	Excavation, vertical coring, seismic methods, impact echo, surface resistivity testing, GPR, borehole radar and sonic
Elevation of the top of pile cap/footing	Excavation, probing, seismic methods, GPR, surface resistivity testing, borehole radar and sonic
Width and length of footing/pile cap	Excavation, probing, seismic methods, GPR, surface resistivity testing
Layout of pile group	Partial excavation, seismic methods, impact echo, GPR

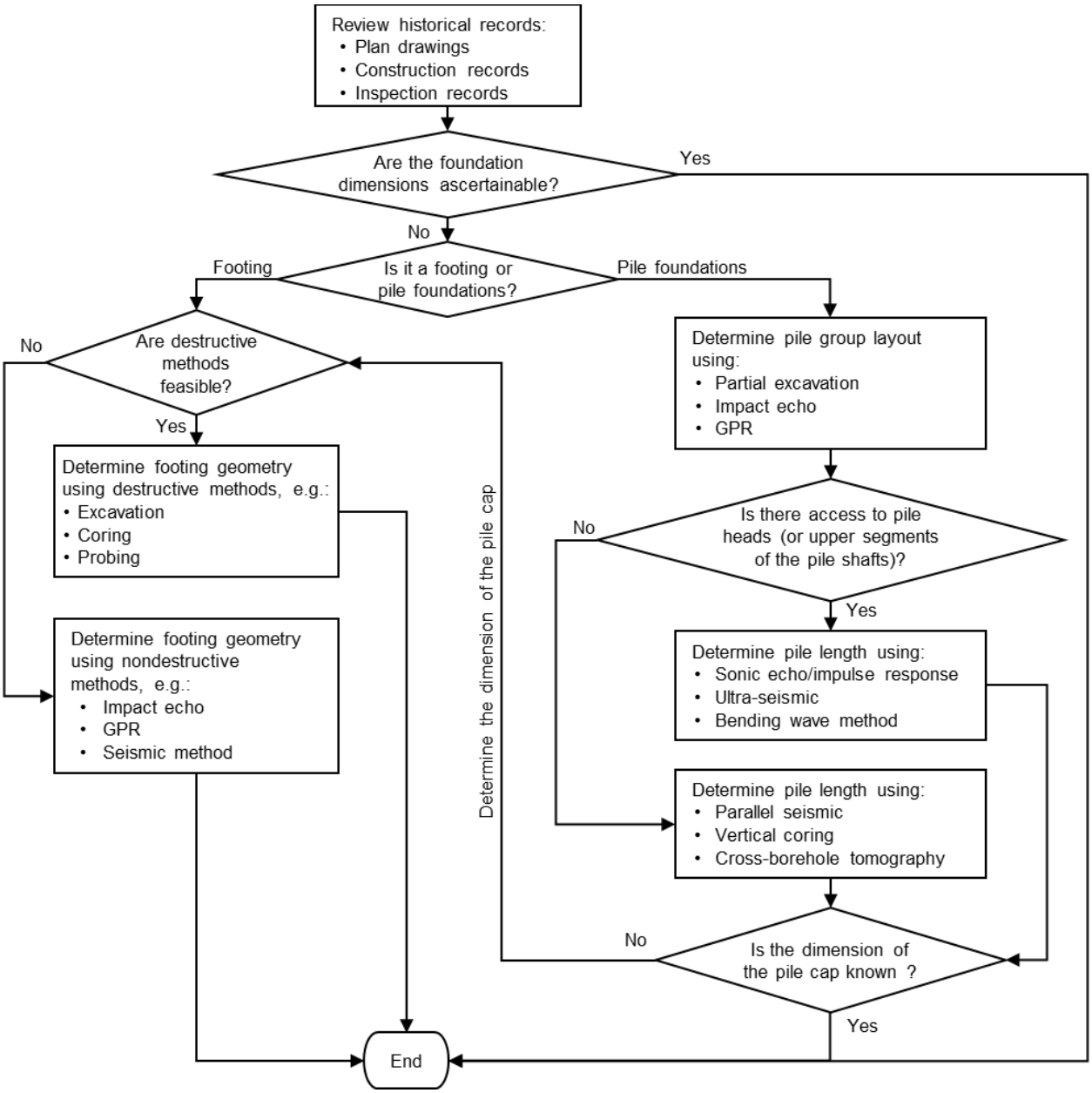

Figure A.2 Flow chart to determine the geometry of the unknown foundation.

A.1.2 Inspection of Structural Integrity of Existing Foundations

After determining the as-built geometry of existing foundations, inspection of structural integrity of existing foundations should be performed and structural integrity of the existing foundations should be assessed. The inspection items and corresponding inspection methods for existing concrete and steel foundations can be found in Table 4.3 and Table 4.4. The detailed inspection methods can be found in Section 4.4 of the report. Figure 4.2 shows the flow chart to inspect three aspects of structural integrity items of existing foundations.

Table A.2 Inspection items and corresponding inspection methods for existing concrete foundations

Item Category	Inspection Items	Methods/Techniques
Material properties	Mix properties, compressive strength, elastic modulus, rebar strength	Review of historical records, destructive methods (sampling and lab testing, vertical coring with wireline logging)
Surface defects	Cracking/crack density, spalling, delamination, patching, discoloration, efflorescence and rust/moist straining, cold joints (lift lines), section loss	Visual observation, destructive methods (excavation)
Internal defects	Cracking, voids, weak zones, honeycombing, location of delamination, presence of water, chloride and salts, presence and extent of corrosion of rebar, section loss	Destructive methods (excavation, vertical coring with wireline logging), nondestructive methods (GPR, ultrasonic pulse velocity, infrared thermography, electrical resistivity, radiography, sonic echo/impulse response method, ultra-seismic, impact echo, SASW, bending wave method)
Geometry	Discontinuities, breaks, rebar layout	Review of historical records, destructive methods (excavation), nondestructive methods (GPR, radiography, cover meters, parallel seismic, induction field testing)

Table 4.4 Inspection items and corresponding inspection methods for existing steel foundations

Item Category	**Inspection Items**	**Methods/Techniques**
Material properties	Yield strength, tensile strength	Review of historical records, destructive methods (sampling and lab testing)
Defects	The location and extent of corrosion, cracks (especially near welds and bolts), surface flaws, condition of fatigue prone elements, condition of cover plate cutoffs, condition of connection details and fasteners, presence of lead paint, section loss	Visual observation, dye penetrant testing, destructive methods (sampling and lab testing), nondestructive methods (magnetic particle testing, Eddy current testing, ultrasonic testing and phased array ultrasonic testing, acoustic emission)
Geometry	Discontinuities, breaks	Destructive methods (excavation), nondestructive methods (GPR, parallel seismic, induction field testing)

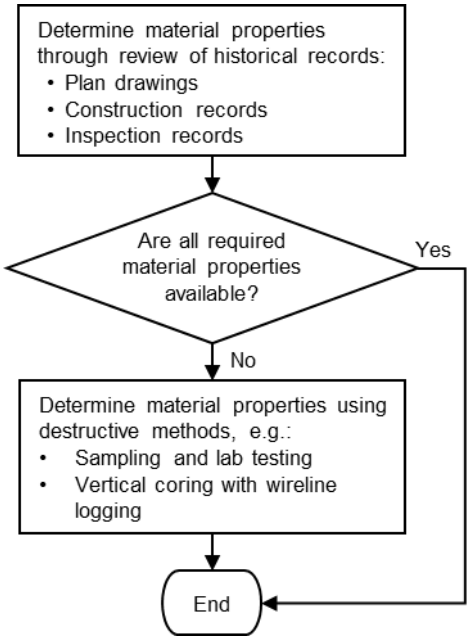

(a)

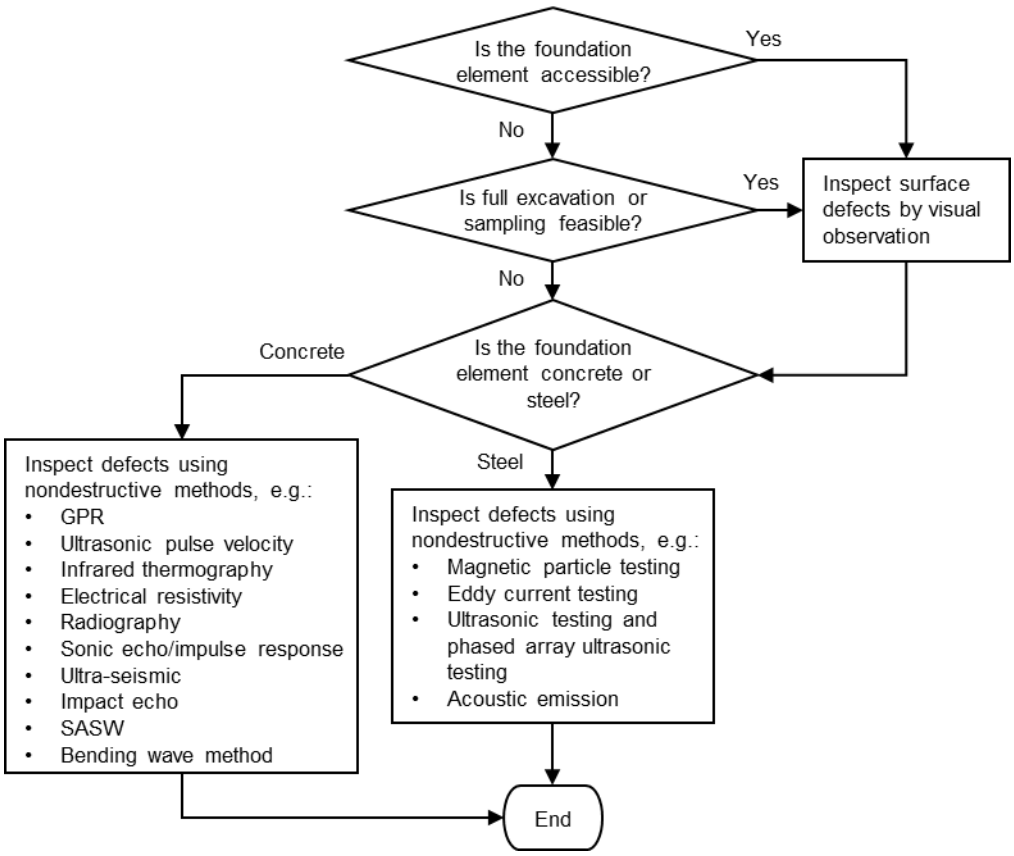
Is the foundation element accessible?
Yes
No
Is full excavation or sampling feasible?
Yes
Inspect surface defects by visual observation
No
Is the foundation element concrete or steel?
Concrete
Steel
Inspect defects using nondestructive methods, e.g.:
• GPR
• Ultrasonic pulse velocity
• Infrared thermography
• Electrical resistivity
• Radiography
• Sonic echo/impulse response
• Ultra-seismic
• Impact echo
• SASW
• Bending wave method
Inspect defects using nondestructive methods, e.g.:
• Magnetic particle testing
• Eddy current testing
• Ultrasonic testing and phased array ultrasonic testing
• Acoustic emission
End

(b)

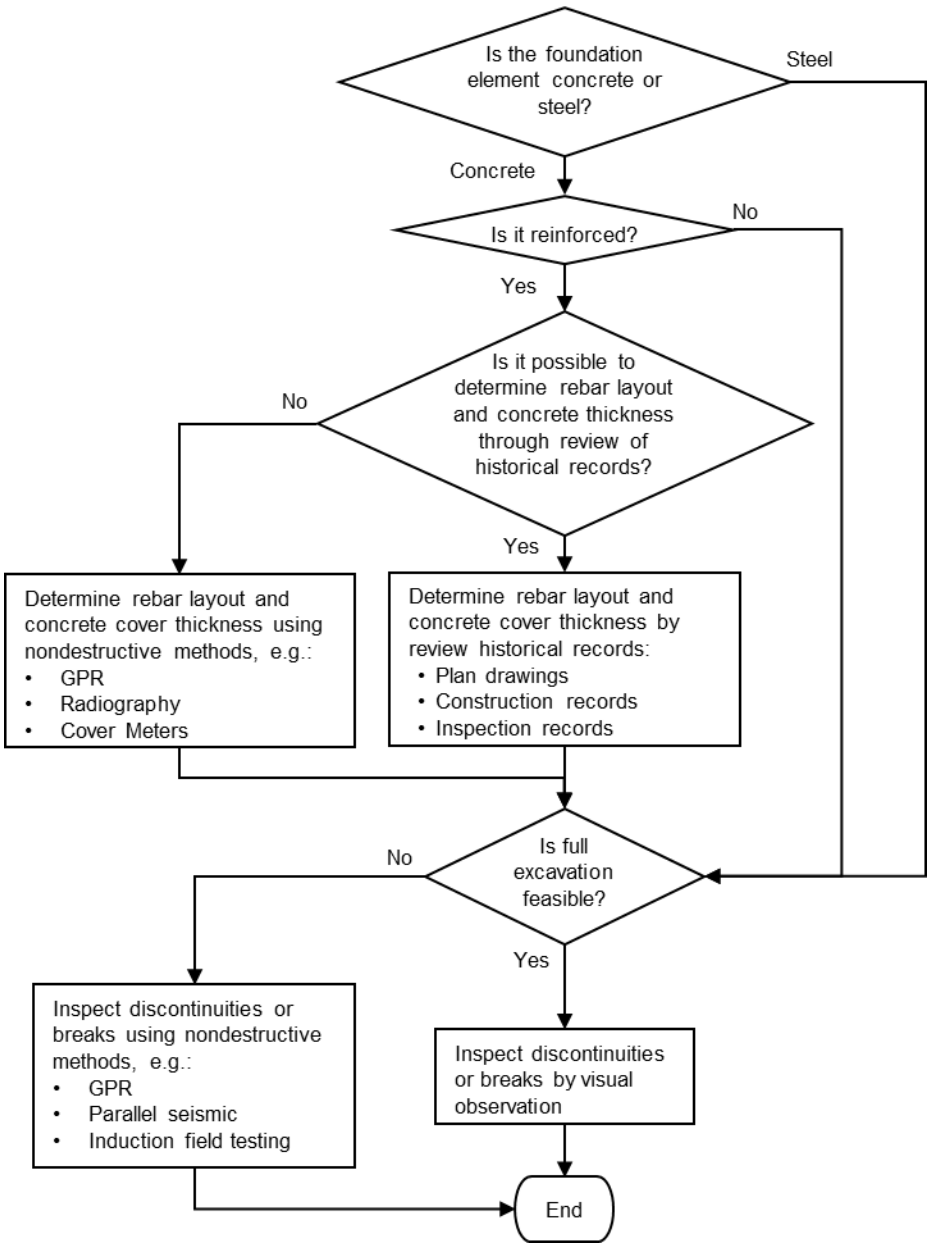

(c)

Figure A.3 Flow chart to inspect three aspects of structural integrity of existing foundations: (a) material properties of foundation elements, (b) defects in existing foundations, and (c) a change in geometry of existing foundations.

A.2 Interpretation of Site Investigation Data

If the structural integrity of existing foundations is sufficient for potential reuse with or without repairs, the available site investigation data should be collected and analyzed. Having an accurate

analyzed site investigation data is very important to estimate the capacities of existing foundations accurately. If necessary, additional site investigations should be performed.

The data that can be used for the analysis include the following.

- Geotechnical logs: soil description, layering, soil density, SPT and/or CPT, water content, groundwater level and flow pattern (i.e., hydrostatic, hydrodynamic, artesian conditions).
- Records of geohazard vulnerability assessments.

Geohazard vulnerability assessments includes vulnerability to scour and seismic hazards (including liquefaction, settlement, slope failure, and fault rupture). Records on corrosive soils, Karst formation, loss of soil foundation support and drainage during or after a rain event can also be used for the analysis.

If available historical records are incomplete and do not provide sufficient information, additional site investigation can be performed in the context of reuse decisions (including deciding which types of *in situ* or laboratory tests are more appropriate for the site conditions). Even when original borings from the time of initial construction are available, further exploration can be done to confirm the available data and the time effect on the current soil profile. If only standard penetration test (SPT) data are available, more reliable tests, such as the cone penetration test (CPT), can be performed.

A.3 Capacity Estimation of Existing Foundations

The current capacity of existing foundations can be estimated from consideration of some of the following.

1. Historical records (original plan drawings, construction records, as-built plans showing the geometry of existing foundations or inspection records).
2. Results inspection or structural integrity evaluations.
3. Site investigation data.
4. Load tests.

Figure A.4 shows the flow chart to estimate capacities of existing foundations. Details on capacity estimation methods can be found in Section 5 of the report.

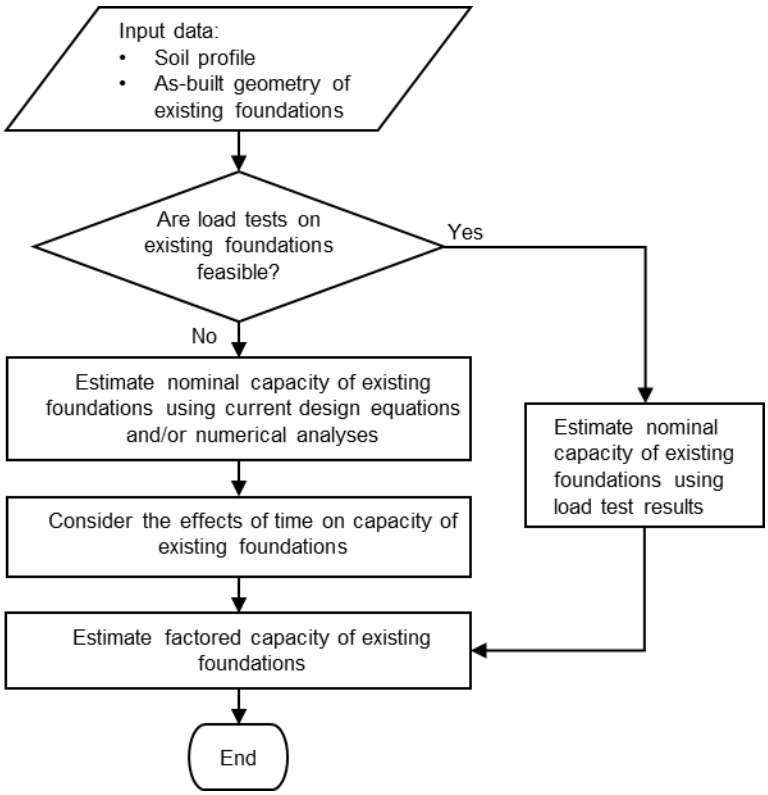

Figure A.4 Flow chart to estimate capacity of existing foundations.

A.4 Design Checks and Selection of Foundation Reuse

Based on the updated design load, current soil profile and estimated current capacity of existing foundations, the design checks for the foundation reuse can be performed. The minimum requirements for foundation reuse may be set as follows.

- Factored resistance > factored load.
- No significant foundation element deterioration.
- Structurally sound foundation elements.
- No significant scour.
- No excessive total and differential settlements.
- No excavations or other work that might lead to loss of foundation support.
- No significant reconfiguration of loads.
- Lack of ability to perform construction as needed for the existing and new foundation elements.

If the existing foundation does not pass design checks, it can be repaired or strengthened to increase its capacity, or the superstructure design load can be revised, as by using light-weight superstructure materials. If none of those methods work, the existing foundation can be completely replaced by new foundations. Figure A.5 shows the flow chart to select foundation

reuse solutions. The detailed foundation reuse solution methods and several factors to be considered can be found in Section 6.

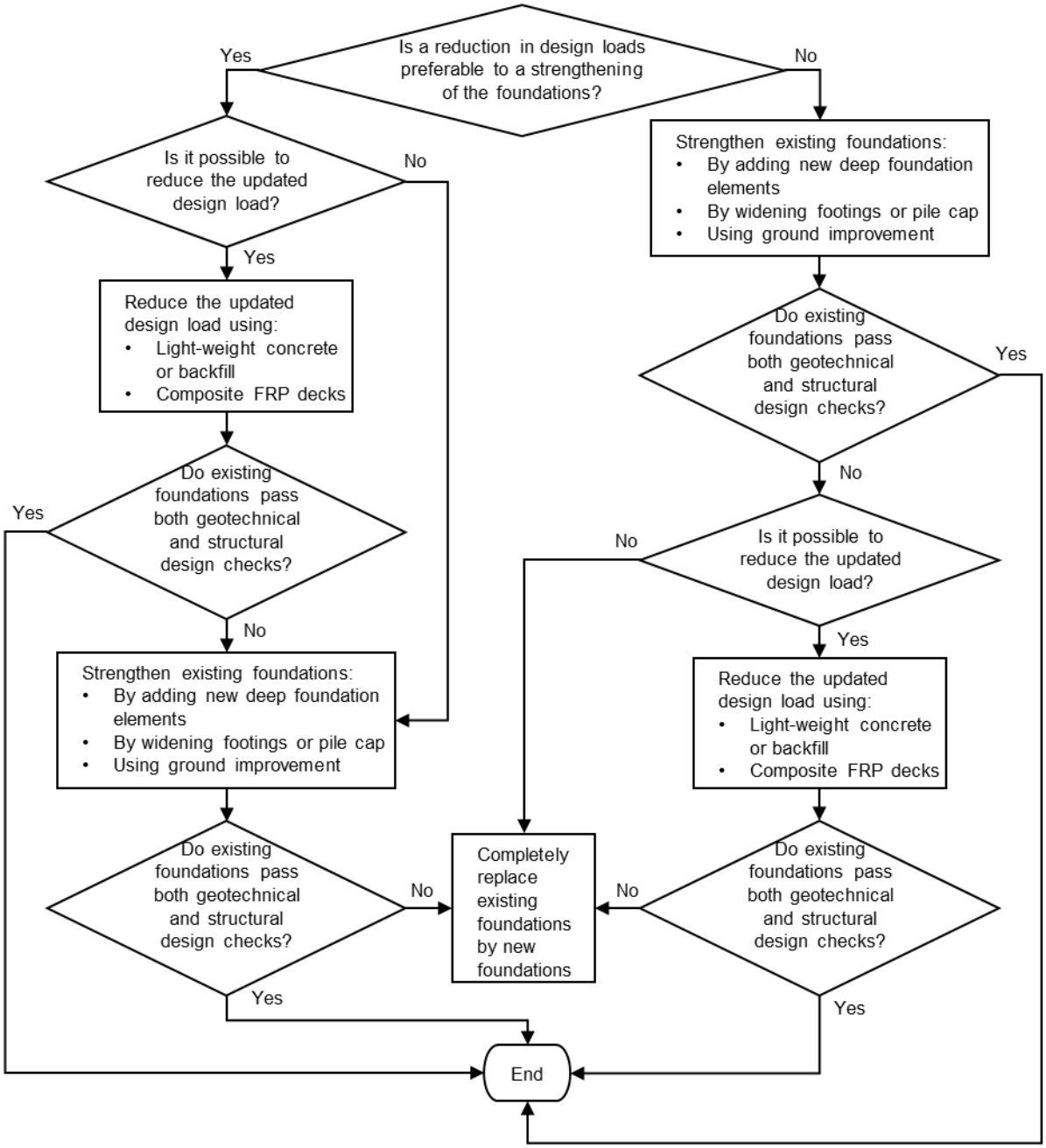

Figure A.5 Flow chart to select foundation reuse solutions.

About the Joint Transportation Research Program (JTRP)

On March 11, 1937, the Indiana Legislature passed an act which authorized the Indiana State Highway Commission to cooperate with and assist Purdue University in developing the best methods of improving and maintaining the highways of the state and the respective counties thereof. That collaborative effort was called the Joint Highway Research Project (JHRP). In 1997 the collaborative venture was renamed as the Joint Transportation Research Program (JTRP) to reflect the state and national efforts to integrate the management and operation of various transportation modes.

The first studies of JHRP were concerned with Test Road No. 1—evaluation of the weathering characteristics of stabilized materials. After World War II, the JHRP program grew substantially and was regularly producing technical reports. Over 1,600 technical reports are now available, published as part of the JHRP and subsequently JTRP collaborative venture between Purdue University and what is now the Indiana Department of Transportation.

Free online access to all reports is provided through a unique collaboration between JTRP and Purdue Libraries. These are available at http://docs.lib.purdue.edu/jtrp.

Further information about JTRP and its current research program is available at http://www.purdue.edu/jtrp.

About This Report

An open access version of this publication is available online. See the URL in the citation below.

Lim, J., Salgado, R., Prezzi, M., Wang, Y., & Han, F. (2023). *Development of protocols for reuse assessment of existing foundations in bridge rehabilitation and replacement projects* (Joint Transportation Research Program Publication No. FHWA/IN/JTRP-2023/23). West Lafayette, IN: Purdue University. https://doi.org/10.5703/1288284317654